Underground Injection Control
Carbon Sequestration
Class VI Permit Application

APPLICATION NARRATIVE
40 CFR 146.82(a)

Four Corners Carbon Storage, LLC
San Juan Basin, New Mexico Carbon Sequestration Project

June 2023

Prepared by:

Kevin Bush (Subsurface Director)
Katy Larson (UIC Coordinator)
Four Corners Carbon Storage, LLC
4200 West 115th Street
Leawood, KS 66211

Numeric Solutions, LLC
1536 Eastman Ave., Suite D
Ventura, CA 93003

TABLE OF CONTENTS

List of Figures

List of Tables

LIST OF EQUATIONS

Plan revision number: 0
Plan revision date: 6/9/2023

List of Attachments

File Name / Folder	Description
FourCornersCarbonSJ_geodatabase.gdb	An ESRI file geodatabase containing project specific data (proposed well locations, AoR boundary, etc.) and other pertinent spatial data referenced in the application narrative
References	A folder containing references cited
2.1.2_RegionalTopographicMap.pdf	Regional topographic map of the Northern San Juan Basin showing the location of the proposed injection well (blue) and AoR. Regional topographic map of the Northern San Juan Basin showing the location of the proposed injection well (blue) and AoR. The approximate extent of the San Juan Basin is shown with a dashed dark red line and the approximate Central Basin extent is shown with a thin dotted red line
2.1.3_TypeWellLog.pdf	Type well log for the project area showing all key stratigraphic markers and zones from surface down to the lower confining zone
2.2.1a_FourCornersCarbon_Inj1_AoR_Map_ArchD_1-18k_land-topo.pdf	A map of the AoR with all required information per 14 CFR §146.82 at a scale of 1 in. to 1,500 ft (1:18,000).
2.2.1b_FourCornersCarbon_Inj1_AoR_Map_ArchD_1-12k_SatImage.pdf	An AoR basemap version at 1:12,000 scale with a recent satellite imagery basemap
2.2.1c_AoRMap-let.pdf	A smaller scale letter sized version of the AoR basemap
[redacted]	Large scale structure contour map on the top of the proposed injection zone, [redacted]
[redacted]	Large scale structure contour map on the top of the upper confining zone, [redacted]
2.2.3_CrossSections.pdf	Structural cross section A and B running NW-SE and SW-NE, respectively, through the proposed injection well location
2.3.1_BasementFaultsMap.pdf	Map of approximate locations of basement faults (after Taylor and Huffman 1998)
2.4.1a_[redacted]	[redacted] structure contour map at 1:250k scale
2.4.1b_[redacted]	[redacted] gross isopach map at 1:250k scale
2.4.2a_[redacted]	[redacted] structure contour map at 1:250k scale
2.4.2b_[redacted]	[redacted] gross isopach map at 1:250k scale
2.5.3_WSMLetter-final.pdf	Basin scale stress orientations map from the World Stress Map database
2.6.2_SeismicHistoryMap.pdf	Seismic events map of the SJ basin from the USGS
2.7.3_AoRWaterWellsBasemap.pdf	Map of water wells within the AoR
3.4.1a_AoR Oil and Gas Well List (NM OCD)-dist.xlsx	Spreadsheet with a list of all oil and gas wellbores within the AoR and pertinent information (depths etc.) from the New Mexico Oil Conservation Division.
3.4.1b_AoR Water Well List (NM OSE PODs)-dist.xlsx	Spreadsheet with all water wells within the AoR from the New Mexico Office of the State Engineer's Points of Diversion database.
3.4.1c_Oil and Gas Well Files NM-OCD.zip	Well files and logs for all oil and gas wells within the AoR
3.4.1d_Water Well Files_NM-OSE.zip	Well files for all water wells within the AoR
13.1a_EJ_Addresses Map.pdf	Map showing address points within and adjacent to the AoR
13.1b_EJ_Sat Image.pdf	Google Earth satellite imagery map of the AoR
13.2_HistoricPlacesMap.pdf	Map of the proposed injection well and the area of review showing the nearest Historic Places.

ACRONYMS AND ABBREVIATIONS

Note: All terms are written as used in the text.

°	degrees
%	percent
µmho	micromhos
µS	microSiemens
2D	two dimensional
A	
AOI	area of interest
AoR	Area of Review
API	American Petroleum Institute
ATSM	American Society for Testing and Materials
AWRI	Annis Water Resources Institute
B	
bbl	barrel(s)
Bcf	billion cubic feet
bgs	below ground surface
BHP	bottomhole pressure
BHT	bottomhole temperature
BOP	blowout preventer
C	
CBL	cement bond log
CCS	carbon capture and storage
CCUS	carbon capture, utilization, and storage
CEJST	Climate and Economic Justice Screening Tool
CFR	Code of Federal Regulations
CO_2	carbon dioxide (may also refer to other carbon oxides)
COGCC	Colorado Oil and Gas Conservation Commission
CRA	corrosion resistant alloy
D	
DIC	dissolved inorganic carbon
DITF	drilling-induced tensile fractures
DOC	dissolved organic carbon
DOE	Department of Energy
E	
ECOS	Environmental Conservation Online System
EHS	environmental, health and safety
EJ	environmental justice
ELAN	elemental analysis
EOS	equation of state

EPA	Environmental Protection Agency
ERP	emergency response plan
ERRP	emergency and remedial response plan
ESHIA	Environmental, Social and Health Impact Assessment
F	
F	Fahrenheit
FMI	formation microimager
Four Corners Carbon	Four Corners Carbon Storage, LLC
ft	feet / foot
ft/D	feet per day
ft/mile	feet per mile
ft^2/D	square feet per day
ft^3/sec	cubic feet per second
G	
g/cc	grams per cubic centimeter
gpm	gallons per minute
GR	gamma ray
GSDT	Geologic Sequestration Data Tool
H	
HHRA	Human Health Risk Assessment
I	
IEA	International Energy Agency
in.	inch
L	
lbm	pound mass
lbf	pound force
M	
Ma	million years
mD	millidarcy (1 mD = 9.86923e-16 m^2)
MD	measured depth
MDT	Modular Formation Dynamics Tester
MEM	mechanical earth model
mg/L	milligrams per litter
MICP	mercury injection capillary pressure
MIRU	move in and rig up
MIT	mechanical integrity test
MM	million
MMCF	million cubic feet
MMT	million metric tons
Mt	megatonne / million metric tons
Mt/yr	million metric tons per year
Mta	million metric tons per annum

mV	millivolt
N	
NHD	National Hydrography Dataset
NMBGMR	New Mexico Bureau of Geology & Mineral Resources
NMOCD	New Mexico Oil Conservation Division
NMR	Nuclear Magnetic Resonance
NPDES	National Pollutant Discharge Elimination System
O	
OCD	Oil Conservation Division (New Mexico)
OD	outside diameter
ohm-m / Ωm	ohm meters – unit of resistivity
OSE	Office of State Engineer (New Mexico)
OSHA	Occupational Safety and Health Administration
P	
P&A	plug and abandon
PGA	peak ground acceleration
PISC	post-injection site care
PLSS	Public Land Survey System
POD	point of diversion
Pp	pore pressure
ppm	parts per million
Program	Department of Energy CarbonSAFE Phase III Program
psi	pounds per square inch
psi/ft	pounds per square inch per foot
psig	pounds per square inch gauge
Q	
Quanti.Elan™	SLB's mineralogical inversion application that provides quantitative formation evaluation of open hole logs level by level
R	
RCA	routine core analysis
RCRA	Resource Conservation and Recovery Act
RHOB	bulk density log
Rmf	resistivity of mud filtrate
Rw	resistivity of connate water
S	
SCADA	supervisory control and data acquisition
SCAL	special core analyses
sc-CO_2	supercritical carbon dioxide
SCP	State Cleanup Program
SEM	scanning electron microscope

SHmax	maximum horizontal stress
SHmin	minimum horizontal stress
SP	spontaneous potential
SRT	step-rate test
SS	subsea
SSTVD	subsea true vertical depth
Sv	vertical stress
SWD	saltwater disposal
T	
Tallgrass	Tallgrass Energy, L.P.
TCS	triaxial compressive strength
TD	total depth
TDS	total dissolved solids
ThruBit™	SLB through-the-bit logging - an openhole logging tool that is deployed from within drill string for difficult logging jobs
TVD	true vertical depth
TVDSS	true vertical depth subsea
U	
UIC	Underground Injection Control
US	United States
USDW	Underground Source of Drinking Water
USFWS	U.S. Fish & Wildlife Service
USGS	U.S. Geological Survey
UST	underground storage tanks
W	
WHP	wellhead pressure
wt%	weight percent
X	
XRD	X-ray diffraction
XRF	X-ray fluorescence

1.0 PROJECT BACKGROUND AND CONTACT INFORMATION

According to the International Energy Agency (IEA), 40 million metric tons (Mt) of carbon dioxide (CO_2) are captured annually in the world.[1] By 2070, the world will need to capture and store more than 10,000 Mt of CO_2 to meet the IEA's Sustainable Development Scenario plan—making new projects and investment paramount to achieving these goals.[2] As of the 2015 Paris Agreement, North America planned to create a carbon emission-free power sector by 2035. This goal would require the elimination of approximately five billion metric tons per year by 2035.[3]

Tallgrass Energy, L.P. (Tallgrass), headquartered in Leawood, Kansas, is a committed leader at the forefront of the United States' decarbonization efforts. Tallgrass is a pipeline and gas storage company that enables a high quality of life through the delivery of energy and services that fuel homes and businesses. Tallgrass' subsidiary, Four Corners Carbon Storage, LLC (Four Corners Carbon), was formed to focus on Tallgrass' carbon sequestration efforts.

Tallgrass and predecessor companies have operated natural gas storage fields for more than 70 years. Tallgrass currently operates 90 wells, 74 billion cubic feet (Bcf) of underground natural gas storage capacity, and 20,470 compression horsepower across Huntsman and East Cheyenne, Wyoming underground gas storage fields. These gas storage operations provide Tallgrass with critical subsurface working knowledge and skillsets that transfer directly to the sequestration of CO_2, specifically the injection, monitoring, and storage of gaseous fluids in porous reservoirs.

Four Corners Carbon proposes drilling and completing a carbon sequestration injection well (Injector 1) and monitoring well (Monitor 1) for the safe sequestration of carbon dioxide (the "Project") in northern San Juan County, [redacted]. Strat 1[4] is utilized as the project characterization well. **Table 1.1** provides the Project information including the well names, well utilizations, and coordinates.

Table 1.1—Project information.

Well Name	Use	Latitude*	Longitude*	PLSS
Injector 1	Injection	[redacted]	[redacted]	[redacted]
Monitor 1	Monitoring			
Strat 1	Characterization			

*North American Datum 1983

This application will:

- Characterize the geology and reservoir characteristics of the proposed injection well location to verify that the proposed injection reservoir and seal are suitable for long-term CO_2 storage.
- Describe the methodology for determining the AoR and review any potential requirements for corrective-active measures.

1 https://www.iea.org/reports/about-ccus
2 https://www.whitehouse.gov/briefing-room/statements-releases/2021/04/22/fact-sheet-president-biden-sets-2030-greenhouse-gas-pollution-reduction-target-aimed-at-creating-good-paying-union-jobs-and-securing-u-s-leadership-on-clean-energy-technologies/
3 https://www.usgs.gov/faqs/how-much-carbon-dioxide-does-united-states-and-world-emit-each-year-energy-sources
4 [redacted]

- Describe the engineering design of the injection well and monitoring wells.
- Provide an overview of the Project-related operational plans including:
    - Pre-Operational Logging and Testing
    - Testing and Monitoring
    - Emergency Response
    - Financial Assurance assessment informed by a risk assessment approach
- Review the plugging of the injection and monitoring wells, post-injection site care, and site closure. In accordance with all federal regulations for Class VI wells; the permit will be updated every two years during active well injection and every five years post-injection.
- Evaluate the AoR for environmental justice (EJ) related impacts during Project operation and post-injection monitoring.

1.1 Project Goals

Drill a CO_2 injection and sequestration well into [redacted] to sequester [redacted] of CO_2 for approximately [redacted] years for a cumulative injected mass of [redacted] Mt. This project will not be on non-native lands, with the injection well positioned on private lands and the overall sequestration project occupying private and BLM lands. The Standard Industrial Classification (SIC) code for this project is 4953 – Refuse Systems (nonhazardous waste disposal sites).

1.2 Project Partners and Collaborators

A list of all groups responsible for funding and/or contributing technical material to the Project is provided in **Table 1.2**.

Table 1.2—Applicant, project partners, and collaborators.[5]

Category	Company Name	Role
Applicant	Four Corners Carbon	UIC Permit Operator, UIC Applicant and authorship, technical feasibility, technical modeling
Industrial Collaborators	Numeric Solutions, LLC	UIC authorship, technical modeling
	SLB	Technical feasibility, technical modeling
	Acorn International	Community engagement plan

1.3 Project Timeframe

Figure 1.1—Project timeline from feasibility through post-injection site care and closure (PISC).

1.4 Proposed Injection Mass/Volume and CO_2 Source

The proposed injection volume is [redacted] for [redacted] years, which would amount to a total injected volume of [redacted] The source of the CO_2 to be injected has not yet been determined, but Four Corners Carbon will advise the permitting authority of the source of the CO_2 once it has been identified.

[5] Four Corners Carbon utilized data from the Strat 1 well to help prepare a Class VI permit for an injection well in the San Juan Basin.

1.5 Injection Depth Waver and/or Aquifer Exemption

1.5.1 Injection Depth Waiver

No injection depth waiver is requested nor is it required for the proposed Project. All injection and storage is proposed to occur below the lowermost underground source of drinking water (USDW) in the area.

1.5.2 Aquifer Exemption

No new or expanded aquifer exemption is requested nor required for the proposed Project as all injection and storage will occur in zone(s) that are currently non-USDWs.

1.6 List of Permits or Construction Approvals [40 CFR 144.31I(6)]

No permits or construction approvals have been applied for or received at the time of this initial Class VI application submission. Federal, state, and local permitting and notifications will commence upon submission of this Class VI application. **Table 1.3** identifies the potential environmental permits that Four Corners Carbon may need to obtain pursuant to 40 CFR 144.31(e)(6).

Table 1.3—Permit approvals and submissions.

Agency/Permit Type	Permit No.	Status
RCRA - Hazardous Waste Management	TBD	Not filed
UIC - Underground Injection of Fluids	TBD	Not filed
NPDES Discharge of Surface Water	TBD	Not filed
PSD - Air Emissions from Proposed Sources	TBD	Not filed
Non-attainment Program Under the Clean Air Act	TBD	Not filed
National Emissions Standards for Hazardous Air Pollutants Pre-Construction Approval Under the Clean Air Act	TBD	Not filed
Dredge and Fill Permitting Program Under Section 404 of the Clean Water Act	TBD	Not filed
State and Local Permits	TBD	Not filed

NPDES==National Pollutant Discharge Elimination
PSD==Prevention of Significant Deterioration

Four Corners Carbon intends to file a Notice of Intent (NOI) for a Universal Application with the New Mexico Environmental Department (NMED) per 20.2.73. The NOI is not a permit but will give notice to the NMED of the Project and initiate a pre-application meeting to determine permitting requirements that will be required by NMED for the construction of this Project.

1.7 List of State, Tribe, and Territory Contacts [40 CFR 146.82(a)(20)]

Table 1.4—State, tribe, and territory contacts.

Agency	Phone Number
San Juan County New Mexico Sheriff's Office	505-334-6107
San Juan County Fire Department Administration	505-334-1180
New Mexico State Police	505-325-7547
New Mexico Department of Homeland Security & Emergency Management	505-476-9600
Environmental Services Contractor	312-269-2318
Underground Injection Control (UIC) Program Director	214-665-8473
U.S. Environmental Protection Agency National Response Center (24 hours)	800-424-8802
U.S. Environmental Protection Agency, Region 6	800-887-6063
New Mexico Energy, Minerals, and Natural Resources Department	505-564-7600
New Mexico Bureau of Geology & Mineral Resources	575-835-5490
New Mexico Oil Conservation Division (Aztec)	505-320-0243
New Mexico Environment Department	505-566-9741
Bureau of Land Management (Farmington, New Mexico)	505-564-7600

1.8 Contact Information

Kyle Quackenbush | Segment President – Liquids (Crude Oil and CO_2)
Four Corners Carbon Storage, LLC
370 Van Gordon Street
Lakewood, CO 80228
kyle.quackenbush@tallgrass.com
T: 303-763-3319

Katy Larson | UIC Coordinator
Four Corners Carbon Storage, LLC
370 Van Gordon Street
Lakewood, CO 80228
katy.larson@tallgrass.com

2.0 SITE CHARACTERIZATION

The site characterization provides text, tables, and figures to fulfill the site characterization requirements listed at 40 CFR §146.82(a)(2), (3), (5), and (6). References are appropriately cited and provided in **Literature.zip**. A guide of detailed site characterization discussions is provided in **Table 2.1**—Site characterization summary.

The subject sequestration Project is proposed for the [redacted] region of the San Juan Basin, in northwestern New Mexico. [redacted]

Data, information, and interpretations described in this section are summarized in the following text, demonstrating the location of Injector No. 1 and the AoR to be geologically and hydrologically favorable for the permanent storage of CO_2:

- The extent and structure of the San Juan Basin, along with its tectonic setting, are an ideal location for CO_2 storage. Much of the Central Basin consists of relatively simple structures with shallow dips (less than one degree) and is without recent faulting. No significant seismic hazards are present in the AoR (Sections 2.1, 2.3).
- The regional geologic setting is well constrained due to tens of thousands of wellbore penetrations from petroleum exploration and production that began in the 1940s within the San Juan Basin (Section 2.2).
- Within the AoR [redacted] is an excellent reservoir with high porosity (average [redacted] v/v [volume over volume] net) and permeability (approximately [redacted] millidarcy mD). (Sections 2.4.1, 2.5).
- Within the AoR, [redacted] is saline with no economic quantities of hydrocarbons (Sections 2.1.4, 2.8.1).
- [redacted] is encountered at ideal depths for pressures and temperatures favorable for the storage of supercritical CO_2, thousands of feet below currently exploited groundwater aquifers and the lowermost USDW (Sections 2.4.1, 2.7).
- [redacted] is laterally extensive with no known structural or stratigraphic traps within the AoR. No faulting was identified in the AoR or the surrounding area (Section 2.2).
- [redacted] has the pore volume to store, many times more CO_2 than proposed by this Project (Section 2.10.2).
- [redacted] is vertically bound by the laterally continuous [redacted] confining layer consisting of approximately 100 ft of low permeability limestones and shales (Sections 2.4.2, 2.10.3).
- [redacted] is an open saline aquifer with no known lateral flow barriers, CO_2 would be confined vertically by the overlying [redacted] while lateral confinement would initially occur via residual and solubility trapping then ultimately via mineral trapping (**Figure 2.1**) [redacted] (Sections 2.2.3, 2.10.2).

- No detrimental geochemical interactions are expected between the injectate and the formations or formation fluids. This will be confirmed via future core and fluid analyses along with geochemical modeling (Section 2.8).
- No artificial penetrations penetrate the injection or upper confining zones within the AoR. Injection and in-zone monitoring wells will be engineered to prevent the migration of fluids from the approved injection zone (Sections 2.2, 3.4.1, 5.0).

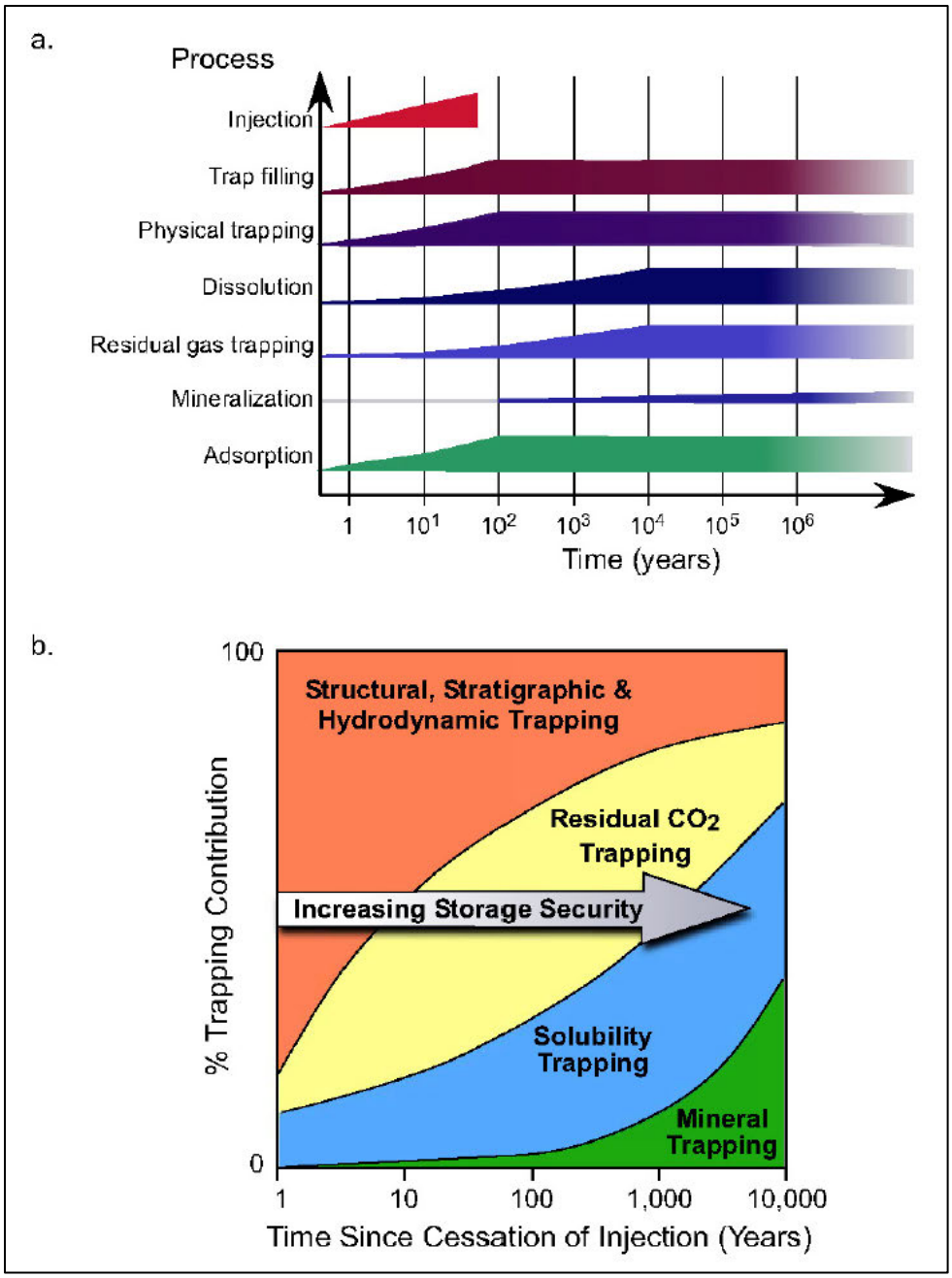

Figure 2.1—(a) Time scale of various CO_2 storage process in deep saline aquifer; (b) storage security of the CO_2 with the advancement of these processes (Bachu 2006).

Table 2.1—Site characterization summary.

CFR	Section Title	Section No.	Sub-Section Title	Sub-Section No.
40 CFR 146.82(a)(3)(iii)	Regional Geology, Hydrology, and Local Structural Geology	2.1	Tectonic History	2.1.1
			Structure	2.1.2
			Stratigraphy	2.1.3
			General Hydrogeology	2.1.4
40 CFR 146.82(a)(2), 146.82(a)(3)(i)	Maps and Cross Sections of the Area of Review	2.2	Map of Area of Review	2.2.1
			Structure Maps of the Injection and Confining Zones	2.2.2
			Cross Sections	2.2.3
40 CFR 146.82(a)(3)(ii)	Faults and Fractures	2.3	Literature Review	2.3.1
			Well Data	2.3.2
40 CFR 146.82(a)(3)(iii)	Injection and Confining Zone Details	2.4	Injection and Confining Zone Details	2.4
			Data on the Injection Zone(s)	2.4.1
			Reservoir Properties	2.4.1.1
			Geochemical Reactions	2.4.1.2 2.4.2.2
			Additional Data Required	2.4.1.3
			Data on the Confining Zone(s)	2.4.2
			Zone Properties	2.4.2.1
			Capillary Pressures	2.4.2.3
40 CFR 146.82(a)(3)(iv)	Geomechanical and Petrophysical Information	2.5	Fractures	2.5.1
			Stress	2.5.3
			Ductility	2.5.4
			Rock Strength	2.5.5
			In-Situ Fluid Properties	2.5.6
40 CFR 146.82(a)(3)(v)	Seismic History	2.6	Summary of Seismic History and Available Data	2.6.1
			Seismic Risk	2.6.2
40 CFR 146.82(a)(3)(vi), 146.82(a)(5)	Hydrologic and Hydrogeologic Information	2.7	Hydrostratigraphy and Underground Sources of Drinking Water	2.7.1
			Springs	2.7.2
			Water Wells Within the AoR	2.7.3
40 CFR 146.82(a)(6)	Geochemistry	2.8	Fluid Chemistry	2.8.1
			Solid Phase Geochemistry	2.8.2
			Geochemical Modeling	2.8.3
40 CFR 146.83	Site Suitability	2.10	Structural and Tectonic Suitability	2.10.1
			Injection Zone Suitability	2.10.2
			Confining Zone Suitability	2.10.3
			Mechanical Suitability	2.10.4

2.1 Regional Geology, Hydrogeology, and Local Structural Geology [40 CFR 146.82(a)(3)(vi)]

2.1.1 Tectonic History

The San Juan Basin is an asymmetric structural depression covering approximately 21,600 square miles of the east-central Colorado Plateau area in northwestern New Mexico, southwestern Colorado, a small portion of northeastern Arizona, and southeastern Utah (**Figure 2.2**; Craigg 2001). It was formed during the Late Cretaceous to Eocene age Laramide Orogeny, which occurred approximately 75 to 35 million years ago (Ma) (Kirk and Condon 1986; Dickinson and Snyder 1978). Strata in the basin reaches a maximum thickness of 14,000 feet and consists primarily of sedimentary and igneous rocks ranging in age from Devonian to Lower Tertiary. Faulting is prevalent along the basin margins and in the northeastern, southeastern, and south-central portions of the San Juan Basin.

The tectonic evolution of the San Juan Basin began by at least the late Paleozoic Period following Precambrian metamorphism, deformation, erosion, and subsequent burial. There is little evidence to suggest a structural depression existed during the Precambrian. Recurrent tectonism adjacent to the present-day San Juan Basin began during the late Paleozoic and extended through Mesozoic Periods, forming the building blocks of the future San Juan, Zuni, Defiance, and Nacimiento uplifts. Although minor deformation and uplift occurred throughout most of the Mesozoic, the San Juan Basin began to resemble its current configuration during the Laramide Period (Lorenz and Cooper 2001).

The Hogback monocline, a feature that bounds the northwestern limit of the central San Juan Basin, was initiated during the early Laramide orogeny (Figure 2.2 and **Figure 2.3**). Other bordering uplifts, including the Defiance to the southwest, the Zuni to the south, the San Juan to the north, and the Nacimiento to the east, were recurrently active during both the Paleozoic and Mesozoic periods; however, these uplifts were far more pronounced during late Cretaceous and the earliest phase of the Eocene Laramide Orogeny (Kelley 1951). Based on the distribution of post-Cretaceous sediments, uplift of the outer rim areas was localized during the earliest phase of the Laramide Orogeny and was gradually spread to the inner rim of the basin during the later phase that concluded by the end of the Eocene (Kelley 1951).

Middle and late Tertiary deposits unconformably rest on much older strata, including wide regions of Precambrian rocks exposed in the cores of some of the earlier uplifts. By the Pliocene, both the San Juan Basin and Colorado Plateau were uplifted, resulting in drainages developing to both the east and west of the continental divide. These drainages incised into the basin filling sediments and removing much of the late and middle Tertiary deposits from the central portion of the basin (Kelley 1951).

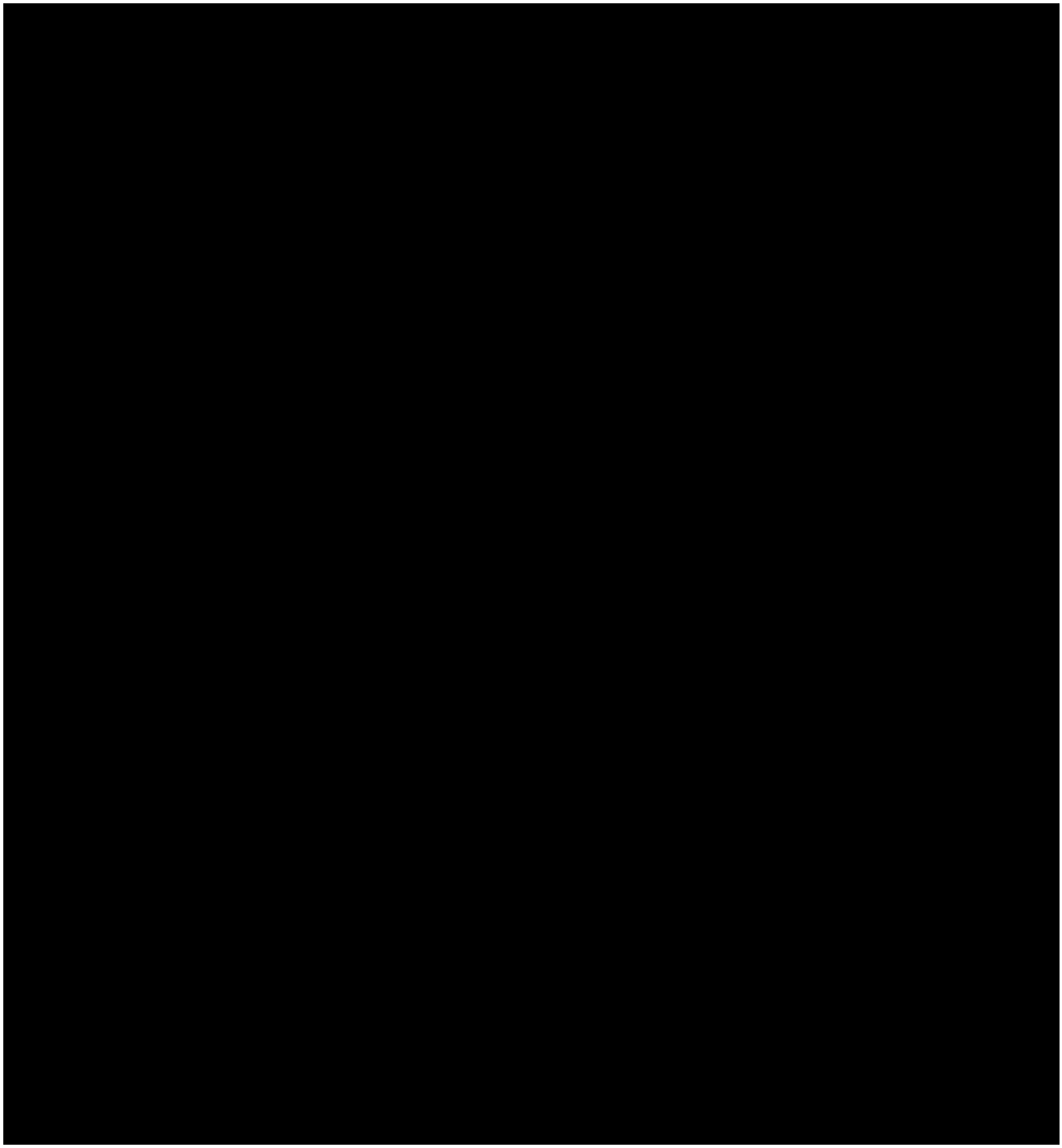

Figure 2.2—Structural elements of the San Juan Basin. San Juan structural basin shown in red outline (after Merrill et al. 2016). Arrows along monoclines point in the downdip direction.

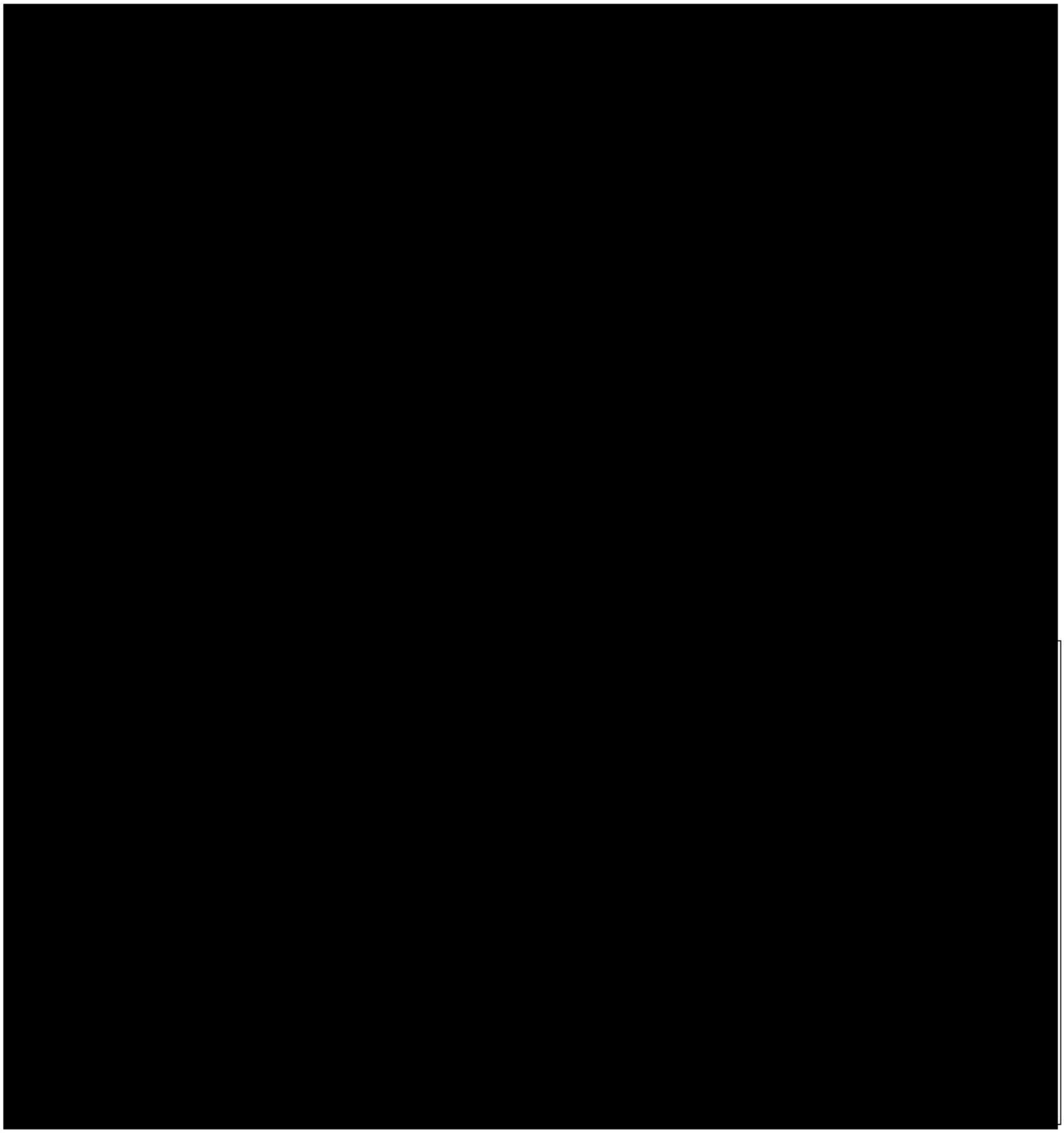

Figure 2.3—(a) Schematic (not to scale) west to east cross section through the San Juan Basin at the approximate latitude of the proposed injection well showing [redacted] injection zone [redacted]). (b) Schematic (not to scale) northeast to southwest cross section ([redacted]).

2.1.2 Structure

The AoR is located [redacted] region of the San Juan Basin (Figure 2.2 and **Figure 2.4)**. The interior of the basin consists of strata that exhibit a gentle, regional dip with numerous tectonic features that surround the perimeter of the basin, separating it from the Colorado Plateau. These tectonic features played a predominant role in

generating the present basin configuration. The major structural features adjacent to and within the San Juan Basin are categorized into three types: large uplifts, low structural arches and embayments, and monoclines (Figure 2.2). The Nacimiento fault, on the eastern margin of the basin, resulted in Precambrian granite being uplifted to the east. It is an example of a fault determining a basin boundary. The Defiance and Nutria monoclines are also clear basin-bounding features. Features like the Gallup and Acoma sags form less distinct boundaries where the San Juan Basin merges across structural saddles with adjacent basins or embayments (Kernodle 1996). Figure 2.2 depicts the major structural features bounding the San Juan Basin. These features are discussed in the following text beginning with those in the central portion of the basin and then moving in a clockwise direction around the perimeter features beginning in the north and concluding with a summary of prominent intra-basin structural features.

Figure 2.4—Regional topographic map of the Northern San Juan Basin showing the location of the proposed injection well (blue) and AoR. Regional topographic map of the Northern San Juan Basin showing the location of the proposed injection well (blue) and AoR. The approximate extent of the San Juan Basin is shown with a dashed dark red line and the approximate Central Basin extent is shown with a thin dotted red line.

2.1.2.1 Central/Inner Basin

The central region of the San Juan Basin has an approximate diameter of 100 miles and covers approximately 7,500 square miles (Figure 2.2). The basin is asymmetric with the northwest-striking axis along the northeastern rim (Figure 2.3, Lorenz and Cooper 2001). Monoclines bound the basin on the west, north, and eastern margins. Dips on these structures range from 20° to 40° in contrast to internal basin strata that dip at less than 1° (Fassett 1989). Along the Nacimiento Uplift, on the eastern margin of the basin, beds are near-vertical to overturned at some locations (Baltz 1967). The basin interior is underlain by a Proterozoic crystalline basement containing several northeast to southwest and northeast to southeast faults that were reactivated repeatedly throughout geologic history (Taylor and Huffman 1988).

2.1.2.2 Chaco Slope

The Chaco Slope marks the transition between the Zuni Uplift and the San Juan Basin's interior (Figure 2.2 and Figure 2.3). This region consists of strata gently dipping to the north to northeast at values ranging from 2° to 10° (Lorenz and Cooper 2001). The strata in this area are broadly folded and faulted due to several deformational events, including the Zuni Uplift that occurred during the Laramide Orogeny (Chamberlin and Anderson 1989). Fault intensity generally increases from west to east across the slope. Faults along the western half of the structure generally exhibit a northerly strike but shift to the northeast along the eastern half (Kirk and Condon 1986).

2.1.2.3 Zuni Uplift

The Laramide-aged Zuni Uplift is a northwest-striking asymmetric feature with a steeply dipping southwestern edge (Figure 2.2). Deformation associated with this structure is the primary cause of fracturing in the Cretaceous strata (Lorenz and Cooper 2001). The Zuni Uplift is slightly less than 2,500 square miles (70 miles by 35 miles). There is 8,000 ft of structural relief and 13,000 ft elevation difference between the uplift and the deepest part of the basin (Woodward and Callender 1977).

The Zuni Uplift merges with the Chaco Slope to the north along a mostly continuous northwestern trending boundary that is sometimes disrupted by short monoclines. Where the Zuni Uplift and the Chaco Slope come together, strata dips between 3° to 10° to the northeast and the area is disrupted by many 18-to-30-mile straight-line segments of north- to northeast-striking fault zones and sets of smaller scale northeast- to east-northeast-striking faults (Thaden and Zech 1984). The Zuni Uplift is bound to the west by the 32-mile-long Nutria monocline on which stratal dip ranges from low angles to overturned (Kelley 1967).

The Zuni Uplift's tectonic history extends to at least the Paleozoic period, when Pennsylvanian-aged strata thickened north of the uplift, suggesting contemporaneous differential movement (Jentgen 1977). Depositional patterns and folding within the Morrison Formation indicate uplift during the Jurassic period, which terminates in an unconformity at its top prior to Cretaceous Dakota Sandstone deposition.

2.1.2.4 Gallup Sag

The Gallup Sag, a 70-mile-long geologic feature that ranges from 8 miles to 28 miles in width, is located between the Zuni Uplift to the east and the Defiance Uplift to the west (Figure 2.2). The Gallup Sag gently plunges approximately 60 feet per mile (ft/mile) to the north and has a relatively flat base (Kelley 1967). It is described as a narrow embayment extending southward from the San Juan Basin (Kelley 1967). The synclinal axis of this asymmetrical sag lies closer to the west side of the Zuni Uplift, mirroring the axis of the Acoma Sag located east of the Zuni Uplift. This juxtaposition indicates that the Zuni Uplift was thrust over and onto the adjacent sag segments (Lorenz and Cooper 2001).

2.1.2.5 Acoma Sag

The Acoma Sag is bounded to the west by the Zuni Uplift, the Chaco Slope to the northwest, the Rio Puerco fault zone to the northeast, and the Lucero Uplift to the southeast (Figure 2.2). The synclinal axis of the Acoma Sag, the McCarty syncline, covers approximately 1,250 square miles (25-miles wide by 50-miles in length), and is situated adjacent to the eastern margin of the Zuni Uplift (Lorenz and Cooper 2001). The syncline gently plunges to the north and has been intruded by the Mount Taylor volcanics.

2.1.2.6 Defiance Uplift

The Defiance Uplift covers approximately 3,300 square miles (95-miles long by 35-miles wide) and marks the westernmost boundary of the San Juan Basin (Figure 2.2). The Defiance Uplift is described as a north-striking asymmetric uplift with its steepest limb along the eastern edge of the feature. The eastern-dipping limb forms the Defiance monocline and dips from 20° to 90° to the east (Lorenz and Cooper 2001). The monocline is disrupted by several southeast-plunging anticlinal and synclinal cross folds that exhibit an *en echelon*[6] character, indicating right-lateral movement (Kelley 1967).

2.1.2.7 Four Corners Platform

The Four Corners Platform is a broad, northeast-trending structural element along the northwestern boundary of the San Juan Basin to the west of the Hogback monocline and between the Defiance and San Juan uplifts (Figure 2.2 and Figure 2.3). Although there is minimal topographic relief across the extent of The Four Corner's Platform, it has 4,000 ft of structural relief and is expressed as a relatively flat and wide feature (Thaden and Zeck 1984). It is difficult to delineate the transition between the platform and the interior Central Basin even though this area has several anticlines/domes, suggesting that the boundary between them may be the result of wrench faulting along an irregular fault (Lorenz and Cooper 2001).

2.1.2.8 San Juan Uplift

The San Juan Uplift, also termed the San Juan Dome, is a roughly circular feature approximately 60-miles in diameter that marks the northern boundary of the San Juan Basin (Figure 2.2). The

[6] Describing parallel or subparallel, closely-spaced, overlapping or step-like minor structural features that are oblique to the overall structural trend. https://glossary.slb.com/en/terms/e/en_echelon. Accessed April 2023

difference in structural relief between the highest point of the uplift and the deepest portion of the basin is approximately 20,000 ft (Lorenz and Cooper 2001).

The southwestern edge of the San Juan Uplift is marked by the Needle Mountains which contain abundant sedimentary structures in the early Tertiary fluvial Ojo Alamo Sandstone. Analysis of the sediments suggests a south to southeast flow from the developing uplift (Steven 1975). During the Tertiary Period, volcanic and volcaniclastic strata generated by the active San Juan volcanic center covered much of the uplift and the northern region of the basin. The upper Animas Formation is age equivalent to the Tertiary volcanic activity and is composed of volcanic-rich coarse-grained sandstones and conglomerates (Lorenz and Cooper 2001). The Animas Formation has a maximum thickness of 2,700 ft along the northern region of the basin, suggesting that the northern edge of the basin was subsiding at that time (Fassett 1991).

2.1.2.9 Archuleta Anticlinorium

The Archuleta Anticlinorium, or Archuleta Arch, consists of a series of northwest-striking, parallel folds that form the northeastern boundary of the San Juan Basin separating it from the adjacent Chama Basin to the east Figure 2.2). The Archuleta Arch exhibits approximately 13,000 ft of structural relief in the San Juan Basin but only 1,500 ft of relief when contrasted with the Chama Basin (Lorenz and Cooper 2001).

2.1.2.10 Nacimiento Uplift

The Nacimiento Uplift is a well-documented transpressional[7] structure consisting of a series of north-striking, tilted, Precambrian blocks protruding along the southeastern edge of the San Juan Basin (Figure 2.2 and Figure 2.3). The Nacimiento Uplift has an approximate 10,000 ft of structural relief relative to the adjacent Chama Basin. North-striking normal faults are parallel to the main region of the Nacimiento front and delineate smaller tilted fault blocks (Lorenz and Cooper 2001). Other segmented blocks are separated by east-west, northeast, and northwest striking faults that are interpreted to have absorbed some of the differential movement between individual blocks (Woodward and Callender 1977). The northern region of the Nacimiento Uplift merges with the Archuleta Anticlinorium creating a faulted anticline that plunges 10° to 20° to the north and smaller folds that subsequently end in the south (Slack 1973).

The Nacimiento Uplift is marked by two phases of tectonism that occurred during the Laramide Orogeny. The first phase consisted of right-lateral displacement (2 miles to 3 miles) exhibited by remnants of north northwest to south southeast-striking *en echelon* folding along the western margin of the uplift (Baltz 1967). The second phase consisted of transpressive, right-lateral wrench faulting (Woodward 1983). During the late Tertiary Period, secondary reactivation of the uplift occurred due to extensional faulting along the Rio Grande rift (Kelley 1957).

2.1.2.11 Rio Puerco Fault Zone

The Rio Puerco Fault Zone lies between the Nacimiento and Lucero uplifts along the southeastern margin of the San Juan Basin (Figure 2.2). This fault zone comprises northwest-striking *en echelon* folds, northeast-striking *en echelon* normal faults, and a monocline (Slack and Campbell 1976).

[7] A segment along a transform or strike-slip fault which has a compressional component, sometimes creating related thrust faulting and mountains. https://opengeology.org/textbook/glossary/transpression/. Accessed March 2023.

The northeast-striking *en echelon* folds extend along the western margin of the Nacimiento Uplift, with some folds near the plunging southern area of the Nacimiento Uplift striking approximately north-south. The *en echelon* folds and normal faults are related to an early phase of Laramide deformation resulting in approximately 1.5 miles of right-lateral wrench offset (Slack and Campbell 1976).

2.1.2.12 Hogback Monocline

The Hogback Monocline is a long, arcuate structural feature that borders the Central Basin in all directions except the south and southwest (Figure 2.2 and Figure 2.3). The monocline, [redacted] is one of the most prominent structural features in the San Juan Basin, creating a subbasin within the basin (Kelley 1951). No other basin on the Colorado Plateau has such a clearly marked, continuous "monoclinal" feature (Kelley 1951). The Hogback Monocline dips steeply toward the Central Basin to the southeast. Along the Nacimiento Uplift, the Hogback Monocline is complexly faulted, and beds are locally overturned.

The Hogback Monocline is interpreted as an eastward- to southeastward-directed thrust fault (Lorenz and Cooper 2001). Near the Farmington, New Mexico area, the Hogback Monocline generally strikes to the northeast. The Hogback Monocline consists of a sinuous rim of southeastward-dipping strata with overlying transpressional thrust faults disrupting the basement and above affecting Paleozoic strata (Lorenz and Cooper 2001). Two-dimensional (2D) seismic lines across this structure reveal a downward-flattening fault that exhibits both normal and reverse displacement depending on the age of offset (Taylor and Huffman 1988). Seismic cross-sections published in Huffman and Taylor (1999) display inward-directed, "sled-runner" thrust planes in front of many of the basin monoclines that have loosely connected segments of variable dip and displacement. The "sled-runner" thrust planes are aligned expressions of *en echelon* segments of right-lateral displacement along the eastern and western margins of the basin as well as southward-verging thrust faulting resulting from the San Juan Uplift at the northern edge of the basin (Lorenz and Cooper 2001).

2.1.3 Stratigraphy

The San Juan Basin contains a thick sequence of sedimentary and igneous rock ranging from the Devonian Period to the Tertiary Period with the largest section deposited from Pennsylvanian Period to the Tertiary Period. The maximum thickness of the San Juan sedimentary sequence is approximately 14,400 ft within the Central Basin region (Figure 2.3). **Figure 2.5** from Craigg (2001) presents the stratigraphic framework and nomenclature of the San Juan Basin. **Figure 2.6** presents the stratigraphic framework and nomenclature specific to the AoR and this Project while **Figure 2.7** provides a type well log for the AoR.

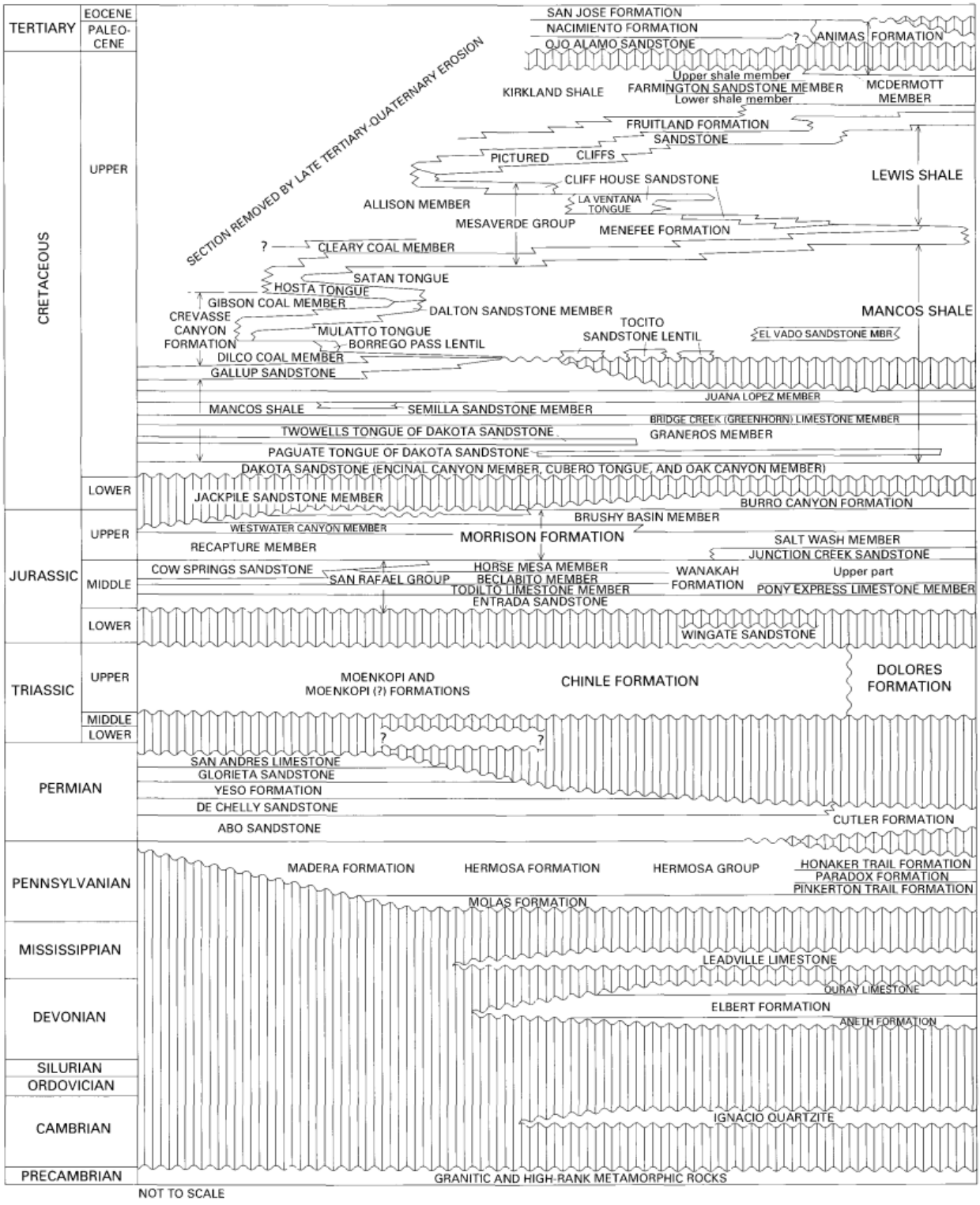

Figure 2.5—Stratigraphic framework and nomenclature of the San Juan Basin (Craigg 2001).

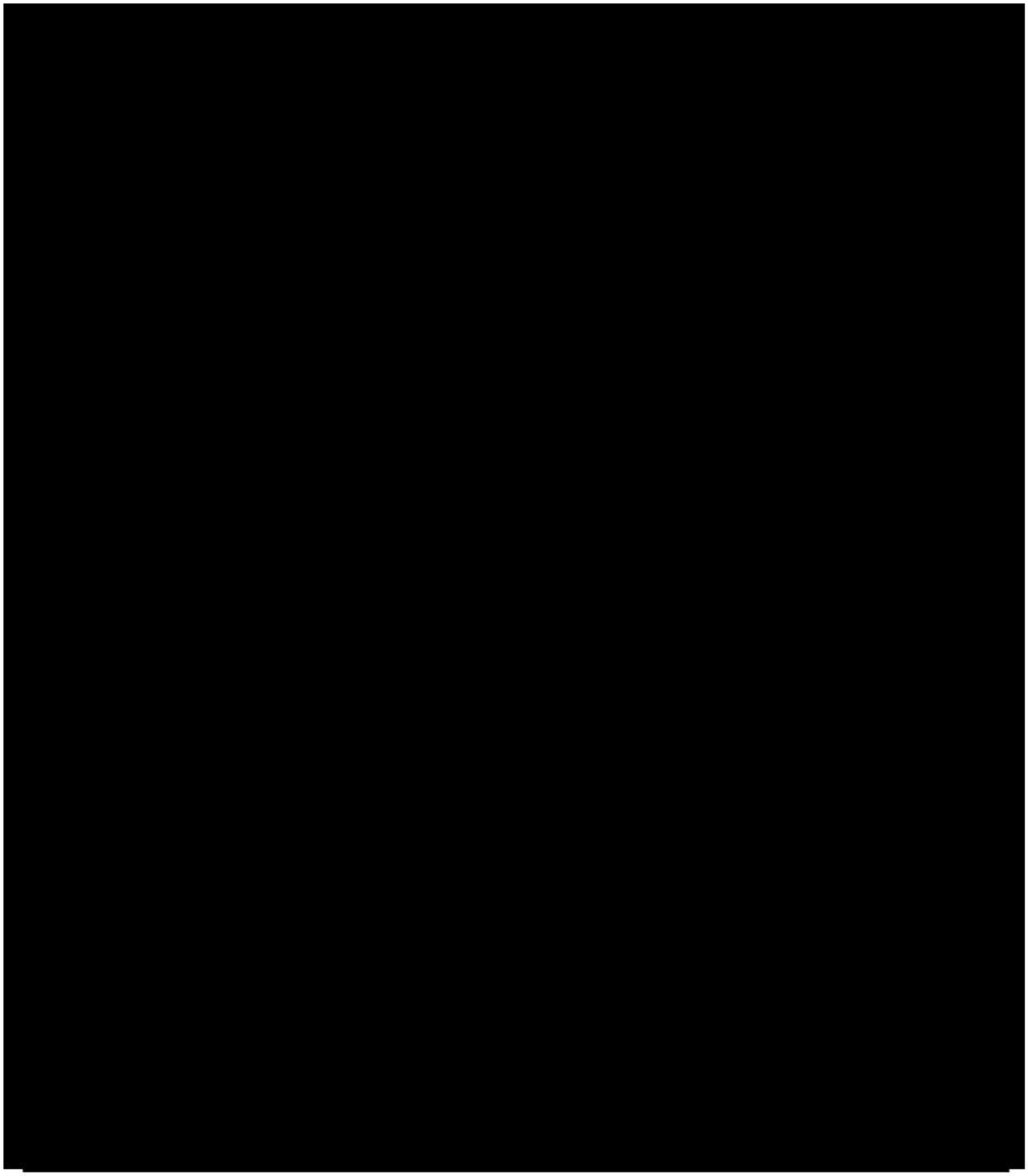

Figure 2.6—AoR specific stratigraphic column and UIC significance.

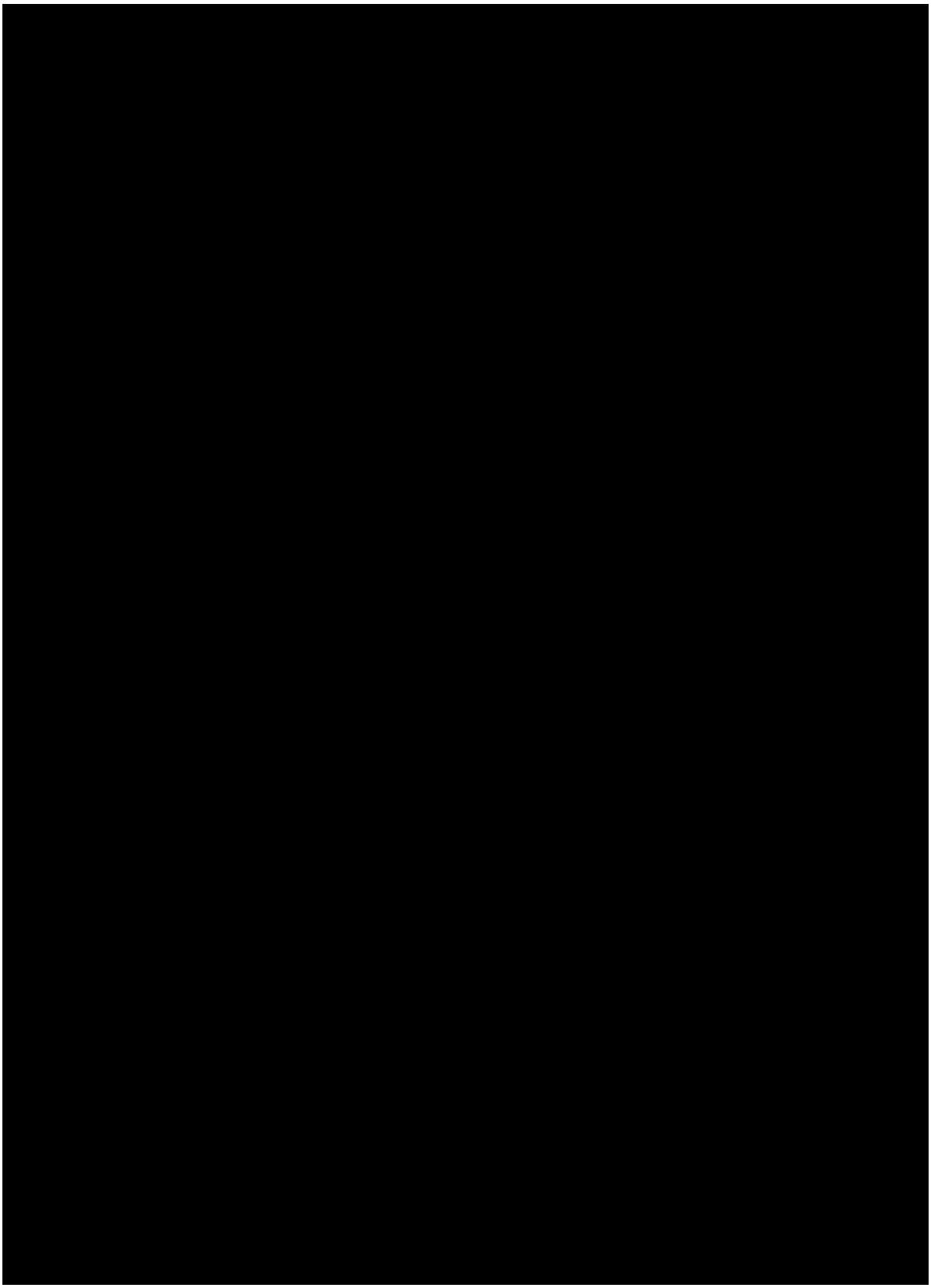

Figure 2.7—Type well log for the project area showing all key stratigraphic markers and zones from surface down to the lower confining zone. Track 1 provides period and zone, track 2 contains gamma ray (GR), and track three contains shallow (ILS) and deep resistivity (ILD).

The principal aquifers and confining intervals are Jurassic to Cenozoic Periods age (described in detail in Section 2.1.4—General Hydrogeology and Section 2.7—Hydrologic and Hydrogeologic Information). Triassic strata are generally considered confining units in the San Juan Basin, although minor aquifers may be present (Craigg 2001). **Table 2.2** provides a generalized stratigraphic summary of the San Juan Basin (Kelley et al. 2014).

Table 2.2—Generalized description of the Cenozoic, Cretaceous, and Jurassic rock units in the San Juan Basin (after Kelley et al. 2014). Note: the Gallup Sandstone is within the Mancos Shale, not above it as depicted below.

	Formation	Rock Type (major rock listed first)	Depositional Environment	Resources	Geologic Symbol
Cenozoic	San Jose Fm	Sandstone and shale	Continental rivers	Water, Gas	Tsj
	Nacimiento Fm	Shale and sandstone	Continental rivers	Water, Gas	Tn
	Ojo Alamo Sandstone	Sandstone and shale	Continental rivers	Water, Gas	Toa
Cretaceous	Kirtland Shale	Interbedded shale, sandstone	Coastal to alluvial plain	Water, Oil, Gas	Kk
	Fruitland Fm	Interbedded shale, sandstone, and coal	Coastal plain	Coal, CBM[8]	Kf
	Pictured Cliffs Sandstone	Sandstone	Regressive marine, beach	Oil, Gas	Kpc
	Lewis Shale	Shale, thin limestones	Offshore marine	Gas	Kls
	Cliff House Sandstone	Sandstone	Transgressive marine, beach	Oil, Gas	Kch
	Menefee Fm	Interbedded shale, sandstone, and coal	Coastal Plain	Coal, CBM[8], Gas	Kmf
	Point Lookout Sandstone	Sandstone	Regressive marine, beach	Oil, Gas, Water	Kpl
	Crevasse Canyon Fm	Interbedded shale, sandstone, and coal	Coastal Plain	Coal	Kcc
	Gallup Sandstone	Sandstone, a few shales, and coals	Regressive marine to coastal deposit	Oil, Gas, Water	Kg
	Mancos Shale	Shale, thin sandstones	Offshore marine	Oil, Gas	Kmf
	Dakota Sandstone	Sandstone, shale, and coals	Transgressive coastal plain to marine shoreline	Oil, Gas, Water	Kd
Jurassic	Morrison Fm	Mudstones, sandstone	Continental rivers	Uranium, Oil, Gas, Water	Jm
	Wanakah Fm	Siltstone, sandstone	Alluvial plain and eolian		
	Entrada Sandstone	Sandstone	Eolian sand dunes	Oil, Gas, Water	Je

2.1.3.1 Triassic Formations

Triassic age sedimentary rocks in the San Juan Basin, from oldest to youngest, are the Early Triassic Moenkopi, which is generally absent from the basin, and the Late Triassic Chinle and Dolores formations that outcrop along the basin margins and are present throughout the subsurface

[8] Coalbed methane

(Craigg 2001). The [redacted] is the lower confining unit for Injector No. 1. It has eight members in stratigraphic ascending order: the Shinarump, Monitor Butte, Petrified Forest, Owl Rock, Rock Point, Agua Zarca Sandstone, Salitral Shale Tongue, and Poleo Sandstone Lentil. The Upper, Middle, and Lower Members of the Dolores Formation are roughly time-equivalent to the Chinle Formation. The members of the Chinle and Dolores formations disconformably overlay Permian aged strata across much of the basin, except for the eastern and northern regions where they overlie Pennsylvanian strata or Precambrian basement. Late Triassic strata are unconformably overlain by the Jurassic age Entrada Sandstone across much of the basin.

Late Triassic rocks in the San Juan Basin were deposited mostly in non-marine environments including stream channel, flood plain, eolian, and lacustrine environments (Craigg 2001). The Chinle and Dolores Formations are generally regional confining layers. Upper Triassic rocks are absent in the northeast San Juan Basin then thicken to a maximum of 1,600 ft in the southwestern part of the basin. [redacted] **Table 2.3** briefly summarizes the lithology, location, and thickness of Triassic strata within the San Juan Basin.

Table 2.3—Triassic stratigraphy of the San Juan Basin (data from Craigg 2001).

Geologic Unit	Geologic Member	Lithology Description	Hydrologic Unit	Basin Location	AoR Presence	Thickness (ft)
Dolores	Upper	siltstone with minor sandstone	Dolores confining unit	SW Colorado	[redacted]	<550
	Middle	siltstone/sandstone/ conglomerate				130–270
	Lower	silty sandstone				20–160
Chinle	Poleo Sandstone Lentil	fluvial sandstone	Chinle confining unit	N-central & E	[redacted]	0–130
	Salitral Shale Tongue	lacustrine shale		N-central & E	[redacted]	110–300
	Agua Zarca Sandstone	fine-coarse conglomeratic sandstone		N-central & E	[redacted]	0–250
	Rock Point	siltstone and fine sandstone		SW	[redacted]	<500
	Owl Rock	silty shale w/ limestone		W & NW	[redacted]	0–300
	Petrified Forest	mudstone/shale w/ interbedded sandstone/conglomerate		Widespread	[redacted]	500–1,100
	Monitor Butte	interbedded mudstone/sandstone/ siltstone/conglomerate		SW	[redacted]	0–300
	Shinarump	fluvial sandstone w/ mudstone		W & S	[redacted]	25–210

2.1.3.2 Jurassic Formations

From oldest to youngest, Jurassic age rocks in the San Juan Basin are the Wingate Sandstone, Entrada Sandstone, Wanakah Formation, Cow Springs Sandstone, and the Morrison Formation (Merrill et al. 2016). The Jurassic formations were deposited in non-marine environments, including stream channels, flood plains, lakes, dunes, and sabkhas. The strata collectively reach a

maximum thickness of approximately 1,500 ft in the west-northwestern region of the San Juan Basin. They are progressively truncated southward until the entire Jurassic section is eroded south of the Zuni Uplift. **Table 2.4** briefly summarizes the lithology, location, and thickness of Jurassic strata in the San Juan Basin.

Table 2.4—Jurassic stratigraphy of the San Juan Basin (data from Craigg 2001).

Geologic Unit	Geologic Member	Lithology Description	Hydrogeologic Unit	Basin Location	AoR Presence	Thickness (ft)
Morrison Formation	Jackpile Sandstone	alluvial and fluvial sandstone, mudstone	Morrison aquifer (Westwater Canyon)	SE	[redacted]	200–1,100
	Brushy Basin			Widespread	[redacted]	
	Westwater Canyon			Widespread	[redacted]	
	Recapture Shale			Widespread	[redacted]	
	Salt Wash			N/NW	[redacted]	
	Junction Creek Sandstone			SW Co/N Basin	[redacted]	
Cow Springs Sandstone/ Bluff Sandstone		eolian sandstone	Cow Springs aquifer	Widespread	[redacted]	90–300
Wanakah	Todilto - Upper Facies (Beclabito/Horse Mesa Members equivalent)	eolian fine-coarse-grained sandstone	Wanakah confining unit	NE AZ & NW NM	[redacted]	40
		claystone, siltstone and fine sandstone		NE AZ & NW NM	[redacted]	125–200
	Todilto- Lower Facies	lacustrine limestone, anhydrite, siltstone and sandstone		NM/CO Stateline	[redacted]	0–100
Entrada Sandstone		eolian sandstone	Entrada aquifer	Widespread	[redacted]	60–300
Wingate Sandstone		eolian sandstone	Wingate aquifer	NW basin margin	[redacted]	No Data

Wingate Sandstone

The Wingate Sandstone is found only along the farthest northwestern margin of the San Juan Basin [redacted]. This formation unconformably overlies the Chinle Formation and is unconformably overlain by the Entrada Sandstone. The Wingate is an eolian sandstone consisting of blocky, light to reddish-brown to orange, very fine- to medium-grained sandstone. Due to the Wingate Sandstone's limited extent, it is not considered an important regional aquifer (Craigg 2001).

Entrada Sandstone [redacted]

The Entrada Sandstone is ubiquitous across the San Juan Basin and adjacent Colorado Plateau. Throughout most of the San Juan Basin, the Entrada unconformably overlies the Chinle Formation and its equivalents except for the northwest portion where the Entrada unconformably overlies the Wingate Sandstone (Craigg 2001). The Entrada outcrops at the basin margins where it forms steep cliffs above the Chinle Formation.

The Entrada Sandstone consists of reddish orange, mottled red and white to light-brown silty sandstone and very fine- to medium-grained, well-sorted, quartz sandstone interbedded with thinner reddish-brown siltstone (Craigg 2001). The red color variation is the result of differing proportions of ferrous and ferric iron (Ridgley et al. 1978). Like the underlying Wingate Sandstone, the Entrada is characterized by high-angle, large-scale crossbedding associated with deposition in an eolian environment. The siltstone intervals within it indicate deposition in interdune and sabkha environments (Green and Pierson 1977).

The San Juan Basin Entrada Sandstone ranges from 60 ft to 330 ft thick with the maximum thickness encountered in the center of the basin (Green and Pierson 1977). Along the eastern basin margin, Entrada Sandstone thicknesses range from 100 ft to 300 ft; [redacted]

[9] https://wwwapps.emnrd nm.gov/OCD/OCDPermitting/Data/Wells.aspx. Accessed 05/2023.

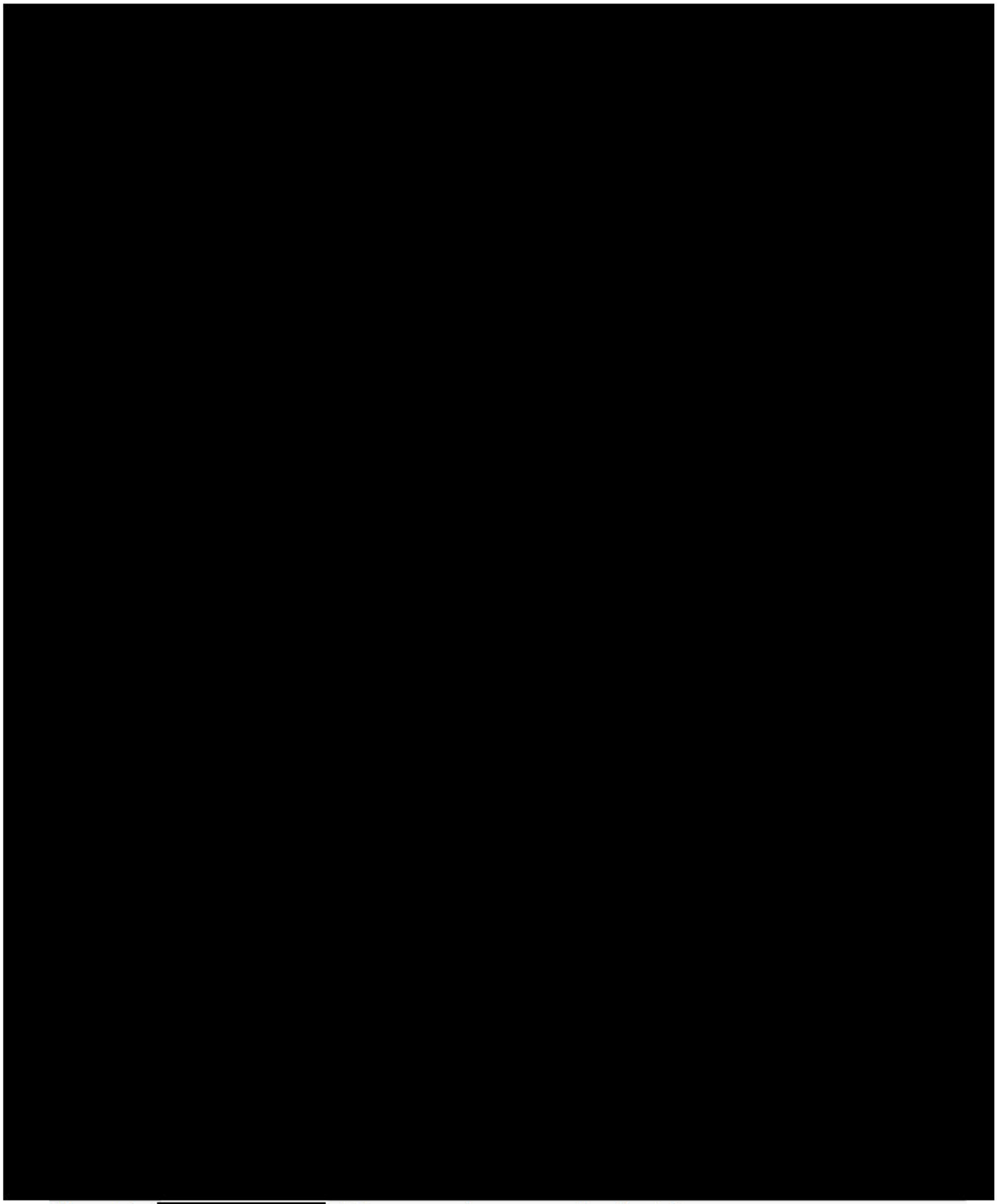

Figure 2.8— [redacted] TDS concentrations surrounding the AoR.

Wanakah Formation

The Wanakah Formation is named for exposures in the Wanakah mine located north of Durango, Colorado, and contains strata between the Entrada and younger Junction Creek Sandstones (Craigg 2001). The Wanakah Formation, in New Mexico, comprises three members in stratigraphic ascending order: the Todilto Limestone, Beclabito, and Horse Mesa Members (Condon and Huffman 1988). The Beclabito Member is also referred to as the Summerville Formation by authors (e.g., Condon and Peterson 1986, Craigg 2001, Kelley et al. 2014). For simplicity, the Todilto limestone Member is combined with the overlying Beclabito and Horse Mesa Members into a single Todilto Member. The Todilto Limestone is henceforth referred to as the lower facies of the Todilto Member, and the overlying Beclabito and Horse Mesa Members are termed the upper facies of the Todilto Member.

Todilto Member [redacted]

The lower facies of the Todilto Limestone Member contains two major lithofacies: a lower gray limestone unit and an upper gypsum and anhydrite unit that contains siltstones and sandstones (Green and Pierson 1977). The limestone facies has a maximum thickness of 40 ft and is present throughout the San Juan Basin, except in the extreme northwest area and the Gallup Sag. [redacted] The massive light gray to white gypsum and anhydrite facies reaches a maximum thickness of 100 ft and is only encountered beneath the eastern half of the basin (Green and Pierson 1977). The depositional environment for these facies is either a fresh to saline inland lake or a restricted marine basin (Condon and Huffman 1988).

The upper facies of the Todilto Member is encountered throughout northeastern Arizona and northwestern New Mexico. The upper facies of the Todilto was deposited either in a marginal lacustrine or marginal marine (sabkha) environment (Craigg 2001) and ranges in thickness from 125 ft to 200 ft. The upper facies of the Todilto Member has both a conformable and gradational contact with the underlying lower facies of the Todilto Member in the western and southwestern region of the basin and inter-tongues with the Cow Springs Sandstone (Condon and Huffman 1988). The upper facies of the Todilto Member consists of interbedded white to reddish-orange and reddish-brown claystone, massive or planar-bedded to cross bedded siltstone, and silty, very fine- to fine-grained sandstone (Green and Pierson 1977). The basal facies of the member grades into a coarse-grained fluvial conglomerate south and southeast of Grants, New Mexico.

Cow Springs Sandstone/Horse Mesa Member/Bluff Sandstone

The Cow Springs Sandstone overlays the upper Todilto Member of the Wanakah Formation (Beclabito Member/Summerville Formation/Horse Mesa equivalent) and underlies the Morrison Formation (Craigg 2001). Literature also refers to the Cow Springs Sandstone as the Bluff Sandstone or Wanakah Formation Horse Mesa Member. Stone et al. (1983) classifies the Cow Springs and Bluff Sandstone formations together because they are closely related stratigraphically and probably behave as a single hydraulic unit. The Bluff Sandstone is believed to be a tongue of the Cow Springs, but because of the Bluff's homogeneous mappable character and areal extent, it is considered a separate formation assigned to the San Rafael Group. The Cow Springs and Bluff Sandstone display an inter-tonguing relationship with both the underlying upper facies of the Todilto Member of the Wanakah Formation and the overlying Recapture Shale Member of the

Morrison Formation (Stone et al. 1983). The Bluff Sandstone is a medium-grained, mature arkose with an estimated thickness ranging from a few feet up to 300 ft.

The Cow Springs Sandstone outcrops in the southwestern region of the basin and inter-tongues with the upper Todilto Member of the Wanakah Formation throughout much of this portion of the basin. To the east and northeast, the Cow Springs Sandstone thins and inter-tongues with the Horse Mesa Member of the Wanakah Formation, forming a broad, vertical intergradational zone with the Wanakah Formation (Condon and Huffman 1988). The Cow Springs Sandstone contains eolian and interdune environments consisting of cross-bedded to flat-bedded, greenish-gray, light yellowish-gray, and light-brown, well-sorted, fine- to medium-grained quartzose and arkosic sandstone (Green and Pierson 1977). It has a maximum thickness of approximately 300 ft but decreases to approximately 200 ft northward, just south of Crystal, New Mexico. Cow Springs thickness also decreases to approximately 90 ft eastward near Thoreau, NM (Craigg 2001). Cooley and Weist (1979) report that the Cow Springs Sandstone member yields some water to wells where it is hydraulically connected with the Morrison Formation in the southwestern region of the basin. No wells are known to produce water from the Cow Springs exclusively, but it is productive in combination with overlying and underlying zones.

Condon and Huffman (1988) note that the lower facies of the Junction Creek Sandstone is correlative to the upper portion of the Todilto Member (Horse Mesa Member equivalent) and consists of cliff-forming, white to orange and red, planar-bedded and cross bedded, very fine- to coarse-grained quartzose sandstone (Condon and Huffman 1988).

Morrison Formation

The Morrison Formation is ubiquitous throughout the San Juan Basin, outcrops along the basin margins, and contains the most prolific regional aquifers in the basin (Craigg 2001). It is not classified as a USDW within the AoR. The Morrison Formation conformably overlies the Wanakah Formation and Cow Springs Sandstone throughout most of the San Juan Basin, but conformably overlies and inter-tongues with the Junction Creek Sandstone in the northern region of the basin. (Dam 1995; Craigg 2001). A disconformity separates the Morrison Formation from the overlying Dakota Sandstone, except in the northern region where the Burro Canyon conformably rests on the Morrison (Green and Pierson 1977). The Morrison Formation consists of yellowish-tan to pink, fine- to coarse-grained, locally conglomeratic sandstone interbedded with sandy siltstone and green to reddish-brown shale and claystone with occasional, minor beds of limestone (Craigg 2001). In the San Juan Basin, Morrison Formation thickness ranges from 200 ft near Grants, New Mexico to approximately 1,100 ft in the northwestern region of the basin (Dam et al. 1990).

The Morrison Formation is composed of six members which are in ascending order: the Junction Creek Sandstone, Salt Wash Member, Recapture Member, Westwater Canyon Member, Brushy Basin Member, and Jackpile Sandstone Member (Grean and Pierson 1977). **Table 2.5** summarizes the lithology, location, and thickness of each member.

Table 2.5—Summary of the lithology and thickness of Morrison Formation members (data from Craigg 2001).

Geologic Unit	Geologic Member	Lithology Description	Hydrologic Unit	Basin Location	AoR Presence	Thickness (ft)
Morrison Fm.	Jackpile Sandstone	medium-coarse sandstone w/ mudstone	Morrison aquifer (Westwater Canyon)	SE	[redacted]	100–300
	Brushy Basin	claystone/mudstone w/ fine-medium sandstone		Widespread	[redacted]	150–250
	Westwater Canyon	fine-coarse sandstone w/shale/claystone		Widespread	[redacted]	100–300
	Recapture Shale	fluvial sandstone w/claystone/siltstone		Widespread	[redacted]	75–300
	Salt Wash	fine-medium fluvial sandstone/claystone		N/NW	[redacted]	<200
	Junction Creek Sandstone	fine-coarse sandstone		SW CO/N Basin	[redacted]	200–500

2.1.3.3 Cretaceous Formations

Cretaceous strata reaching approximately 6,500 ft of thickness overly the Jurassic and Triassic sediments in the San Juan Basin. Cretaceous formations were deposited in continental, marginal marine, and marine environments resulting from transgressing and regressing shorelines. The Dakota and Gallup sandstones are the most prominent regional aquifers. **Table 2.6** summarizes the lithology, location, and thickness of Cretaceous strata within the San Juan Basin.

Table 2.6—Cretaceous stratigraphy of the San Juan Basin. Pictured cliffs sandstone and Crevasse Canyon data from Stone et al. 1983. All other data from Craigg 2001.

Geologic Unit	AoR Unit/Member	Lithology Description	Hydrogeologic Unit	Basin Location	AoR Presence	Thickness (ft)
Fruitland/ Kirtland Shale	Fruitland/ Kirtland Shale	fluvial sandstone, mudstone; coal measures	Fruitland/ Kirtland aquifer	N/NE	[redacted]	0–2,000
Pictured Cliffs Sandstone	Pictured Cliffs Sandstone	marine sandstone	Pictured Cliffs aquifer	N Half	[redacted]	0–400
Lewis Shale	Lewis Shale	marine claystone, siltstone	Lewis confining unit	WS	[redacted]	0–2,400
Cliff House	Cliff House/Ventana Tongue	marine sandstone	Cliff House aquifer	WS/ N-NE	[redacted]	0–300
Menefee	Menefee	coal measures	Menefee confining unit	WS	[redacted]	0–3,000
Point Lookout Sandstone	Point Lookout Sandstone	marine sandstone	Point Lookout aquifer	WS	[redacted]	40–415
Crevasse Canyon	NP	coal measures, marine sandstone	Fruitland/Kirtland aquifer	SSW only in NM/AZ	[redacted]	420–700
Gallup Sandstone	NP	marine sandstone	Gallup aquifer	SW only in NM/AZ	[redacted]	0–300
Mancos Shale	Mancos Shale	shale, claystone	Lower Mancos confining unit	WS	[redacted]	2,300
Dakota Sandstone	Dakota Sandstone	marine sandstone, coal measures	Dakota aquifer	WS	[redacted]	200–500
Burro Canyon	Burro Canyon	eolian sandstone and conglomerate	Burro Canyon aquifer	SW CO/NW NM	[redacted]	30–200

NP=not present, WS=widespread

Burro Canyon Formation

The Burro Canyon Formation is limited to southwestern Colorado, but formation lenses are present in northwestern New Mexico, northeastern Arizona, and southeastern Utah. The Burro Canyon conformably overlies the Brushy Basin Member of the Morrison Formation and likely records continuous deposition from Late Jurassic through Early Cretaceous time (Craigg 2001). Lenses of the Burro Canyon Formation inter-tongue with mudstone of the Bushy Basin Member in the Four Corners region. A disconformity separates the Burro Canyon from the overlying Dakota Sandstone.

Burro Canyon Formation sediments were deposited in various fluvial environments including high-energy braided streams (upper Burro Canyon), low-energy meandering streams (lower Burro Canyon), and floodplains (lower Burro Canyon). The stratigraphy of this interval includes lenticular white, light gray, and pale brown to tan, fine- to coarse-grained sandstone, and conglomeratic channel sandstone. Burro Canyon thicknesses range from 30 ft to 200 ft and average approximately 150 ft in the northwestern region of the San Juan Basin. The formation pinches out to the northeast and to the south, toward the San Juan River (Craigg 2001).

Dakota Sandstone

The Dakota Sandstone is late Cretaceous in age in the San Juan Basin and was deposited on a regional erosional surface, recording a transition from continental alluvial plain (lower Dakota Sandstone) to marine shore zone (upper Dakota Sandstone). It disconformably overlies the Bushy Basin Member of the Morrison Formation across much of the basin except where it also disconformably overlies other members of the Morrison Formation, including the Westwater Canyon (southwest San Juan Basin), Jackpile Sandstone (southeast San Juan Basin), and Burro Canyon Formation (north San Juan Basin) (Craigg 2001). The Dakota Sandstone is conformably overlain by the Mancos Shale except where the two formations inter-tongue near their contact (Owen 1973).

There are three principal lithologic units in the Dakota Sandstone. They are in ascending order:

1) A sequence of buff to brown, cross bedded, poorly sorted, coarse-grained conglomeratic sandstone and moderately sorted, medium-grained sandstone (lower);
2) Dark-gray carbonaceous shale with brown siltstone and lenticular sandstone beds (middle); and
3) Yellowish-tan, fine-grained sandstone interbedded with gray shale (upper).

The total Dakota formation thickness ranges from 30 ft to 500 ft, though 200 ft to 300 ft is commonly encountered (Dam 1995). Subsurface data indicates that Dakota thicknesses increase from the western, northwestern, and northern margins of the basin toward the eastern, southeastern and southern margins of the basin (Dam 1995; Craigg 2001). [redacted]

Mancos Shale

The Mancos Shale is an Upper Cretaceous aquitard throughout the San Juan Basin. Shallow marine deposits consisting of gray to black shale and claystone with discontinuous yellowish-gray, calcareous siltstone and sandstone are characteristic of the Mancos. The Mancos contains thin bentonite beds, mostly in the lower formation, as well as calcareous concretions, thin limestone beds, and offshore sandstone bar deposits, are mostly present in the lower formation. The Mancos Shale conformably overlies and intertongues with the transgressive Dakota Sandstone and is conformably overlain by and inter-tongued with the regressive marine Point Lookout Sandstone which is a local transgressive marine sandstone (Craigg 2001).

The Mancos Shale in the north San Juan Basin that reaches a maximum thickness of approximately 2,300 ft. Regionally, this shale is a confining unit, but locally, sandstone bodies within it yield small quantities of water to wells. [redacted]

Gallup Sandstone

Where it is present, Gallup Sandstone lithologies include conglomerate, sandstone, shale, carbonaceous shale, and coal (Craigg 2001). Sandstone bodies are characteristically pink to light gray, fine- to medium-grained, and are moderately to well sorted. Total interval thickness decreases from 300 ft near the outcrop along the southwestern basin to zero ft in the northwest

region of the San Juan Basin. The Gallup thins southeastward from the Nutria monocline to the Arroyo Chico-Puerco area (Craigg 2001).

Point Lookout Sandstone

The Point Lookout Sandstone is the oldest formation of the Mesa Verde Group and the most extensive regressive marine beach sandstone within the San Juan Basin (Molenaar 1977). It outcrops outside the Central Basin area of the San Juan Basin typically forming cliffs, cap mesas and buttes, or erosion-resistant dip slopes and hogbacks. The Point Lookout Formation conformably overlies the Mancos Shale across the entire San Juan Basin. This contact is characterized by interbedded thin sandstone, siltstone, and shale that record a distinct offshore marine transition. It is conformably or disconformably overlain by the Menefee Formation with some inter-tonguing at the contact. Thickness of the Point Lookout Sandstone ranges from approximately 100 ft in the southern region of the San Juan Basin to 350 ft near the Colorado-New Mexico state line.

Menefee Formation

The Menefee is the middle formation of the Mesa Verde Group and outcrops beyond the margins of the Central Basin (**Figure 2.9**). It is characterized by an erosion-resistant sandstone that frequently caps isolated buttes and hillocks as well as shale sections that form slopes and broad valleys. Depending on the location, the Menefee either conformably or disconformably overlies the Point Lookout Sandstone and conformably or disconformably is overlain by the Cliff House Sandstone. It is usually mapped as an undivided formation, but in the southern region of the basin it is subdivided into three members which are in stratigraphic ascending order:

1) the Clearly Coal Member, which contains carbonaceous shale and coal beds;
2) the Allison Member, which contains thick stacked channel sands; and
3) the upper Coal-Bearing Member like the Clearly Coal Member which contains carbonaceous shale and coal beds.

The sandstone is lenticular, light brown to gray, thick to very thickly bedded, and fine- to medium-grained with a clay matrix and various cement types. The siltstone is gray, thin to thickly bedded and tabular. The Menefee Formation thickness increases from north to south. pinching out in the northeastern region of the basin and thickening to a maximum of approximately 3,000 ft to the south (Cooley and Weist 1979). [redacted]

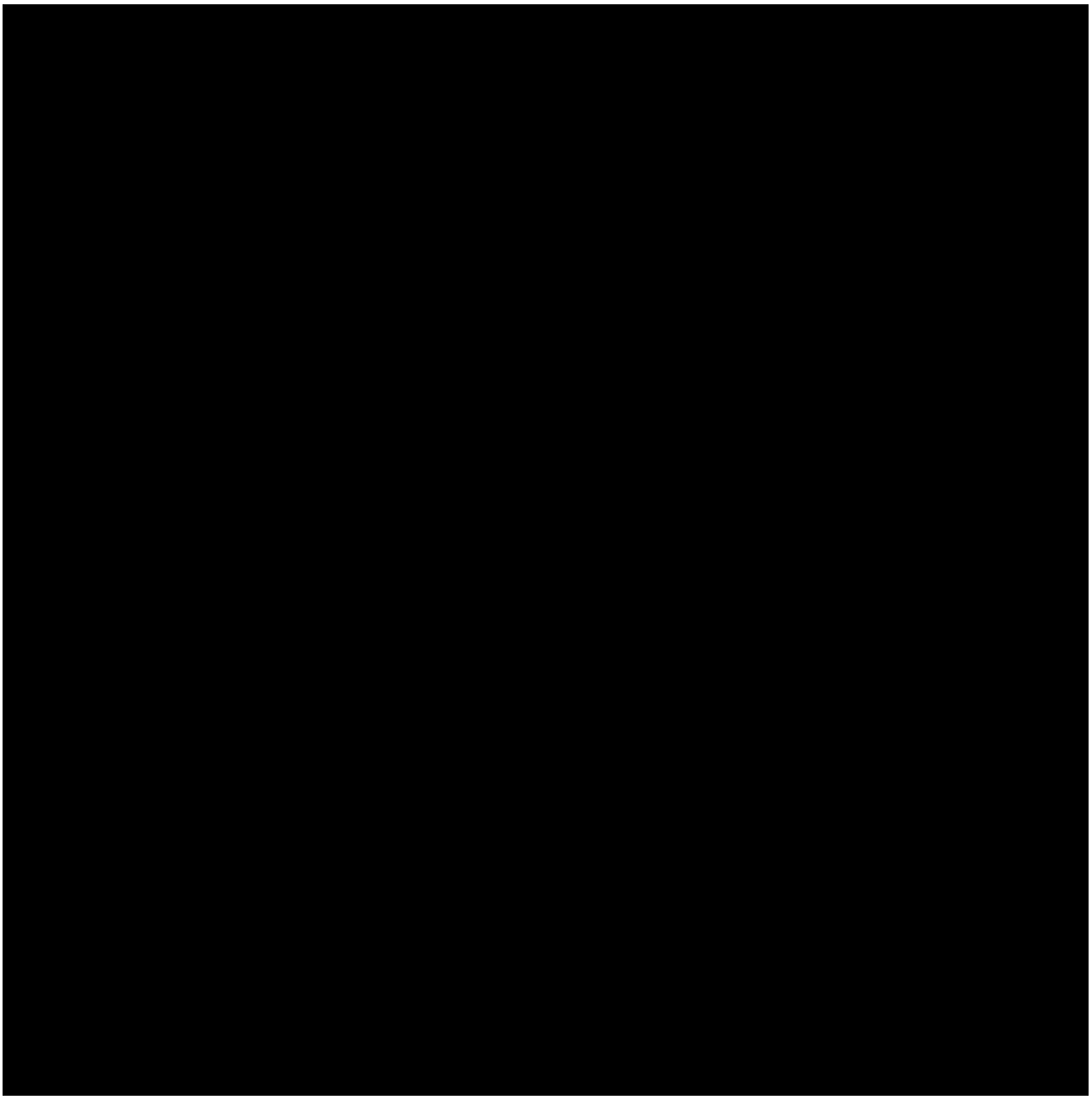

Figure 2.9—A simplified geologic map of the San Juan Basin (after Pecha et al. 2018).

Cliff House Sandstone

The Cliff House Sandstone is the uppermost formation in the Mesaverde Group (Craigg 2001). It is present in the northeastern region of the San Juan Basin and outcrops along the margins of the Central Basin where it caps mesas, and forms erosion-resistant dip slopes and hogbacks (Figure 2.9). The Cliff House is conformably overlain by and inter-tongues with the Lewis Shale. The Menefee Formation is both conformably and unconformably overlain by the Cliff House and Lewis Shale in some regions where the Cliff House tongues pinch out.

The Cliff House Sandstone consists of tan, light-brown, or yellowish brown, thick to very thick-bedded and locally cross-bedded, very fine- to fine-grained sandstone with calcite or silica cement

and clay. Interbeds of gray shale and silty shale are common. The Cliff House attains a maximum thickness of 400 ft but is generally less than 200 ft across much of the eastern region of the San Juan Basin (Cooley and Weist 1979). Thickness variations are due to local inter-tonguing with the overlying Lewis Shale and underlying Menefee Formation.

Lewis Shale

The Lewis Shale is present in the northeastern region of the San Juan Central Basin and outcrops along its inside margin [redacted] (Figure 2.9). Locally, erosion-resistant siltstone and sandstone cap isolated buttes while less resistant shale forms slopes and broad valleys or flats. The Lewis Shale was deposited in an offshore marine environment. It conformably overlies and inter-tongues with the Cliff House Sandstone, and conformably overlies both the Menefee Formation and Pictured Cliffs Sandstone. Strata in this formation represent the final major transgression of the Cretaceous Seaway in the San Juan Basin and are the youngest marine shale in the basin (Craigg 2001).

The Lewis Shale consists of dark gray claystone and siltstone with thin platy beds of fine-grained sandstone and concretionary and shaley limestone. In the eastern region of the basin, the Lewis Shale contains zones of shaley sandstone (Cooley and Weist 1979). The shale progressively thickens eastward from its pinch-out near the "big bend" of the Chaco River to approximately 2,000 ft to 2,700 ft of total thickness in Colorado (Cooley and Wiest 1979).

Pictured Cliffs Sandstone

The Pictured Cliffs Sandstone is present in the northeastern region of the San Juan Basin (Cooley and Wiest 1979) and conformably overlies the Lewis Shale. It outcrops along the inside basin margin to the northeast and northwest where the sandstone caps mesas and buttes or forms erosion-resistant dip slopes (Figure 2.9). As the name implies, the Pictured Cliffs Sandstone is a cliff former, except along the southeastern outcrop belt, where it forms very thin, low, non-resistant slopes (Craigg 2001). Molenaar (1977) describes the Pictured Cliffs Sandstone as a regressive marine beach deposit.

The Pictured Cliffs Sandstone consists of an upward-coarsening sequence of light gray to yellowish gray, thick- to very thick-bedded, very fine- to medium-grained, locally cross-bedded and bioturbated sandstone with frequent thin beds of dark marine shale in the lower section of the formation. According to Molenaar (1977), the unit's thickness varies from 0 ft to 400 ft, though the average is approximately 200 ft.

Fruitland Formation

The Fruitland Formation is present in the northeastern region of the San Juan Basin (Cooley and Wiest 1979) and outcrops along the inside margins of the Central Basin (Figure 2.9). It forms erosion-resistant sandstone that commonly caps isolated buttes and hillocks. Less resistant shale forms slopes, broad valleys, or flats. The Fruitland conformably overlies the Pictured Cliffs Sandstone local intertonguing at the contact, and conformably underlies the Kirtland Shale (Craigg 2001).

The Fruitland Formation consists of lenticular beds of mudstone, siltstone, silty sandstone, sandstone, and coal. Total thicknesses range from less than 200 ft in the eastern basin to 250 ft and 400 ft in Colorado, and then to a maximum of 700 ft in the southwestern region of the basin.

Even though the Fruitland Formation yields small quantities of water to wells, it does form a confining layer above the Pictured Cliffs Sandstone (Cooley and Weist 1979). Information noted in well histories posted by the NMOCD indicate that the combined Fruitland Formation and Kirtland Shale are a significant source of coalbed methane production with associated water as a byproduct. The produced saline water is injected into [redacted]. Geochemical water sampling data supported by petrophysical analysis of wireline logs collected near the AoR, indicate that the estimated TDS concentrations for the [redacted] refer to 2.8.1 Fluid Chemistry for details).

Kirtland Shale

As with the Fruitland Formation, the Kirtland Shale is present in the northeastern region of the basin (Cooley and Wiest 1979) and outcrops along the inside margins of the Central Basin Figure 2.9). The Kirtland Formation generally forms steep slopes below mesa or buttes that are capped by the overlying, resistant Ojo Alamo Sandstone (Craigg 2001). The Kirtland Shale conformably overlies the Pictured Cliffs Sandstone and is unconformably overlain by the Tertiary Ojo Alamo Sandstone.

The Kirtland Shale is subdivided into three members: the Lower Shale Member, the Farmington Sandstone Member, and the Upper Shale Member. All of the members are generally composed of mudstone, siltstone, silty sandstone, and sandstone with minor beds of coal (Craigg 2001).

Kirtland Shale thicknesses range from less than 200 ft in the eastern region of the basin, to 700 ft south of Farmington and then to as much as 1,200 ft in Colorado. Sandstone lenses within the Farmington Sandstone Member attain a combined thickness of as much as 350 ft (Cooley and Weist 1979).

The Kirtland Shale yields only small quantities of water to wells in a few places outside of the AoR. South of the city of Farmington, New Mexico, the middle sandstone member contains a limited quantity of water of poor chemical quality (Cooley and Weist 1979). As noted in the Fruitland Formation section, the combined Fruitland Formation and Kirtland Shale are a significant source of coalbed methane production and its associated water. The produced saline water is injected into [redacted]. Based on geochemical water sampling data, supported by petrophysical analysis of wireline logs collected near the AoR, TDS concentrations for [redacted]

2.1.3.4 Tertiary Formations

The Tertiary San Juan Basin is one of several intra-foreland basins that developed within the larger Cordilleran Foreland Basin concurrently with adjacent uplifts. Tertiary strata represent the Cordilleran Foreland Basin fill and increase in thickness northeastward towards the Archuleta anticlinorium (Hart 2001). Cather (2004), states that lower Paleocene strata were deposited during a second phase of the Laramide Orogeny, which was characterized by rapid subsidence and

sediment accumulation, particularly in the northeastern region of the San Juan Basin. The final phase of subsidence was initiated in the Early Eocene Period and was after a period of non-deposition and erosion. The entire Tertiary section consists of nonmarine clastic deposits.

Early Tertiary sedimentary strata in the Central Basin include the Ojo Alamo Sandstone, upper Animas Formation strata, the Nacimiento Formation, and the San Jose Formation. In the western region of the San Juan Basin, the Chuska Sandstone caps the Chuska Mountains. Within the Central Basin, Tertiary strata disconformably overlie Upper Cretaceous strata. **Table 2.7** briefly summarizes the lithology, location, and thickness of Tertiary strata in the San Juan Basin.

Table 2.7—Tertiary stratigraphy of the San Juan Basin (all data from Craigg 2001 unless noted).

Geologic Unit	Lithology Description	Hydrogeologic Unit	Basin Location	AoR Presence	Thickness (ft)
Valley Fill & Terrace Deposits	unconsolidated fluvial, colluvial, eolian deposits	Alluvial aquifer	Widespread	[redacted]	<100[1]
Chuska Sandstone	eolian sandstone, lacustrine mudstone	Chuska aquifer	Widespread	[redacted]	500–1,200
San Jose	alluvial sandstone, mudstone	San Jose aquifer	NM & CO	[redacted]	200–2,700
Nacimiento	lacustrine and fluvial interbedded shale and sandstone	Nacimiento aquifer	N/NE	[redacted]	500–1,300
Animas	alluvial and fluvial sandstone and mudstone	Animas aquifer	N only	[redacted]	230–2,700
Ojo Alamo Sandstone	alluvial and fluvial sandstone and mudstone	Ojo Alamo aquifer	NE; Mostly NM; pinch-out bet. Farmington and CO state line	[redacted]	20–400

[1] Data from Stone et al. (1983).

Ojo Alamo Sandstone (Underground Source of Drinking Water)

The Paleocene Ojo Alamo Sandstone is present in the east-central region of the San Juan Basin and outcrops inside the Central Basin as cliffs, dip slopes, low mesas caps, and rounded hills (Figure 2.9). The formation is primarily found in New Mexico and pinches out in the northwest between Farmington, New Mexico and the Colorado state line, west of La Plata River. The Ojo Alamo Sandstone disconformably overlies the Kirtland Shale, except where the Kirtland and Lewis shales were removed by erosion. Deposition of the base of the Ojo Alamo Sandstone is on an extensive channeled, wavy erosional surface that occasionally cuts more than 50 ft or more into the underlying shale/sandstone of the Fruitland Formation/Kirtland Shale (Craigg 2001).

The Ojo Alamo Sandstone is composed of overlapping stream channel deposits with occasional floodplain deposits suggesting an alluvial plain depositional model (Craigg 2001). Strata consist of overlapping sheetlike sequences of sandstone and conglomeratic sandstone locally containing interbedded shale lenses. The Ojo Alamo is an arkosic, light brown to rusty brown or buff and tan

sandstone containing abundant silicified wood (Craigg 2001). The sandstone is medium- to coarse-grained and commonly conglomeratic, containing pebbles that decrease in size and quantity from west to east across the Central Basin.

Baltz (1967) reported interval thicknesses between 70 ft and 200 ft, while Stone et al. (1983) reported thicknesses ranging from 70 ft to 300 ft, with 50 ft to 150 ft being the most common range of values.

Nacimiento Formation (Underground Source of Drinking Water)

The Paleocene Nacimiento Formation is present in the northeast region of San Juan Basin and conformably overlies the Ojo Alamo Sandstone [redacted] This formation outcrops inside the southern and western margins of the Central Basin (Figure 2.9). It also outcrops in a narrow band along the western face of the Nacimiento Uplift. The Nacimiento Uplift is a non-resistant unit that erodes to low, rounded hills or forms a badlands topography. It grades laterally into the upper strata of the Animas Formation along a zone connecting the La Plata River valley near the New Mexico-Colorado state line (Craigg 2001).

The Nacimiento Formation strata were mostly deposited in lake beds and less predominately in stream channels. It consists of interbedded black and gray shale with discontinuous white, medium- to very coarse-grained arkosic sandstone (Craigg 2001). Baltz (1967) noted that sandstone percentages increase northward. Stone et al. (1983) suggested that the formation may contain more sandstone than reported due to misinterpretation of poorly consolidated slope-forming sandstones as shale.

Molenaar (1977) presents the thickness of the Nacimiento Formation as ranging from 500 ft to 1,300 ft. Baltz (1967) noted that it generally thickens from the Central Basin margins toward the center, but the thickness and extent of sandstone lenses decrease due to their depositional in localized stream channels.

San Jose Formation (Underground Source of Drinking Water)

The Eocene San Jose Formation is present in New Mexico and Colorado [redacted]
It is the youngest sedimentary formation in the San Juan Basin, except for an area near the western edge where the Chuska Sandstone is present. The basal contact of the San Jose Formation varies depending on location within the San Jose Basin. Along the basin margins, the contact is a disconformity, along the Nacimiento Uplift the contact is an angular unconformity, and in the Central Basin the contact is conformable (Baltz 1967).

The San Jose Formation strata were deposited in a variety of fluvial environments and consist of an interbedded sequence of sandstone, siltstone, and variegated shale. The sandstone is buff to yellow and rust colored, cross bedded, very fine- to coarse-grained arkose that is locally conglomeratic and contains abundant silicified wood (Baltz 1967). The thickness of the San Jose Formation generally increases from west to east (Craigg 2001) and attains a maximum thickness of 2,400 ft in the east-central portion of the Central Basin. Stone et al. (1983) report a range of thicknesses from approximately 200 ft in the west and south, to nearly 2,700 ft in the center of the basin.

Quaternary Alluvium (Underground Source of Drinking Water)

Quaternary alluvium occurs along most of the stream channels in the San Juan Basin [redacted] The Alluvium consists of a heterogeneous mixture of sand, silt, and clay, as well as gravel and boulders in the larger channels. All drainages in the basin contain alluvial valley fill, and the valleys of the San Juan River contain extensive terrace deposits (Stone et al. 1983).

Terrace deposits typically do not exceed 30 ft in thickness and consist of boulder-sized gravel resting on benches cut into Tertiary bedrock units. These very well-rounded boulders are various igneous and metamorphic rocks, including cross-bedded quartzite. The terrace deposits were sourced from late Pleistocene glacial moraines in the Colorado mountains and are in disconformable contact with all of the underlying units (Stone et al. 1983). Within the valleys of the San Juan River and its tributaries, alluvium thickness generally does not exceed 100 ft, except in the Chaco Canyon area where thicknesses are at most 125 ft (Stone et al. 1983).

Most water wells completed within the alluvium yield sufficient quantities of water for livestock and domestic use. The alluvium is often too thin and limited in extent to support continuous, large withdrawals except along the San Juan River (Cooley and Weist 1979).

Throughout most of the basin, alluvium containing water flows toward the nearby streams and receives recharge from runoff from nearby hillsides, percolation from stream channels, and, occasionally, from underlying bedrock aquifers.

2.1.4 General Hydrogeology

2.1.4.1 Precipitation

The climate of the San Juan Basin is classified as arid to semiarid with varied precipitation across the region. Annual precipitation is most plentiful (20 in. to 30 in.) in the mountain regions but the central region of the San Juan Basin receives less than ten inches of precipitation per year. The San Juan River west of Farmington, New Mexico and the north-flowing reach of the Chaco River receive less than eight inches of precipitation per year (Stone et al. 1983). Most precipitation occurs during the summer months due to local, intense thunderstorms. The summer moisture source originates from the Gulf of Mexico while the source of winter precipitation is the Pacific Ocean. The arid character results from mountain barriers and long distances lying between both sources and northwest New Mexico (Stone et al. 1983).

2.1.4.2 Surface Water Resources

Colorado River Drainage Basin

Both the San Juan and Animas rivers flow into New Mexico from Colorado. [redacted] is joined by the [redacted] and flows westward along an arcuate course, leaving the state near Four Corners (Stone et al. 1983). San Juan River flow ranges from 1,975 cubic feet per second (ft^3/sec) (Farmington, New Mexico) to 2,175 ft^3/sec (Shiprock, New Mexico). San Juan River tributaries that contribute large quantities of water during stormflow periods include Canon Largo River, Gallegos Canyon River, Chaco River, and the La Plata River.

Table 2.8 (Stone et al. 1983) is a summary of discharge and water quality at selected surface water stations for the Colorado River and Rio Grande drainage basins within the San Juan Basin.

Table 2.8—Summary of discharge and water quality at selected surface water stations for the Colorado River and Rio Grande drainage basins (from Stone et al. 1983).

		Water Discharge			Water Quality		
Station Number	Station Name	Period of Record	Drainage Area (mi^2)	Mean (ft^3/s)	Period of Record	Specific Cond. Mean (µmhos)	Sediment Conc. Mean (mg/L)
Colorado River Drainage Basin							
9355500	San Juan River near Archuleta	1955-77	3,260	1,304	1955-78	311	4,831
9364500	Animas River at Farmington	1912-77	1,360	909	1940-78	606	3,003
936500	San Juan River at Farmington	1912-77	7,240	2,370	1962-78	548	-
9367500	La Plata River near Farmington	1938-77	583	24	-	2,262	3,888
9367561	Shumway Arroyo near Waterflow	1974-77	73.8	-	1974-78	6,481	14,653
9367680	Chaco Wash at Chaco Canyon National Monument	1976-77	578	-	1976-78	470	30,033
9367710	De-Na-Zin Wash near Bisti Trading Post	1975-77	184	-	1975-78	709	54,162
9367930	Hunter Wash at Bisti Trading Post	1975-77	45.6	-	1975-78	1,074	46,250
9367930	Chaco River near Waterflow	1975-77	4,350	-	1976-78	1,878	48,674
9368000	San Juan River at Shiprock	1927-77	12,900	2,175	1941-45, 1951-78	748	12,691
9395500	Puerco River at Gallup	-	558	-	1975-77	898	-
Rio Grande Drainage Basin							
8334000	Rio Puerco above Arroyo Chico, near Guadalupe	1951-77	420	13.0	-	-	-
8340500	Arroyo Chico near Guadalupe	1943-77	1,390	21.8	-	-	-
8343500	Arroto Chico near Guadalupe	1936-77	2,300	6.49	-	1,315	-
8349800	Rio San Jose near Grants	1976-77	107	-	-	1,657	-
8351500	Rio San Jose at Correo	1943-77	3,660	11.7	-	-	-
8352500	Rio Puerco at Rio Puerco	1934-77	6,590	57.0	-	-	-

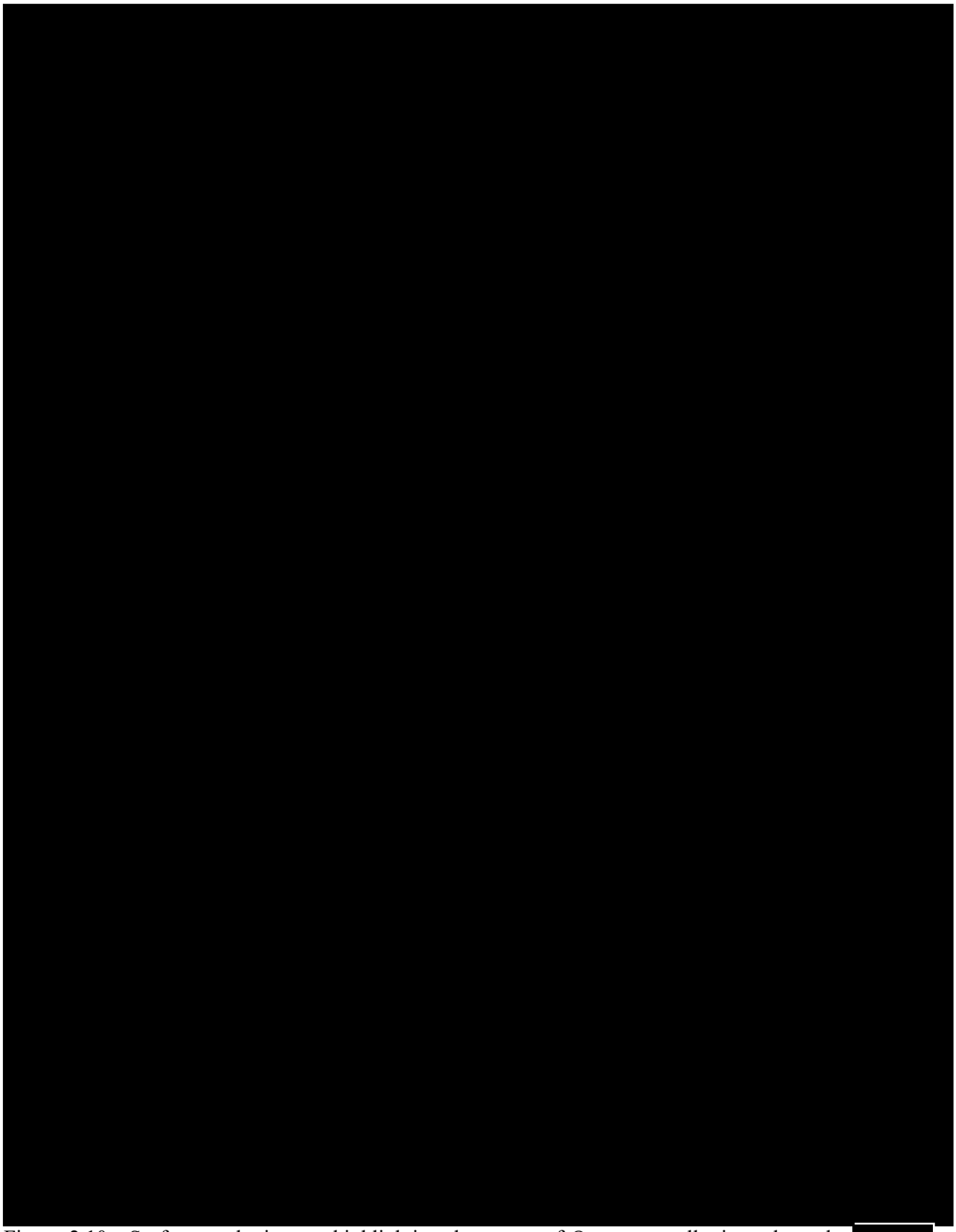

Figure 2.10—Surface geologic map highlighting the extent of Quaternary alluvium along the [redacted] rivers (after Scholle 2003).

La Plata River

The La Plata River flows at a rate of less than 5 ft^3/sec [redacted] New Mexico. Most of the flow in the downstream La Plata River near the New Mexico-Colorado state line is diverted for irrigation.

2.1.4.3 Regional Hydrogeology

Table 2.9 is a summary of the stratigraphy, a description of aquifers, and a description of confining units within the AoR. Preliminary screening of USDWs was accomplished by reviewing multiple literature sources including:

- Hydrologic Assessment Map [redacted]—thickness, TDS, discharge, and specific capacity data
- [redacted]—thickness, transmissivity, and TDS data
- [redacted]—thickness data
- [redacted]—thickness, porosity, and permeability data
- [redacted]—transmissivity, discharge, and specific capacity data
- [redacted]—specific capacity data for the [redacted]
- [redacted]—discharge data for Quaternary valley fill and terrace deposits

Of the units listed as aquifers within the basin, [redacted] These USDW aquifers will be described in greater detail in Section 2.7 (Hydrologic and Hydrogeologic Information [40 CFR 146.82(a)(3)(vi), 146.82(a)(5)]).

2.1.4.4 Regional Aquifers and Confining Units/Aquitards

Apart from pre-Jurassic units, the following formations are listed in Table 2.9 in descending age and are identified as either major or marginal aquifers or as confining units within the basin.

Table 2.9—Regional aquifers and aquitards.

Major Aquifers		Marginal Aquifers		Confining Units/Aquitards	
Hydrogeologic Unit	**Age**	**Hydrogeologic Unit**	**Age**	**Hydrogeologic Unit**	**Age**
Valley-Fill and Terrace Deposits	Quaternary	Chuska Sandstone	Eocene/ Oligocene	Lewis Shale	Late Cretaceous
San Jose Formation	Eocene	Nacimiento/ Animas Formations	Paleocene	Menefee Formation	Late Cretaceous
Ojo Alamo Sandstone	Paleocene	Fruitland Formation- Kirtland Shale	Late Cretaceous	Crevasse Canyon Formation	Late Cretaceous
Pictured Cliffs Sandstone	Late Cretaceous	Point Lookout Sandstone	Late Cretaceous	Mancos Shale	Late Cretaceous
Cliff House Sandstone	Late Cretaceous	Junction Creek Sandstone	Upper Jurassic	Wanakah Formation (Todilto, Beclabito, Horse Mesa Members)	Middle Jurassic
Gallup Sandstone	Late Cretaceous	Cow Springs-Bluff Sandstone	Late Jurassic	Dolores Formation	Upper Triassic
Dakota Sandstone	Late Cretaceous	Entrada Sandstone	Late Jurassic	Chinle Formation (Salitral Tongue, Owl Rock Members)	Upper Triassic
Morrison Formation	Late Jurassic	Wingate Sandstone	Lower Jurassic		

Table 2.10 provides a summary of hydrologic characteristics, including transmissivity, storage coefficient, hydraulic conductivity, discharge, and specific capacity, of the hydrogeologic units within the San Juan Basin.

Table 2.10—Summary of hydrologic characteristics of hydrogeologic units in the San Juan Basin.

Hydrogeologic Unit	Porosity (v/v)[4]	Transmissivity (ft^2/D)[2]	Storage Coefficient[5]	Hydraulic Conductivity (ft/D)[5]	Discharge (gpm)[1]	Sp. Capacity (gpm/ft)[1]
Alluvial aquifer	No Data	<1,000–40,000			10–20 [7]	No Data
Nacimiento aquifer	0.18	<100			44	0.24–2.3 [6]
Ojo Alamo aquifer	0.18	50–250			40–45	0.02–2.04
Fruitland/Kirtland aquifer	0.1-0.3	0.6–130 [5]	0.00001		1-12	0.001–0.42 [5]
Pictured Cliffs aquifer	0.15	0.00—3.0 [5]		0.007	1-40 [6]	N/A
Lewis confining unit	0.05	N/A			N/A	N/A
Cliff House aquifer	0.12	2.1 [5]		0.0015	1-40 [5]	0.01–0.15 [5]
Menefee confining unit	0.12	<50		0.017	N/A	N/A
Point Lookout aquifer	0.12	0.4–236 [5]	0.000041	0.0058	1–360 [5]	0.02–1.67 [5]
Lower Mancos confining unit	0.12	N/A			N/A	N/A
Dakota aquifer	0.1	100	0.00004–0.000057	0.03	1.25–75	0.03–3.67
Morrison aquifer	0.15	<500	0.00002–0.0002	0.025-0.39	18	0.01
Cow Springs aquifer	N/A	<50 to 300			N/A	N/A
Wanakah confining unit	0.08	N/A			N/A	N/A
Entrada aquifer	0.18	<50 to >100		0.5-5	105 [5]	0.33 [5]
Chinle confining unit	0.12	N/A			N/A	N/A

[1] Data from HA720 series map plates unless otherwise noted.
[2] Transmissivity values from Stone et al. 1983 unless otherwise noted.
[3] Data from Craigg 2001.
[4] Data from Haerer & McPherson 2009.
[5] Data from Levings et al. 1996.
[6] Data from Kernodle 1996.
[7] Data from Brown and Stone 1979.

2.1.4.5 Hydrologic Properties

Transmissivity of San Juan Basin aquifers range from a maximum of 450,000 square feet per day (ft^2/D) near Bluewater, New Mexico where there are cavernous limestones associated with the Glorieta Sandstone-San Andreas Limestone aquifer, to less than 1 ft^2/D for the finer-grained, well-cemented sandstones, such as the Pictured Cliffs Sandstone within the central region of the basin

(Stone et al. 1983). Better yielding sandstone aquifers of Tertiary through Jurassic age have transmissivities ranging from 25 ft^2/D to 500 ft^2/D. Specific storage, which is a function of aquifer porosity as well as aquifer and water compressibility, is similar for all confined aquifers and is approximately 10^{-6}/ft of thickness (Lohman 1972). The specific yield of unconfined aquifers, including alluvial deposits and sandstones in or near outcrop areas, ranges from 0.1 to 0.3 (Lohman 1972).

2.1.4.6 Regional Flow

Regional flow originates from topographically high outcrop areas toward lower outcrop areas as much of the aquifer recharge within the New Mexico region of the San Juan Basin occurs along the flanks of the Zuni, Chuska, and Cebolleta mountains (**Figure 2.11**). Recharge in topographically high areas along the northern and northeastern basin margins, including the San Juan Mountains in Colorado, also contributes to the regional flow systems (Stone et al. 1983). The main discharge regions of the basin include the San Juan River valley in the northwest and tributaries of the Rio Grande in the southeast. Steady-state analysis yields inflow and outflow rates of less than 20 ft^3/sec for Tertiary aquifers and approximately 40 ft^3/sec for Cretaceous and Jurassic sandstone aquifers (Lyford and Stone 1978).

Numerous ephemeral alluvial-filled stream channels are principal sources of groundwater recharge in some regions, or principal locations of discharge in others. Most discharge to alluvial channels is lost to evapotranspiration; however, some of the water also moves as subsurface flow.

Inter-aquifer movement of water, termed leakage, contributes to the San Juan Basin groundwater flow system. Differences in hydraulic head exceeding 200 ft, common between aquifers of the San Juan Basin, provide the driving mechanism for inter-aquifer movement. The geologic section displayed in Figure 2.11 (Kelley et al. 2014), depicts with arrows the likely direction of flow through confining beds.

The amount of vertical movement between aquifers is difficult to ascertain; however, substantial differences in hydraulic head (more than 200 ft), as well as water quality between vertically adjacent aquifers, imply that leakage rates through intervening confining layers are low in most areas (Stone et al. 1983). Zones of high vertical permeability are characteristic of highly fractured areas, such as those along the Hogback monocline near the Four Corners region in the northwest, and the Rio Puerco fault zone in the southeast, though few permeability data are available.

Figure 2.11—Schematic west to east cross section through the San Juan basin at the approximate latitude of the proposed injection well showing [redacted]njection zone (E) as well as the overlying USDWs: [redacted] Other intervening non-USDW aquifers and confining layers are also shown (after Kelley et al. 2014).

2.1.4.7 Water Quality

Water quality is measured as specific conductance in micromhos (µmho). Total dissolved solids is equivalent to approximately 0.7 times the specific conductance. Basin specific conductance ranges from less than 500 micromhos (µmho)[10] (350 mg/L TDS) for water near outcrops of some of the more transmissive rocks, such as the Ojo Alamo Sandstone, to more than 100,000 µmho (70,000 mg/L TDS) for water in deeper, less transmissive units, such as the Cow Springs Sandstone (Stone et al. 1983).

Alluvium-filled aquifers, though highly variable, have specific conductance values from less than 1,000 µmho in headwater areas, where water is received from percolating storm and snowmelt flows, to more than 4,000 µmho in lower reach areas, where it receives discharge from bedrock sources. Infiltration from irrigation also decreases specific conductance.

The concentrations of major chemical constituents do not appreciably vary between aquifers. Analysis of water reporting a specific conductance of less than 1,000 µmho generally contains sodium and sulfate as major constituents with elevated levels of bicarbonate. Chloride is a common

[10] The unit of measurement for conductivity is expressed in either microSiemens (uS/cm) or micromhos (umho/cm) which is the reciprocal of the unit of resistance, the ohm. Grand Valley State University. Instructor's Manual - Conductivity - Robert B. Annis Water Resources Institute (AWRI) - Education & Outreach - Grand Valley State University (gvsu.edu). Accessed March 2023.

constituent of water quality values when values exceed a specific conductance of 4,000 µmho (Stone et al. 1983).

Section 2.7—Hydrologic and Hydrogeologic Information provides a detailed discussion of hydrologic properties of each USDW within the AoR. Figure 2.11 provides a discussion of aquifers above the [redacted] that are not USDWs within the AoR but are in other regions of the San Juan Basin.

2.1.4.8 Non-Underground Sources of Drinking Water Aquifers

[redacted]

Recharge to [redacted] Injector No. 1 designated injection zone, principally occurs near topographically high outcrop areas flanking the [redacted] e San Juan Basin either by direct infiltration or by leakage of stratigraphically continuous aquifers (Lyford 1979). Groundwater flow is generally toward outcrops in Utah and near Four Corners. The approximate depth to the [redacted] ft true vertical depth subsea (TVDSS). The Strat 1 well, drilled approximately [redacted] of the AoR, indicates that [redacted] has an approximate thickness of [redacted]

Transmissivity values are less than 50 ft^2/D along the southern edge of the San Juan Basin but greater than 100 ft^2/D near the basin center (Stone et al. 1983). Levings et al. (1996) (Table 2.10) indicates a [redacted] Hydraulic conductivity values from selected oil wells yield a range of 0.5 ft to 5 ft/D, which support transmissivities above 100 ft/D (Craigg 2001). Discharge ranges from 8 to 616 gallons per minute (gpm).

Near recharge areas have a specific conductance of over 1,500 µmhos that can increase to more than 10,000 µmhos in deeper portions of the San Juan Basin. Water quality deteriorates toward the center of the San Juan Basin as dissolved solid concentrations increase in the direction of flow toward the basin center. Concentrations exceeding 10,000 mg/L are attributed to the dissolution of soluble carbonate minerals and the dissolution of evaporitic deposits from the [redacted] Within the AoR, the [redacted] contains high concentrations of TDS, well above the 10,000 mg/L criterion for classification as a USDW (refer to Section 2.8.1 Fluid Chemistry). Data collected by the Colorado Oil and Gas Conservation Commission (COGCC) surrounding the AoR is presented in Figure 2.8 along with identified [redacted] TDS concentrations ranging from [redacted]

[redacted]

[redacted]. As with [redacted], recharge occurs either by direct infiltration or from leakage of overlying and underlying aquifers near topographically high outcrop areas flanking the edge of the San Juan Basin (Cooley and Weist 1979). [redacted] groundwater flow is generally toward outcrops in Utah and Four Corners mimicking the flow of the overlying Morrison Formation. The approximate depth to the [redacted] in the AoR is -

[redacted]. The Strat 1 test well drilled approximately [redacted] of the AoR indicates that the [redacted] an approximate thickness of [redacted]

Although most hydrologic data for the [redacted], several sources report a transmissivity of approximately 50 ft^2/D for most of the San Juan Basin increasing up to 300 ft^2/D in the Four Corners area (Stone et al. 1983). Specific conductance and TDS are generally low (less than 2,000 µmhos or 1,600 mg/L) in or near outcrops but are likely to be much greater in the deeper portions of the basin. Petrophysical and geochemical analysis of wells in the AoR suggest that the TDS concentrations within [redacted] are greater than 10,000 mg/L. Refer to 2.8.1 Fluid Chemistry for a detailed discussion on measured and calculated TDS values within the AoR.

[redacted] noted that small to moderate amounts of water, [redacted], are from a multiple-aquifer system. No wells are known to exclusively produce water from [redacted], but rather combined with over- and underlying zones.

[redacted]

Recharge to [redacted] occurs on or near high outcrop regions near Four Corners (**Figure 2.12**). Groundwater flow is generally toward outcrops in Utah and near Four Corners. Discharge regions for [redacted] are present in the northwestern region of the San Juan Basin near Four Corners where the San Juan River breached [redacted] The depth of the [redacted] is approximately [redacted] in the AoR. The Strat 1 test well [redacted] the AoR indicates [redacted]

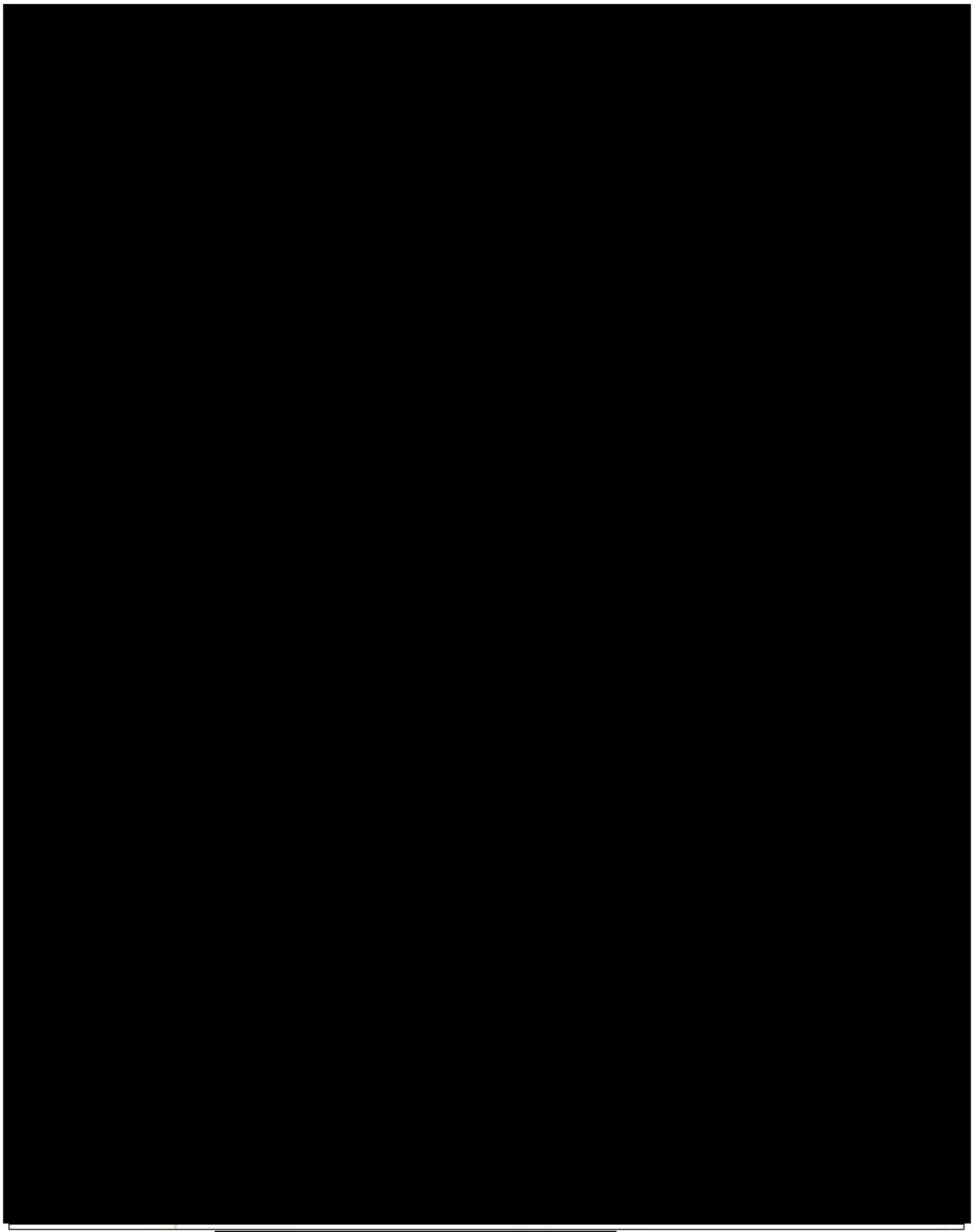

Figure 2.12—Depth to [redacted]

The Morrison aquifer is a hydrogeologic unit that corresponds to the Morrison Formation. The conceptual model of the ground-water flow system is based on work by Kelly (1977) that assumed

the Westwater Canyon Member is the only significant regional aquifer; however, the other Morrison aquifer members are important local aquifers. The Brushy Basin and Recapture Members function as semi-confining layers above and below the Westwater Canyon Member throughout the San Juan Basin except in the southwestern region of the basin where the Brushy Basin Member is absent (Dam 1995). The Morrison Formation is the source of the Crownpoint, New Mexico public water supply and supplies water to the city of Gallup, New Mexico along with the Gallup Sandstone in the southern region of the San Juan Basin (Stone et al. 1983).

The Westwater Canyon Member is the principal water-yielding unit of the Morrison transmissivity within the Morrison Formation and ranges from lower than 50 ft^2/D in the northeast San Juan Basin to as high as 300 ft^2/D at the southwest end of the basin (Lyford 1979). Levings et al. (1996) published hydraulic conductivity values that range from 0.025 ft/D to 0.39 ft/D. Discharge ranges from 1.3 gpm to 2,258 gpm with a median discharge of 32 gpm (Dam 1995) and specific capacity varies from 0.01 gallons per minute per foot (gpm/ft) to 3.98 gpm/ft drawdown. Even with a low specific capacity, yields of several hundred gpm may be obtained before the water level would draw down to the top of the aquifer. The Morrison Formation has an average porosity of 15 v/v and average permeability 37 mD (Haerer and McPherson 2009).

Stone et al. (1983) notes that the Morrison Formation of San Juan Basin has some of the lowest ground water TDS values along the shallow basin fringes where the formation outcrops. Specific conductance may exceed 10,000 µmhos, or 8,000 mg/L in the central and northeast regions of the basin (Lyford 1979). Within the AoR, petrophysical and geochemical analysis of nearby wells indicate [redacted]. Refer to 2.8.1 Fluid Chemistry for a detailed discussion on measured and calculated TDS values within the AoR.

Dakota Sandstone/Burro Canyon Formation

The Burro Canyon Formation is a minor hydraulic unit that is only present in the northern San Juan Basin and is typically mapped with the overlying Dakota Sandstone (Craigg 2001). Craigg (2001) further notes that in the Four Corners region sandstone lenses locally intertongue with mudstone of the Brushy Basin Member of the Morrison Formation. The Burro Canyon ranges in thickness from 30 ft to 200 ft, but hydraulic data is minimal due to the limited subsurface extent of the formation. The Burro Canyon yields small quantities of water to wells and springs (Cooley and Weist 1979). Levings et al. (1996) reports a specific conductance of 1,300 µmhos or 1,040 mg/L) a single sample from an undisclosed location.

Recharge to the Dakota Sandstone occurs on or near high outcrops near the Four Corners region (**Figure 2.13**). Dakota Sandstone groundwater flow is generally toward the Four Corners outcrops. The Dakota Sandstone discharges in the Four Corners region where the San Juan River breaches the Morrison aquifer (Dam 1995). [redacted] According to Craigg (2001), the thickness of the Dakota ranges from 200–500 ft but is [redacted] within the AoR.

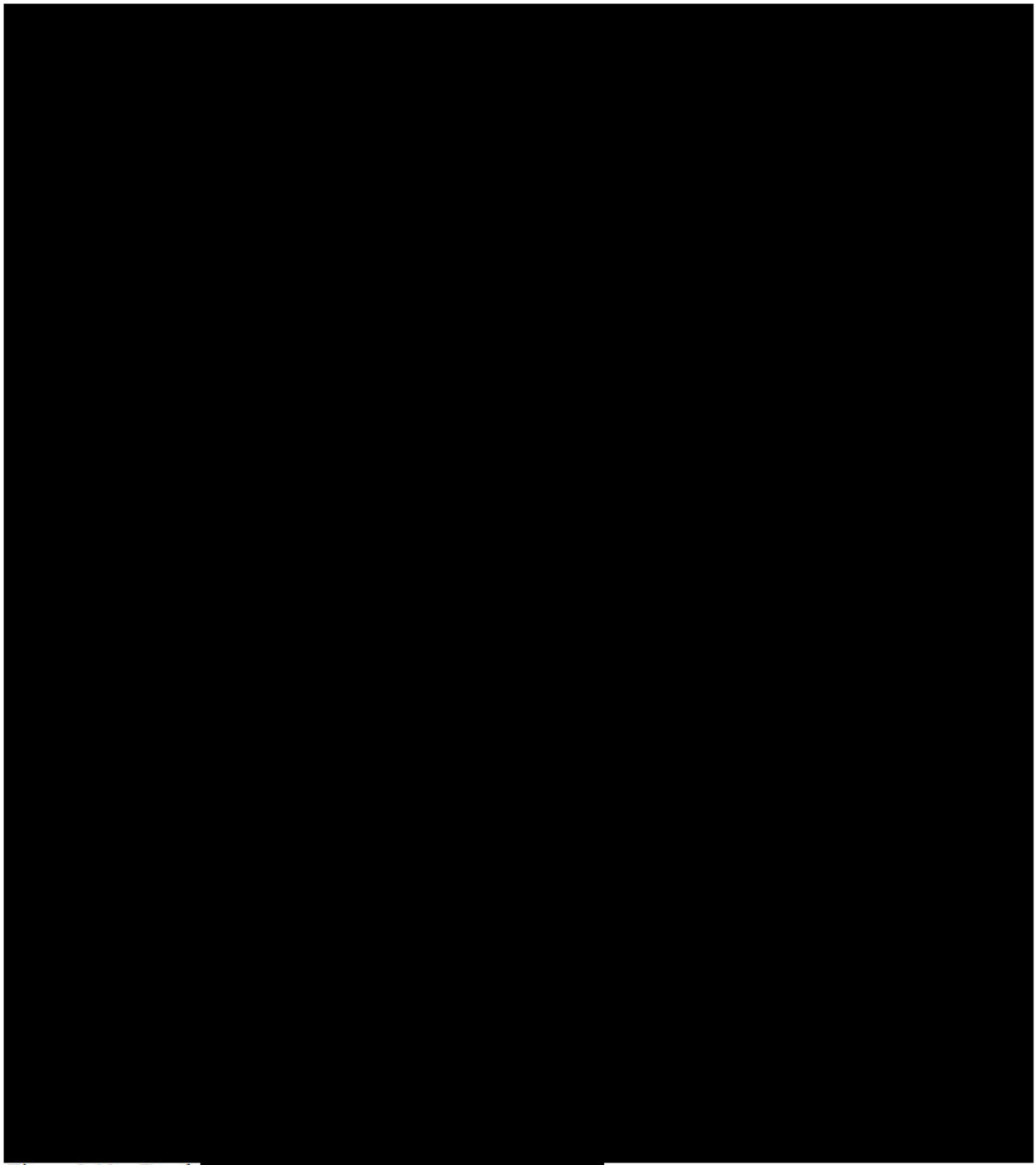

Figure 2.13—Depth

Levings et al. (1996) reported average hydraulic conductivity of 0.03 ft/D from oil and gas test holes. Discharge values ranges from 1.25 gpm to 75 gpm with a median discharge of 13 gpm (Dam 1995) and specific capacity ranges from 0.03 gpm/ft to 3.67 gpm/ft drawdown. Hydraulic conductivity data from oil-producing zones averages approximately 0.03 ft/D. The Dakota

Sandstone has an average porosity of 10 v/v and permeability 255 mD (Haerer and McPherson 2009). Much lower values of transmissivity are expected in oil- and gas-producing zones in the deeper strata of the San Juan Basin (Stone et al. 1983).

The Dakota Sandstone is a dependable, low yield aquifer throughout much of the San Juan Basin (Craig 2001). Specific conductance increases from less than 2,000 µmhos (1,600 mg/L) near recharge areas to more than 10,000 µmhos (8,000 mg/L) in the deeper strata of the basin (Stone et al. 1983).

The Dakota aquifer is a USDW at the San Juan Basin margins and is utilized as a source of water for domestic, livestock, and industrial purposes. The aquifer occurs under both unconfined and artesian conditions. The Dakota aquifer is recharged through infiltration of precipitation and streamflow on outcrops as well as vertical leakage through confining beds. Most water wells are completed in both the Dakota Sandstone and Morrison Formation, which have a higher quality of fresh water than the Dakota (Cooley and Weist 1979). USDW viability data includes geochemical water sampling data and petrophysical analysis of wireline logs near the AoR. Within the AoR, the TDS concentrations within [redacted]. Refer to 2.8.1 Fluid Chemistry for a detailed discussion on measured and calculated TDS values within the AoR.

Point Lookout Sandstone

The Point Lookout Sandstone is present throughout the San Juan Basin and is a source of water for domestic and livestock use in regions with suitable water quality and reasonable operation economics. Water wells are generally located on or near outcrop areas. [redacted]. Within the AoR, the [redacted] base is approximately [redacted] above [redacted] injection zone, and the thickness is approximately [redacted]

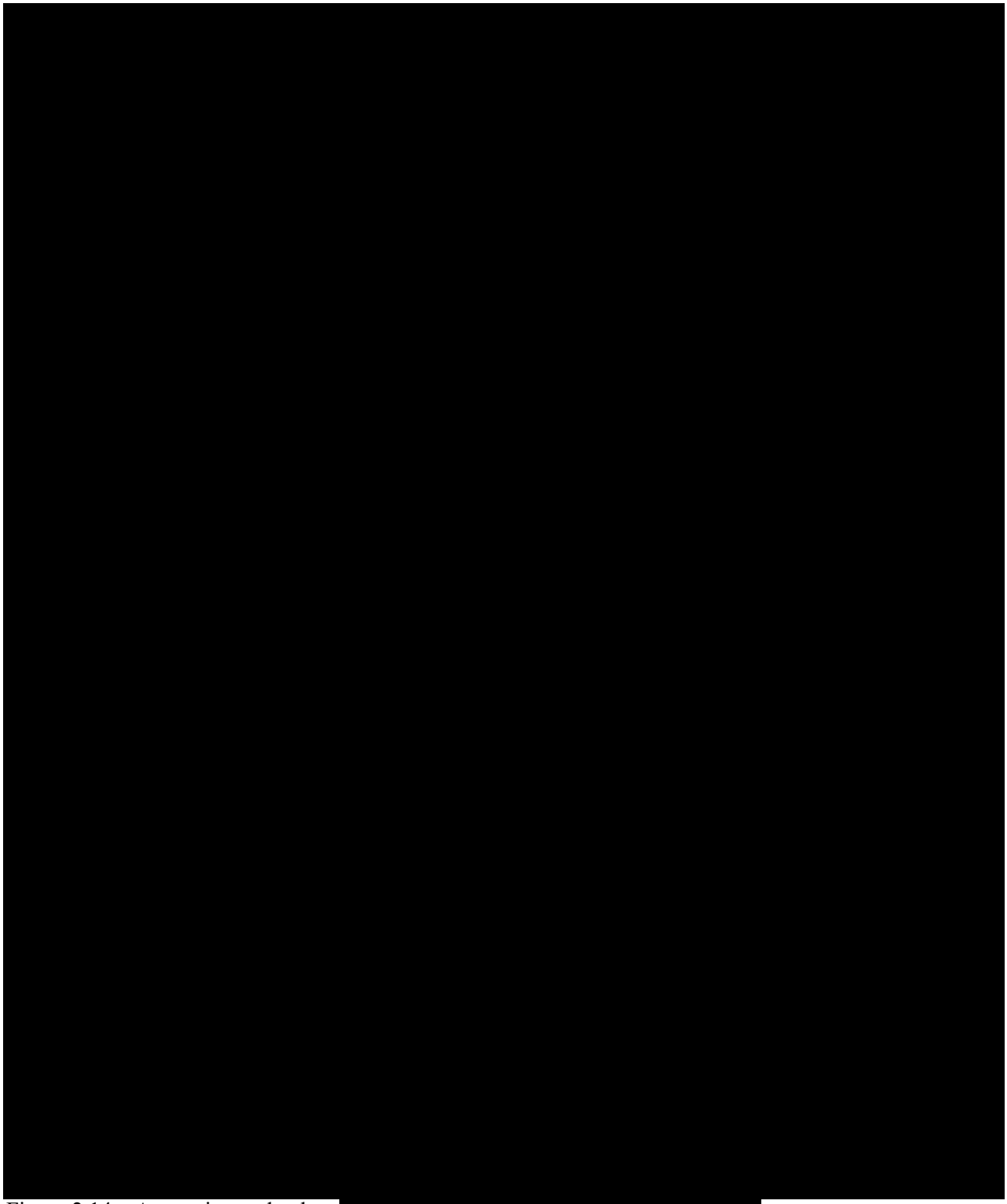

Figure 2.14—Approximate depth to

The Point Lookout Sandstone is Water wells are located outside the AoR and produce only small quantities from this interval. Petrophysical analysis of wells near the AoR indicates the TDS concentrations within the

Point Lookout Sandstone to be [redacted] Refer to 2.8.1 Fluid Chemistry for a detailed discussion on measured and calculated TDS values within the AoR.

Cliff House Sandstone

The Cliff House Sandstone is present throughout the San Juan Basin and has an approximate depth of [redacted] true vertical depth (TVD) within the AoR. Within the AoR it is approximately [redacted]

Cooley and Weist (1979) noted that the Cliff House Sandstone is a persistent, low yielding aquifer that supplies water for both agricultural and municipal purposes. Several wells produce water from this interval for stock and domestic use near outcrops in the central region of the San Juan Basin. The Cliff House provides water to stock wells south of Farmington, New Mexico as a water supply for the Chaco Canyon National Monument (Cooley and Weist 1979). The Cliff House may provide larger water yields where the formation sandstones are better developed. Based on geochemical water sampling data and petrophysical analysis of wireline logs near the AoR, the TDS concentrations for the Cliff House Sandstone [redacted]. Refer to Section 2.8.1—Fluid Chemistry for a detailed discussion on measured and calculated TDS values within the AoR.

Pictured Cliffs Sandstone

The Pictured Cliffs House Sandstone is present throughout the northern half of the basin, with an approximate depth to the formation top of [redacted] TVD within the AoR (Dam et al. 1990; **Figure 2.15).** Within the AoR its base is [redacted] above the [redacted] injection zone with an average thickness of [redacted] (Stone et al. 1983).

The Pictured Cliffs Sandstone forms a thin, low-yielding aquifer that furnishes water to a few stock wells and springs. Water flow is generally westward and discharges to the San Juan and Chaco rivers east and south of Shiprock, New Mexico with some water discharges to the Rio Puerco south of Cuba (Cooley and Weist 1979). Although some stock wells produce water from this formation, it cannot be considered a major aquifer because it is only a water producing zone in proximity to the overlying coals in the Fruitland Formation (Stone et al. 1983).

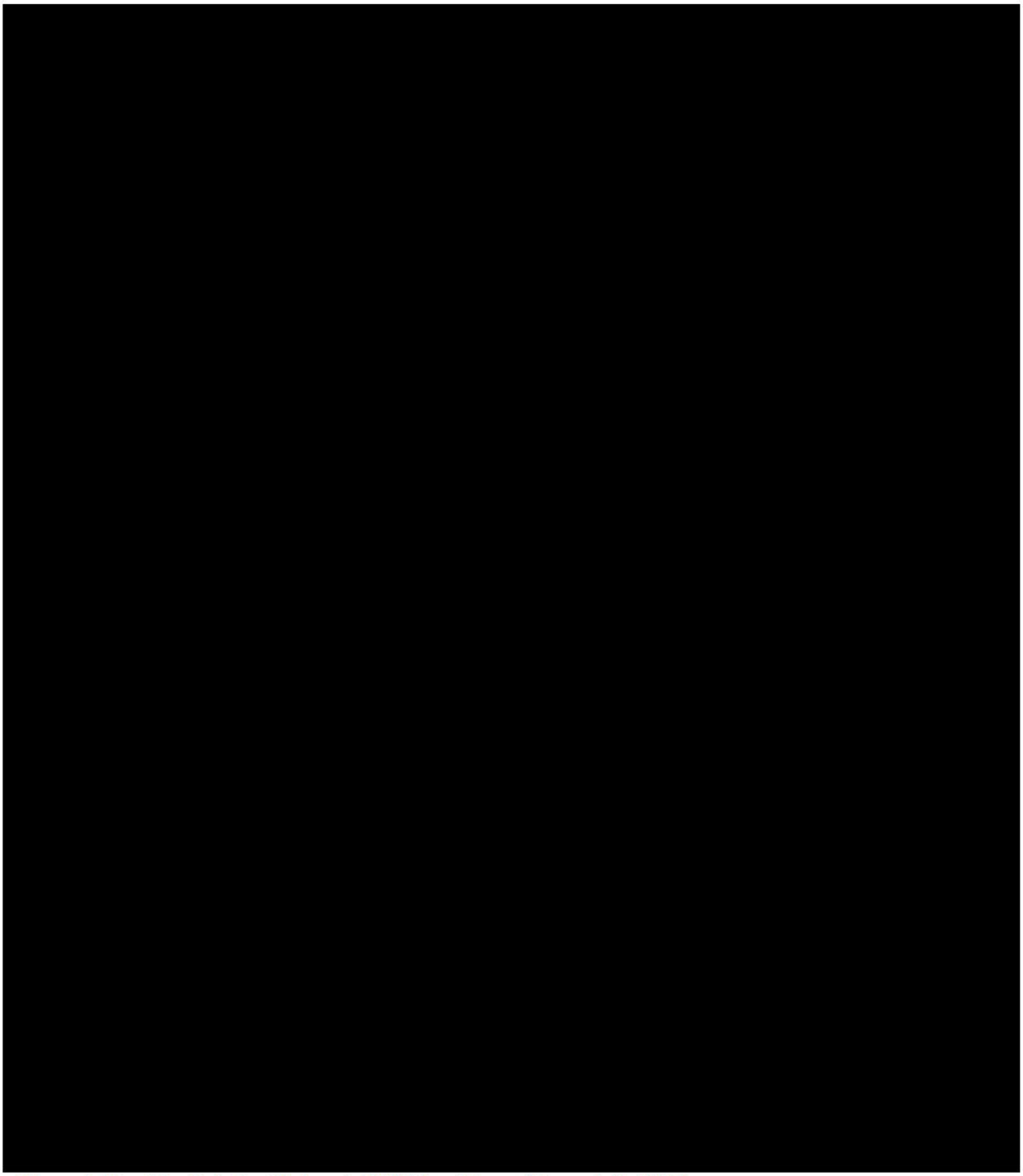

Figure 2.15—Depth to top Pictured Cliffs Sandstone (Dam et al. 1990).

Dissolved solids concentrations near recharge areas can be as low as 1,300 mg/L but increase from 30,000– mg/L to 40,000 mg/L in the deeper regions of the basin (Dam et al. 1990). Data collected up dip and down dip of the AoR provide a range of TDS concentrations between 1,300 mg/L and 7,490 mg/L (Dam et al. 1990). Geochemical water sampling data and petrophysical analysis of wireline logs near the AoR indicate TDS concentrations for the Pictured Cliffs Sandstone

[redacted] therefore, [redacted]. Refer to 2.8.1 Fluid Chemistry for a detailed discussion on measured and calculated TDS values within the AoR.

2.2 Maps and Cross Sections of the Area of Review [40 CFR 146.82(a)(2), 146.82(a)(3)(i)]

The majority of the AoR is located in a [redacted] region of the San Juan Basin and is located away from the steeper dips observed at the San Juan Basin's fringes (Figure 2.4). The AoR has no folds or faults. The [redacted] is continuous across the San Juan Basin and does not pinch-out. Well log mapping confirms the [redacted] continuity.

2.2.1 Map of Area of Review

2.2.1a_FourCornersCarbon_Injector_1_AoR Map ArchD_1-18k_land-topo.pdf is a map of the AoR with all required information per 14 CFR §146.82 at a scale of 1 in. to 1,500 ft (1:18,000). A smaller scale (1:55,000) version is also included in **Figure 2.16.** A version at 1:12,000 scale with a recent satellite imagery basemap is provided in: **2.2.1b_FourCornersCarbon_Injector_1_AoR Map ArchD_1-12k_SatImage.pdf**.

All data that informs the map is provided in an ESRI file geodatabase (**FourCornersCarbonSJ_geodatabase.gdb**). Data sources of artificial penetrations, clean-up sites, hydrologic data, mines and quarries, faults, and structures are summarized as follows:

Artificial Penetrations

Oil and Gas Wells

Well locations, including production wells, abandoned wells, plugged wells, dry holes, stratigraphic boreholes, and injection wells, are sourced from the New Mexico Oil Conservation Division's (OCD) well database[11]. For all wells identified, available files from the New Mexico OCD were downloaded and reviewed to confirm total depth and zones penetrated. [redacted] wells within the AoR [redacted] A list of all oil and gas wells within the AoR is provided in **3.4.1a_AoR Oil and Gas Well List (NM OCD)-dist.xlsx**. Well files for all wells within the AoR are provided in **3.4.1c_Oil and Gas Well Files_NM-OCD.zip**.

Water Wells

Water well locations were obtained from the New Mexico Office of the State Engineer's (OSE) points of diversion (POD) database[12]. The records in this database are sourced from the OSE's Water Administration Technical Engineering Resource System database (updated March 1, 2023).

There are [redacted] water wells identified located within the AoR. All wells are active; [redacted] The deepest well is drilled to 195 ft below ground surface (bgs). A list of water wells within the AoR is provided in **3.4.1b_AoR**

[11] https://ocd-hub-nm-emnrd.hub.arcgis.com/ - Accessed 1/17/2023
[12] https://services2.arcgis.com/qXZbWTdPDbTjl7Dy/arcgis/rest/services/OSE_PODs/FeatureServer – Accessed 3/31/2023

Water Well List (NM OSE PODs)-dist.xlsx. Well files for all water wells within the AoR are provided in **3.4.1d_Water Well Files_NM-OSE.zip**.

Clean-Up Sites

EPA clean-up site data is from the United States Environmental Protection Agency (EPA) Region 06 Geospatial Data of Regulated Facilities or Cleanup Locations database[13]. No EPA cleanup sites are identified within the mapped area.

State clean-up sites are sourced from the online New Mexico Environment Department's State Cleanup Program (SCP) database[14] and no active cleanup sites are present within the AoR or mapped area.

Hydrologic Data (Surface Water and Springs)

Hydrologic data is sourced from the USGS National Hydrography Dataset (NHD)[15]. Aside from seasonal washes and arroyos, no significant surface waters or springs are present within the AoR.

Mines and Quarries

Locations of mines and quarries are from the New Mexico Energy, Minerals and Natural Resources Department, Mining and Minerals Division[16]. There are no mines within the AoR. The nearest is [redacted] of the proposed Injector No. 1 location.

Faults

Surface fault locations are sourced from the USGS Quaternary Fault database[17] as well as regional geologic mapping by Scholle (2003). Neither source identifies surface faults within the AoR.

Structures Intended for Human Occupancy

There are no structures intended for human occupancy identified within in the AoR. Potential structures are sourced from the New Mexico Department of Finance and Administration Address Point database via RGIS[18]. Points within the AoR were reviewed in conjunction with satellite imagery to confirm if a structure is present. The nearest potential structure for human occupancy is [redacted] t of the AoR and [redacted] from the proposed injection site.

[13] https://www.epa.gov/frs/epa-frs-facilities-state-single-file-csv-download
[14] https://data-nmenv.opendata.arcgis.com/maps/85f43fe83e564d89a1d3b4b2d6a7129b/about, accessed January 9, 2023
[15] https://www.usgs.gov/national-hydrography/national-hydrography-dataset
[16] https://catalog newmexicowaterdata.org/dataset/emnrd-mmd-gis – Accessed 1/30/2023
[17] U.S. Geological Survey and New Mexico Bureau of Mines and Mineral Resources, Quaternary fault, and fold database for the United States, accessed 1 March 2023, at: https://www.usgs.gov/natural-hazards/earthquake-hazards/faults
[18] https://rgis.unm.edu/rgis6/dataset.html?uuid=cef558f9-9312-45b4-8e84-93450b38278e – accessed 4/10/2023

Tribal Boundaries

Tribal boundaries are sourced from the Bureau of Land Management's National Surface Management Agency database from the National Operations Center—Division of Information Resource Management[19].

[19] https://gis.blm.gov/arcgis/rest/services/lands/BLM_Natl_SMA_Cached_without_PriUnk/MapServer – access 3/9/2023

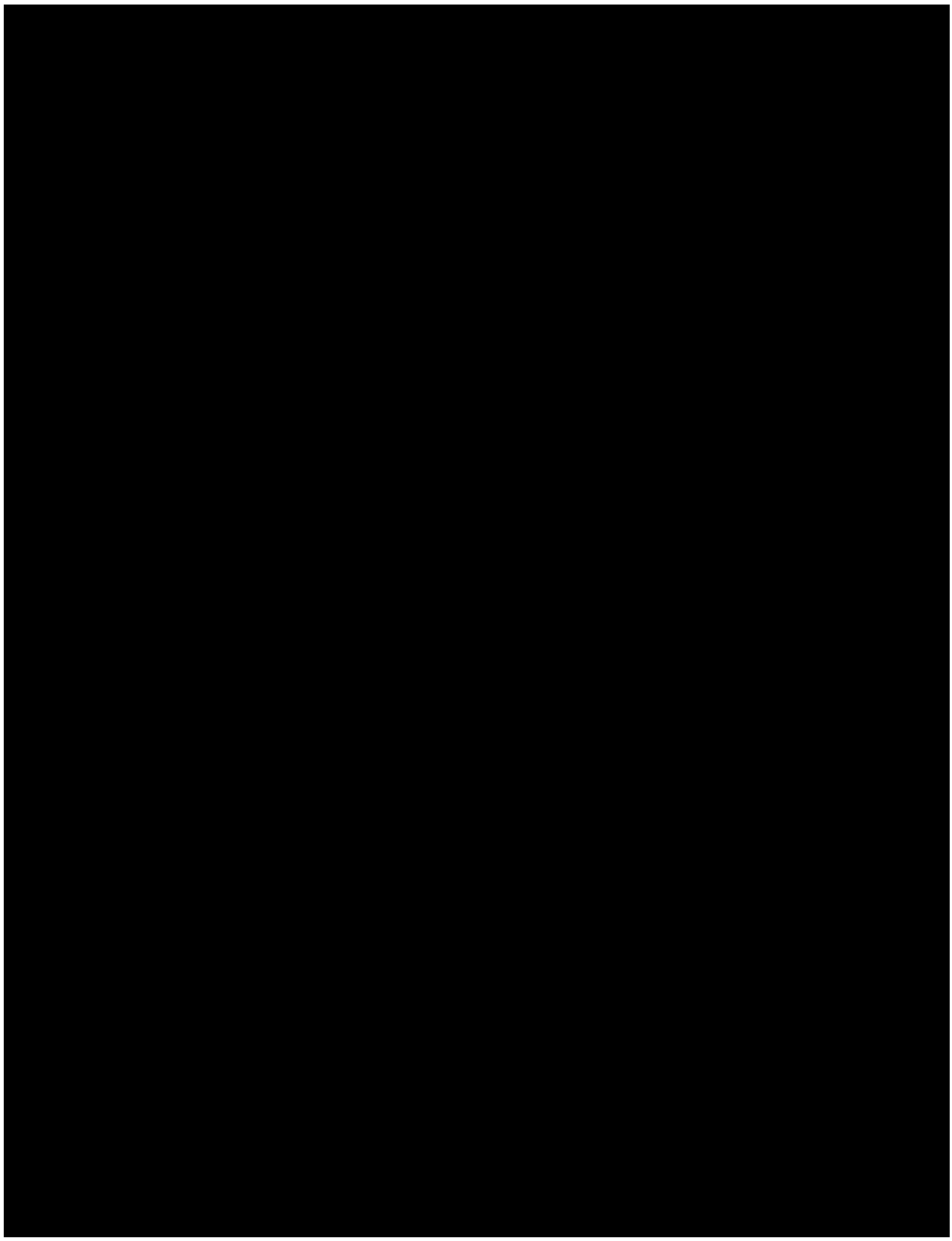

Figure 2.16—Area of Review basemap showing the location of the project wells: Injector 1, Monitor 1, and the Strat 1 and existing artificial penetrations in the mapped area, including oil and gas wells, water wells, and mines.

2.2.2 Structure Maps of the Injection and Confining Zones

Structure maps on the top of the injection [redacted] and confining [redacted] zones at 1:250,000 scale are provided in **Figure 2.17** and **Figure 2.18**, respectively. More detailed maps, using a scale of 1:24,000 showing all artificial penetrations, are provided in files uploaded separately: **2.2.2_[redacted] Structure Contour Map_1-24k_ArchE.pdf** and **2.2.2_[redacted] Structure Contour Map_1-24k_ArchE.pdf**.

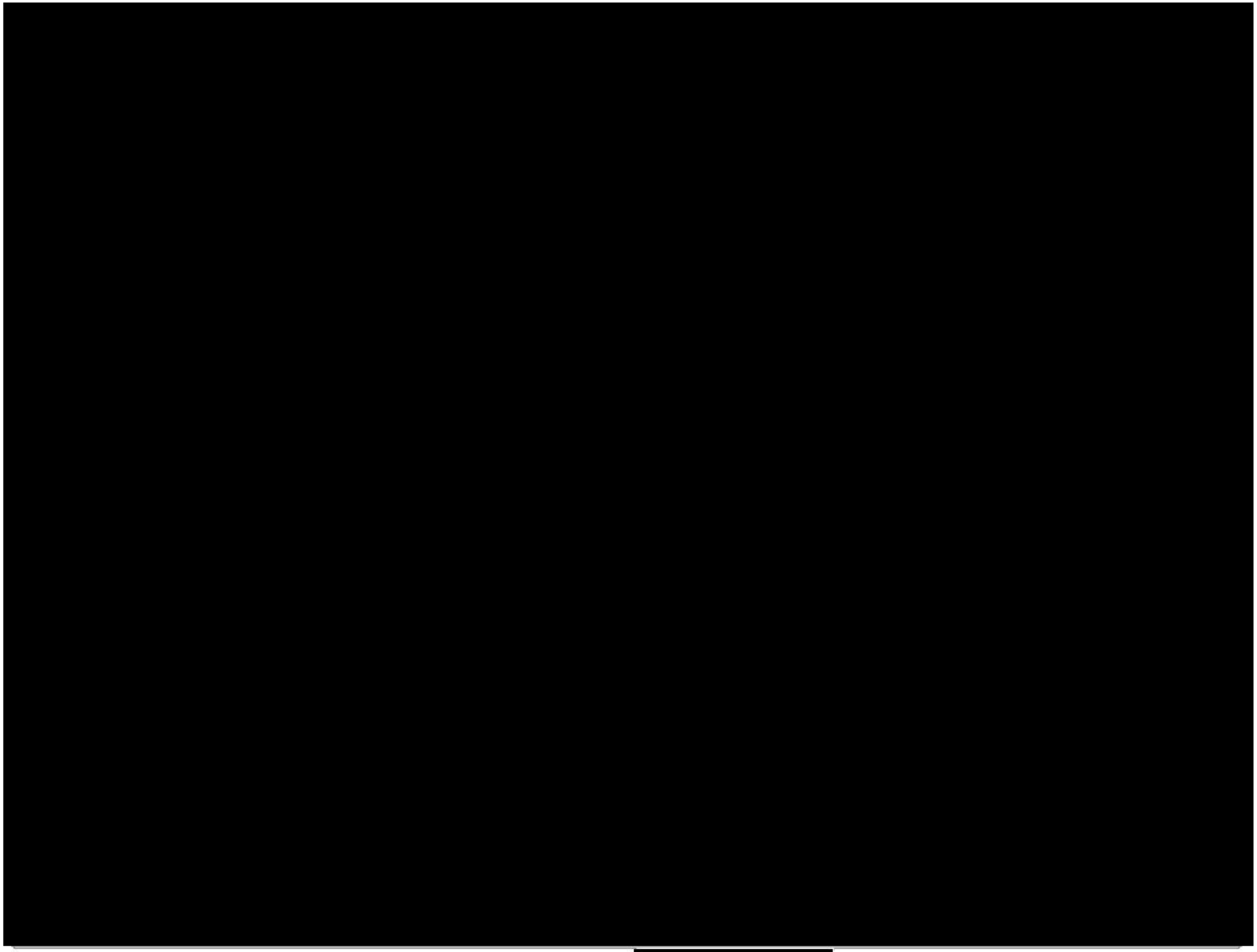

Figure 2.17—Structure map on the top of the proposed injection zone, [redacted]. Red marker tops are shown for wells penetrating the [redacted] and used to generate the contours. The structure was conformably gridded to overlying horizons [redacted] with significantly more well control. Orange and purple lines signify the location of cross sections A and B provided in Section 2.2.3.

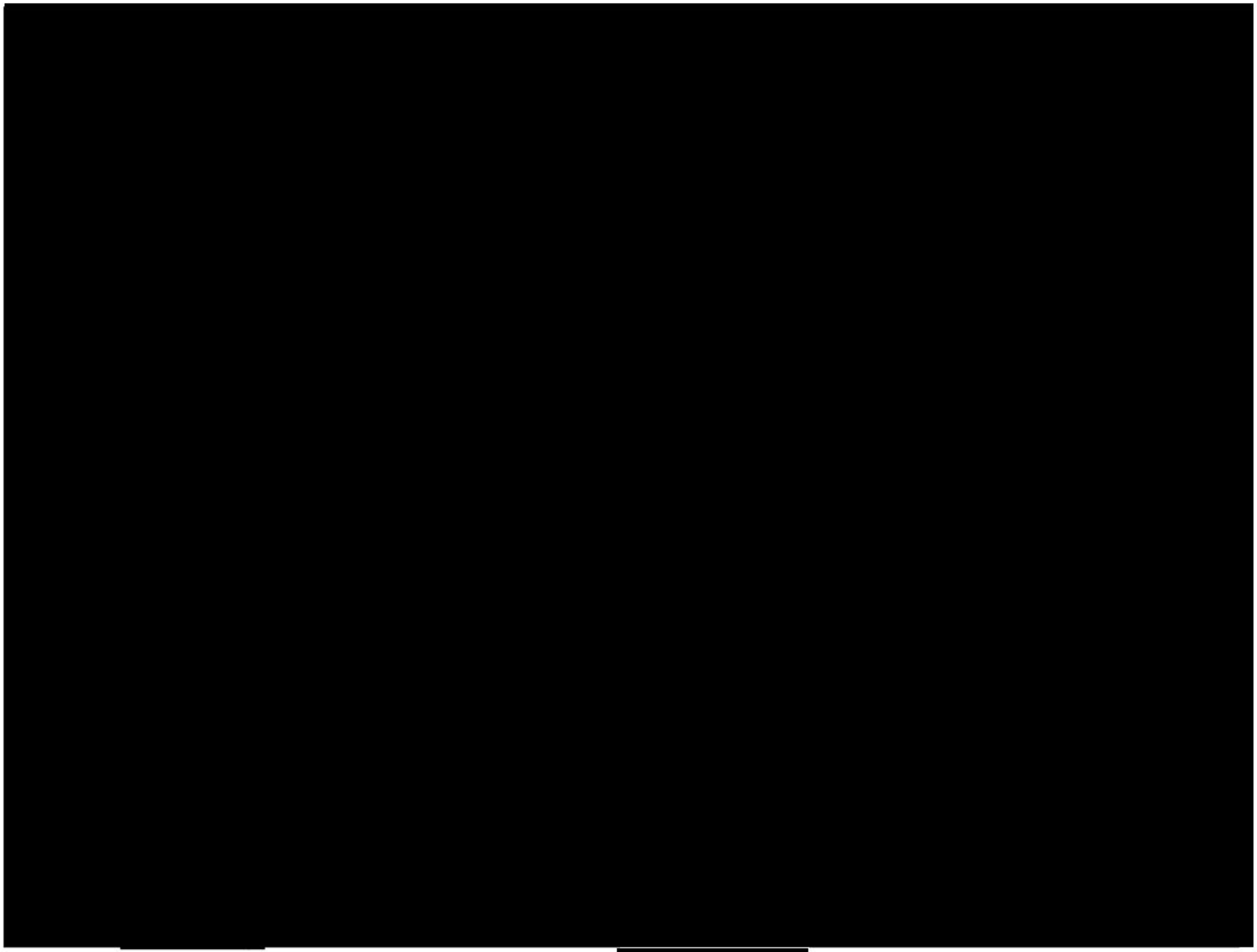

Figure 2.18—Structure map on the top of the upper confining zone [redacted]. Blue marker tops are shown for wells penetrating [redacted] and used to generate the contours. The structure was also conformably gridded to overlying horizons with significantly more well control. Orange and purple lines signify the location of cross sections A and B provided in Section 2.2.3.

2.2.3 Cross Sections

Two cross sections, extending from surface to below the proposed injection zone [redacted]), running through the proposed injection well location are provided in **Figure 2.19** These sections demonstrate that the location of the proposed injection well (Injector 1) is within [redacted] Injector No. 1 is observed to be within [redacted] are continuous across the proposed injection site. All wells on the sections show similar thickness in [redacted], thus no significant structural thinning nor pinch-out is expected or observed. In addition, no faults are observed crossing [redacted]. While no confining zones aside from the [redacted] are required to contain CO_2 sequestered in the [redacted] there are many additional low permeability shale and claystone intervals present in the stratigraphic section separating the lowermost USDW ([redacted] from the [redacted]

Figure 2.19—Geologic cross sections A and B running through the proposed injection well location extending from surface to below the base of the proposed injection zone (The nearest offset wells penetrating are included. All significant stratigraphic zones are shown and USDWs are labeled and shown in blue. Well logs show gamma ray on the left track and deep and shallow resistivity on the right track.

2.3 Faults and Fractures [40 CFR 146.82(a)(3)(ii)]

This section is a review of available literature and data used to characterize faults and fractures within the AoR. It focuses on potential hazards related to CO_2 containment. A literature and data review informs Four Corners Carbon's understanding and conceptual model of the distribution and character (e.g., density, spacing, orientation and mode) of potential fractures and faults induced by historical regional stress regimes related to the tectonic history of the San Juan Basin. Data from well logs and core adjacent to the AoR were reviewed to determine if faults and fractures exist. Core, open-hole logs, and image log data were collected across the confining and injection intervals in the Strat 1 well, [redacted] of the AoR, to determine if faults or fractures are present in the injection and/or confining zones at that location. To augment this review, with additional data acquisition, Four Corners Carbon plans to collect whole core and rotary sidewall core as well as resistivity and acoustic image logs from Injector No. 1 across the confining and injection intervals within the AoR (Figure 2.16).

2.3.1 Literature Review

The AoR is in the Central Basin region of the San Juan Basin, an area that has not undergone significant tectonic deformation (Kelley 1951; Craigg 2001). The general tectonic history of the San Juan Basin is spatially and temporally complex (refer to Section 2.1.1—Tectonic History). The San Juan Basin is bounded by structural uplifts and monoclines that initiated as early as the late Paleozoic with additional and further deformation occurring during the Laramide Orogeny (Kelley 1951; Craigg 2001). During this time, the Zuni and San Juan uplifts converged, generating basement thrust faults along the northern and southern margins of the basin. Strain from this compressional event was predominately accommodated by north-south oriented vertical fractures observed in outcropping Cretaceous rocks as well as in the subsurface throughout the basin (Figure 2.19; Lorenz and Cooper 2001; Lorenz and Cooper 2003). Uplifted basement blocks subjected to transpressive right lateral wrench faulting are present on the western and eastern basin margins bordering the Defiance and Hogback monoclines and the Nacimiento Uplift.

Stratigraphy in the Central Basin of the San Juan Basin exhibits gentle regional dips of less than 1° and low amplitude flexures possibly resulting from movement of underlying basement faults (Taylor and Huffman 1998). [redacted] (**Figure 2.20**). Shallow faults are interpreted close to structurally complex areas near the Central Basin margins [redacted]

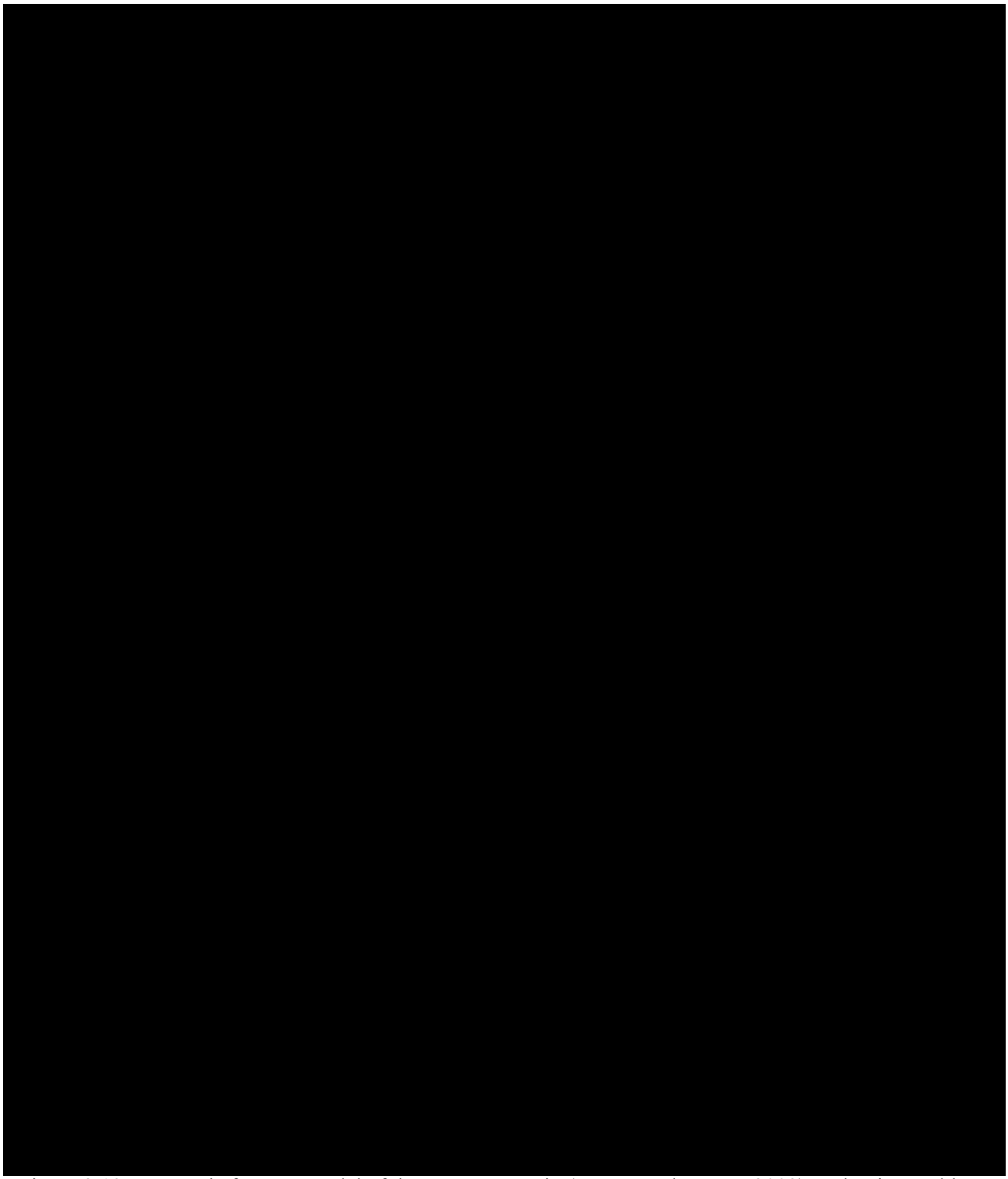

Figure 2.19—Tectonic fracture model of the San Juan Basin (Lorenz and Cooper 2003). A dominant oldest set of vertical extension fractures striking primarily north northeast-south southwest was observed across the basin. These features are primarily the result of southward and northward indentation of the San Juan and Zuni uplifts.

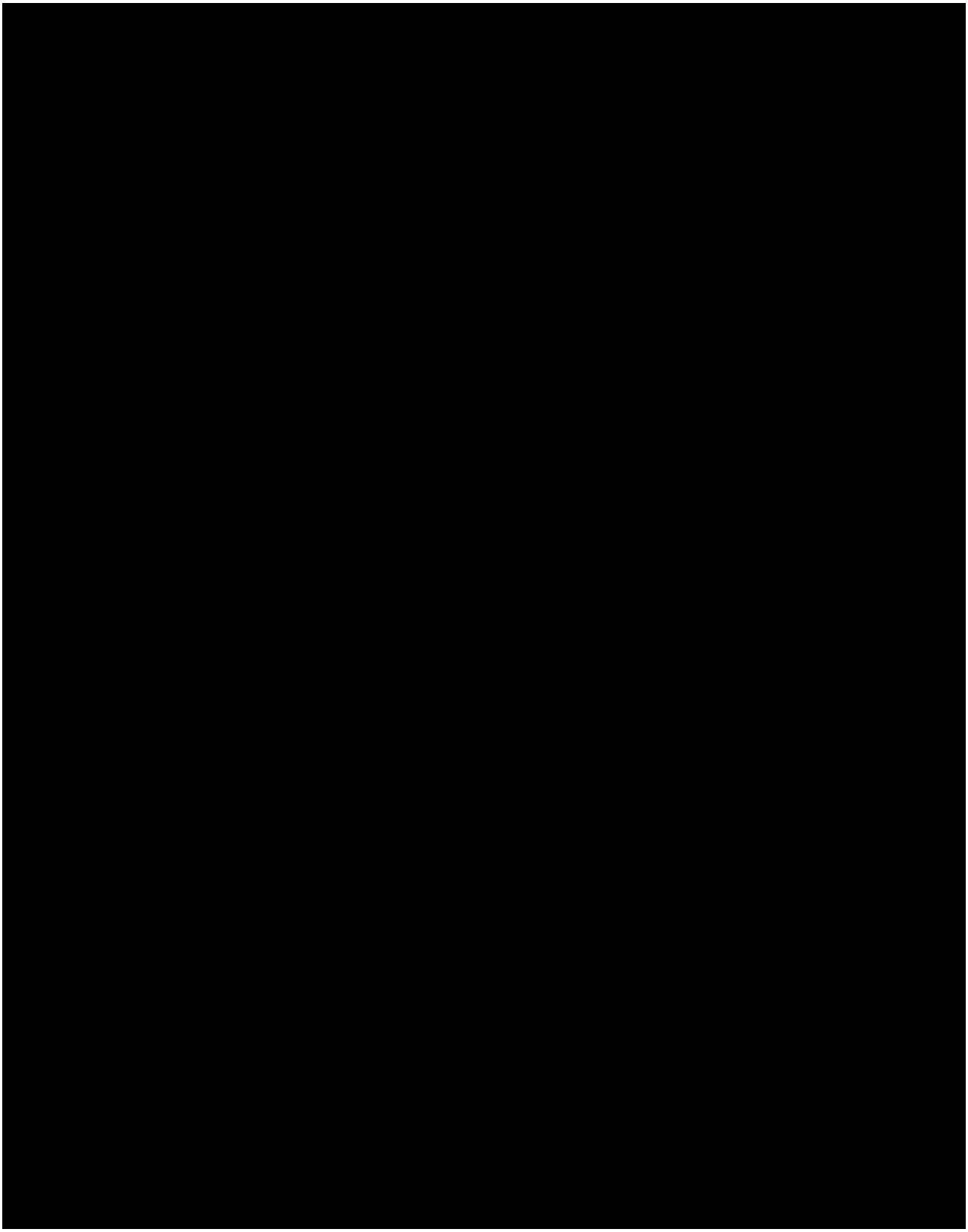

Figure 2.20—Locations and strikes of the five basement fault types (after Taylor and Huffman 1998).

2.3.2 Well Data

No faults were interpreted from well data within a 20-mile buffer of the Injector No. 1 well.

Whole core and resistivity image logs were collected in Strat 1. Interpretation of these resistivity image logs informed Four Corners Carbon on the expected fracture types (e.g., drilling induced, cemented, or uncemented natural fractures) and their orientation near the AoR. Results indicate there are no open fractures present in either the injection or the primary confining zones. The [redacted] the primary confining interval that directly overlies [redacted] and the [redacted] contain cemented fractures that are oriented northeast to southwest with dips less than 70°. Open fractures oriented north northeast to south southeast with dips greater than 70° are present within the [redacted] (**Figure 2.21**), but the primary confining interval is free of open or conductive fractures (**Figure 2.22**). The [redacted] open fracture density is low and additional data collection is planned to resolve whether these are an isolated occurrence or not (**Figure 2.23)**.

Prior to CO_2 injection, Four Corners Carbon plans to confirm an adequate sealing interval is present. Whole core, rotary sidewall core, and resistivity and acoustic image logs are planned in Injector No. 1 to provide a near wellbore assessment of faults and fractures in the injection and confining zones. Together resistivity and acoustic image logs will characterize open versus closed fractures, fracture aperture, and orientation. Interpreted near wellbore fault and fracture data from Injector No. 1 and Strat 1 will be compared to ascertain the regional extent of faulting and fracturing. Acoustic logs will be collected from Injector No. 1 to calculate rock mechanical properties including Youngs Modulus, Poisson's ratio, and to provide seismic tie-in for future 2D seismic surveys. Youngs Modulus and Poisson's ratio are key parameters in determining rock strength and ductility.

Figure 2.21—Rose diagram of Strat 1 resistivity image log analysis showing open fractures in [redacted] The brown shaded regions summarize the orientation and frequency of cemented fractures. The farther radially a particular slice is shaded represents a higher number of fractures with that orientation. Note: Predominant fracture orientation has a [redacted] strike with dips between [redacted]

Figure 2.22—Strat 1 resistivity image log analysis showing cemented fractures within the [redacted]. The pink shaded regions indicate the orientation and frequency of cemented fractures. The farther radially a particular slice is shaded represents a higher number of fractures with that orientation. Predominant fracture orientation has a [redacted] strike with dips between [redacted]

Figure 2.23—Fracture classification, density, and orientation from preliminary resistivity image log interpretation report of Strat 1.

2.4 Injection and Confining Zone Details [40 CFR146.82(a)(3)(iii)]

2.4.1 Data on the Injection Zone(s)

[redacted] is ubiquitous throughout the subsurface of the San Juan Basin and adjacent Colorado Plateau (**Figure 2.24**). This formation was deposited [redacted] that covered a sizable portion of the southwestern United States during [redacted] is an oil and gas reservoir producing from [redacted] In the northern region of the San Juan Basin, [redacted] is used as an analog to study potential fluid-rock interactions related to CO_2 sequestration because it is [redacted]

Figure 2.24—Approximate depositional extent of the [redacted] Study locations where solid-phase geochemical data were collected are shown as blue stars.

2.4.1.1 Reservoir Properties

[redacted]

Table 2.11—Summary of solid-phase geochemical data for [redacted]

Study Area	Sample Type	Rock Mineralogy				Cement Mineralogy			
		Quartz	K-Feldspar	Plagioclase	Trace	Calcite	Quartz	Dolomite	Smectite
[redacted]									
[redacted]									
[redacted]									

[redacted]

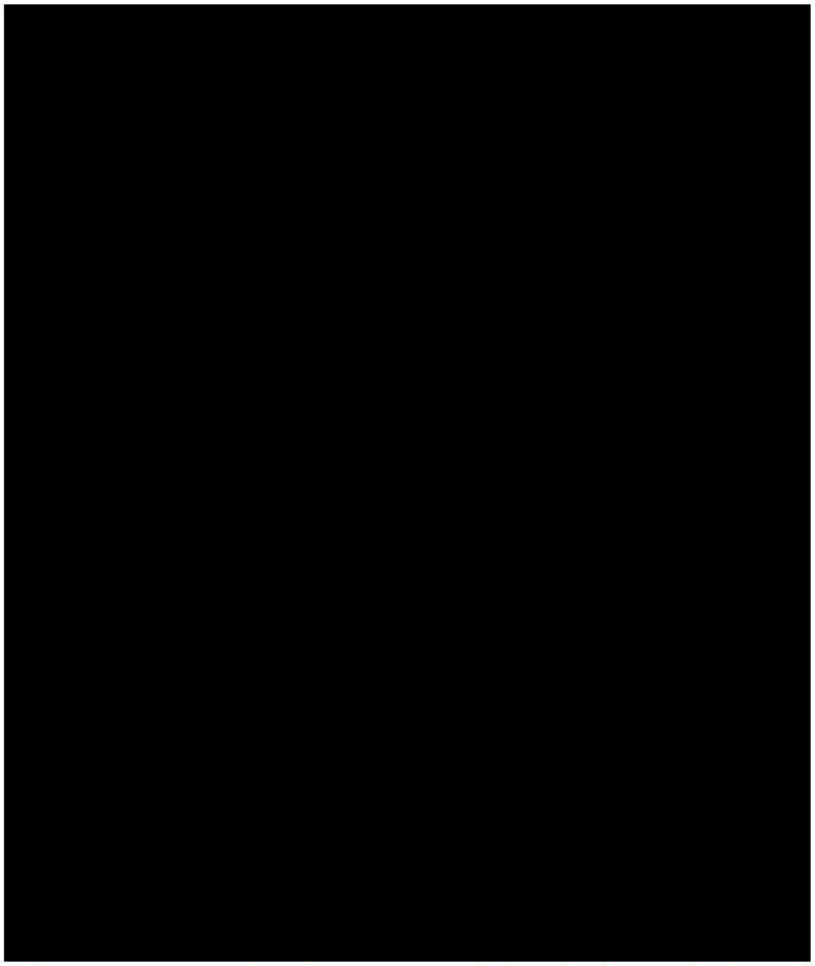

Figure 2.25—Type log from Strat 1 well showing intervals from which conventional core was cut.

Core will be collected from Four Corners Carbon Injector No. 1 prior to injection. These data will verify the mineralogy and composition at the proposed injection site.

[redacted]

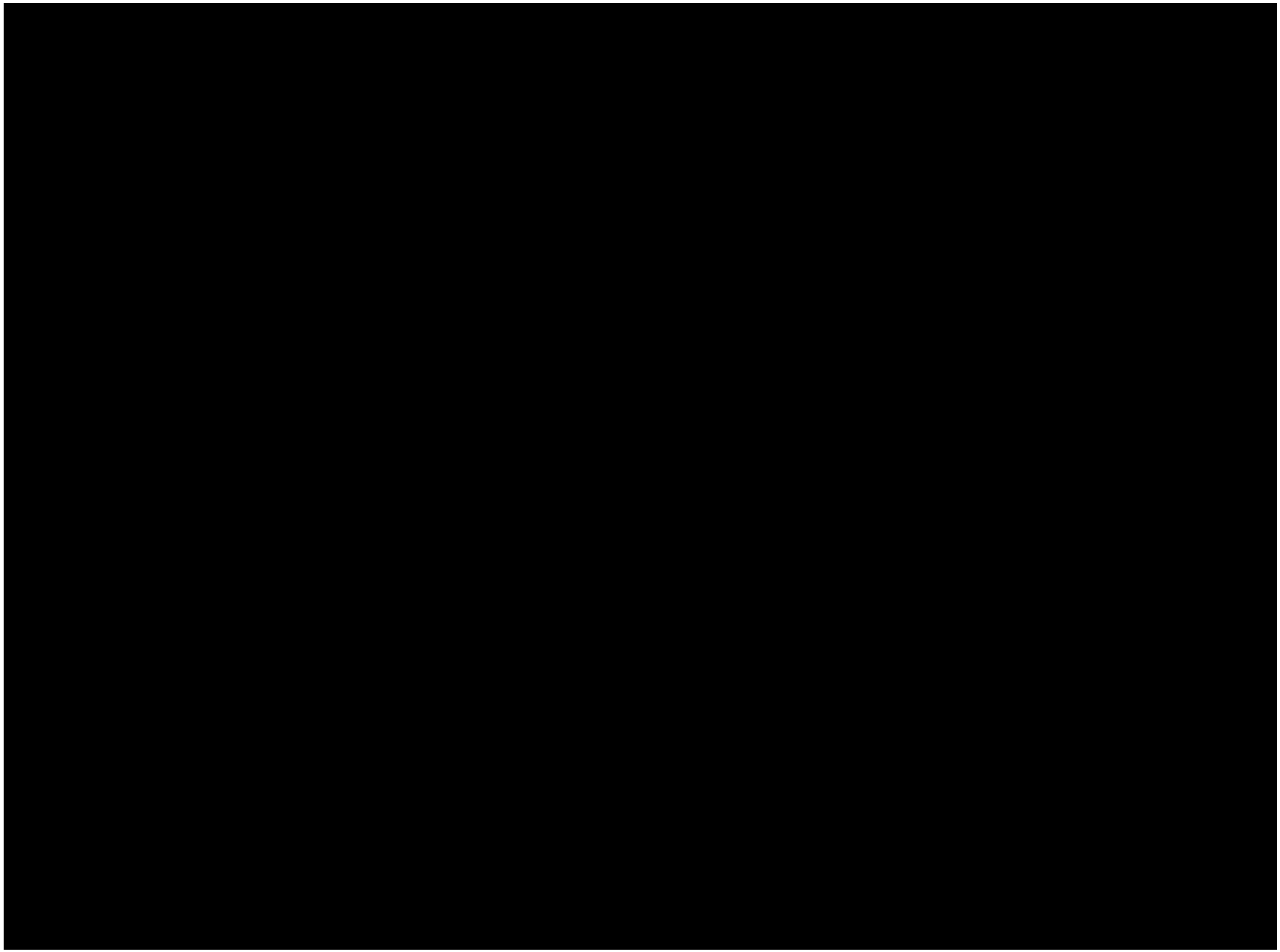

Figure 2.26— [redacted] structure contour map (TVDSS) near the AoR.

Figure 2.27— thickness map (TST) near the AoR.

Table 2.12—Average porosity and permeability parameters for the net reservoir quality section of [redacted] by Strat 1.

Zone	Net to Gross	Thickness (ft)	Avg Total Porosity (v/v)	Avg Permeability (mD)
[redacted]				

Note: Net reservoir is [redacted] or greater porosity.

2.4.1.2 Geochemical Reactions

Four Corners Carbon does not anticipate adverse chemical reactions in the [redacted] from CO_2 injection. [redacted] Four Corners Carbon plans to model potential chemical reactions in [redacted] after analyzing site-specific data.

2.4.1.3 Additional Data Required

Measurements of [redacted] zone injectivity are planned for the cores cut from in Strat 1. Both routine core analyses (RCA) and Special Core Analyses (SCAL) are planned as detailed in Table 2.13 and **Table 2.14**. Relative permeability and wettability testing at reservoir conditions will be conducted to clarify transient wettability behavior. The relative permeability and capillary pressure of the formation fluids will evaluate multiphase fluid-rock compatibility and potential reservoir damage, such as fines migration or clay swelling. Water-rock interaction flow-through experiments with brine equilibrated with CO_2 will measure and quantify absolute permeability, strength, and elasticity changes. Beyond RCA and SCAL, Nuclear Magnetic Resonance (NMR) logs are planned for Injector No. 1. NMR log measurements are the most accurate porosity log measurements and provide an estimate of pore size distribution as a proxy of capillary pressure.

Table 2.13—Summary of required geomechanical characterization per 40 CFR 146.82(a)(3)(iv), and forthcoming data to address requirements.

UIC-Class VI requirements for 40 CFR 146.82(a)(3)(iv)	Data Acquisition Planned for Well Injector 1	
	Wireline	Core
Fractures	•	
Ductility	•	

UIC-Class VI requirements for 40 CFR 146.82(a)(3)(iv)	Data Acquisition Planned for Well Injector 1	
	Wireline	Core
Rock strength	• [redacted]	[redacted]
In situ stress field	[redacted]	[redacted] ge logs or other wellbore information).
Pore pressure	• [redacted]	[redacted]

Table 2.14—Summary of required rock properties of the confining and injection zone per 40 CFR 146.82(a)(3)(iii) and forthcoming data to address requirements.

UIC-Class VI required data [40 CFR 146.82(a)(3)(iii)]	Data Acquisition Planned for Injector 1	
	Wireline	Core
Mineralogy	[redacted]	[redacted]
Porosity	[redacted]	[redacted]
Permeability	[redacted]	[redacted]
Capillary pressure	[redacted]	[redacted]
Geology/facies changes	[redacted]	[redacted]

2.4.2 Data on the Confining Zone(s)

[redacted].

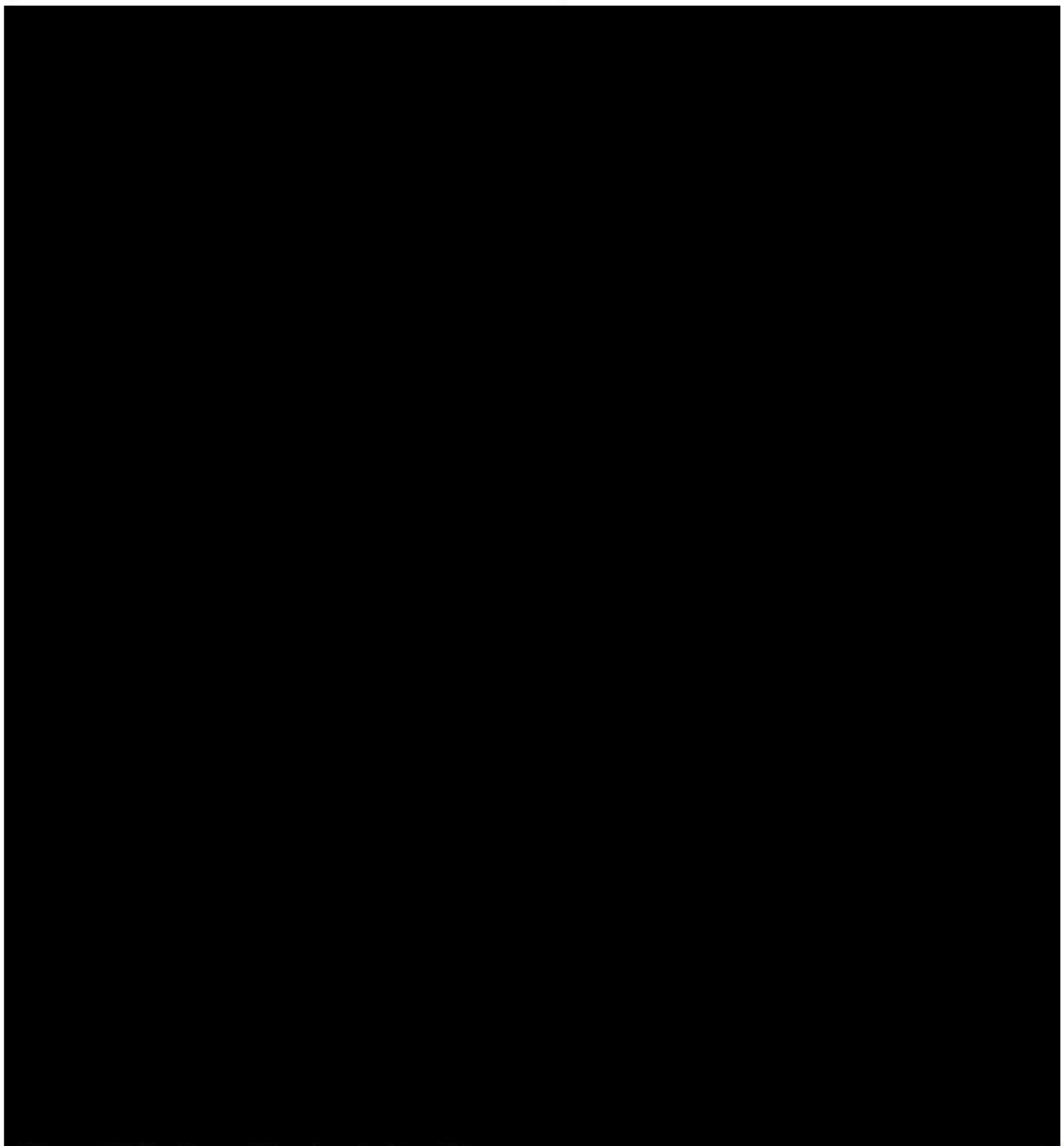

Figure 2.28—Depositional extents of [redacted] Solid-phase geochemical data was collected at sample sites shown on map ([redacted].

Table 2.15—Summary of solid-phase geochemical data for [redacted].

Sample Location / Sample Study		[redacted]
Rock Mineralogy	Quartz	
	K-Feldspar	
	Plagioclase	
	Zircon	
	Muscovite	
	Lithics	
	Calcite	
	Organics	
Cement	Calcite	
	Sericite	
	Quartz	

2.4.2.1 Zone Properties

An abundance of data exists on the mineralogy and petrology of [redacted]. The average composition of the lower unit is more than [redacted] (Table 2.15). The major constituents of the silts and fine sands [redacted] petrographically analyzed three outcrop samples to describe the upper [redacted] as a silty sandstone (Table 2.15). Point count results indicate that the [redacted] Core collected from Strat 1 located [redacted] AoR is being analyzed for mineralogy and elemental composition to confirm the geochemistry of [redacted] Core will be collected and analyzed across [redacted] from the Injector No. 1 well, to be drilled by Four Corners Carbon within the AoR prior to injection (Figure 2.16).

The physical properties of [redacted] vary throughout the San Juan Basin. It outcrops along the basin margins and reaches depths greater [redacted]. Within the AoR [redacted] (**Figure 2.29**). [redacted] penetrations within the AoR; therefore, openhole log interpretations from adjacent wells were used to estimate its thickness within the AoR. The combined thickness [redacted] (**Figure 2.30**). Current estimates of porosity and permeability for the confining zone in the AoR are based on neutron-density cross-plot porosity and porosity-based intrinsic permeability calculations (Juhasz 1979; **Table 2.16**). They will be supplemented with NMR- and core-based permeability as additional data is available.

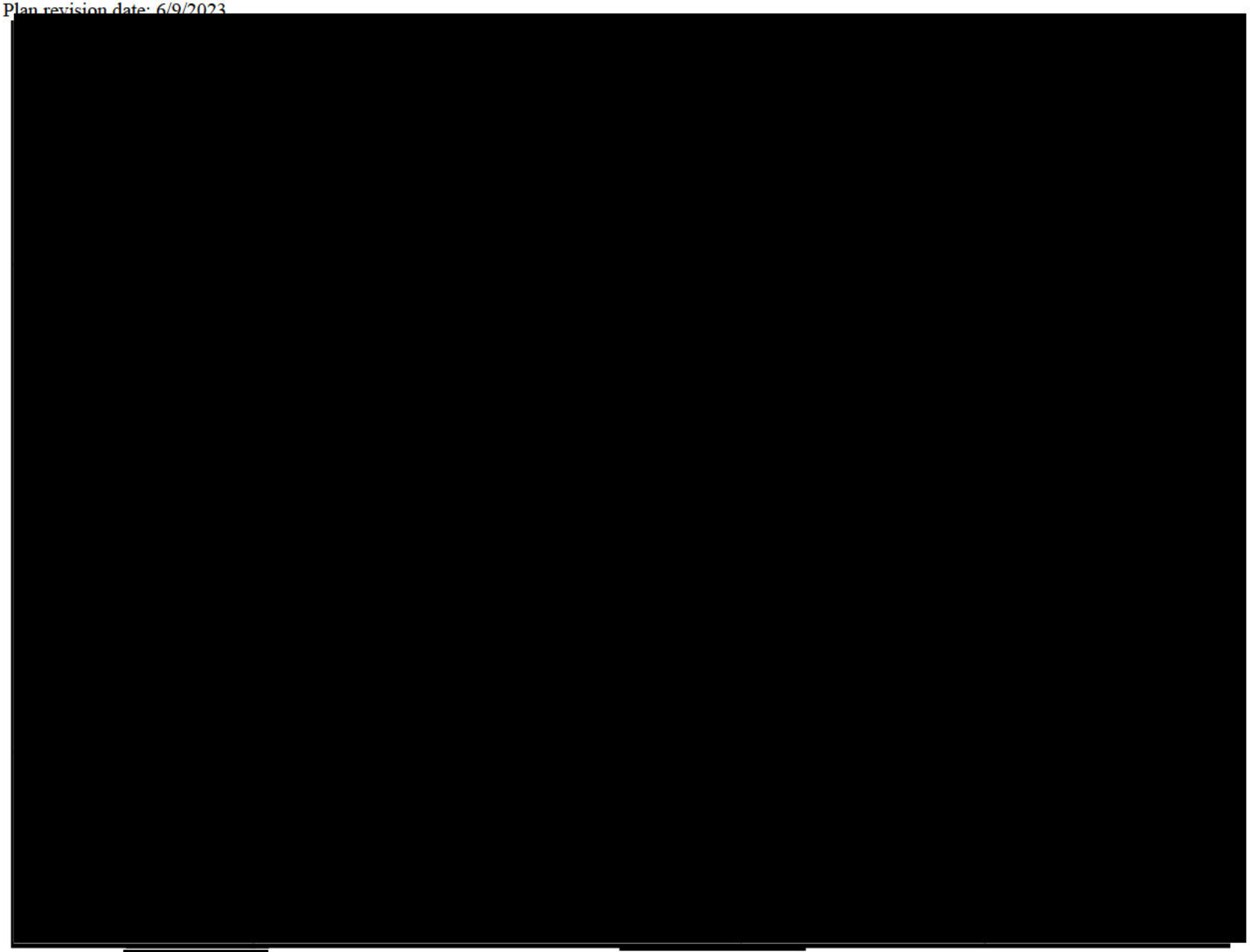

Figure 2.29— [redacted] structure contour map (TVDSS) near the AoR.

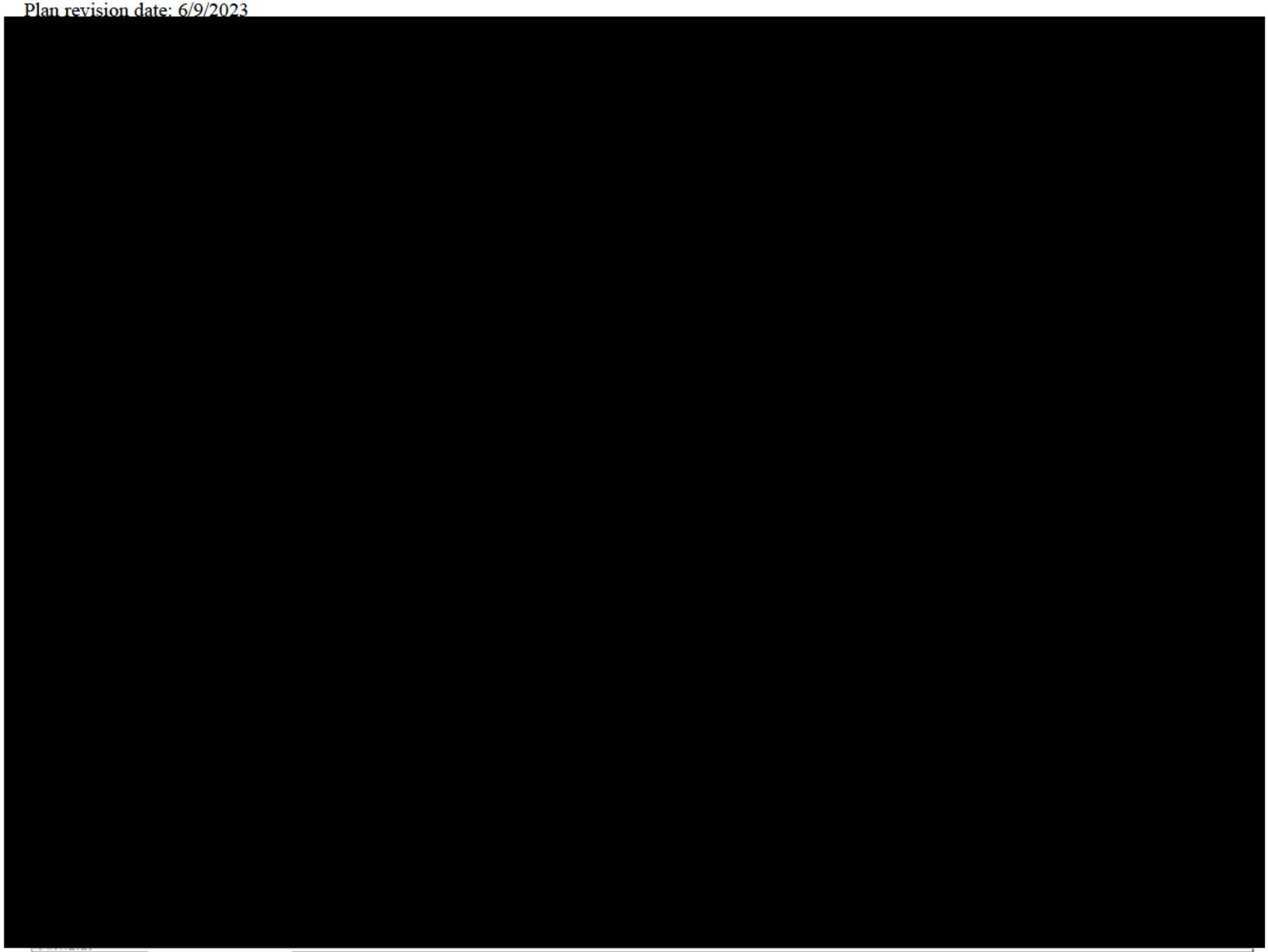

Figure 2.30— [redacted] thickness map (TST) near the AoR.

Table 2.16—Average ELAN porosity and permeability for [redacted] based on data recorded in the Strat 1 well.

Zone	Gross Thickness (ft)	Net Confining Thickness (ft)	Total Porosity (v/v)	Permeability (mD)
[redacted]				
[redacted]				

2.4.2.2 Geochemical Reactions

Four Corners Carbon does not anticipate adverse chemical reactions in [redacted]r from CO_2 injection in [redacted]. CO_2 dissolution into pore fluid increases pH, accelerating limestone dissolution. Gherardi et al. (2007) modeled CO_2 injection into a sandstone reservoir with a carbonate cap rock and found that the cap rock self-healed by re-precipitating calcite when the water content of the reservoir is high. Additional research [redacted] confirms that [redacted] is a caprock. Published results [redacted] indicate that the dissolution of carbonates mobilizes carbonate-forming cations which react with CO_2 and lead to carbon mineralization over lengthy periods creating the final trapping mechanism, after physical and solubility trapping, which is considered the most secure form of carbon storage.

2.4.2.3 Capillary Pressure

Measurements of confining zone capacity via capillary pressure measurements are planned for the [redacted] core from the Strat 1 and in future wells to be drilled within the Project AoR. MICP lab studies involve placing a dried rock sample in an evacuated sample chamber and incrementally injecting mercury at increasing pressure, MICP is planned for the injection zone and seal zone while porous plate capillary pressure experiments are planned for the injection zone. During the MICP procedure, the pressure is recorded at each step. The resulting data are plotted to indicate the capillary breakthrough pressure of the sample and provide measurements of the maximum pressure and sealing capacity (i.e. CO_2 column heights). The cap pressure measurements provide pore size distributions that allow for rock typing. Multiphase flow in the upper confining zone will be measured with gas intrusion experiments which will help quantify relative permeability of super critical-CO_2 (sc-CO_2) and will be used to tune simulation models. These results will determine the sealing capacity of [redacted] and define hydraulic flow units in [redacted] injection zone within the AoR. Determination of flow units is critical for tuning the static and dynamic reservoir models and better constraining injectable rock volume.

2.5 Geomechanical and Petrophysical Information [40 CFR 146.82(a)(3)(iv)]

During drilling of the Strat 1 located [redacted] the AoR, [redacted] of conventional core was cut and recovered from [redacted] (**Table 2.17** and **Figure 2.31**).

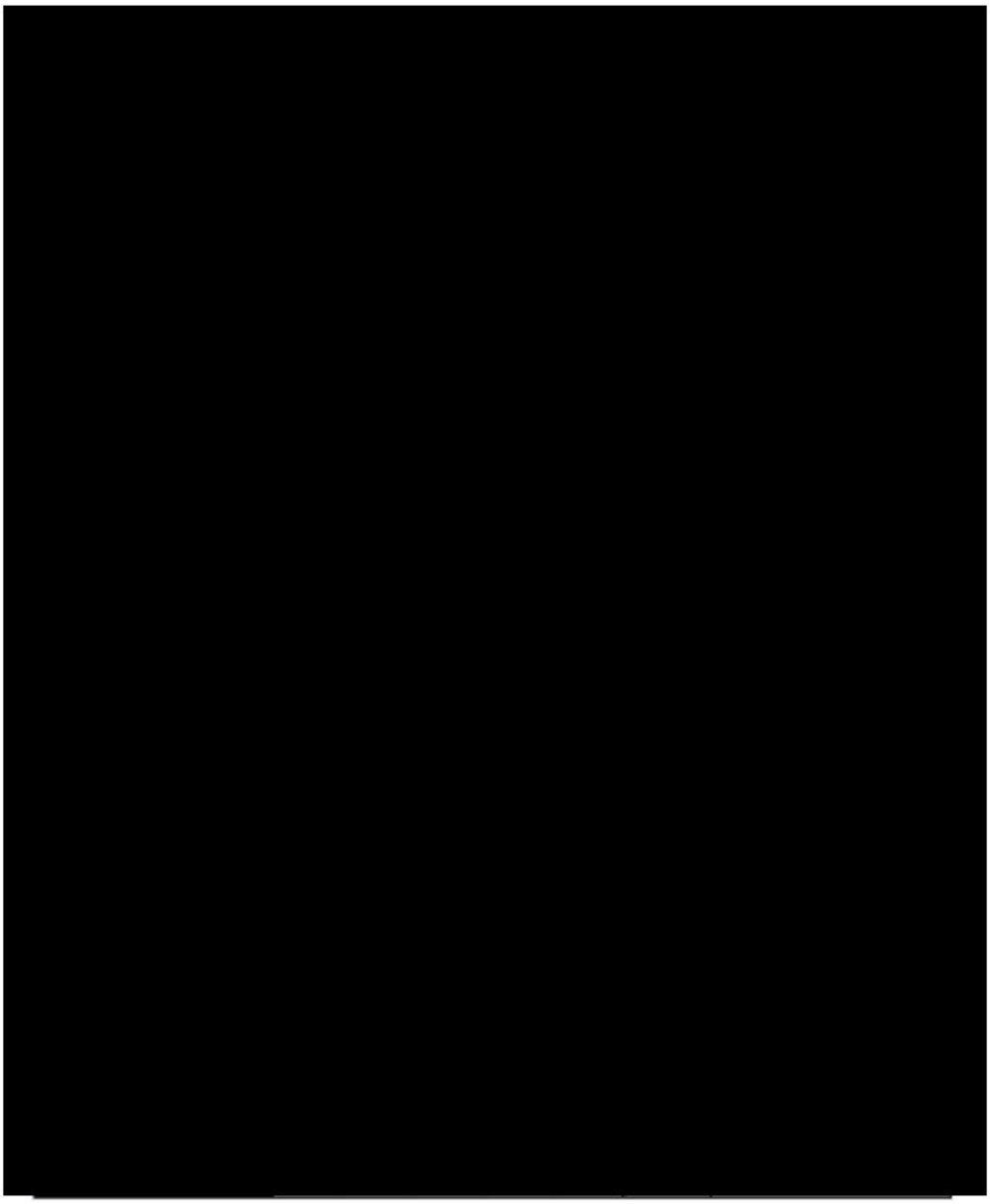

Figure 2.31—Strat 1—Stratigraphic horizons, openhole GR log, and cored intervals.

Table 2.17—Footage of conventional core cut in Strat 1.

Formation	Conventional Core (ft)
[redacted]	[redacted]
[redacted]	[redacted]
[redacted]	[redacted]
[redacted]	[redacted]
[redacted]	[redacted]

Extensive RCA, SCAL, and rock strength tests are planned for the cores. Analyses will include:

- Wettability.
- Capillary pressure.
- Relative permeability and pore water chemistry measurements.
- XRD/X-ray fluorescence (XRF) to determine the injection and confining zone mineralogy.
- Flow-through tests to determine the CO_2-rich fluid-rock compatibility of [redacted] in the vicinity of the AoR.

Prior to injection, additional cores will be collected in the Injector No. 1 well, and the same analyses will be performed for the injection and confining zones.

The Strat 1, [redacted] Injector No. 1, is the closest well to the AoR with log data acquired over [redacted]

[redacted]

Several logs, including [redacted]

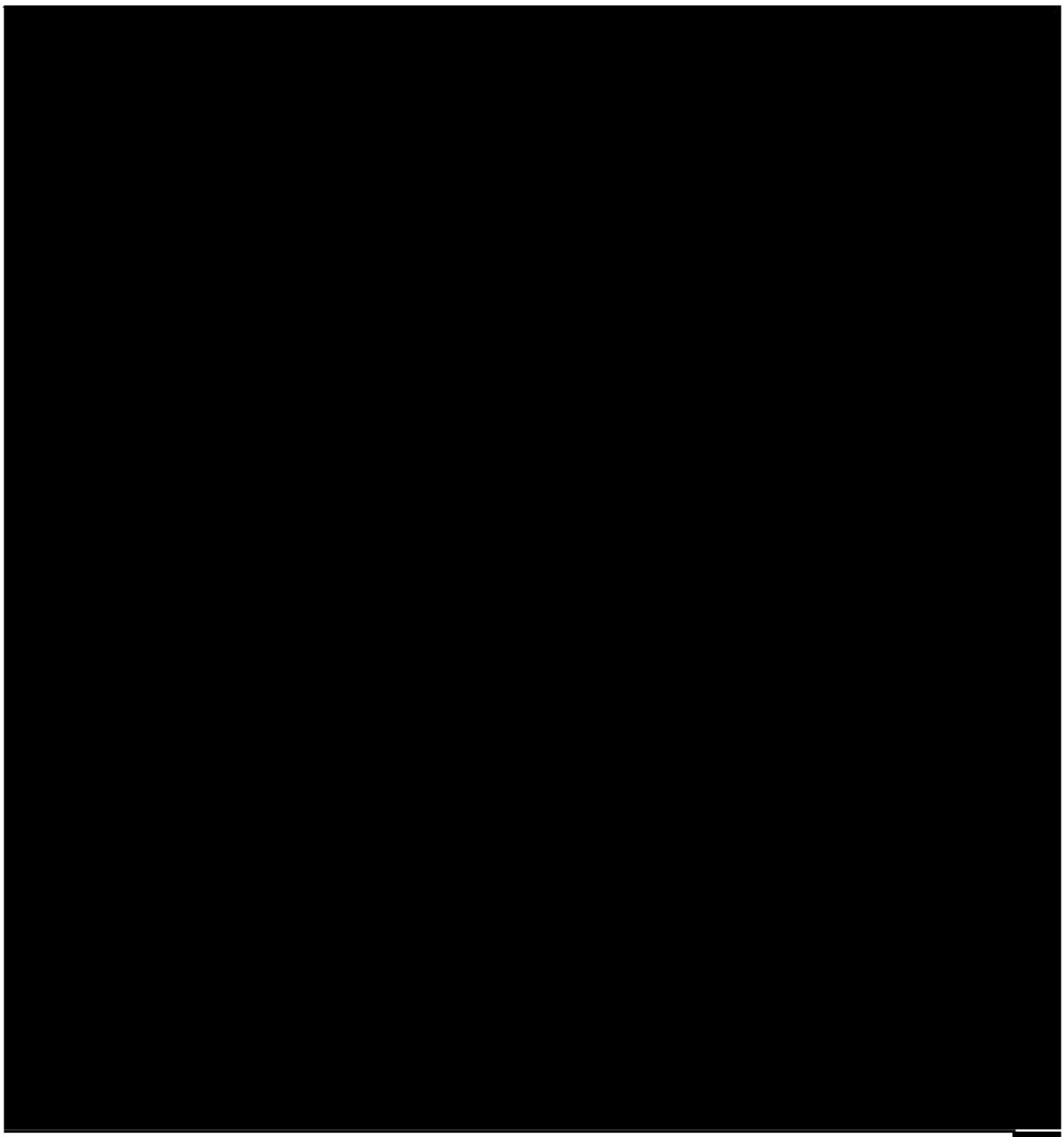

Figure 2.32—Strat 1—Openhole well log and ELAN porosity and permeability interpretations for the [redacted] first permeable interval above confining zone), [redacted] confining zone), [redacted] (injection zone). For the porosity track (second from right), the difference between total and effective porosity is the volume of clay bound water represented as brown shading. [redacted] Log header abbreviations are as follows: measured depth (MD), gamma ray (GR), resistivity (RES), neutron porosity (NPHI), bulk density (RHOB), photoelectric factor (PEF), clay volume (VCl), total and effective porosity (PhiT and PhiE), permeability (PERM).

[redacted]

[redacted] Four Corners Carbon plans to run these advanced well logs in the Injector No. 1 well in addition to standard triple combo logs. Extensive conventional coring is planned in the Injector No. 1 well to characterize the reservoir, along with sealing and geomechanical properties of the confining and injection zones. Furthermore, Injector 1 will be cored extensively with planned core analyses detailed in **Table 2.18**. The wells will be logged with openhole and cased hole logs as detailed in **Tables 2.19** and **Table 2.20**.

Table 2.18—Planned core analyses and how the data will be used to refine static and dynamic models.

Conventional Core Analysis	
Core Property	**Purpose**
Routine Core Analysis	Porosity, permeability
Wettability	Matrix-fluid interaction
Spectral Gamma Ray	Correlation
XRD/XRF	Mineralogy
Geochem	Mineralogy
MICP	Capillary entry pressure, confining layer capacity
Relative Permeability	Multi-phase flow
Electrical Properties	Tuning of reservoir model using log data
Fluid compatibility	Injectate through core to monitor physical/chemical changes
Pore water analysis	Identifications of USDW
Geomechanics	Rock strength, toughness

Notes:
MICP==mercury injection capillary pressure
XRD==X-ray diffraction
XRFS==X-ray fluorescence

Table 2.19—Planned openhole logging. (I-1 refers to Injector 1, M-1 refers to Monitor 1).

Well	Log Type	Purpose	Purpose
I-1, M-1	Caliper	Hole volume, log quality control	Hole volume, log quality control
I-1, M-1	Spectral GR	Lithology, correlation	Lithology, correlation
I-1, M-1	Neutron Porosity	Porosity, lithology	Porosity, lithology
I-1, M-1	Bulk Density	Porosity, vertical stress	Porosity, vertical stress
I-1, M-1	Acoustic log	Porosity, seismic tie in	Porosity, seismic tie in
I-1, M-1	Resistivity	Correlation	Correlation
I-1, M-1	Spontaneous Potential (SP)	Correlation, lithology	Correlation, lithology
I-1, M-1	Caliper	Hole volume	Hole volume
I-1, M-1	Spectral GR	Lithology, correlation	Lithology, correlation
I-1, M-1	Neutron Porosity	Porosity, lithology	Porosity, lithology
I-1, M-1	Bulk Density	Porosity, vertical stress	Porosity, vertical stress
I-1, M-1	Magnetic Resonance	Porosity, permeability	Porosity, permeability
I-1	Dielectric	Water volume, water salinity	Water volume, water salinity
I-1	Neutron-induced GR spectroscopy	Lithology	Lithology
I-1	Compressional/shear acoustic log	Seismic tie, geomechanical properties	Seismic tie, geomechanical properties
I-1	Acoustic imaging	Fracture identification	Fracture identification
I-1	Resistivity imaging	Fracture identification	Fracture identification
I-1	MDT with quicksilver probe	Water sampling, pore pressures, minimum horizontal stress	Water sampling, pore pressures, minimum horizontal stress

Table 2.20—Cased hole logging program for Injector 1 and Monitor 1.

Cased Hole Logging Program		
Interval	**Log**	**Purpose**
0–1,500 ft	Segmented bond log	Quality of cement bond (surface casing only)
	Ultra-sonic cement eval tool	Quality of cement bond (surface casing only)
0–TD	Segmented bond log	Quality of cement bond
	Ultra-sonic cement eval tool	Quality of cement bond
	256-arm caliper tool	Baseline casing condition
	Magnetic flux tool	Baseline casing condition
	Temperature	MIT - External

2.5.1 Fractures

Interpretation of the resistivity image logs for the Strat 1 well informs Four Corners Carbon on the expected fracture types (e.g., drilling-induced, cemented, or uncemented natural fractures), orientation of all fractures, and the minimum and maximum horizontal stress orientations near the AoR. Results indicate no open (conductive) fractures exist in the injection or primary confining zone. [redacted] the primary confining interval directly overlying [redacted], cemented fractures oriented [redacted] and dipping [redacted]° (Figure 2.22) are present. Open fractures oriented [redacted] with dips [redacted] are present within [redacted], directly above the primary confining interval (Figure 2.21). Before future CO_2 injection, Four Corners Carbon intends to collect whole and rotary sidewall cores, resistivity image logs, and acoustic image logs across [redacted] in Injector No. 1. The image logs from Injector No. 1 will allow for near wellbore fault and fracture interpretation

and a determination of how laterally extensive the open fractures within the [redacted] are.

2.5.2 Pore Pressure

Pore pressure within [redacted] was recorded in [redacted] wells within 15 miles of the Injector No. 1 location (**Figure 2.33** and **Table 2.21**). Pore pressures were measured in existing wells by perforating [redacted] and measuring the formation fluid pressure at various depths in wellbore to determine a pore pressure gradient. The average [redacted] pressure gradient calculated from [redacted] Injector No. 1 is proposed to reach the top of [redacted]. The estimated [redacted] pore pressure at this depth is [redacted] based on the average gradient from the adjacent wells. Four Corners Carbon intends to collect pressure data during the drilling of Injector No. 1 to confirm the [redacted] pressure within the AoR.

Figure 2.33—Map showing the location of wells with pore pressure gradient measurements within 15 miles of the proposed injection well.

Table 2.21—Wells with pore pressure measurements within 15 miles of Injector 1.

Well	Pore Pressure Gradient (psi/ft)
[redacted]	[redacted]
[redacted]	[redacted]
[redacted]	[redacted]

2.5.3 Stress

2.5.3.1 Vertical Stress

Measurements, such as RHOB, of the matrix density and pore fluids is required to estimate vertical stress (Sy). The well nearest to the injector with a bulk density log is the Strat 1. The bulk density log provides a preliminary estimate of the vertical stress profile (**Figure 2.34**). [redacted], as described in Section 2.5. the nearest wells with bulk density logs, listed in **Table 2.22**, are incorporated. The vertical stress calculations will be determined when additional log data are recorded in the injector well. Four Corners Carbon plans to utilize best drilling practices to ensure the best borehole conditions in Injector No. 1, so the best quality RHOB log data can be acquired.

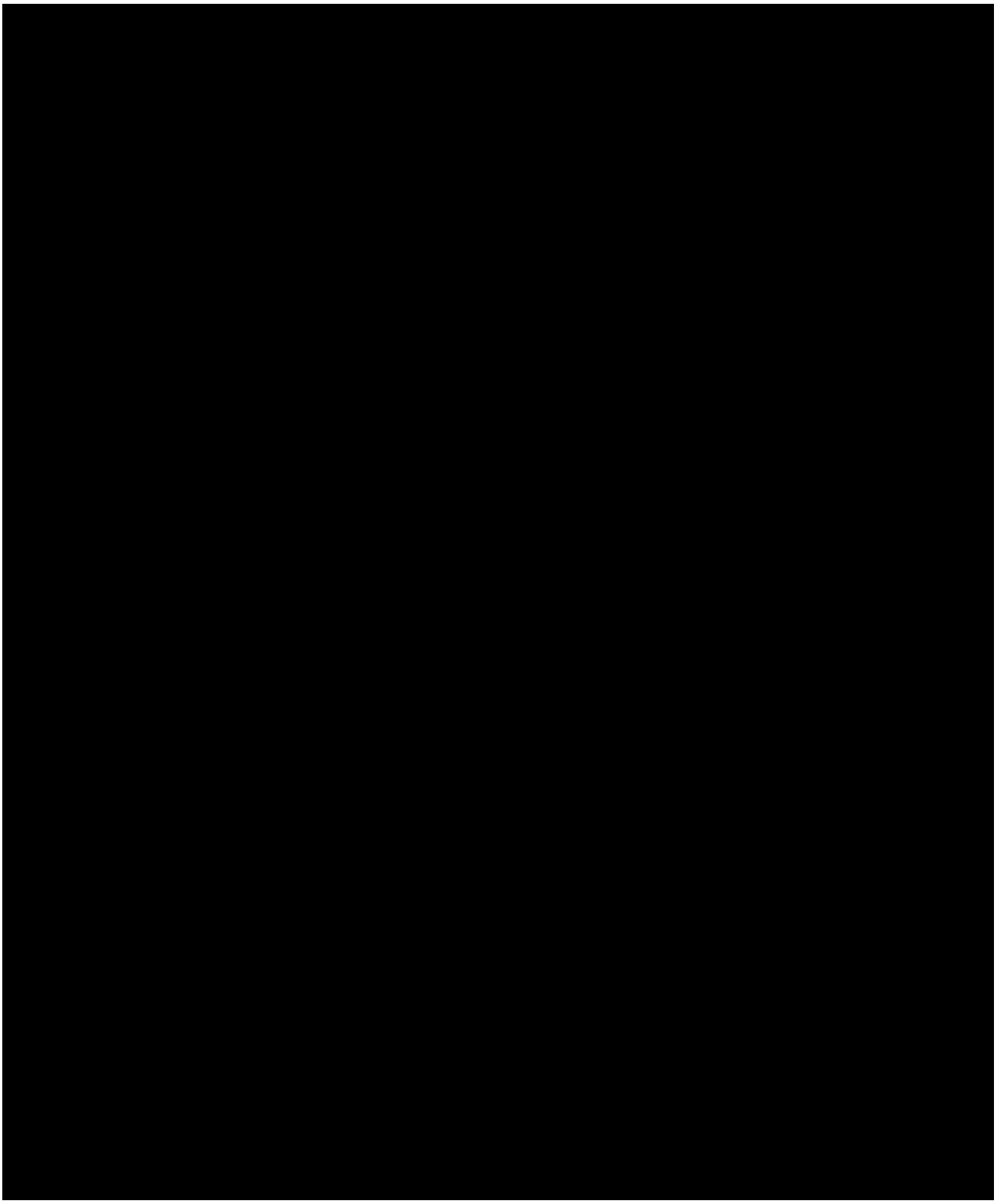

Figure 2.34—Vertical stress gradient and uncertainty range (far right track).

Table 2.22—Wells with bulk density logs nearest the proposed AoR and Strat 1.

Well Name	API	Distance to Strat 1 (miles)
[redacted]	[redacted]	[redacted]

The resulting distributions of RHOB measurements for [redacted]s plus undifferentiated logged intervals [redacted] are provided in **Table 2.23**. The overburden, or vertical stress pressures and gradients, are calculated using **Equation 2.1**, in three scenarios based on the 10th percentile (P10), 50th percentile (P50) and 90th percentile (P90) values of the RHOB log distribution using the wells in Table 2.23. The P10, P50, and P90 values are used in place of the poor-quality RHOB log measurements from [redacted] in the Strat 1. When additional log data are recorded, the vertical stress estimate will be iterated upon.

Table 2.23— Bulk density measurements [redacted] for wells in Table 2.22.

Percentile	Bulk Density (g/cc)
P10	[redacted]
P50	[redacted]
P90	[redacted]

Equation 2.1—Vertical (overburden) stress calculation.

$$S_v = P_0 + g\int_0^z \rho(z)dz$$

Where:

S_v = Vertical stress
P_0 = Pressure at surface
g = Gravitational constant
ρ(z) = Bulk density reading at depth z

Table 2.24 presents the overburden gradients and pressures for the top of the injection zone, upper and lower confining zones for each of the three scenarios.

Table 2.24—Vertical stress pressure and gradients for the key intervals based on interpretation of bulk density log from Strat 1 and offset wells to fill in data gaps.

Interval	Measured Depth at Top of Zone (ft)	Vertical Stress (S_v), psi P50 [P10 – P90]	Vert. Stress Gradient, psi/ft P50 [P10 – P90]
[redacted]	[redacted]	[redacted]	[redacted]

Minimum Horizontal Stress or Fracture Gradient

Minimum horizontal stress (SHmin) are estimated from a pore elastic stress model (**Equation 2.2**, Zoback 2007). A value of Biot's coefficient [redacted] Biot's coefficient relates the relative effect of pore pressure on effective stress and can vary depending on lithology. [redacted]. Poisson's ratio is a measure of the change in width to the change in length as a result of strain. The pore pressure and minimum horizontal stress are presented in **Table 2.25**.

Equation 2.2—Poroelastic stress model.

$$\sigma_h = \frac{\nu}{1-\nu}(\sigma_v - \alpha Pp) + \alpha Pp$$

Where:

σ_h = Minimum horizontal stress (psi)
σ_v = Vertical stress (psi)
α = Biot's Coefficient = 0.75 (unitless)
ν = Poisson's ratio = varies (unitless)
Pp = Pore pressure (psi)

.

Table 2.25—Pore pressure (Pp), minimum horizontal stress, and fracture gradient from pore elastic stress model for key zones.

Interval (Purpose)	Depth at Top of Zone (ft)	Pore Pressure (psi)	Minimum Horizontal Stress (psi)	Fracture Gradient (psi)
[redacted]	[redacted]	[redacted]	[redacted]	[redacted]
[redacted]	[redacted]	[redacted]	[redacted]	[redacted]
[redacted]	[redacted]	[redacted]	[redacted]	[redacted]
[redacted]	[redacted]	[redacted]	[redacted]	[redacted]

2.5.3.2 Maximum Horizontal Stress

Maximum horizontal stress (SHmax) orientation and magnitude will be determined once additional resistivity and acoustic image logs and dipole acoustic logs are run and interpreted in Injector No. 1. Utilizing acoustic and resistivity image logs together provides the best interpretation of stress direction, stress magnitude, and fracture conductivity. The resistivity image log can be used to enhance the interpretation of the lower resolution acoustic image log. The acoustic image log is more sensitive to stress properties than the resistivity image log and has full borehole coverage whereas the resistivity image log typically has gaps between the pads. Acoustic image logs better identify open fractures than resistivity image logs.

2.5.3.3 Stress Orientation

Two technologies are commonly used to determine the azimuth of the maximum horizontal stress: wellbore images and dipole acoustic logs. In the Strat 1 well, a resistivity imaging tool was run from [redacted] to TD. Detailed review of the resulting image log concludes that both drilling induced fractures and bore hole breakouts are present. A dipole acoustic log was also run [redacted] Borehole breakouts provide the azimuth of the minimum horizontal stress and drilling induced tensile fractures (DITF) provide the azimuth of the maximum horizontal stress. A stereonet of breakouts and drilling induced tensile fractures is provided in **Figure 2.35**. [redacted]. The average DITF / SHmax orientation is NE to SW, and the average SHmin is NW to SE. While these observations are not from the confining or injection zone, there are no known faults between these formations and the confining or injection zone, so it is reasonable to assume the stress orientation is similar. Further, the local SHmax orientation of NE-SW is similar to the regional trend from the World Stress Map (Heidbach et al. 2016).

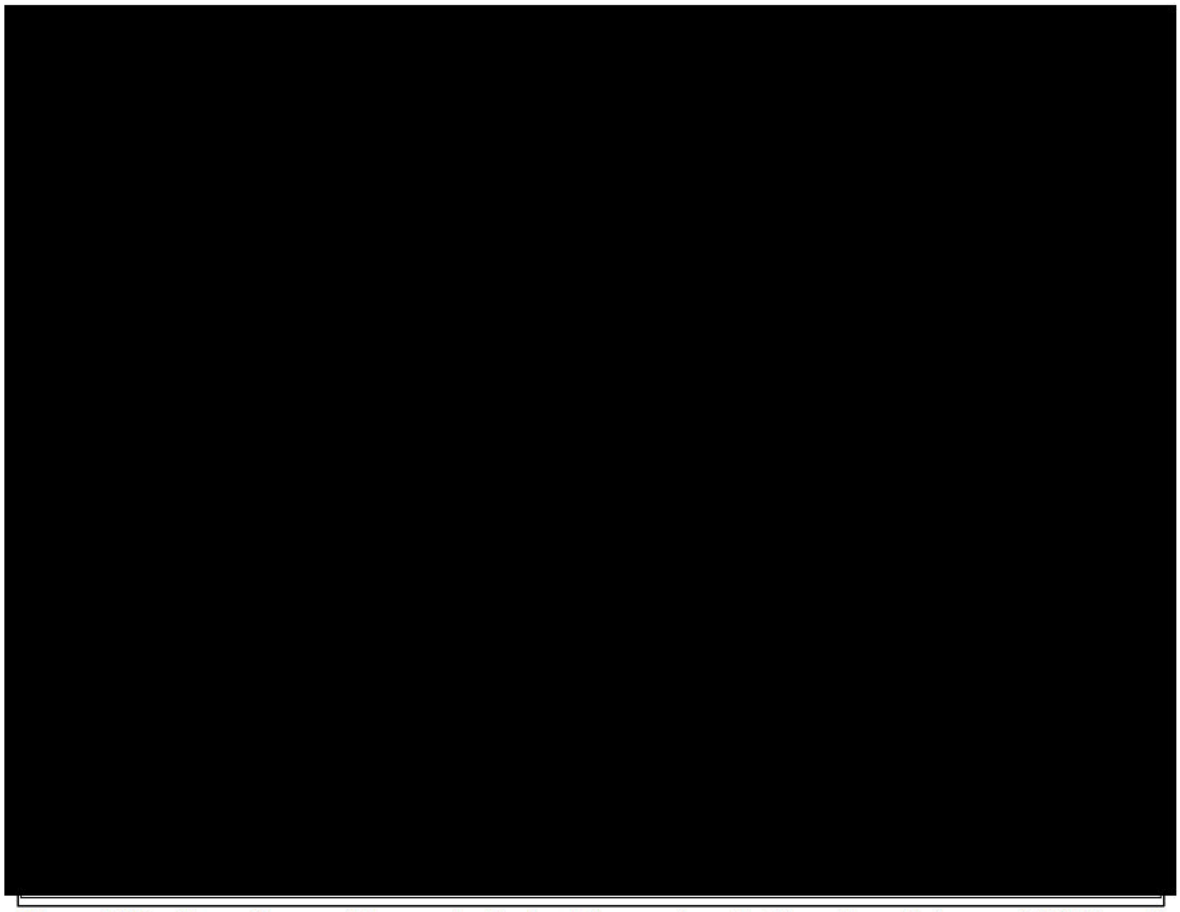

Figure 2.35—Rose diagram/stereo net of orientation and vertical location of observed DITF and borehole breakouts. The blue shaded region represents the orientation of [redacted]. As these appear as planar features cross cutting a wellbore, they are observed in a single plane, 180 degrees from each other and trend [redacted]. The red shaded region represents the [redacted] borehole breakouts and their orientation.

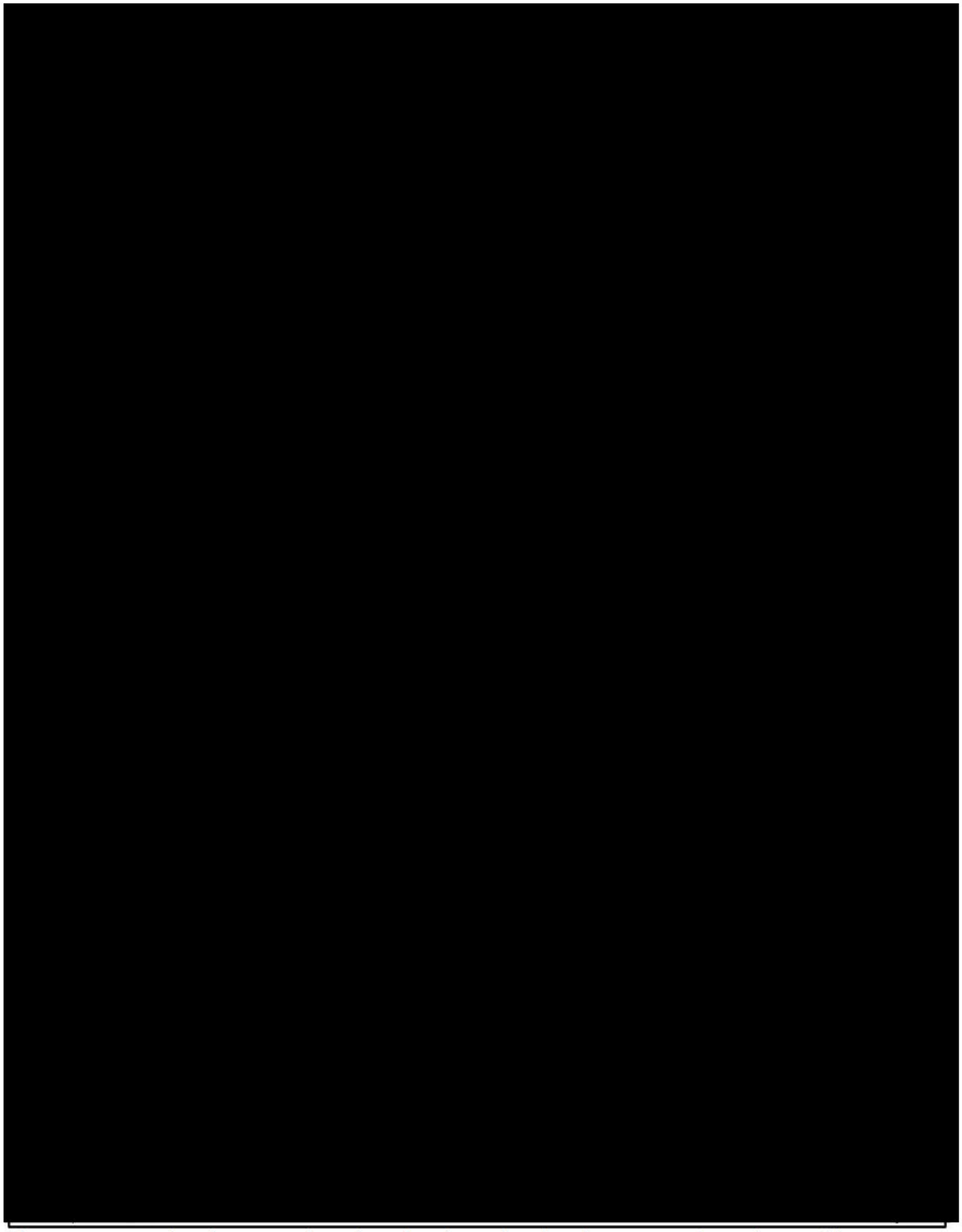

Figure 2.36—Regional stress orientations for the Colorado Plateau area from the World Stress Map (Heidbach et al. 2016).

2.5.4 Ductility

Tri-axial lab tests are planned to characterize the brittle to ductile transition at various confining pressures to better understand the behavior of the injection zone and confining layer when approaching failure. Both reservoir and confining layer samples will be selected to measure the degree of anisotropy and the potential for fracture propagation. The resulting data will be used to calibrate the mechanical earth model using lab measurements. Triaxial tests are planned for the core recovered from Strat 1 and Injector No. 1. The calibrated mechanical earth model will use log data, primarily the acoustic log, to estimate Young's Modulus and Poisson's ratio. The mechanical strength of the confining and injection zones will be compared to in-situ stresses, and, when combined with the tri-axial lab results, provide a better prediction of deformation in a brittle or ductile manner. Additional core recovery and analyses are planned for the Injector No. 1 well prior to injection.

2.5.5 Rock Strength

Rock strength measurements are planned for the core that was recovered in Strat 1. When these measurements become available, they will be used to calibrate a mechanical earth model that calculates the stress state and nature of the expected deformation. The results from triaxial strength testing will be used to define the yield strength, peak strength, and residual strength at in-situ conditions. A dipole acoustic log was acquired in Strat 1 and is currently being evaluated [redacted] Additional acoustic logging is planned for Injector No. 1.

2.5.6 In Situ Fluid Properties

Within the AoR, there are [redacted]. Thus, within the AoR, there are no measured [redacted] fluid analyses nor calculated well log salinities. [redacted] samples will be acquired in the Strat 1 well and are currently being analyzed to provide baseline geochemical information for this formation near the AoR. Adjacent wells are analyzed to interpolate [redacted] salinity within the AoR. Measured TDS values in wells within 20 miles of Injector No. 1 are presented in Table 2.30. The TDS values in these wells range from [redacted] and average [redacted] mg/L (Figure 2.8). [redacted] pore fluid salinity is calculated using the resistivity-porosity method in well [redacted] located [redacted] miles s[redacted] of Injector No. 1 (see Section 2.8 Geochemistry for details on the resistivity-porosity method). The calculated salinity values are [redacted] mg/L, corroborating the measured TDS value of [redacted] mg/L from the same well (**Figure 2.37**). The resistivity-porosity (RP) method tends to under-report salinity if any clay is present and could explain the discrepancy. Regardless, both methods indicate the salinity to be significantly greater than 10,000 mg/L.

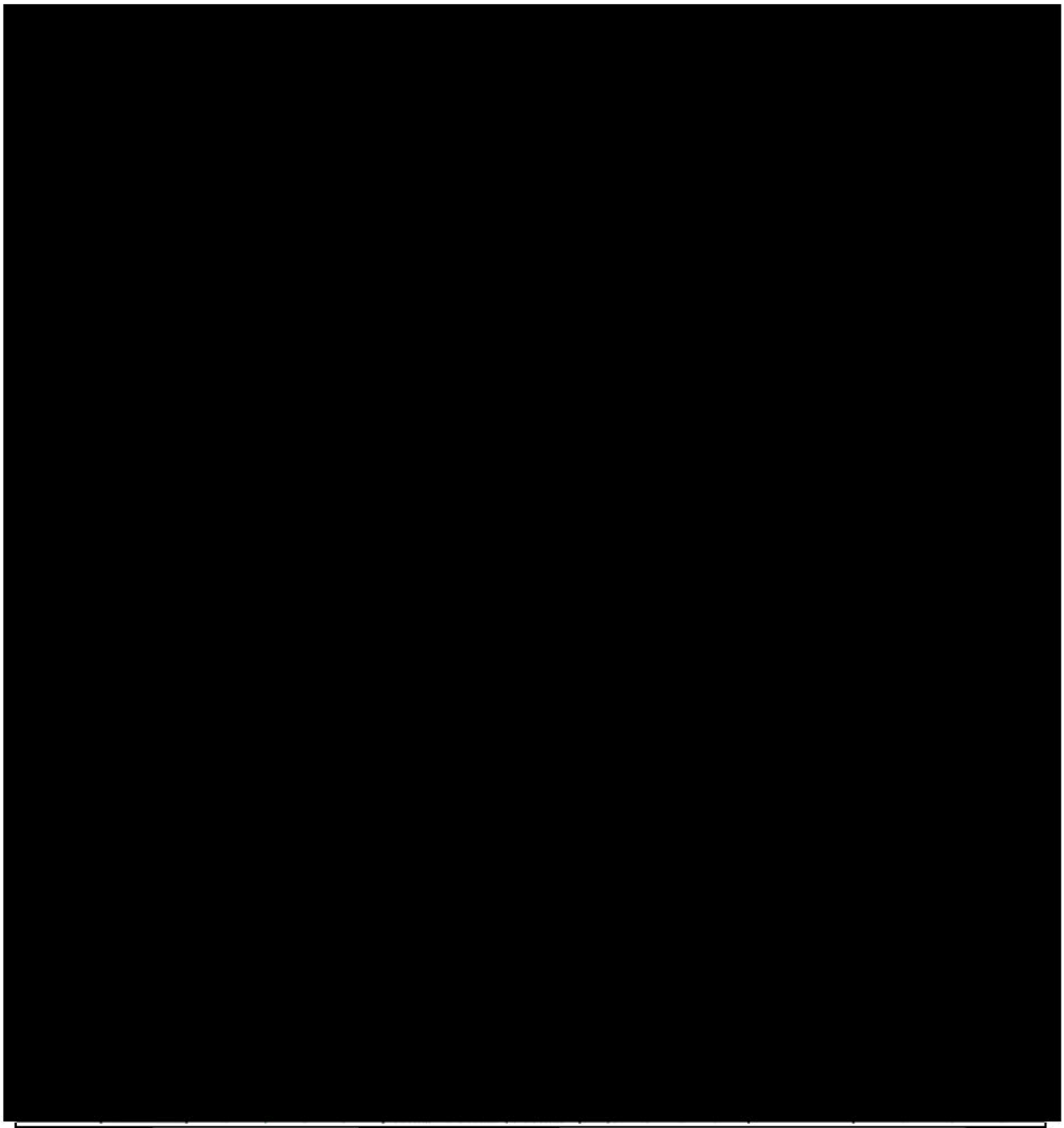

Figure 2.37— [redacted] salinity analysis of [redacted] using the resistivity-porosity method. Only clean reservoir quality sands were selected for calculation as shale and clay render the calculation meaningless.

2.5.7 Geothermal Gradient

The geothermal gradient is assumed to be 1.5°F per 100 ft TVD with a surface temperature of 60°F. These values are supported by the bottom hole temperatures recorded during openhole logging in Strat 1 and will be confirmed when Injector No. 1 is logged.

2.6 Seismic History [40 CFR 146.82(a)(3)(v)]

2.6.1 Summary of Seismic History and Available Data

Publicly available seismicity data in and around the San Juan Basin is reviewed and mapped. The public data includes historical seismic events from the USGS Earthquake Catalog[20], the New Mexico Bureau of Mines and Mineral Resources[21], and the EarthScope USArray Project[22]. Additionally, the newest edition of the USGS National Seismic Hazard Model[23], which predicts the likelihood of damaging earthquake shaking in a given area, was reviewed. Based on these data and models, the Central Basin region of the San Juan Basin is determined to be seismically inactive having very few low magnitude historical seismic events.

No recorded earthquakes had epicenters within the AoR (**Figure 2.38**). Most of the detectable seismic events in the San Juan Basin are due to mining, not earthquakes. Seismic activity from surface mining-related explosions is typically of magnitudes less than 3.0 [redacted]

2.6.2 Seismic Risk

The USGS released an updated National Seismic Hazard Model in 2018[24] to improve earthquake-resilient construction in the United States. This probabilistic model incorporates all known earthquake sources, their distances to sites, and other seismological and geological information to project the potential maximum expected ground motions in an area over a 10,000 year period. The model predicts [redacted][25]. Thus, the AoR is one of the least likely places in the western United States to be impacted by damaging earthquakes (**Figure 2.39**).

[20] https://earthquake.usgs.gov/earthquakes/search/ - accessed 3/15/2023
[21] https://geoinfo nmt.edu/repository/index.cfml?rid=20020001
[22] http://ds.iris.edu/spud/event
[23] https://www.usgs.gov/programs/earthquake-hazards/science/national-seismic-hazard-model
[24] https://www.usgs.gov/programs/earthquake-hazards/science/national-seismic-hazard-model
[25] https://www.usgs.gov/programs/earthquake-hazards/science/introduction-national-seismic-hazard-maps

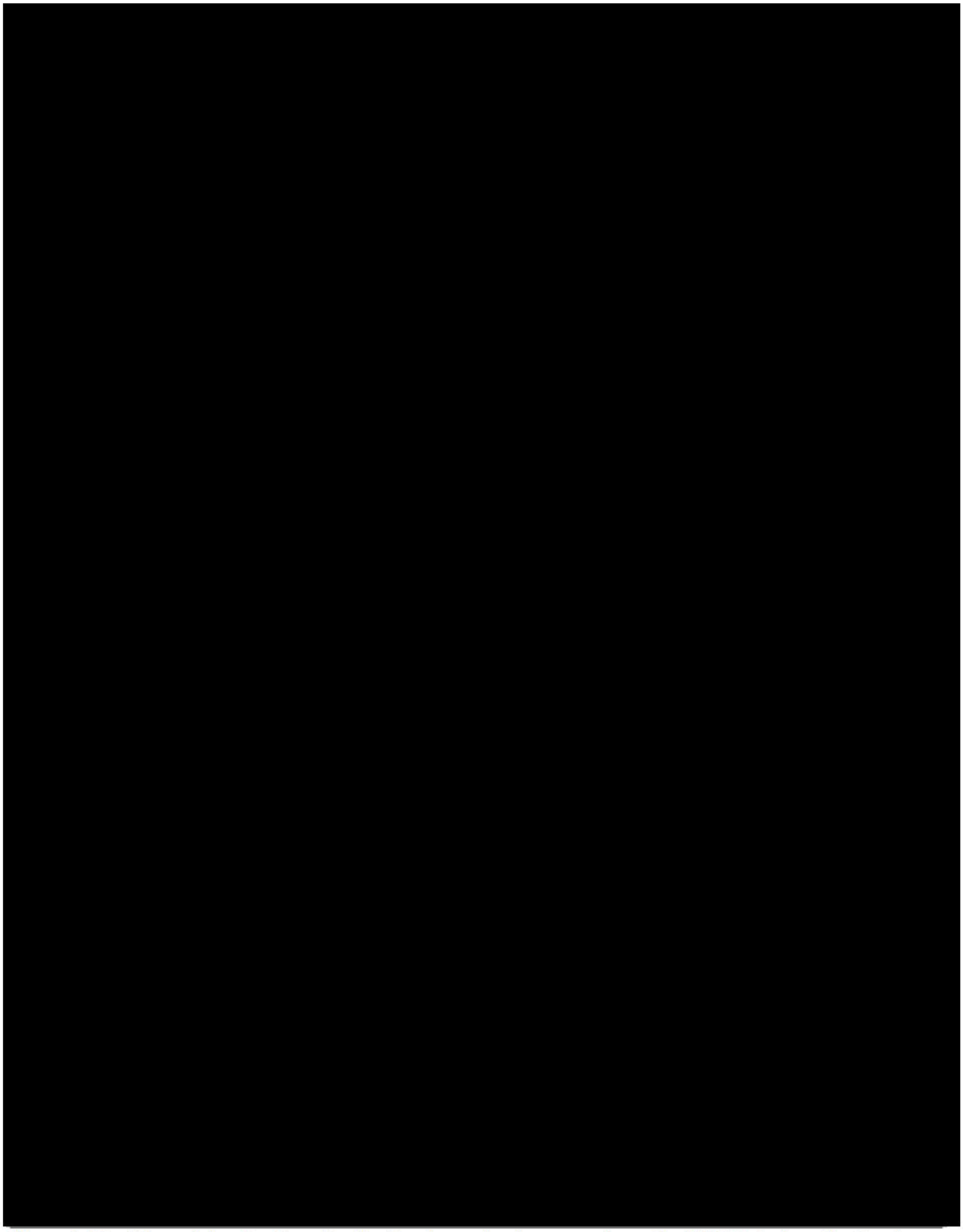

Figure 2.38—Map of the San Juan Basin showing seismic events from the USGS Earthquake Catalogue. Seismic events due to mining explosion and shown with gray circles.

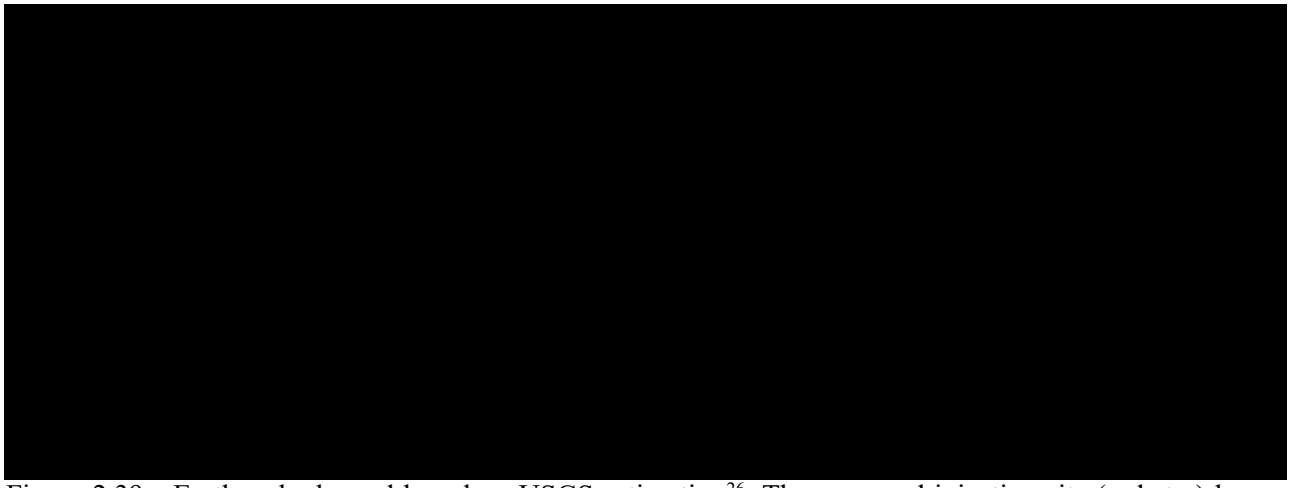

Figure 2.39—Earthquake hazard based on USGS estimation[26]. The proposed injection site (red star) has low earthquake hazard, showing low peak ground accelerations (PGA) with a 2% probability of exceedance in 50 years.

2.7 Hydrologic and Hydrogeologic Information [40 CFR 146.82(a)(3)(vi), 146.82(a)(5)]

2.7.1 Hydrostratigraphy and Underground Sources of Drinking Water

TDS and formation depth have a direct correlation (**Figure 2.40**). Kelley et al. (2014) gathered abundant data and plotted TDS versus depth for each of the water-producing units within the basin including [redacted] in descending stratigraphic order (**Figure 2.41**).

[26] https://www.usgs.gov/programs/earthquake-hazards/science/national-seismic-hazard-model

Figure 2.40—Schematic west to east cross section of the San Juan Basin illustrating that relatively fresh water (white areas) is found along the margins of the basin (after Kelley et al. 2014). Note, the water becomes increasingly saline toward the center of the basin (pink areas). USDWs within the AoR are highlighted in yellow.

Figure 2.41—TDS versus formation depth plots. Mg/L is equivalent to ppm. Expected depths and TDS concentrations within each zone are marked with a red star (after Kelley et al. 2014).

Table 2.26 is a summary of the stratigraphy and a description of major and minor aquifers that are USDWs within the AoR. The summary table provides other hydrologic characteristics including transmissivity, discharge, and specific capacity along with an estimate of vertical separation from [redacted] injection zone labeled "ft Above Inj. Zone." Preliminary screening of USDWs was accomplished by reviewing measured salinity data from literature (i.e., Kelley et al. 2014), oil and gas well data histories[27], and the USGS's Produced Water Database[28]. Site-specific screening for USDWs is refined with petrophysical and geochemical analysis presented in the Geochemistry section (2.8).

Table 2.26—Site specific San Juan Basin Area of Review stratigraphic/hydrologic summary (USDWs above injection zone).

Geologic Unit	Brief Lithology Description[1]	Top Depth (TVD, ft)	Thickness (ft)	ft Above Inj. Zone	Expected TDS (mg/L)[2]	Porosity (v/v)[3]	Transmissivity (ft^2/d)[4]	Discharge (gpm)[5]	Sp. Capacity (gpm/ft)[5]
Nacimiento	[redacted]	[redacted]	[redacted]	[redacted]	[redacted]	[redacted]	[redacted]	[redacted]	[redacted]
[redacted]	[redacted]	[redacted]	[redacted]	[redacted]	[redacted]	[redacted]	[redacted]	[redacted]	[redacted]

[1] Data from Craigg 2001.
[2] Inverse distance weighting from nearby measured TDS values, see Section 2.8.1—Fluid Chemistry for details.
[3] Data from Haerer and McPherson 2009.
[4] Data from Stone et al. 1983.
[5] Data from Levings et al. 1990.

2.7.1.1 Ojo Alamo Sandstone

The Ojo Alamo Sandstone is present in the northern region of the San Juan Basin, but pinches out between Farmington, New Mexico and the Colorado state line (Craigg 2001). [redacted] the AoR as shown in **Figure 2.42**. It lies approximately [redacted] injection zone.

[27] https://wwwapps.emnrd nm.gov/OCD/OCDPermitting/Data/Wells.aspx
[28] http://energy.cr.usgs.gov/prov/prodwat/

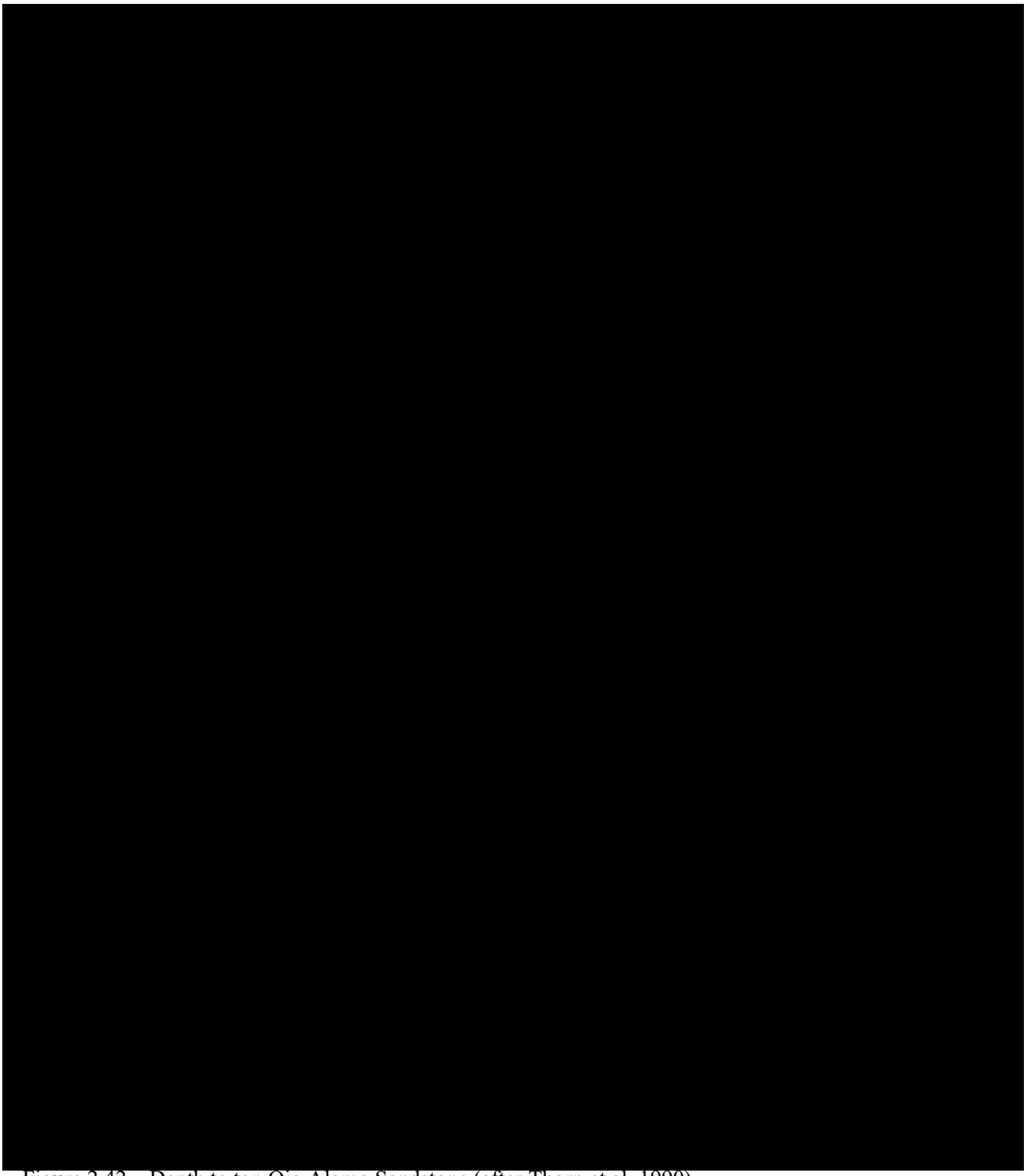

Figure 2.42—Depth to top Ojo Alamo Sandstone (after Thorn et al. 1990).

The Ojo Alamo Sandstone is a widely used source of domestic and stock water in the San Juan Basin. Small springs originate from sandstone beds within this stratigraphic interval, and it is recharged by water discharging from overlying sandstone beds of the Nacimiento Formation.

Cooley and Weist (1979) noted that sandstone beds are moderately cemented by silica, clay and iron-rich minerals and that the presence of cementation is the principal factor controlling permeability and yield. Based on TDS concentration data gathered near the AoR, [redacted] for this project. **Figure 2.43** confirms the USDW character of the aquifer.

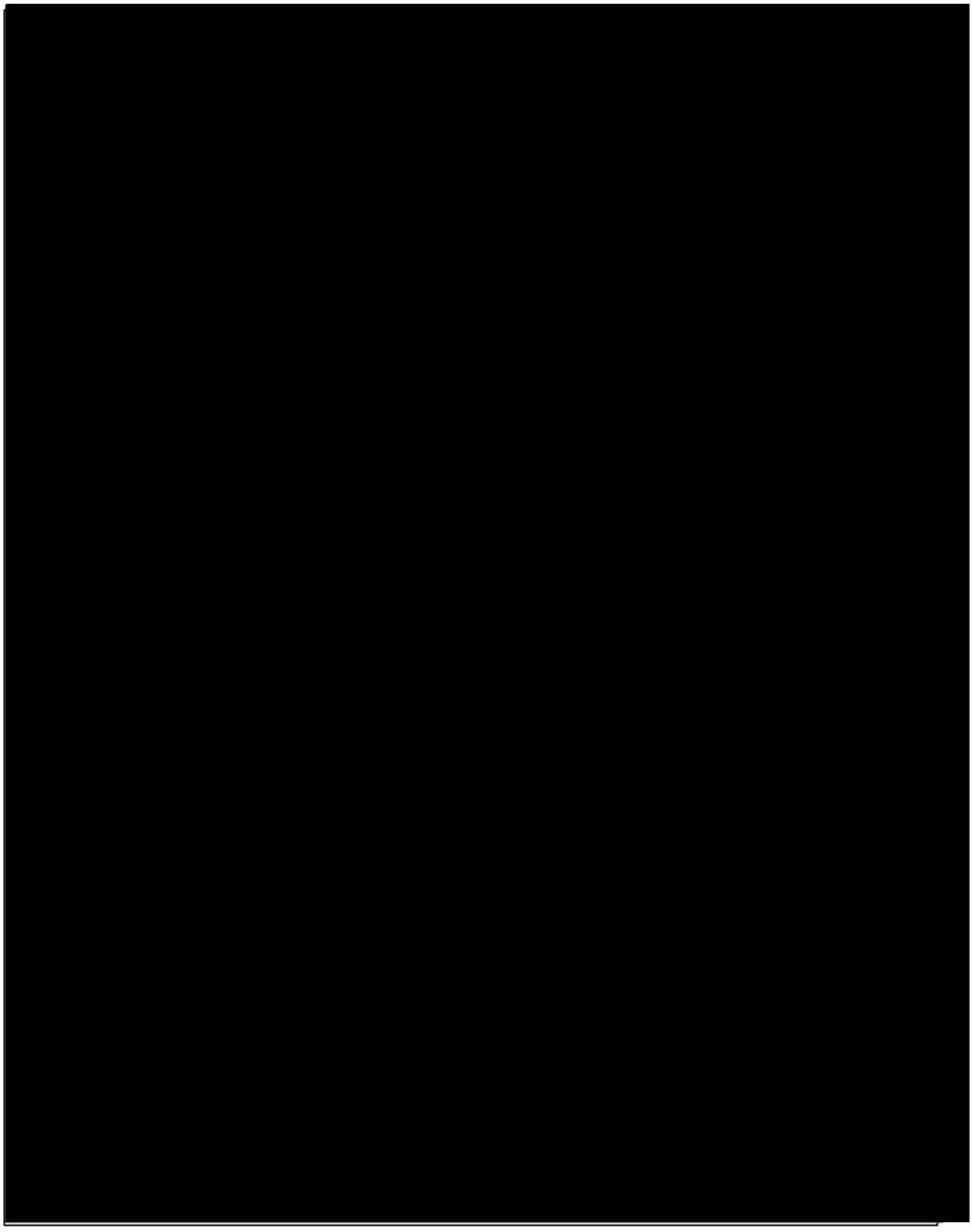

Figure 2.43—Total dissolved solids concentrations of the Ojo Alamo Sandstone within a 20-mile buffer of the Injector No.1 location. Structural contours

Ojo Alamo Sandstone specific capacity varies from 0.02 gpm/ft to 2.04 gpm/ft drawdown with a median of 0.28 gpm/ft (Levings et al. 1996). Discharge rates in the vicinity of the AoR range from [redacted] The Ojo Alamo Sandstone has an average porosity and permeability of 0.18 v/v and 200 mD, respectively for Tertiary sandstone units (Haerer and McPherson 2009).

Specific conductance near recharge areas can be as low as 1,000 µmhos (800 mg/L TDS) but range as high as 9,000 µmhos (7,200 mg/L TDS) in the deeper regions of the basin (Stone et al. 1983). Despite the range in specific conductance, [redacted]

2.7.1.2 Nacimiento Formation

The Nacimiento Formation is present in the northern region of the basin and notably [redacted]. Thickness ranges from 500 ft to 1,300 ft (Craigg 2001) in the basin with approximately [redacted]). The base of the Nacimiento Formation is approximately [redacted]. Based on the general trend of water level elevations data collected in the AoR, the gradient appears to be toward [redacted]

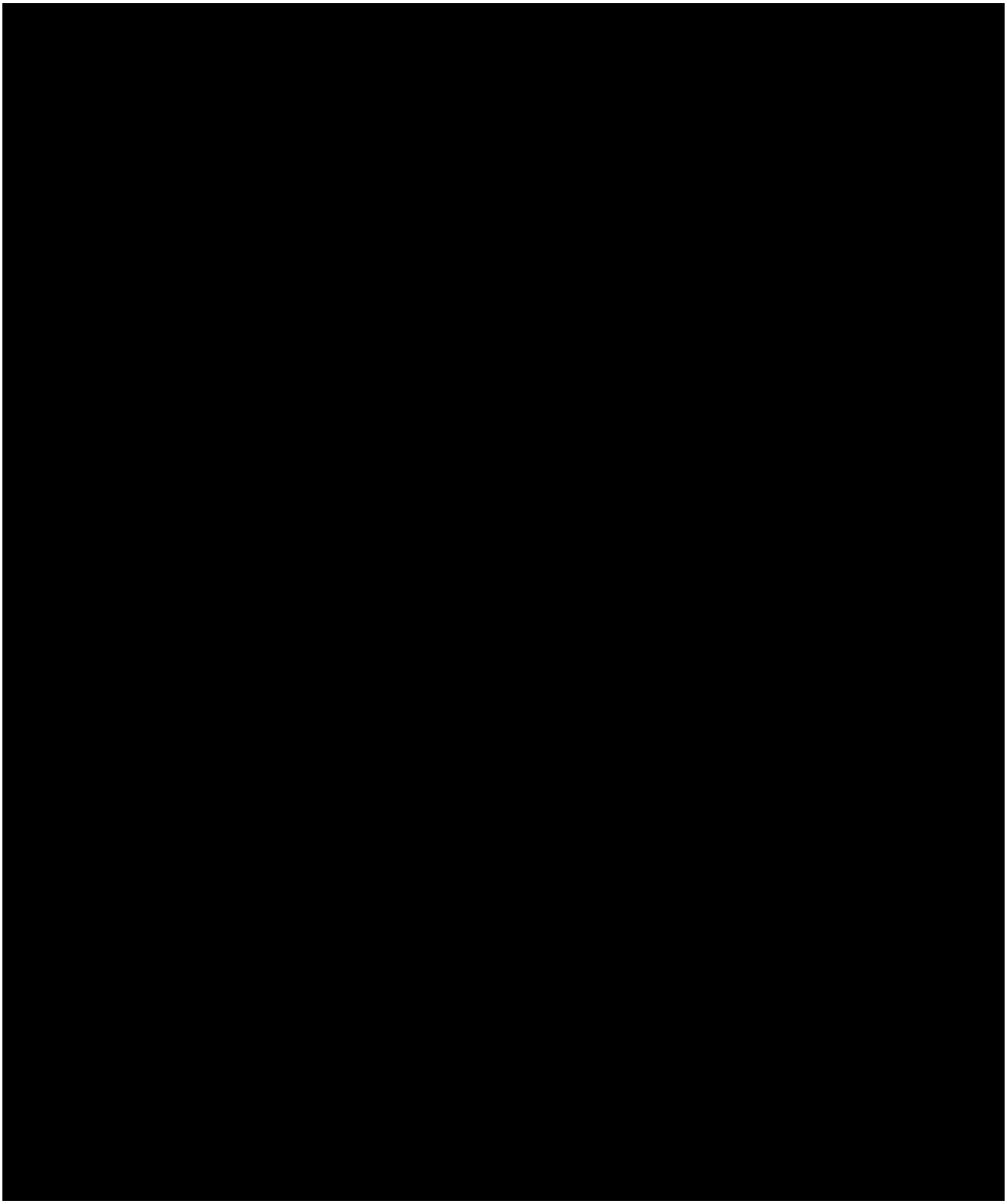

Figure 2.44—San Jose, Nacimiento, and Animas isopachs (after Levings et al. 1990).

The Nacimiento Formation yields small amounts of water to a few wells from discontinuous, fine-grained sandstone bodies indicating that the formation is probably only used as a local aquifer, though sandstones in the northeastern region of the basin may be a source of water to wells. In the southwestern region of the San Juan Basin, a thick shaly sequence in the overlying San Jose Formation separates the San Jose Formation water from the water contained in the underlying Ojo Alamo Sandstone. Water from wells tapping the Nacimiento Formation is used for domestic and stock purposes on ranches; however, it may locally contain high levels of TDS (Cooley and Weist 1979). Based on TDS concentration data collected near the AoR, the [redacted]

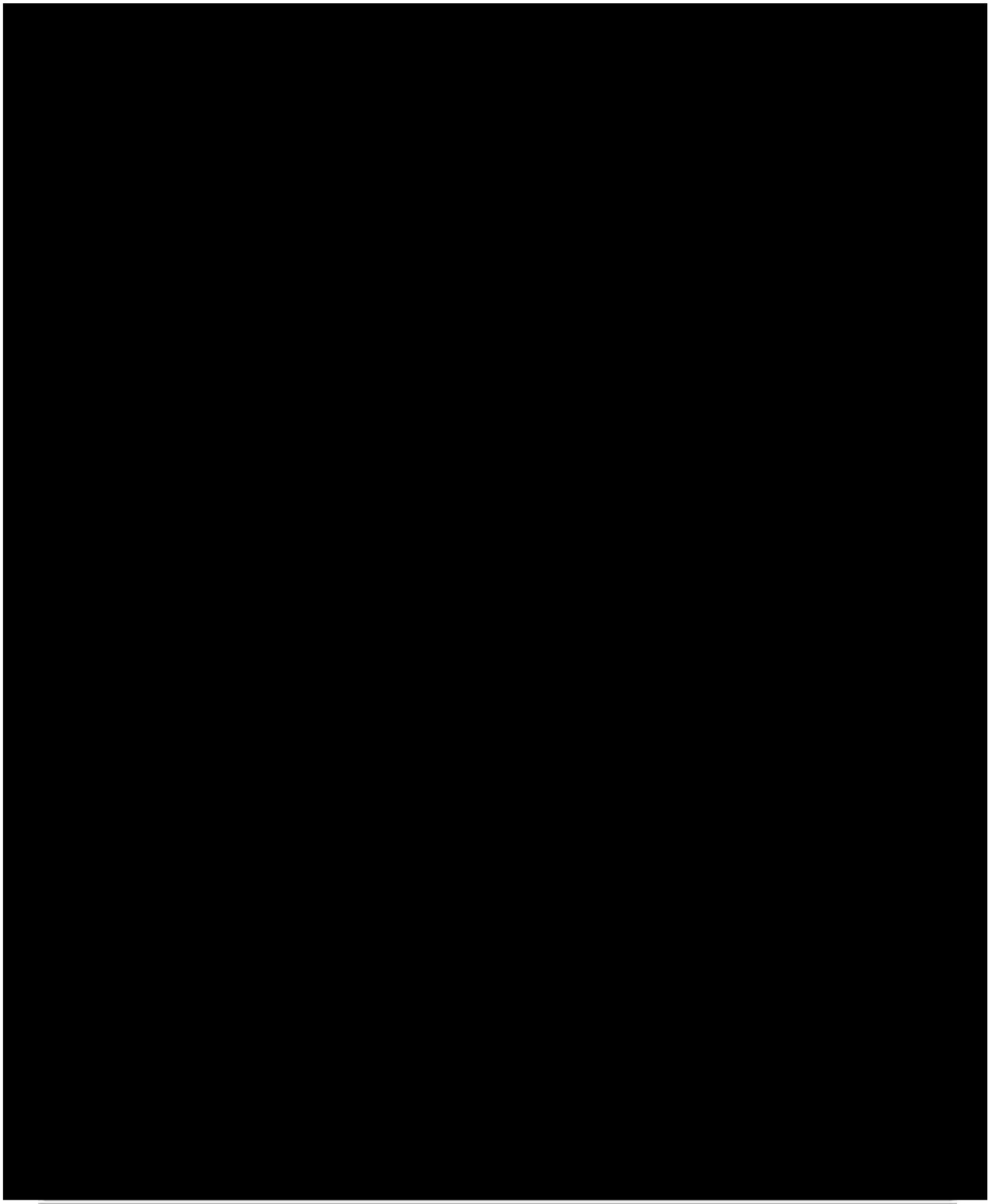

Figure 2.45—TDS concentrations of the Nacimiento Formation within a 20-mile buffer of the Injector 1 location. Structural contours end [redacted]

Specific capacity varies from 0.03 gpm/ft to 0.8 gpm/ft drawdown with a median of 0.24 gpm/ft drawdown (Levings et al. 1996). Discharge rates range from 2 gpm to 70 gpm (Haerer and McPherson 2009) and are [redacted] the AoR (Levings et al. 1990). Stone et al. (1983) noted that transmissivity can be as high as 100 ft^2/D. Specific capacity data cited in Kernodle (1996) suggests a range from 0.24–2.3 gpm/ft drawdown. The Nacimiento Formation has an average porosity and permeability of 0.18 v/v and 200 mD, respectively for Tertiary sandstone units (Haerer and McPherson 2009).

Specific conductance near recharge areas can be as low as 1,500 µmhos (1,200 mg/L TDS) but is generally greater than 2,000 µmhos (1,600 mg/L TDS) in finer-grained strata (Stone et al. 1983). Lyford (1979) noted that salinity increases in the direction of groundwater flow. Water collected from the Nacimiento Formation along the San Juan River yields a specific conductance of 4,000 µmhos (3,200 mg/L TDS). Data reported by Levings et al. (1990) suggests that the TDS concentration in the vicinity of the AoR [redacted]. Given the range in specific conductance, the Nacimiento Formation [redacted]

2.7.2 Springs

There are no springs within the Area of Review. The nearest spring identified in the USGS's NHD[29] is [redacted]

2.7.3 Water Wells Within the Area of Review

There are [redacted] water wells within the Area of Review found in the New Mexico Office of the State Engineer's (OSE) Points of Diversion (POD) database[30] (**Table 2.27**, **Figure 2.46**). All four wells are active— [redacted]
The deepest well is drilled to 195 ft below ground surface (bgs). Based on these depths, [redacted]

Table 2.27—Water well within the Area of Review from the New Mexico Office of the State Engineer's Points of Diversion database. [redacted].

		PLSS			Location (NAD83)		Drill	Depth		
POD Name	Owner	TWS	RNG	SEC	Lat	Lon	Date	(ft, bgs)	Status	Use
[redacted]										

[29] https://www.usgs.gov/national-hydrography/national-hydrography-dataset
[30] https://services2.arcgis.com/qXZbWTdPDbTjl7Dy/arcgis/rest/services/OSE_PODs/FeatureServer – Accessed 3/31/2023

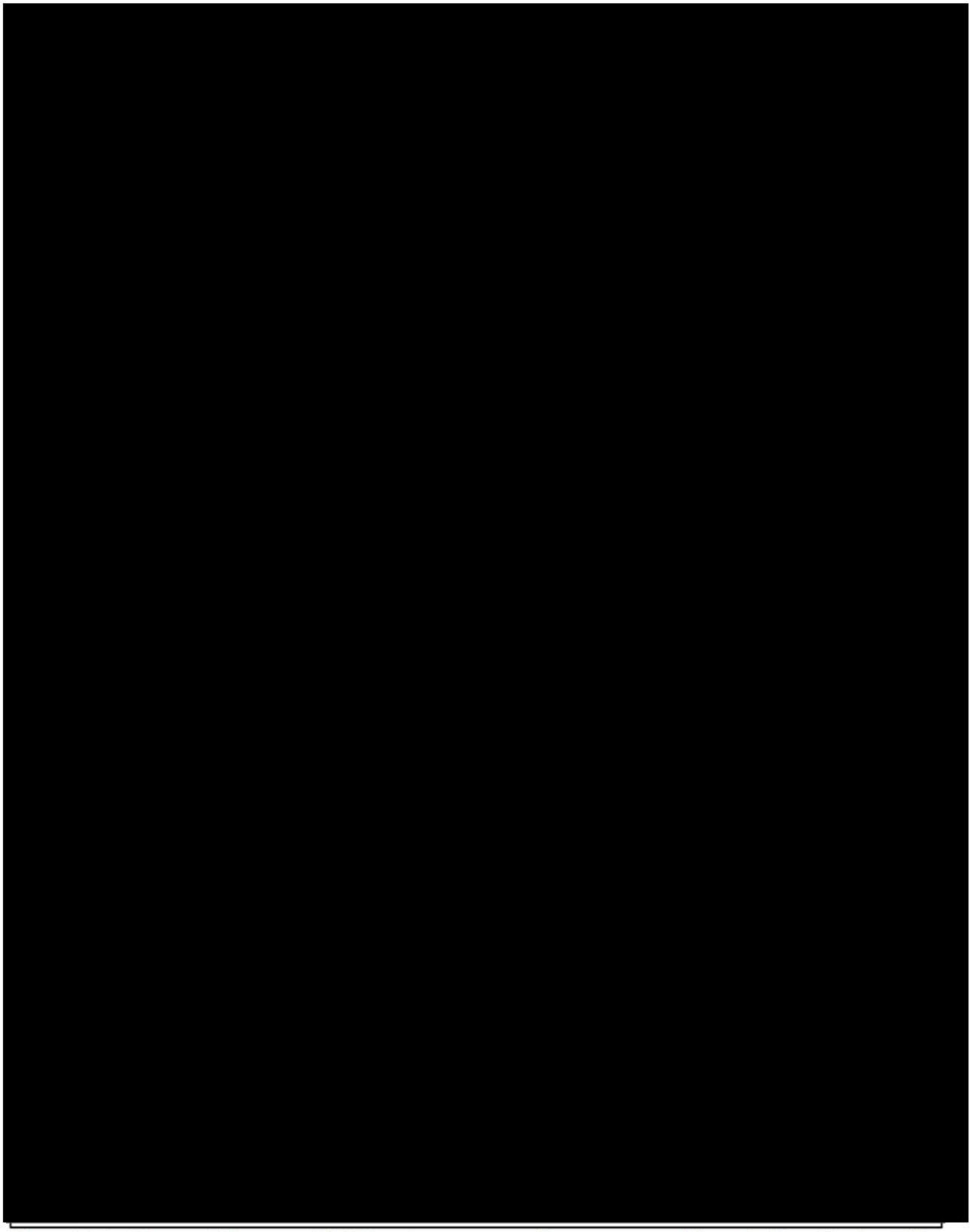

Figure 2.46—Water well basemap. Well locations, status, and use are sourced from the New Mexico Office of the State Engineer's Points of Diversion database. No springs are present within the AoR or mapped area.

2.8 Geochemistry [40 CFR 146.82(a)(6)]

Understanding the geochemistry of aquifers, confining layers, and pore fluids is essential to evaluate the suitability of CO_2 storage sites. Four Corners Carbon reviewed existing fluid- and solid-phase geochemical data of potential injection and confining zones in the San Juan Basin along with geochemical studies in other analogous basins to understand how geochemical reactions may affect CO_2 trapping mechanics, confining zone integrity, and storage capacity at the proposed Project site. This extensive research supports the conclusion that [redacted] has sufficient storage capacity for planned CO_2 injection volumes, has an insignificant risk of releasing trace elements, and has a confining layer capable of confining CO_2 over long periods. These conclusions will be further confirmed via future site-specific data collection from dedicated wells drilled within the AoR. Solid- and fluid-phase geochemistry data will be collected from Four Corners Carbon's Injector No. 1 during and post-drilling, providing baseline geochemical information within the proposed AoR (Refer to Section 6.0, Pre-Operational Logging and Testing).

Solid- and fluid-phase samples have been collected from a stratigraphic characterization well, Strat 1, located [redacted] the AoR and are currently being analyzed. Conventional core was taken across [redacted] which is the first permeable unit above the confining zones, [redacted] confining zone, and the [redacted] injection zone. Core plugs will be taken to evaluate porosity, permeability, total organic carbon, and water content. Petrographic thin-section analysis, electron microscopy, and XRD will be used to assess mineralogy and elemental composition. In addition to core, fluid samples will be collected from [redacted] in Injector No. 1 to confirm that it is not a USDW. Fluid samples from [redacted] will also provide baseline geochemical information including the major ions, pH, alkalinity, total organic carbon, trace metals, stable isotopes, and evaluate CO_2 solubility. Once the collected samples have been analyzed, the data will be used as inputs to model fluid-rock interactions.

No solid- or fluid-phase geochemical data existed in the injection or confining zones within 10 miles of the Injector No. 1 well prior to the Strat 1 being drilled. This initial study included measured and calculated salinity values from nearby wells and incorporated solid-phase data from analogous basins, including the adjacent Paradox and Chama Basins, to compensate for the absence of data. Solid- and fluid-phase geochemical data sources include the USGS Produced Waters Database[31], oil and gas well histories[32], peer-reviewed articles, and dissertations. These data are summarized in **Table 2.29**, in Sections 2.8.1 and 2.8.2, and as an attachment (**Fluid Geochemistry Data.xlsx**).

[redacted] identified as candidates for openhole log-based salinity calculations, [redacted] spontaneous potential (SP) log was used to estimate the pore water salinity. The SP method is a method to calculate formation salinities using SP deflection from a determined baseline, formation temperature, and the resistivity of the mud filtrate. **Table 2.28** provides a description of the parameter inputs and resulting outputs for the equation as follows (**Equation 2.3**; Bassiouni 1994).

[31] http://energy.cr.usgs.gov/prov/prodwat/
[32] https://wwwapps.emnrd nm.gov/OCD/OCDPermitting/Data/Wells.aspx. Accessed 05/2023.

Table 2.28—Various parameter combinations tested for similarity to SP method salinities including water resistivity from temperature and spontaneous potential.

Input	Description
SP Log	Baseline shifted such that shale baseline = 0 mV
Formation Temperature	See discussion. 65°F at surface, 1.5°F/100 ft
Rmf	From log header
Rmf Temperature	Temperature at which Rmf measurement was taken.

Output	Description
RwSP	Resistivity of formation water from SP method (OhmM)
Salinity	Converts Rw to NaCl-equivalent salinity. Salinity = 10^((3.562-LOG$_{10}$(RwSP-0.0123))/0.955) [Baker Atlas 2002]

Equation 2.3—Bassiouni (1994).

$$RwSP = \frac{R_{mf}}{10^{Essp/-K}}$$

Where:

Rmf = resistivity of mud filtrate (Ωm)
Essp = maximum deflection of SP log from shale baseline (mV)
K = 61.3 + 0.133 (formation temp [°F])
Limitations: where Rmf > 0.10 Ωm

A temperature profile was calculated for [redacted] a 60°F formation temperature at the surface, and a temperature gradient of 1.5°F/100 ft. The resulting temperature profile was checked against the recorded bottom hole temperature (BHT) and was determined to be a good approximation and did not warrant further consideration of BHT anomalies due to irregularities in elapsed time since circulation was stopped. The SP log was baseline shifted such that the shale baseline is 0 millivolt (mV). The resulting salinity profile is presented in **Figure 2.48.**

The resistivity-porosity or RP method (**Equation 2.4**) for salinity estimation was applied to [redacted]

Equation 2.4—Resistivity-porosity or RP method for salinity estimation.

$$Rwa = \frac{Rt * \Phi^m}{a}$$

Where:

Rt = true resistivity of formation (usually approximated by deep resistivity)
Φ = total porosity
m = Archie's cementation exponent

No lab measured values for m, the cementation exponent, were available; therefore, the Humble equation coefficients were used. For the Humble equation assumptions, the cementation exponent

[redacted] If any clay is present, the resulting salinity calculation will underestimate salinity rather than overestimate salinity levels.

2.8.1 Fluid Chemistry

Table 2.29—Summary table of measured and calculated TDS values for relevant zones within a 20-mile buffer of the Injector 1 well.

Zone	Significance	Depth to Top of Zone (ft)	Avg. Measured TDS (mg/L)	Log Calc. TDS (mg/L)	Expected TDS (Inverse Distance Weighing, mg/L)
[redacted]					

[1] Utilized a depth versus TDS trend to determine the expected TDS value within the AoR.

2.8.1.1 Injection Zone—[redacted]

[redacted] pore fluids are analyzed in the basin's multiple oil, gas, and water disposal wells. Preliminary results indicate tha[redacted] in the AoR; however, there are [redacted] analyses or wells with logs across [redacted] fluid samples will be collected in the Strat 1 well and are currently being analyzed to provide baseline geochemical information near the AoR. Adjacent wells have been used to interpolate [redacted] salinity within the AoR and these values of measured TDS for wells within 20 miles of Injector No. 1 are presented in **Figure 2.47** and **Table 2.30**.

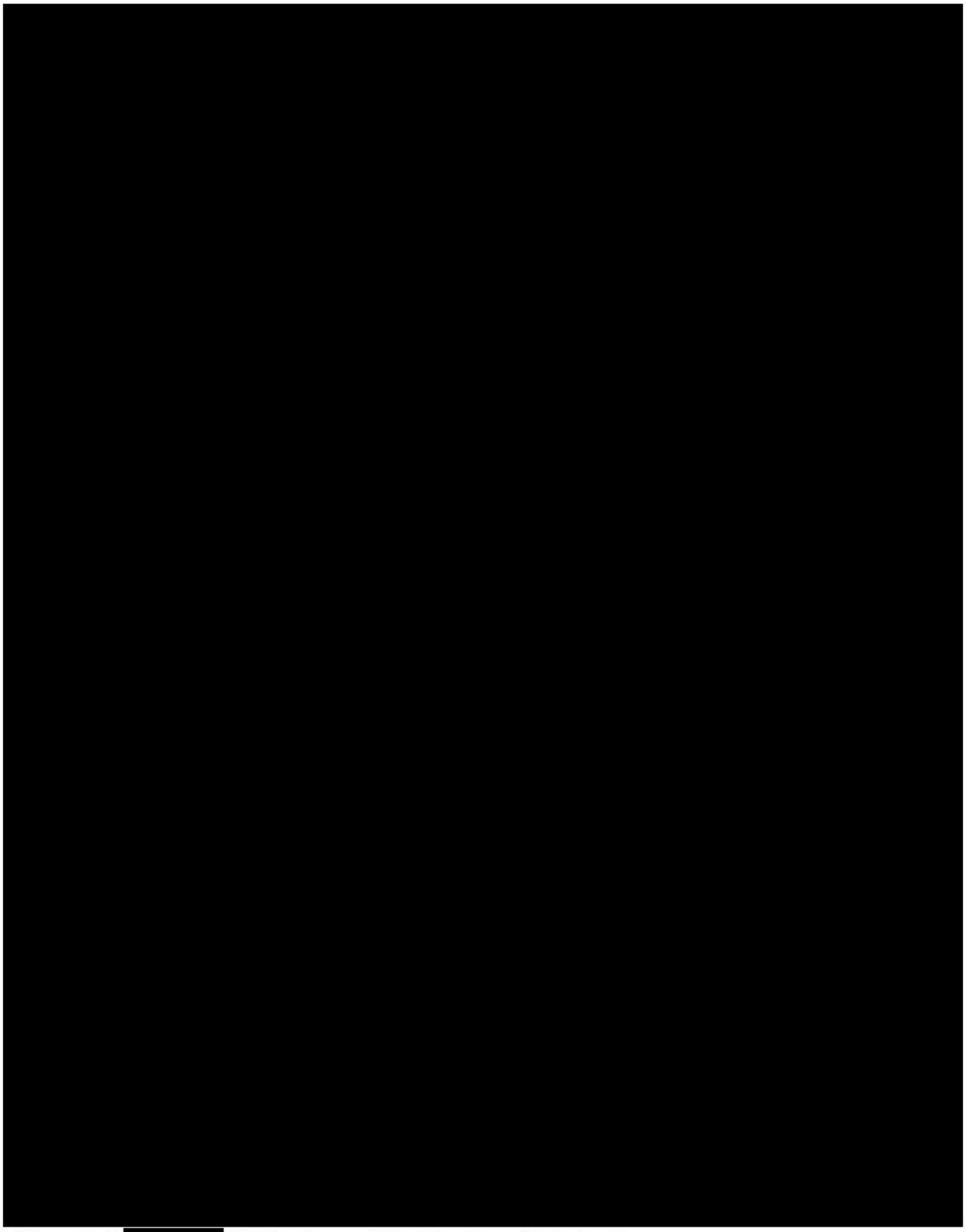

Figure 2.47 [redacted] TDS values within 20 miles of Injector 1

Table 2.30—Measured TDS values of [redacted] pore fluids within a 20-mile buffer of the Injector 1 well.

Well API	Latitude[1]	Longitude[1]	Avg. TDS (mg/L)[2]	Distance to Injector 1 (miles)
[redacted]	[redacted]	[redacted]	[redacted]	[redacted]
[redacted]	[redacted]	[redacted]	[redacted]	[redacted]
[redacted]	[redacted]	[redacted]	[redacted]	[redacted]
[redacted]	[redacted]	[redacted]	[redacted]	[redacted]
[redacted]	[redacted]	[redacted]	[redacted]	[redacted]

[1] NAD83
[2] The average measured TDS value is recorded for wells with multiple fluid analyses.

The TDS values in [redacted] wells range from [redacted] and average [redacted] pore fluid salinity is calculated using the resistivity-porosity method (Equation 2.4) in [redacted] of Injector No. 1 (**Figure 2.48**). The expected [redacted] pore fluid TDS at Injector No. 1 is [redacted]. It is calculated using an inverse distance weighting of all measured TDS values within a 20-mile buffer of Injector No. 1, where the closest TDS data points to Injector No. 1 have a greater impact on the expected TDS value than data points that are farther away.

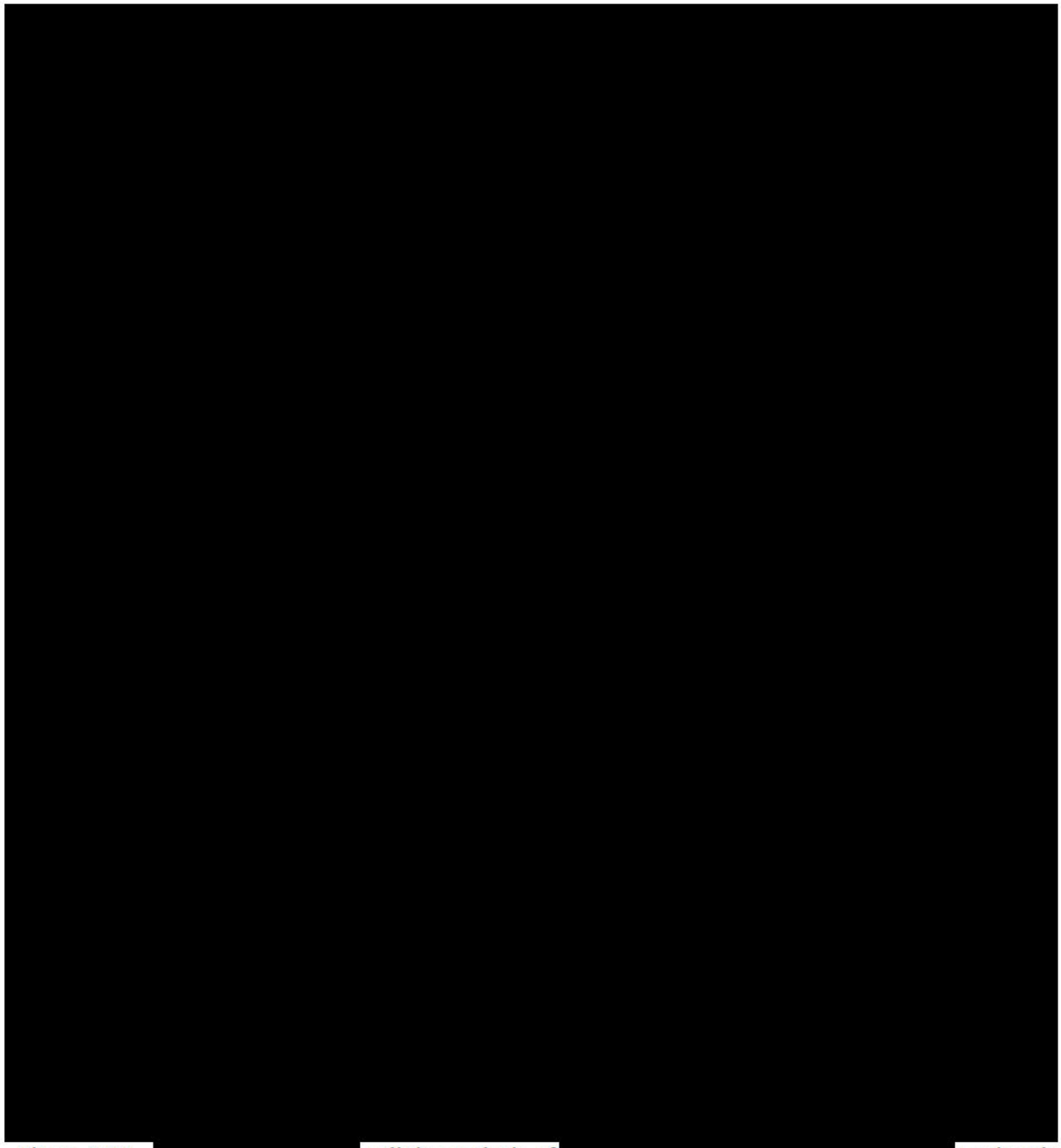

Figure 2.48— salinity analysis of s using the resistivity-porosity method. Only clean reservoir quality sands were selected for calculation as shale and clay render the calculation meaningless.

The calculated salinity values are which corroborates the measured TDS value of from the same well. To confirm this result, Four Corners Carbon plans to collect and analyze fluid samples from Injector No. 1 well before injection to confirm

2.8.1.2 Confining Layer—[redacted]

No analyses of fluid samples collected from [redacted] were located for the Central Basin region of the San Juan Basin. Within the AoR the expected [redacted] porosity ranges from [redacted] and permeability ranges from [redacted].

2.8.1.3 First Permeable Zone Above the Confining Layer—[redacted]

[redacted] fluid samples were collected and analyzed in three wells within 20 miles of the planned Injector No. 1 well. The TDS values in these wells range from [redacted] (**Table 2.31** and **Figure 2.49**).

Table 2.31—Measured TDS values of [redacted] pore fluids within a 20-mile buffer of Injector 1 well.

Well API	Latitude[1]	Longitude[1]	Avg. TDS (mg/L)[2]	Distance to Injector 1 (miles)
[redacted]	[redacted]	[redacted]	[redacted]	[redacted]
[redacted]	[redacted]	[redacted]	[redacted]	[redacted]
[redacted]	[redacted]	[redacted]	[redacted]	[redacted]

[1] NAD83
[2] The average measured TDS value is recorded for wells with multiple fluid analyses.

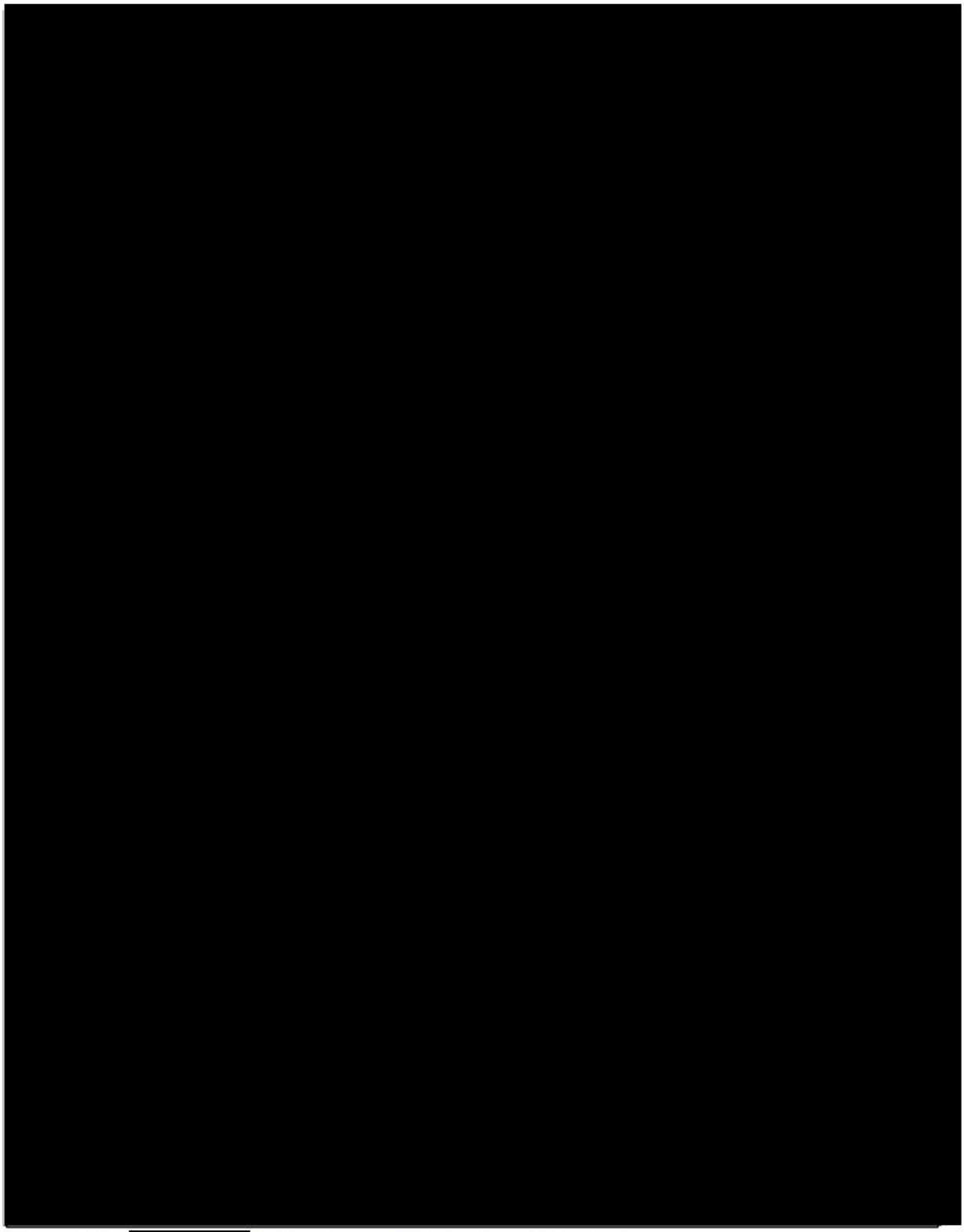

Figure 2.49— [redacted] TDS values within 20 miles of Injector 1.

To supplement the measured TDS values in the vicinity of the AoR, [redacted] pore fluid salinity is calculated using the resistivity-porosity method (Equation 2.4) i [redacted] planned Injector No. 1 well. The calculated salinity value is [redacted] The expected [redacted] TDS at Injector No. 1 is [redacted], which is calculated using an inverse distance weighting method. Based on the measured and calculated salinity values near the AoR, the [redacted] is [redacted]

2.8.1.4 Underground Source of Drinking Water—[redacted]

Fluid samples were collected and analyzed from [redacted] from nine locations within a 20-mile buffer of well Injector No. 1 (**Figure 2.50**). The TDS values in these wells range from [redacted] and average [redacted] Detailed analyses from collected samples are provided in **Table 2.32**. The expected [redacted] pore fluid TDS at Injector No. 1 is [redacted] which is calculated using an inverse distance weighting method. Based on these data, [redacted]

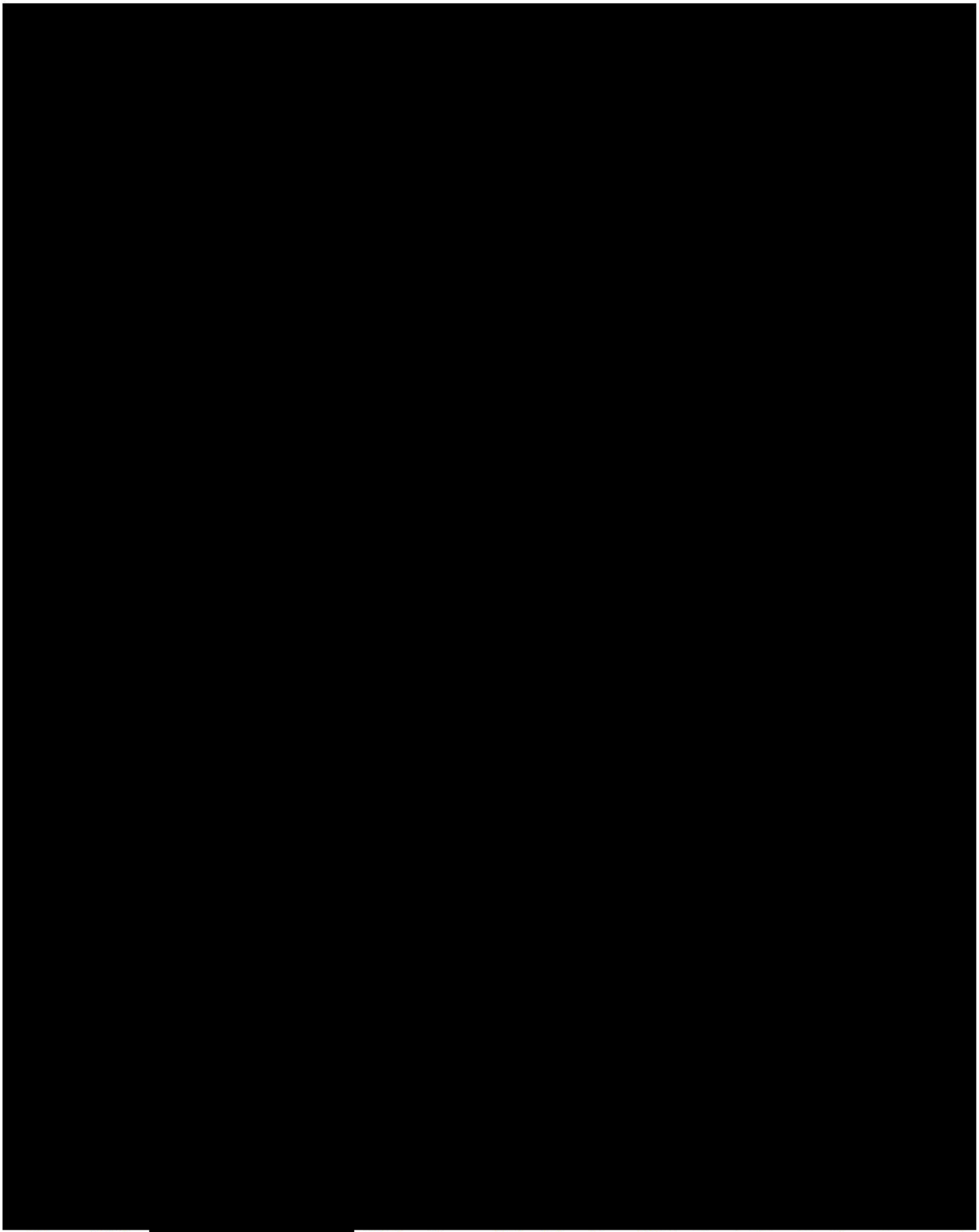

Figure 2.50— TDS values within 20 miles of Injector 1. Structural contours end because the outcrops throughout the study area.

Table 2.32—Measured TDS values of [redacted] fluids within a 20-mile buffer of the Injector 1 well.

Location Identifier	Latitude[4]	Longitude[4]	Avg. TDS (mg/L)[2]	Distance to Injector 1 (miles)
[redacted]				

[1] Data was acquired and measured by [redacted]
[2] The average measured TDS value is recorded for wells with multiple fluid analyses.
[3] Site ID from data collected from the USGS Produced Waters Database (http://energy.cr.usgs.gov/prov/prodwat/). Accessed 4/2023.
[4] NAD83

2.8.1.5 Lowermost Underground Source of Drinking Water—[redacted]

Fluid samples were collected and analyzed from the [redacted] in two locations within a 20-mile buffer of well Injector No. 1 (**Figure 2.51**). The TDS values in these wells range from [redacted] Detailed analyses from collected samples are provided in **Table 2.33**. The expected [redacted] TDS at Injector No. 1 is [redacted] which is calculated using an inverse distance weighting method. Based on these data, [redacted]

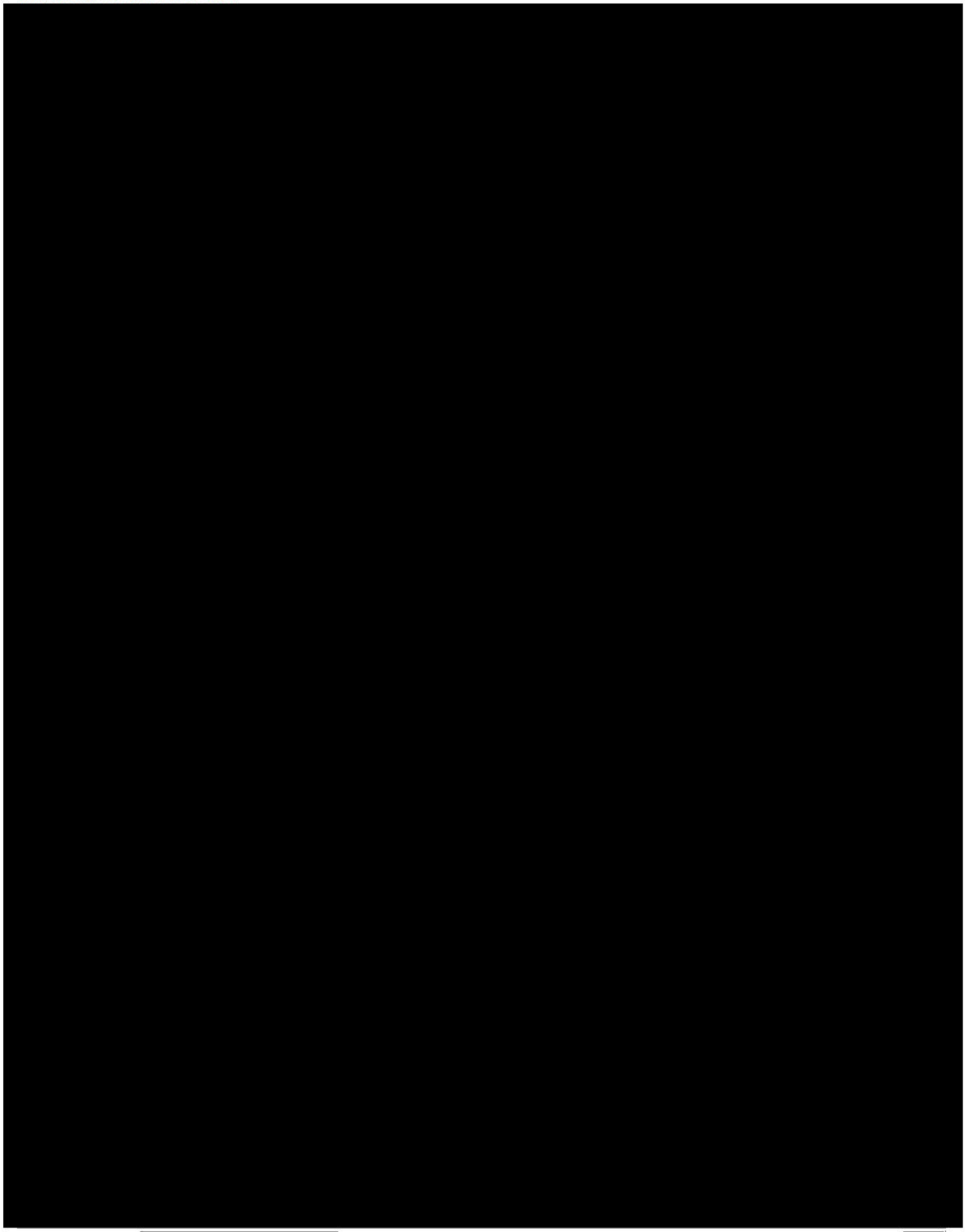

Figure 2.51— TDS values within 20 miles of Injector 1. Structural contours

Table 2.33—Measured TDS values of the [redacted] pore fluids within a 20-mile buffer of the Injector 1 well.

Location Identifier	Latitude[1]	Longitude[1]	Avg. TDS (mg/L)[2]	Distance to Injector 1 (miles)
[redacted]	[redacted]	[redacted]	[redacted]	[redacted]

[1] NAD83
[2] The average measured TDS value is recorded for wells with multiple fluid analyses.
[3] Site ID from data collected from the USGS Produced Waters Database (http://energy.cr.usgs.gov/prov/prodwat/). Accessed 4/2023.

2.8.1.6 Non-USDWs Within the Area of Review

Measured TDS values and petrophysical calculations for wells within a 20-mile buffer of the future Injector No. 1 well suggest that all zones below the [redacted] (Table 2.29).

[redacted]

Within a 20-mile buffer of the Injector No. 1 well, 194 fluid samples were collected and analyzed [redacted]. Average measured TDS for this collection of samples is [redacted] (**Figure 2.52** and **Figure 2.53**). The expected [redacted] pore fluid TDS at Injector No. 1 is [redacted] which is calculated using an inverse distance weighting method.

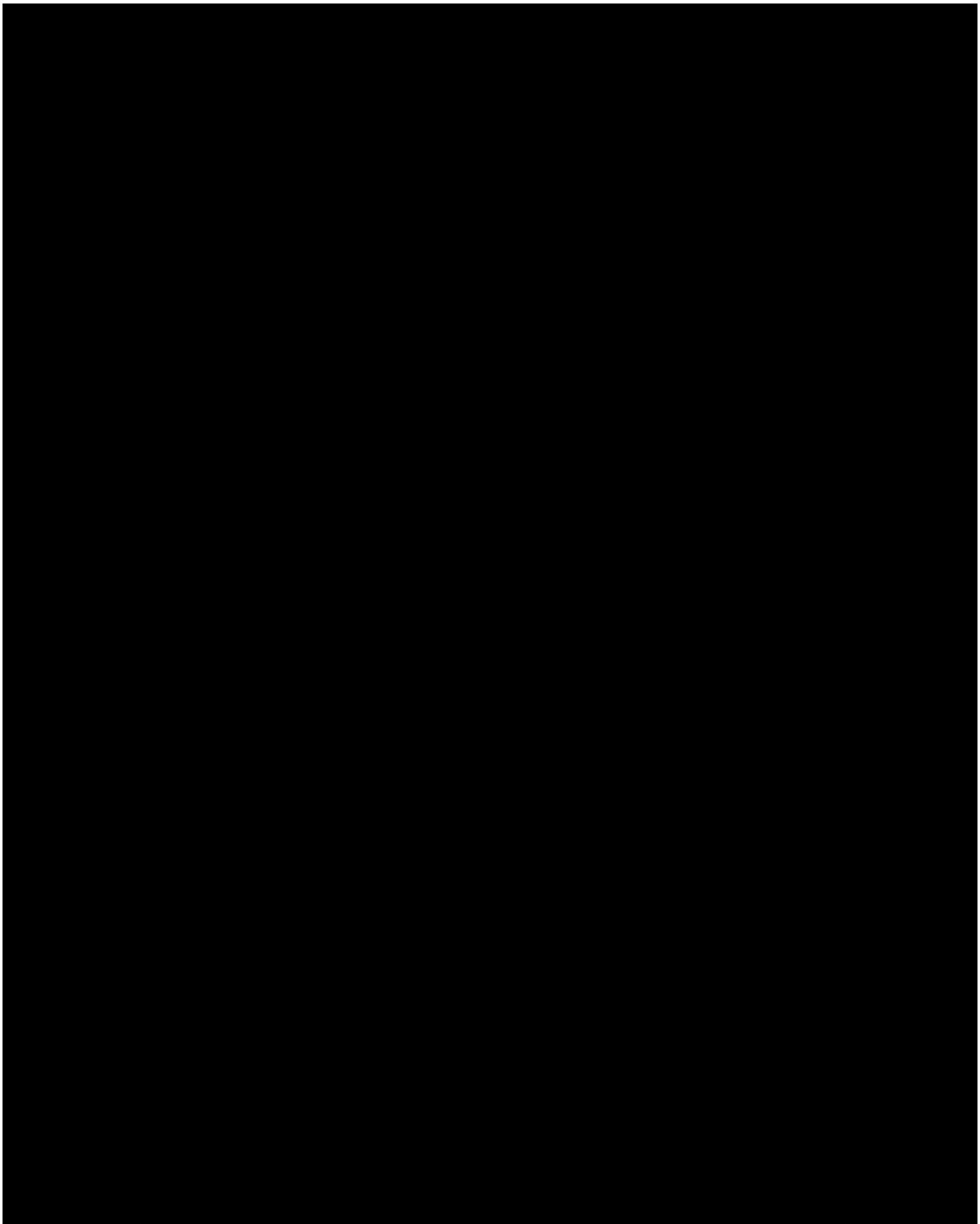

Figure 2.52— TDS values within 20 miles of Injector 1. Structural contours .

Figure 2.53—Histogram of the measured TDS values in the [redacted] within a 20-mile buffer of the AoR [redacted]

[redacted]

The [redacted] unconformably underlies the [redacted] The average measured TDS in the [redacted] from the six samples collected within a 20-mile buffer of the future Injector No. 1 well is [redacted] (**Table 2.34** and **Figure 2.54**). Petrophysical calculations from [redacted] indicate an average salinity of [redacted] using the SP method (**Figure 2.55**). The expected [redacted] e TDS at Injector No. 1 is [redacted] which is calculated using an inverse distance weighting method of measured salinity data.

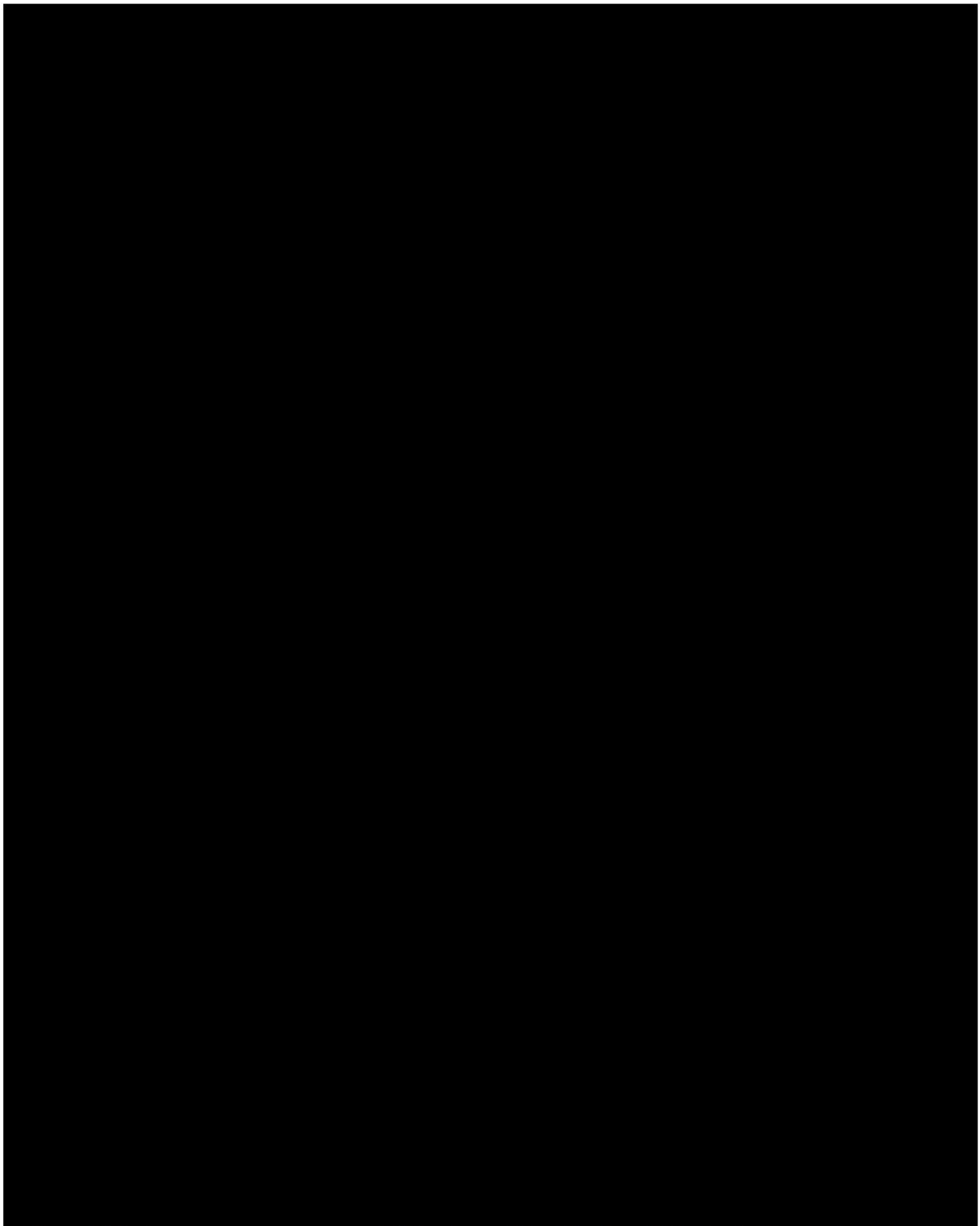

Figure 2.54— TDS values within 20 miles of Injector 1. Structural contours

Table 2.34—Measured TDS values of [redacted] fluids within a 20-mile buffer of the Injector 1 well.

Well API	Latitude[1]	Longitude[1]	Avg. TDS (mg/L)[2]	Distance to Injector 1 (miles)
[redacted]				

[1] NAD83
[2] The average measured TDS value is recorded for wells with multiple fluid analyses.

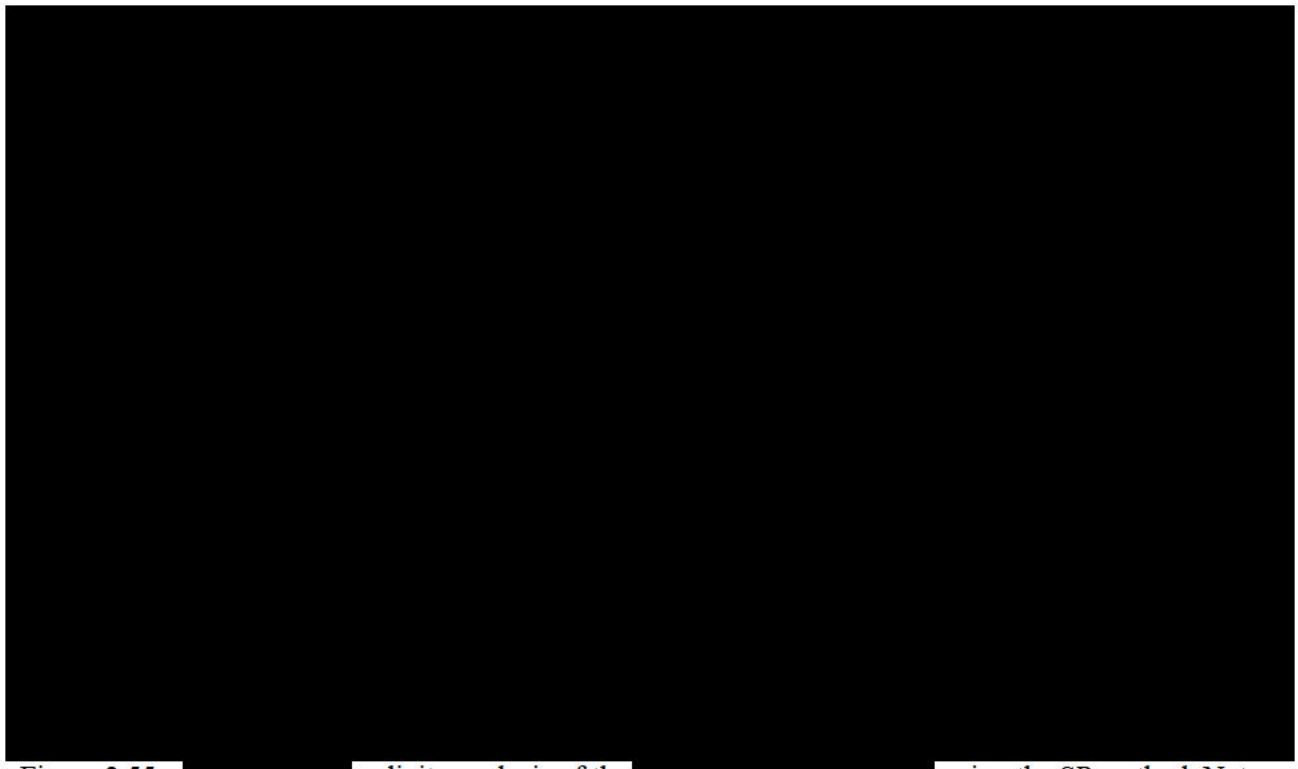

Figure 2.55—[redacted] salinity analysis of the [redacted] using the SP method. Note: The SP based salinity estimate is not valid in shaley sands, shales or thin (less than 10 ft). The track to the right of the resistivity track shows an interval where the SP salinity calculation is valid, and averaged [redacted] mg/L.

[redacted]

Below the [redacted] is the [redacted] which consists of the [redacted] t. Measured TDS values of the [redacted] near the AoR range from [redacted] mg/L and average [redacted] mg/L (**Figure 2.56** and **Table 2.35**).

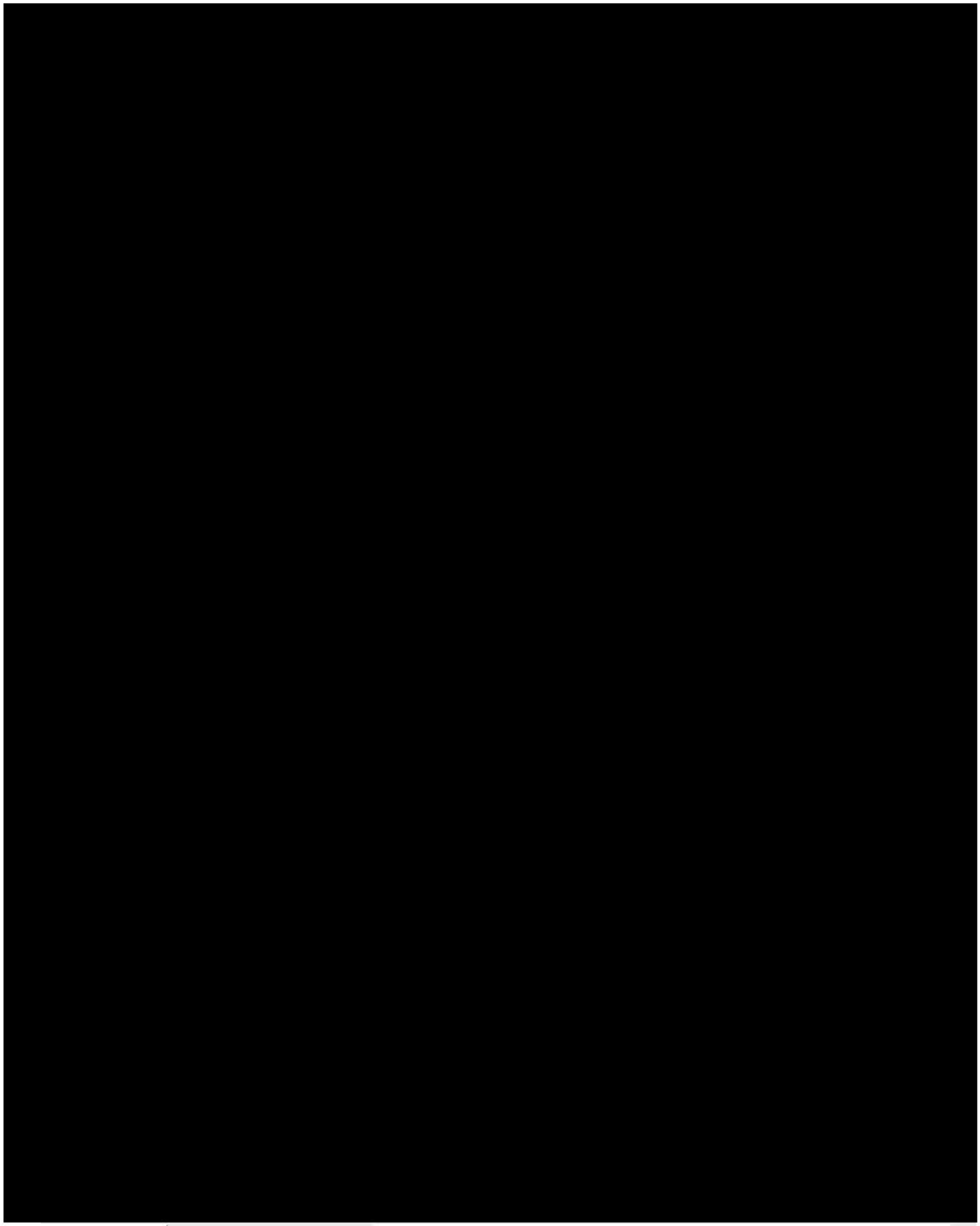

Figure 2.56— TDS values within 20 miles of Injector 1. Structural contours

Table 2.35—Measured TDS values [redacted] fluids within a 20-mile buffer of the Injector 1 well.

Well API / Site ID	Latitude[1]	Longitude[1]	Avg. TDS (mg/L)[2]	Distance to Injector 1 (miles)
[redacted]	[redacted]	[redacted]	[redacted]	[redacted]
[redacted]	[redacted]	[redacted]	[redacted]	[redacted]
[redacted]	[redacted]	[redacted]	[redacted]	[redacted]

[1] NAD83
[2] The average measured TDS value is recorded for wells with multiple fluid analyses.
[3] Site ID from data collected from the USGS Produced Waters Database (http://energy.cr.usgs.gov/prov/prodwat/). Accessed 4/2023.

The lower TDS values are collected near recharge sites where the [redacted] outcrops. Petrophysical calculations from [redacted] indicate an average salinity of [redacted] L using the SP method, like the average measured value for the area (**Figure 2.57**). The expected [redacted] TDS at Injector No. 1 is [redacted] which is calculated using an inverse distance weighting method.

[redacted]

Figure 2.57—[redacted] salinity analysis of the [redacted] using the SP method. Note: The SP based salinity estimate is not valid in shaley sands, shales, or thin sands (less than 10 ft). The track to the right of the resistivity track shows one interval where the SP salinity calculation is valid, and indicated an average salinity of [redacted]

There is a strong correlation between salinity and depth in the [redacted] near the AoR. The average measured TDS values from five fluid samples from [redacted] within a 20-mile buffer of the future Injector No. 1 well is [redacted] (**Figure 2.58,** Figure 2.57**,** and **Table 2.36**). Four Corners Carbon utilized the same inverse distance weighting method to estimate the expected TDS at the Injector No. 1 location. The expected [redacted] pore fluid TDS at Injector No. 1 is [redacted]

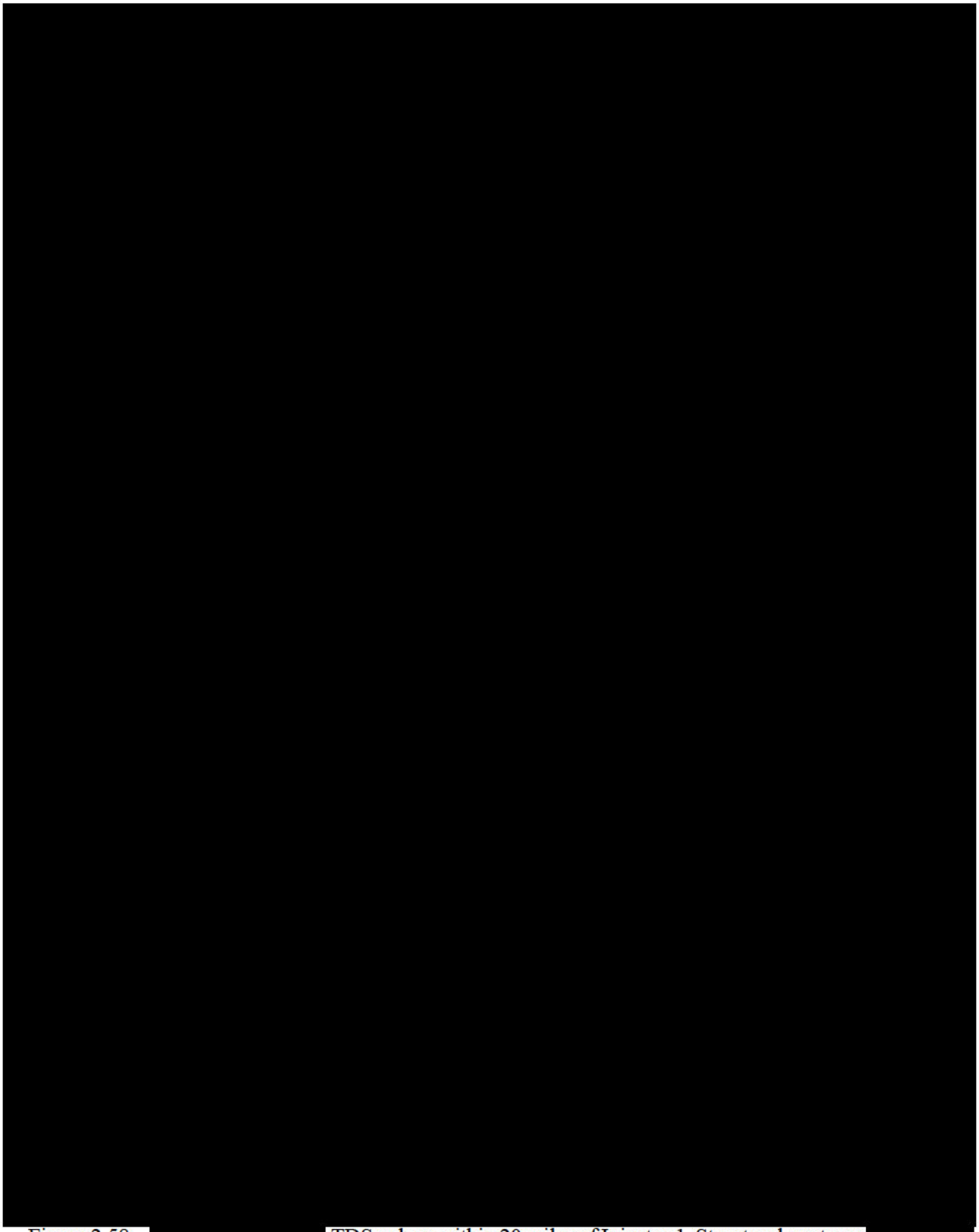

Figure 2.58— TDS values within 20 miles of Injector 1. Structural contours

Table 2.36—Measured TDS values of [redacted] fluids within a 20-mile buffer of the Injector 1 well.

Well API / Site ID	Latitude[1]	Longitude[1]	Avg. TDS (mg/L)[2]	Distance to Injector 1 (miles)
[redacted]				

[1] NAD83
[2] The average measured TDS value is recorded for wells with multiple fluid analyses.
[3] Site ID from data collected from the USGS Produced Waters Database (http://energy.cr.usgs.gov/prov/prodwat/). Accessed 4/2023.

There are no analyzed fluid samples in the [redacted] within a 20-mile buffer of the future Injector No. 1 well. Petrophysical calculations over the P[redacted] indicate a salinity of [redacted] using the SP method (**Figure 2.59**).

[redacted]hod. Note: The SP based salinity estimate is not valid in shaley sands, shales, or thin less than 10 ft. The track to the right of the resistivity track shows one interval where the SP salinity calculation is valid, and indicated an average salinity of [redacted] mg/L.

To supplement the petrophysical calculation, a depth versus measured TDS trend is established in other areas of the San Juan Basin and extrapolated into the AoR (**Figure 2.60**). Based on an average [redacted] depth of [redacted] TVD within the AoR, the estimated salinity from this trend is [redacted]

Figure 2.60—Measured TDS versus depth of the [redacted] for the San Juan Basin. Refer to Figure 2.61 for the sample locations.

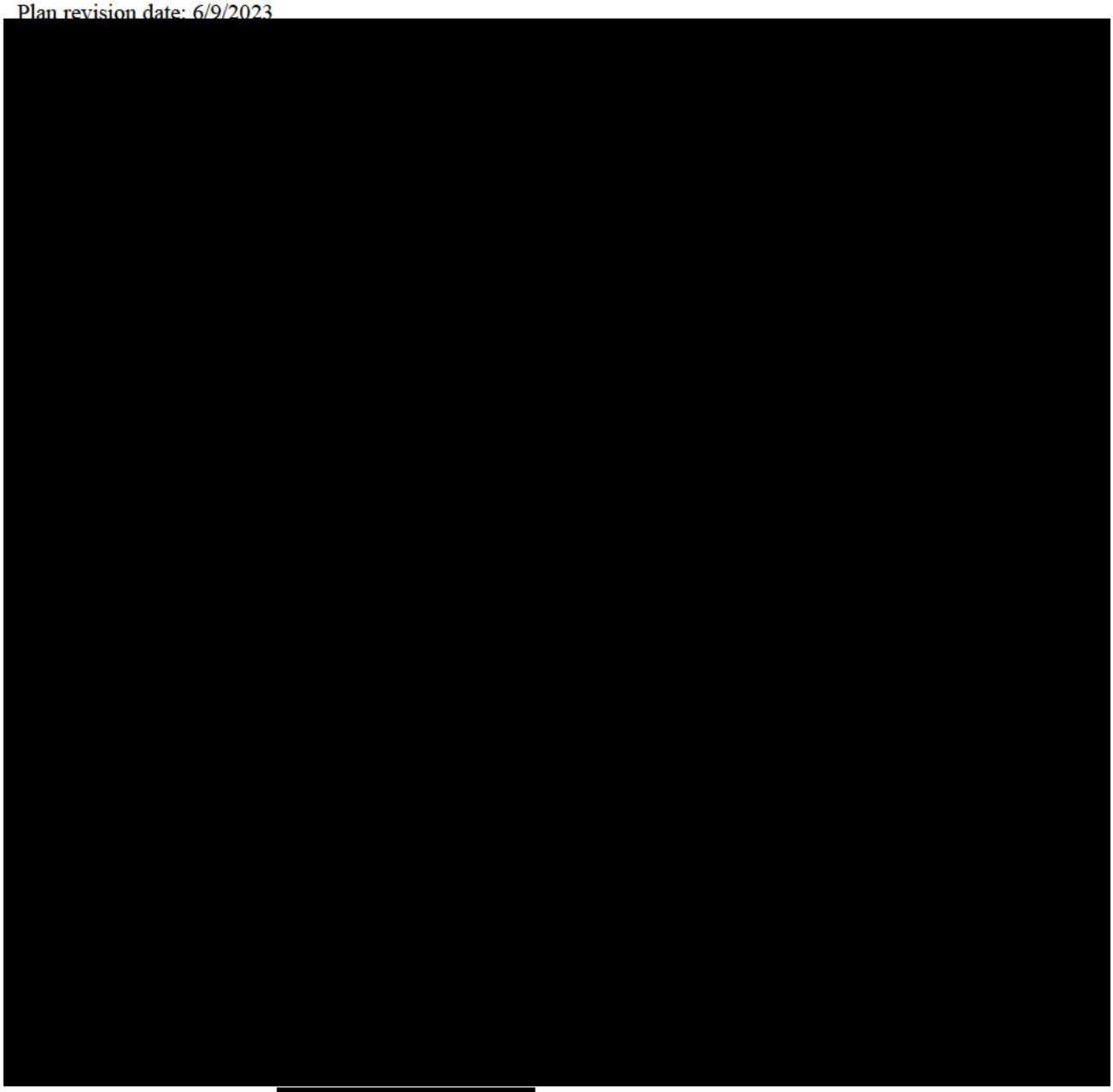

Figure 2.61—Wells with [redacted] measured TDS values that were used to determine a depth versus TDS trend.

[redacted]

Below the [redacted]. The [redacted] measured TDS values within the 20-mile buffer around the future Injector No. 1 well (**Figure 2.62**). The values of measured TDS range from [redacted] (**Table 2.37**). The expected [redacted] TDS at Injector No. 1 is [redacted] mg/L, which is calculated using an inverse distance weighting method.

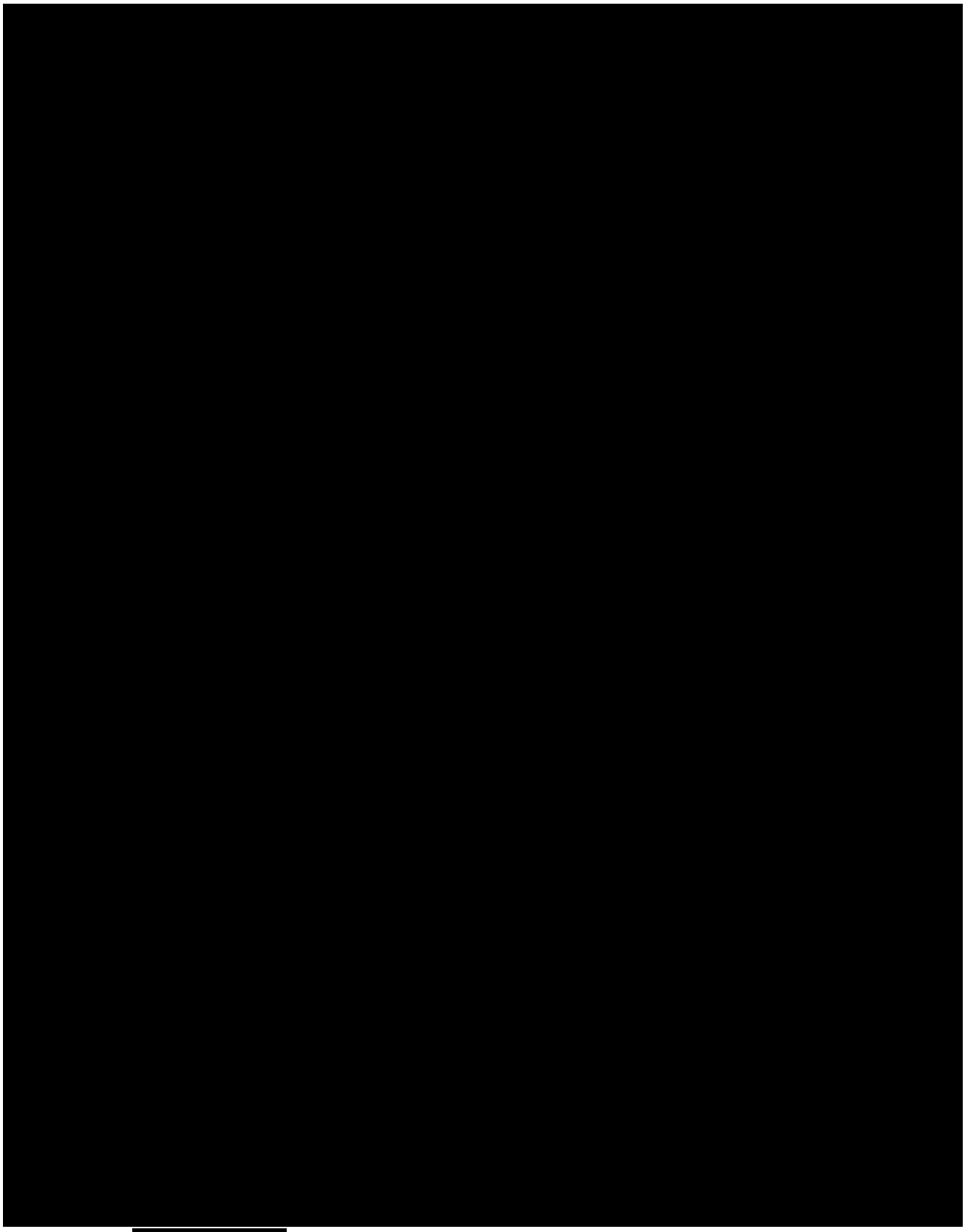

Figure 2.62— [redacted] TDS values within 20 miles of Injector 1.

Table 2.37—Measured TDS values of [redacted] fluids within a 20-mile buffer of the Injector 1 well.

Well API	Latitude[1]	Longitude[1]	Avg. TDS (mg/L)[2]	Distance to Injector 1 (miles)
[redacted]				

[1] NAD83
[2] The average measured TDS value is recorded for wells with multiple fluid analyses.

[redacted]

The [redacted] The [redacted] has [redacted] measured TDS values within the 20-mile buffer around the future Injector No. 1 well (**Figure 2.63**). The values of measured TDS range from [redacted], with an average of [redacted] (**Figure 2.64**). The expected [redacted] TDS at Injector No. 1 is [redacted], which is calculated using an inverse distance weighting method.

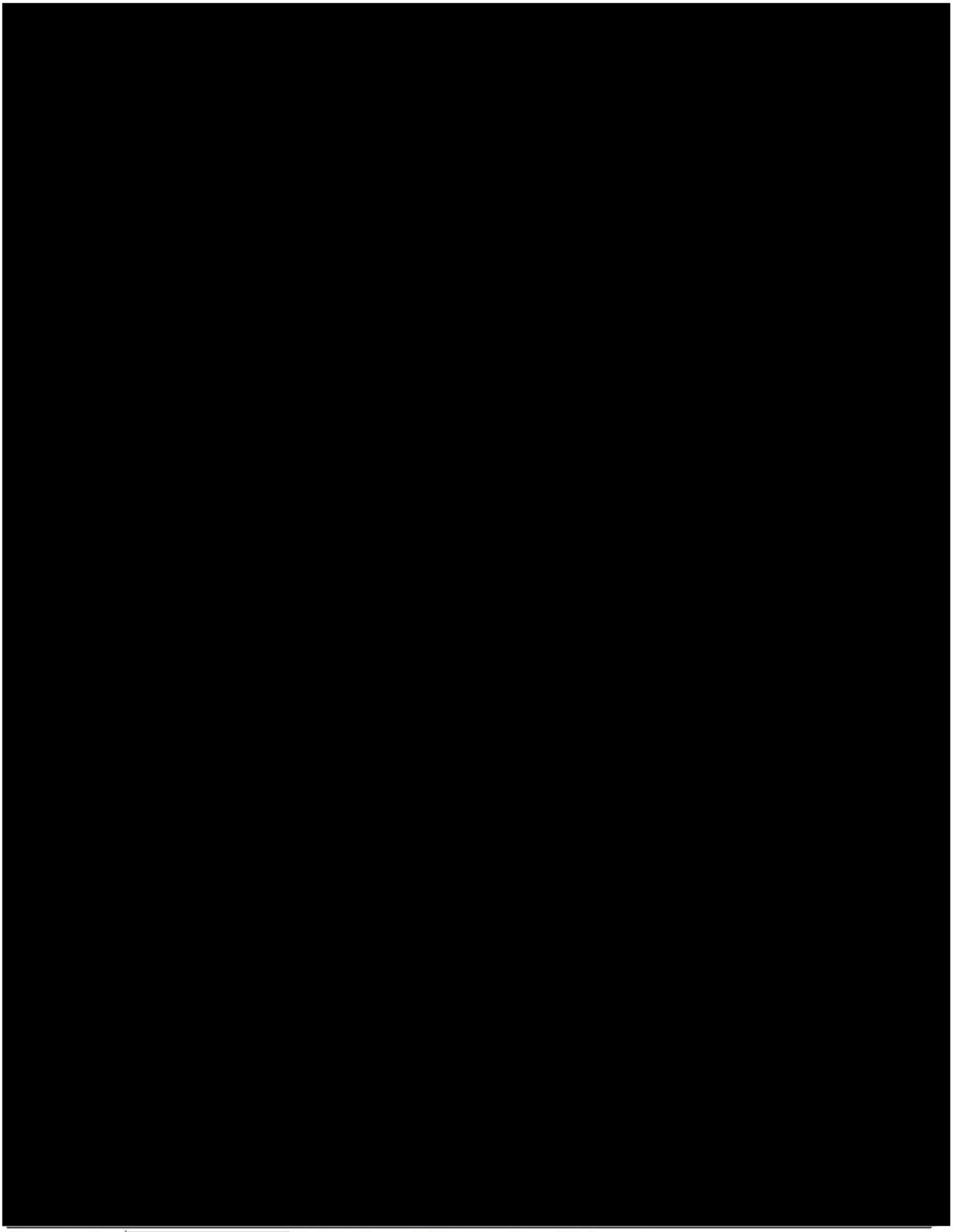

Figure 2.63— [redacted] TDS values within 20 miles of Injector 1.

Figure 2.64—Histogram of the measured TDS values in the [redacted] within a 20-mile buffer of the AoR. Note: [redacted]

[redacted] directly underlies the [redacted] Analysis from two fluid samples shows the measured TDS of the Morrison ranges from [redacted] mg/L and averages [redacted] mg/L in the area (**Figure 2.65** and **Table 2.38**).

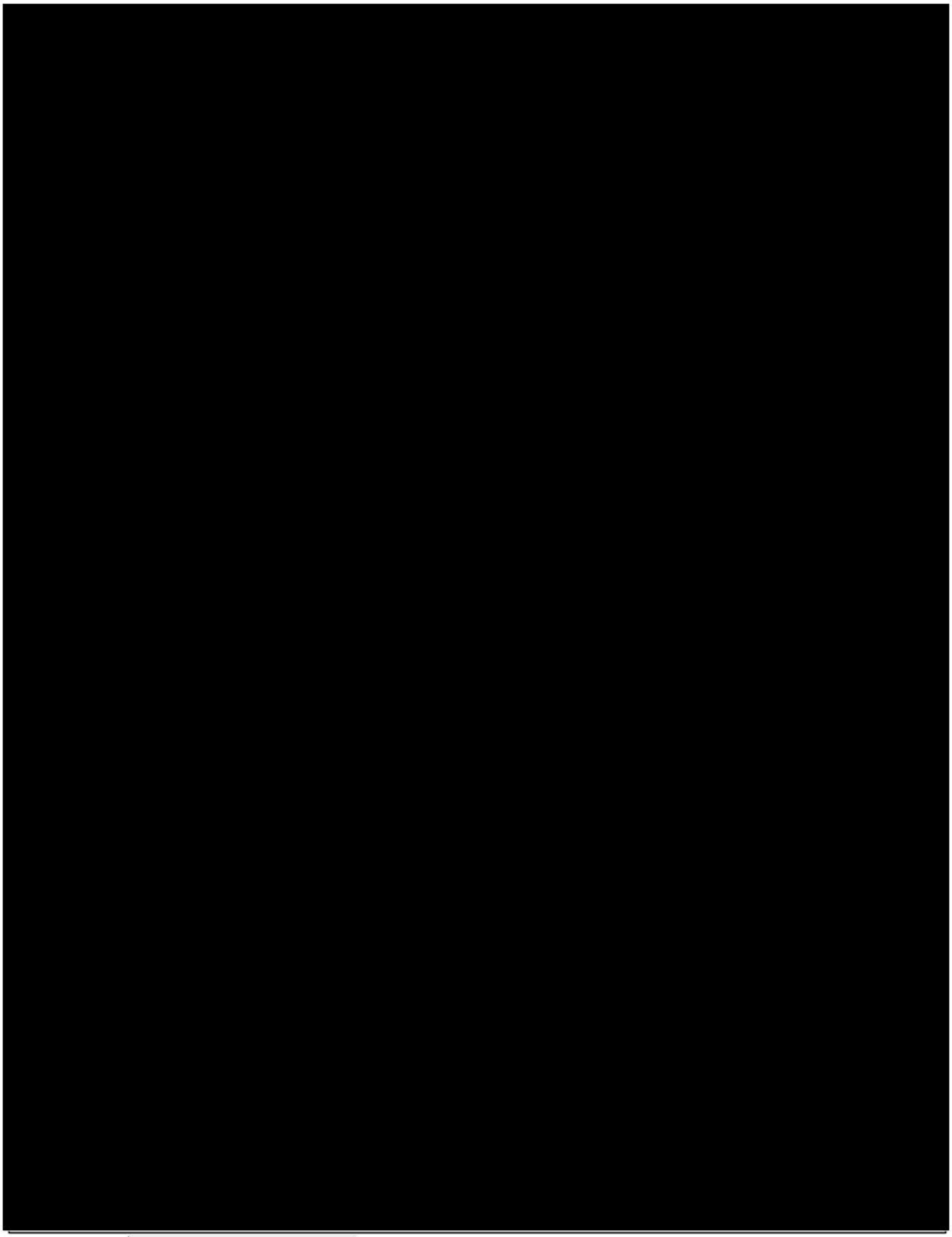

Figure 2.65— [redacted] values within 20 miles of Injector 1.

Table 2.38—Measured TDS values of [redacted] fluids within a 20-mile buffer of the Injector 1 well.

Well API	Latitude[1]	Longitude[1]	TDS (mg/L)	Distance to Injector 1 (miles)
[redacted]	[redacted]	[redacted]	[redacted]	[redacted]

[1] NAD83

Petrophysical calculations using the resistivity-porosity method over the [redacted] in the [redacted] well indicate an average salinity of [redacted] mg/L (**Figure 2.66**). The expected [redacted] TDS at Injector No. 1 is [redacted] mg/L, which is calculated using an inverse distance weighting method. The calculated and measured salinities in the [redacted]

[redacted]

Figure 2.66—[redacted] salinity analysis of the [redacted] using the resistivity-porosity method. Note: The three selected sands all have salinities calculated to be [redacted]

2.8.2 Solid Phase Geochemistry

2.8.2.1 Injection Zone

No solid-phase geochemical data for the [redacted] is found in existing San Juan Basin literature or well files. The [redacted] is present and consistent in composition throughout the [redacted]; therefore, geochemical information is compared across adjacent basins to determine its regional homogeneity (**Figure 2.67** and **Table 2.39**).

Figure 2.67—Approximate depositional extent of the [redacted] Study locations where solid-phase geochemical data were collected are shown as blue stars.

Table 2.39—Summary of solid-phase geochemical data for the Entrada Sandstone.

		Rock Mineralogy				Cement Mineralogy			
Study Area	Sample Type	Quartz	K-Feldspar	Plagioclase	Trace	Calcite	Quartz	Dolomite	Smectite
[redacted]									
[redacted]									

[redacted] utilized thin section petrography, SEM, and XRD to analyze outcrop samples from [redacted] approximately [redacted] of the AoR (Figure 2.67). Detailed results were not reported but the author provided a mineralogic assessment of [redacted] interpreted the [redacted] to be deposited in an [redacted] Because the geochemistry of the [redacted] is similar across the two basins, the geochemistry of the [redacted] at the proposed injection site is assumed to be similar to [redacted] results from the [redacted]. Core collected from well Strat 1, [redacted] of the AoR, is currently being analyzed to determine its mineralogy and elemental composition to confirm the geochemistry of the [redacted] Core will be collected from Injector No. 1 prior to injection to verify the mineralogy and composition from Strat 1.

Four Corners Carbon does not anticipate any adverse chemical reactions from CO_2 injection in [redacted]. The framework grain mineralogy of [redacted] is largely non-reactive or has very slow kinetics under injection conditions [redacted]. Preliminary research has determined no indication of trace metals that could be liberated from formation solids [redacted].

[redacted]

2.8.2.2 Confining Layer

Abundant solid-phase geochemical data for the [redacted] is available throughout the San Juan Basin due to its relevance as an [redacted] rock (e.g., [redacted]), (**Figure 2.68** and **Table 2.40**). [redacted] is comprised of two facies at the Project site: [redacted] and an upper siltstone and silty-sandstone unit.

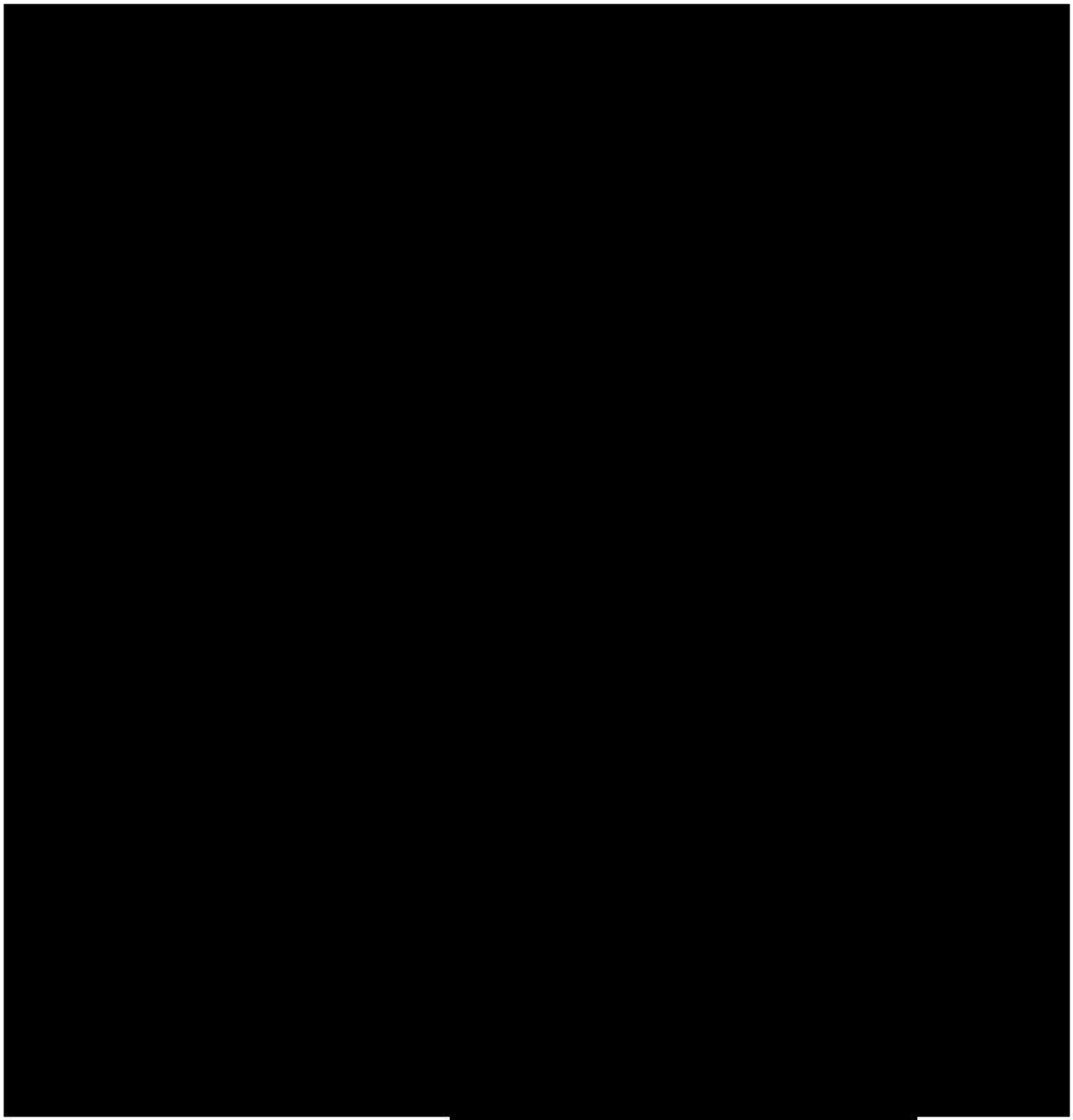

Figure 2.68—Depositional extents of the [redacted]). Note: Solid-phase geochemical data is collected at sample sites shown on map ([redacted]).

Table 2.40—Summary of solid-phase geochemical data for [redacted]

Sample Location / Sample Study		[redacted]
Rock Mineralogy	Quartz	
	K-Feldspar	
	Plagioclase	
	Zircon	
	Muscovite	
	Lithics	
	Calcite	
	Organics	
Cement	Calcite	
	Sericite	
	Quartz	

[redacted] reviewed several published descriptions of the basal [redacted] and analyzed the mineralogy of the unit throughout the San Juan Basin (Figure 2.68). The average [redacted]. The major constituents of the silts and fine sands are quartz, plagioclase, K-feldspar, calcite, muscovite, tourmaline, zircon, glauconite, dolomite, and metamorphic and granitic rock fragments (Table 2.40).

Solid-phase geochemical data of the [redacted] confining unit exists from one outcrop study along the [redacted], approximately [redacted] of the study area (Figure 2.68). [redacted] used petrographic analysis of three outcrop samples to describe the [redacted] as a silty sandstone. Point count results indicate that the [redacted] consists of approximately [redacted] (Table 2.40 provides detailed reports).

Finding an effective and long-term sealing caprock with geochemical stability is an essential criterion for site characterization (Busch et al. 2008; Pearce et al. 2011; Boot-Handford et al. 2014; Tian et al. 2014; Kampman et al. 2016; Patil et al. 2016; Harrison et al. 2019; Schmidt et al. 2019). While [redacted], Four Corners Carbon also finds [redacted] suitable [redacted]

solubility trapping, and widely considered the most secure form of carbon storage. Despite these lines of evidence, site-specific reactive transport models are needed to characterize the likelihood and timescale of these reactions and any possible consequences of their occurrence (Johnson et al. 2004).

2.8.2.3 First Permeable Zone Above Confining Layer

Existing solid-phase geochemical data for the [redacted] were collected in the same study area as the [redacted] confining unit on [redacted] (Figure 2.68). [redacted] analyzed five outcrop samples petrographically to describe the [redacted] Point count results indicate that the [redacted] consists mainly of quartz, with minor feldspar, trace zircon, and lithics, and is cemented by calcite, sericite, and hematite (**Table 2.41**).

Table 2.41—Summary solid-phase geochemical data for the [redacted]

Rock Mineralogy	Sample Location	[redacted]
	Sample Study	[redacted]
	Quartz	[redacted]
	K-Feldspar	[redacted]
	Plagioclase	[redacted]e
	Lithics	[redacted]
	Chert	[redacted]
Cement	Calcite	[redacted]
	Sericite	[redacted]
	Hematite	[redacted]

2.8.2.4 Underground Source of Drinking Water–[redacted]

[redacted] that was formed by the deposition of sediments derived from the erosion of mountains around the edges of the San Juan Basin as it deepened. Its lithology is mostly clay minerals including shrinking-swelling clays, quartz, feldspars and lithics, and some organic-rich horizons that have formed biogenic gas here and elsewhere in the basin ([redacted]).

2.8.2.5 Lowermost Underground Source of Drinking Water—[redacted]

[redacted] was deposited from the [redacted] and consists of fluvial and alluvial sands sourced from the erosion of uplifting mountains as the San Juan Basin deepened. It is a primarily quartz and feldspathic rich sandstone with secondary carbonate, clay, and quartz cements ([redacted]).

2.8.3 Geochemical Modeling

Modeling is the preferred approach to predict changes to water chemistry, mineralogy, reservoir porosity (trapping capacity), sealing performance, and any potential impacts on USDW quality (especially toxic trace metals) over the expected project life and long-term storage (Dai et al. 2020). Reactive transport modeling will be performed for the [redacted] to study fluid-

rock interactions after the analysis of solid- and fluid-phase samples collected from the AoR characterization well. Additionally, salt precipitation modeling will be performed to study potential deposition near the wellbore due to injection where this process is known to cause permeability, porosity, and injectivity reduction (Muller et al. 2009; Pruess and Muller 2009). Reservoir simulators will be employed to perform all of these simulations.

To constrain the changes [redacted] fluid chemistry from CO_2 injection, flow-through experiments were conducted on [redacted] outcrop samples using [redacted] fluid samples that were artificially enriched in CO_2. **Table 2.42** shows the analog [redacted] fluid analysis used to model their brine chemistry, shown in **Table 2.43.** Flow-through experiment statistics are presented in **Table 2.44**. **Figure 2.69** provides the outcrop and fluid sample collection sites used in this experiment. Geochemical modeling of stability indices is also calculated on the initial brine and the effluent. Additional flow-through experiments will be performed prior to injection using core and fluid samples from within the AoR once these data are available.

Table 2.42—[redacted] water chemistry.

pH	Ca (mg/L)	Mg (mg/L)	Na (mg/L)	CO_3 (mg/L)	HCO_3 (mg/L)	Cl (mg/L)	SO_4 (mg/L)	TDS (mg/L)
[redacted]								

Table 2.43—Reservoir conditions used in experiments including fluid chemistry used to create a synthetic brine. Data is from well reports and logs.

Reservoir Conditions	
Pore pressure [Bar]	[redacted]
Mean (confining) stress [Bar]	[redacted]
Temperature [°F]	[redacted]
Brine Chemistry	
Na^+ [ppm]	[redacted]
Ca^{2+} [ppm]	[redacted]
Mg^{2+} [ppm]	[redacted]
Cl^- [ppm]	[redacted]
HCO^{3-} [ppm]	[redacted]
CO_3^{2-} [ppm]	[redacted]
SO_4^{2-} [ppm]	[redacted]
TDS	[redacted]
pH	[redacted]

Table 2.44—Experimental statistics for all cores.

Sample ID	Experiment Type	Flow Rate (ml/min)	Length (days)	Total Pore Volumes
[redacted]	[redacted]	[redacted]	[redacted]	[redacted]
[redacted]	[redacted]	[redacted]	[redacted]	[redacted]
[redacted]	[redacted]	[redacted]	[redacted]	[redacted]

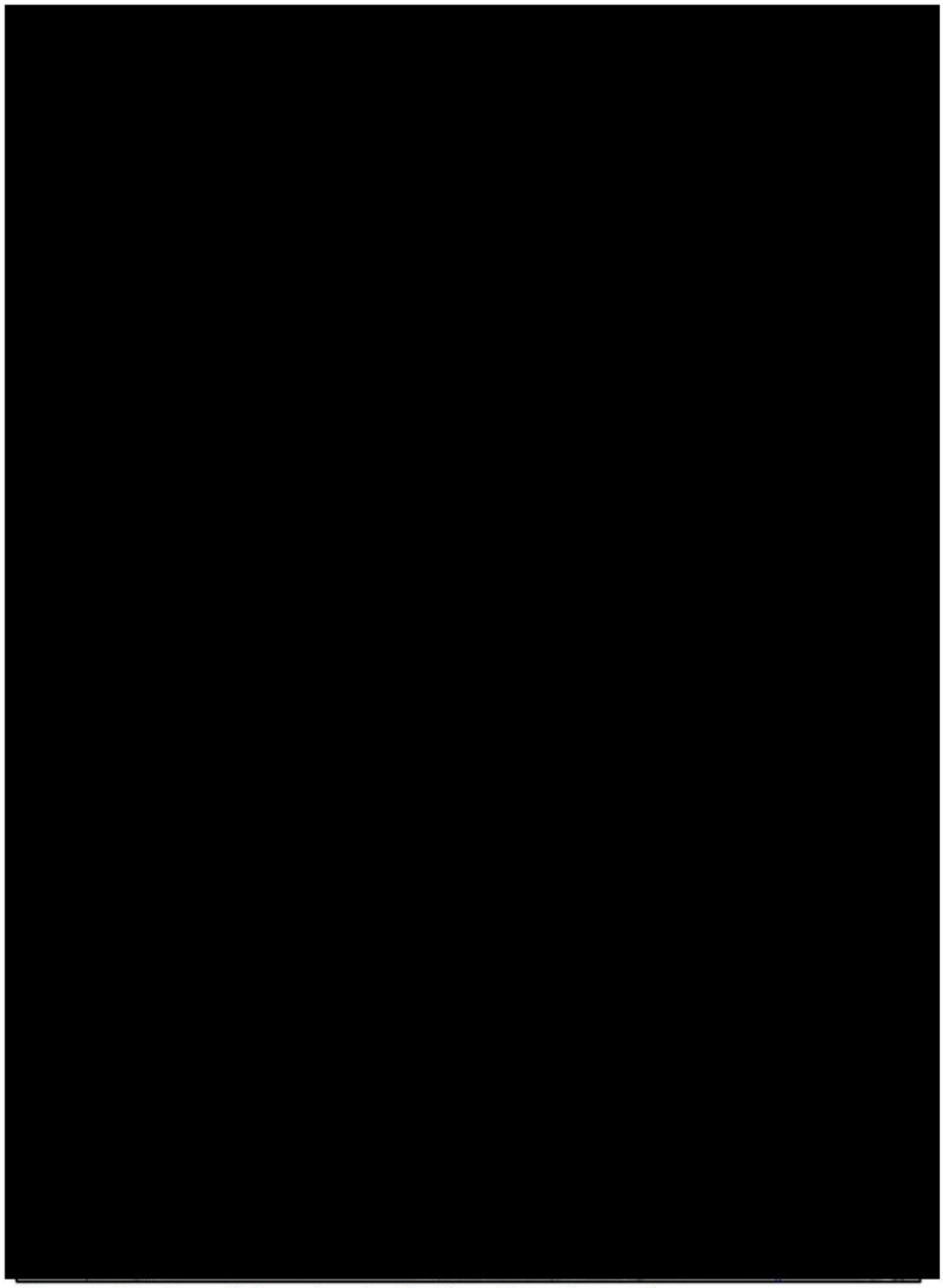

Figure 2.69—Sample location site for flow through experiments.

Fluid samples were collected and analyzed throughout the experiment to document chemical changes from fluid-rock interaction. Results shown in **Figure 2.70** reveal initial peak concentrations in calcium (Ca) and magnesium (Mg) that decrease with reaction progress indicating dissolution of carbonate cement and a reduction in the available reactive surface through time. Furthermore, iron (Fe) and potassium (K) generally increased and decreased with reaction progress respectively, and silicon (Si) is more stable on average. The increasing Fe concentrations may suggest increasing dissolution of Fe-rich phases and/or a reduction in secondary mineralization with time.

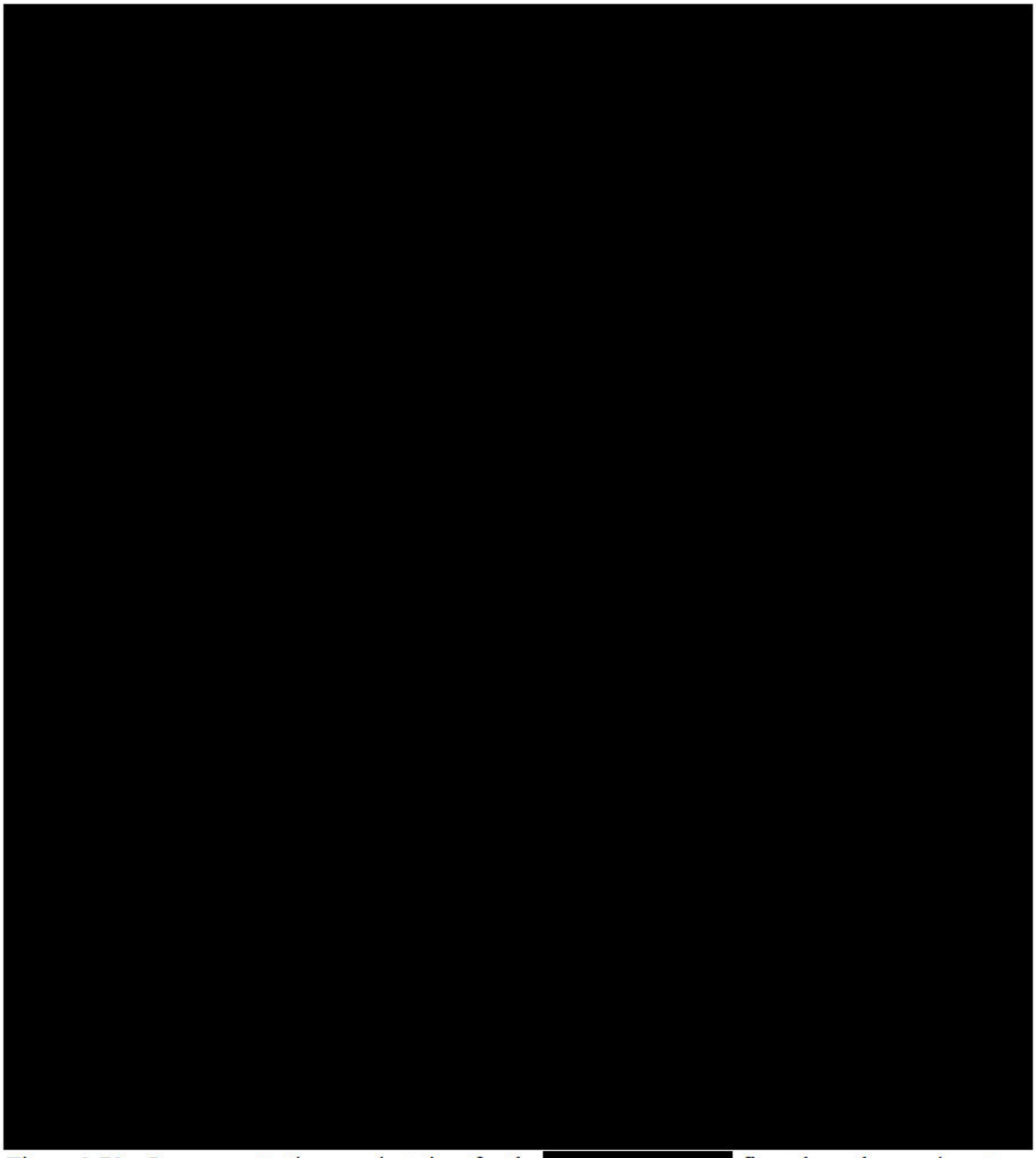

Figure 2.70—Ion concentrations against time for the [redacted] flow-through experiment.

Saturation indices were calculated with The Geochemist's Workbench™, an interactive software that solves problems in aqueous chemistry. Fluid chemistry indicates that calcite, dolomite, and anhydrite are near equilibrium, and the indices rose from the initial fluid upon flowing through the cores (**Figure 2.71**). Even with the relatively short reaction time, these calculations indicate that the fluids are near equilibrium with carbonate mineral phases. All experiments were supersaturated with respect to clay minerals and near saturation with respect to quartz, but feldspar minerals ranged from above to below saturation.

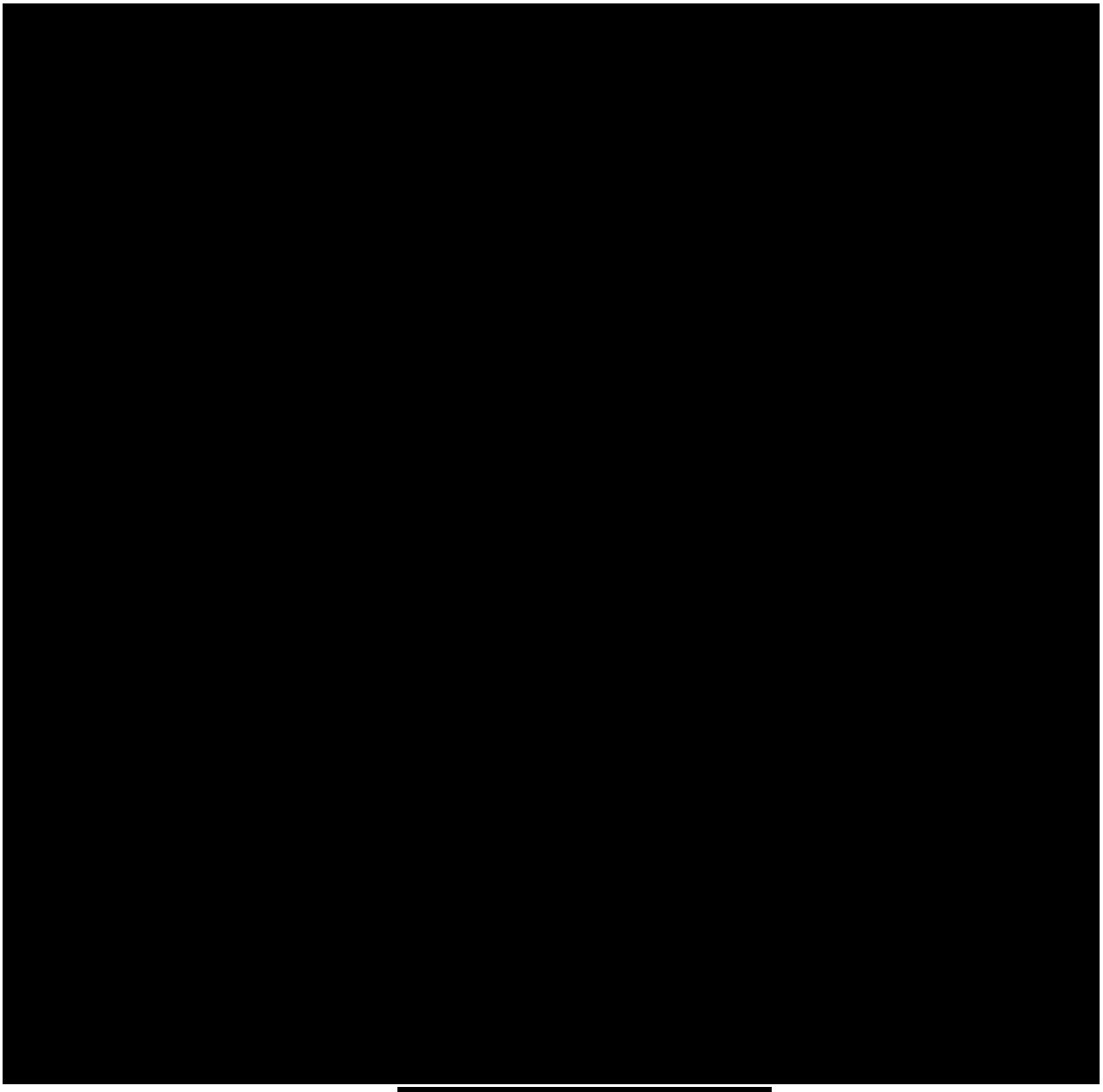

Figure 2.71—Saturation indices for the [redacted] experiments.

The combination of flow-through experiments and saturation index modeling demonstrates that the [redacted] is expected to perform similarly in other siliciclastic reservoirs that undergo

CO_2 injection. Carbonate and sulfate minerals in formation will be quickly dissolved until saturation is reached, likely near the CO_2-brine front. As the CO_2 plume dissolves into the formation waters, carbonate minerals can be expected to precipitate, while silicate mineral such as quartz can be expected to precipitate over a much longer period because they are kinetically many orders of magnitude slower than carbonate dissolution and precipitation (Black et al. 2015; Palandri and Kharaka 2004).

Because of the rapid equilibration of the fluids and the large volume of CO_2 being proposed, Four Corners Carbon expects mineral trapping over the duration of injection will be minor. The primary trapping mechanism implied by geochemical modeling is physical trapping.

2.9 Other Information

Not Applicable

2.10 Site Suitability [40 CFR 146.83]

2.10.1 Structural and Tectonic Suitability

The extent and structure of the San Juan Basin, along with its tectonic setting, make it an ideal location for CO_2 storage. The proposed injection site is located within the Central Basin region of the San Juan Basin (**Figure 2.72**). The Central Basin's geologic setting is well constrained due to the tens of thousands of wellbore penetrations from oil and gas exploration and production. Unlike the monoclines and uplifts that bound the basin, well-log data indicates this region has not undergone significant deformation. Within the Central Basin and the AoR, the [redacted] (injection zone) and [redacted] (confining zone) beds generally dip [redacted] (**Figure 2.73** and **Figure 2.74**). Well data mapping by Four Corners Carbon has not revealed any faults or open fractures in the [redacted] within nor near the AoR. No significant seismic hazards have been identified within the AoR and there have been no recorded earthquakes with epicenters within the AoR[33,34,35]. [redacted]

[33] https://earthquake.usgs.gov/earthquakes/search/
[34] https://geoinfo nmt.edu/repository/index.cfml?rid=20020001
[35] http://ds.iris.edu/spud/event

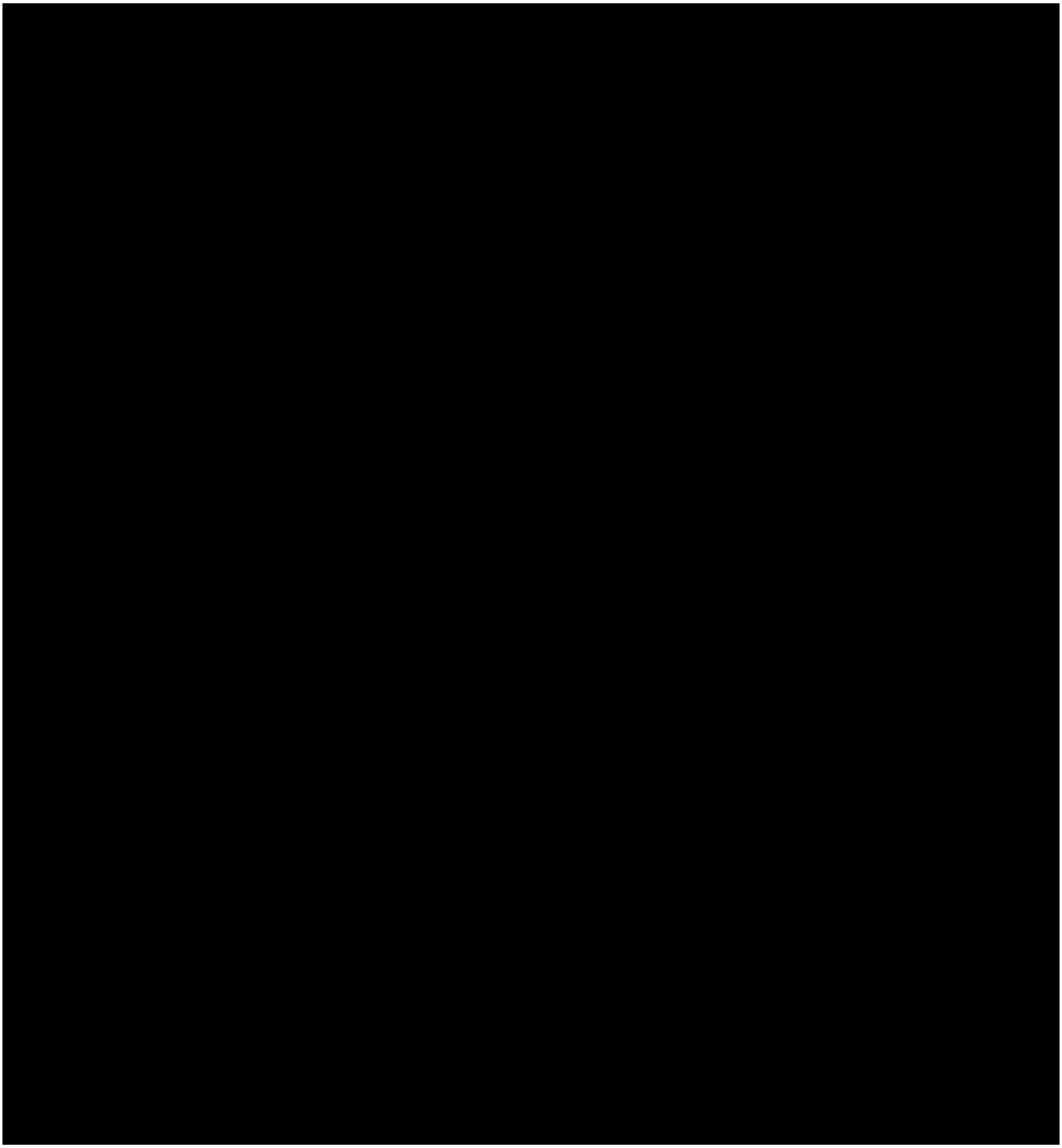

Figure 2.72—Structural elements of the San Juan Basin. San Juan structural basin shown in red outline (after Merrill et al. 2016). Arrows along monoclines point in the downdip direction.

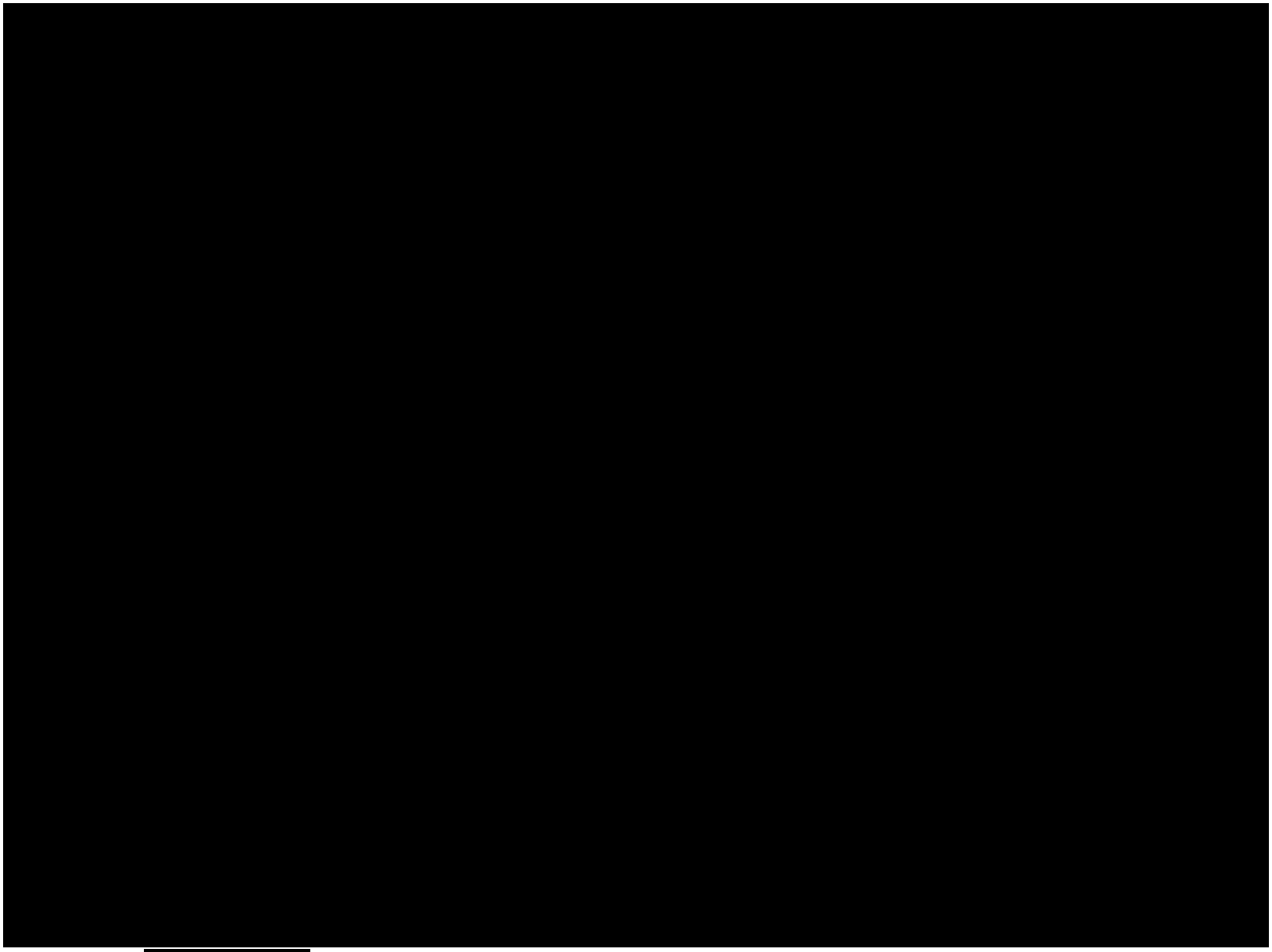

Figure 2.73— [redacted] structure contour map (TVDSS) near the AoR.

Figure 2.74— structure contour map (TVDSS) near the AoR.

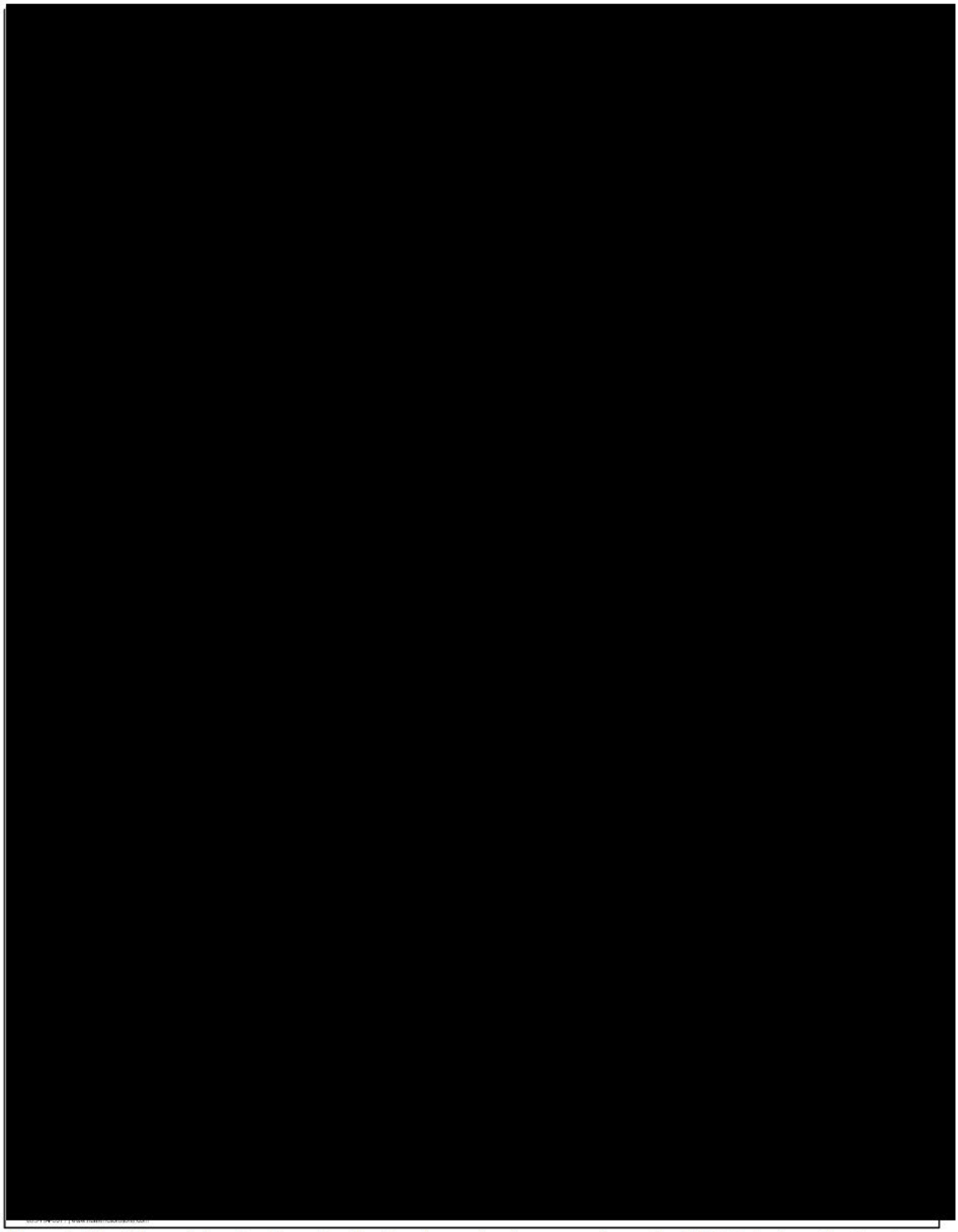

Figure 2.75—Map of the San Juan Basin showing seismic events from the USGS Earthquake Catalogue. Seismic events due to mining explosion are shown with gray circles.

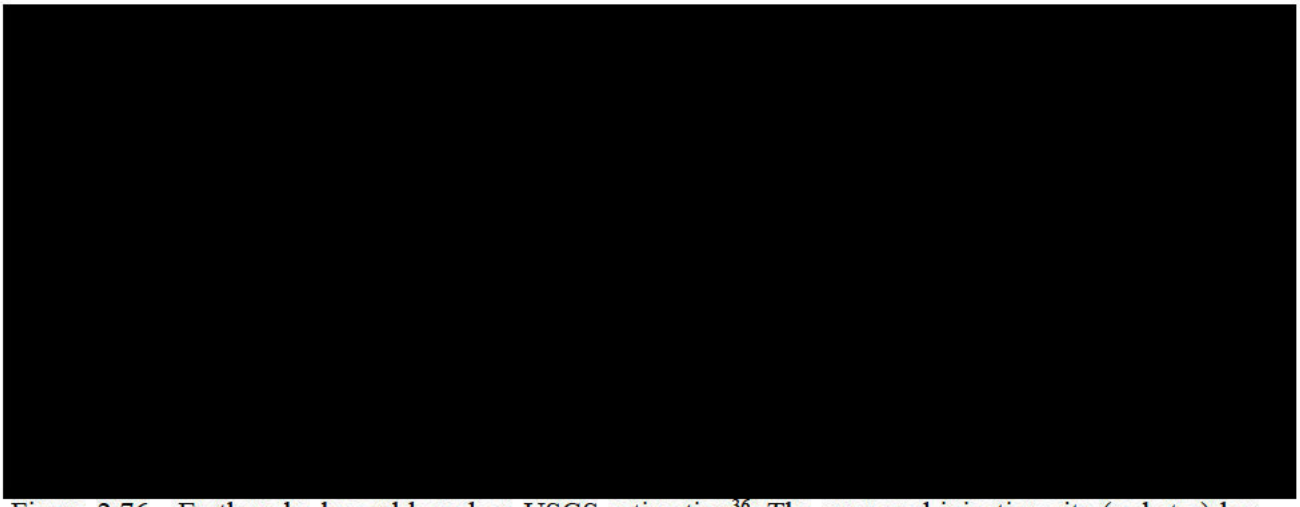

Figure 2.76—Earthquake hazard based on USGS estimation[36]. The proposed injection site (red star) has low earthquake hazard, showing low peak ground accelerations (PGA) with a 2% probability of exceedance in 50 years.

2.10.2 Injection Zone Suitability

The [redacted] is an ideal reservoir to sequester CO_2. Deposited as a widespread [redacted] Colorado Plateau (**Figure 2.77**). Petrographic and geochemical analysis of [redacted] outcrop and core samples indicate that the zone is a relatively [redacted]. The [redacted] is an open aquifer with no known lateral flow barriers or stratigraphic traps that would impact CO_2 plume migration at the proposed injection site (**Figure 2.78**). It is vertically bound by laterally continuous confining layers of the overlying [redacted], composed of low permeability limestones, siltstones, and shales.

[redacted] (Figure 2.73) and ranges in thickness from [redacted] (**Figure 2.79**). Current estimates of porosity and permeability for the [redacted] within the AoR are based on ELAN™ multi-mineral porosity and porosity-based intrinsic permeability from Strat 1 (**Table 2.45**; Juhasz 1979). These data will be supplemented with Nuclear Magnetic Resonance (NMR) and core-based permeability from Injector No. 1 once it is drilled. In addition to core permeability, MICP and porous plate capillary pressure measurements will be taken from Injector No. 1 core to improve estimates of hydraulic flow conductivity and sealing capacity.

[36] https://www.usgs.gov/programs/earthquake-hazards/science/national-seismic-hazard-model

Figure 2.77—Approximate depositional extent of the [redacted]). Study locations where solid-phase geochemical data were collected are shown as blue stars.

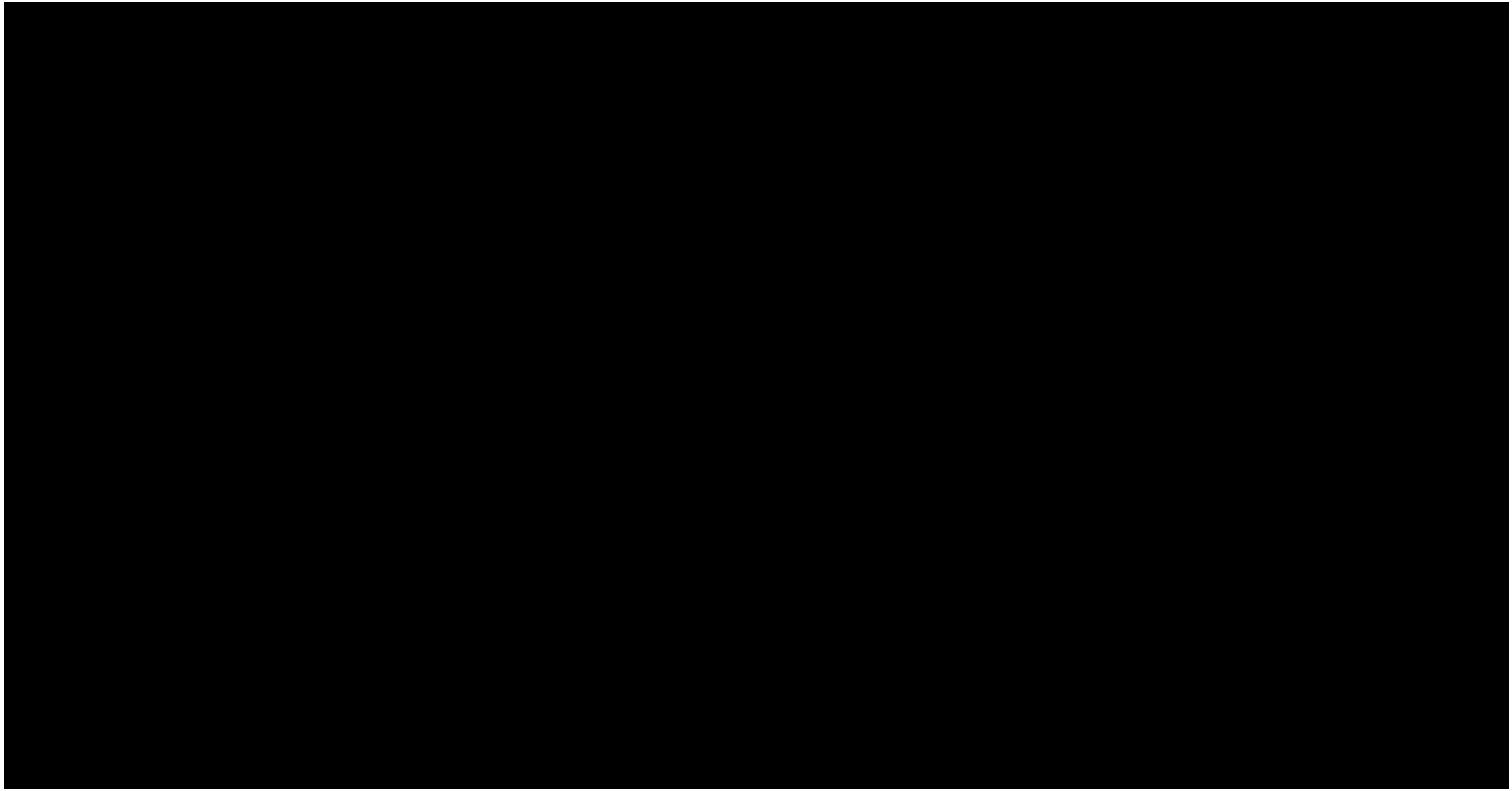

Figure 2.78—Regional cross section that highlights injection and confining zone lithologic homogeneity across the AoR.

Figure 2.79— thickness map (TST) near the AoR.

Table 2.45—Average porosity and permeability parameters for the net reservoir quality section of the intersected by Strat 1.

Zone	Net to Gross	Thickness (ft)	Avg. Total Porosity (v/v)	Avg. Permeability (mD)

The (**Figure 2.80**). Analysis of nearby pore fluids indicates that they contain high concentrations of dissolved solids (more than 10,000 mg/L); thus, the is not a USDW (**Table 2.46** and **Figure 2.81**). Based on measured TDS values and petrophysical calculations, the expected TDS of within the AoR is greater than mg/L. Further, the is encountered at greater than TVD below the lowermost USDW ( ) within the AoR (**Figure 2.82**). it does not contain detectable quantities of hydrocarbons within the AoR. Within the AoR, the occurs at a depth

providing ideal pressures (estimated [redacted] psi) and temperatures ([redacted] °F) to store supercritical CO_2.

Figure 2.80—[redacted] saltwater disposal wells adjacent to the AoR.

Table 2.46—Measured TDS values of [redacted] pore fluids within a 20-mile buffer of the Injector 1 well.

Well API	Latitude[1]	Longitude[1]	Avg. TDS (mg/L)[2]	Distance to Injector 1 (miles)
[redacted]	[redacted]	[redacted]	[redacted]	[redacted]
[redacted]	[redacted]	[redacted]	[redacted]	[redacted]
[redacted]	[redacted]	[redacted]	[redacted]	[redacted]
[redacted]	[redacted]	[redacted]	[redacted]	[redacted]
[redacted]	[redacted]	[redacted]	[redacted]	[redacted]

[1] NAD83
[2] The average measured TDS value is recorded for wells with multiple fluid analyses.

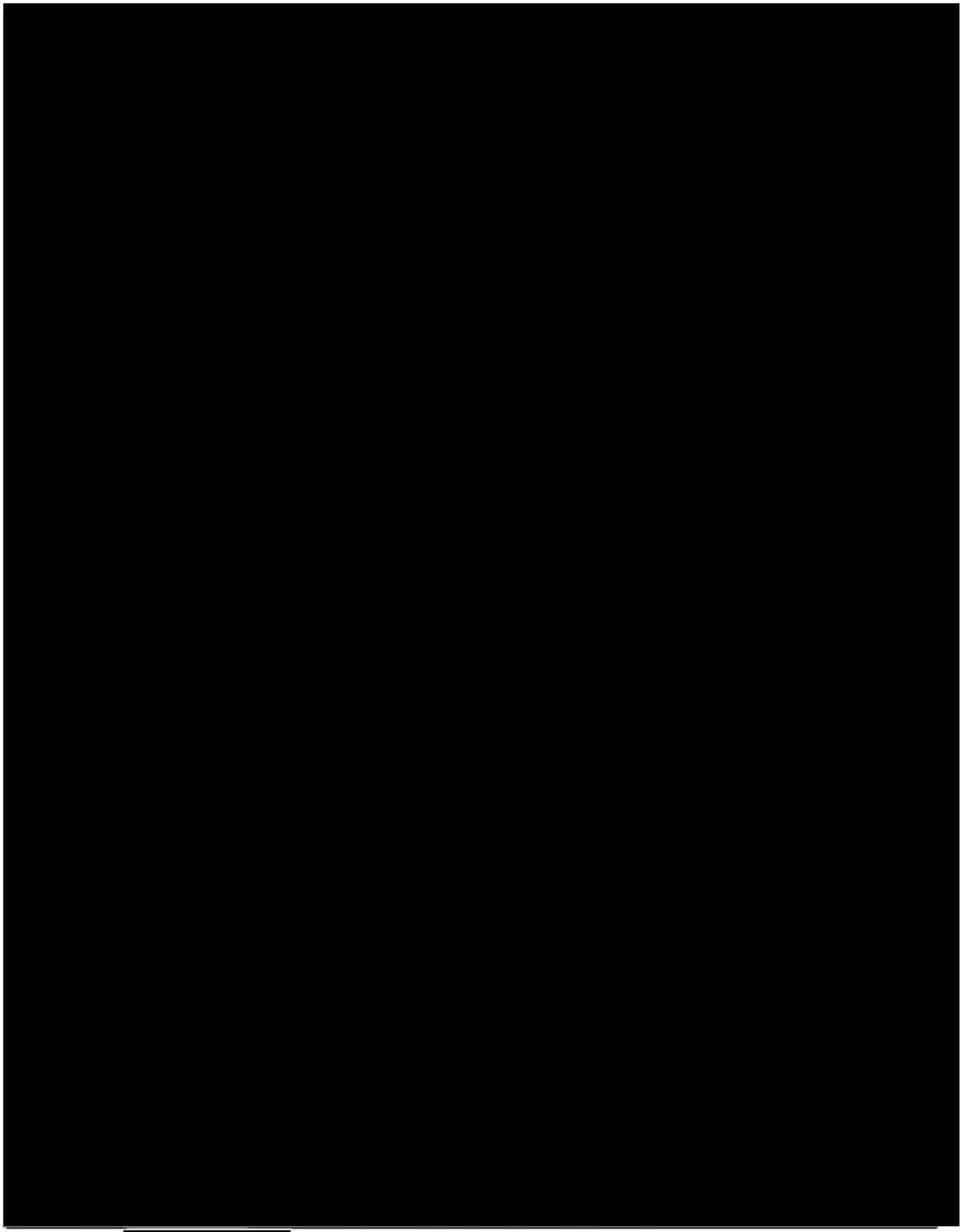

Figure 2.81— [redacted] TDS values within 20 miles of Injector 1.

Figure 2.82—Geologic cross sections A and B running through the proposed injection well location extending from surface to below the base of the proposed injection zone ( ). The nearest offset wells penetrating the Entrada are included. All significant stratigraphic zones are shown, and USDWs are labeled and shown in blue. Well logs show gamma ray on the left track and deep and shallow resistivity on the right track.

Four Corners Carbon does not anticipate adverse chemical reactions in the [redacted] from CO_2 injection. The framework grain mineralogy is largely non-reactive or has very slow kinetics under injection conditions ([redacted]). Preliminary research found no indication of trace metals that could be liberated from formation solids ([redacted]). The dissolution of calcite, dolomite cement (measured in [redacted] samples), would release carbonate-forming cations into the aquifer, enabling injected CO_2 to mineralize faster ([redacted] than if cation abundance is low ([redacted] provide circumstantial evidence that CO_2-rich fluids dissolve [redacted] cement, releasing iron into the formation fluid and bleaching the sandstone. No other mineralogic differences are reported from CO_2-rich fluid interacting with [redacted] rock ([redacted]). After analyzing site-specific data, Four Corners Carbon will employ reactive transport and flow-through models to determine if there will be any adverse geochemical reactions between the [redacted] and the injection fluid.

2.10.2.1 Storage Capacity of the Injection Zone

[redacted] is basin-wide interval spanning thousands of square miles (Figure 2.77). As the formation is an open aquifer, there are no stratigraphic, structural traps or spill points to use to define a storage area. Thus, the potential storage volume is primarily a function of the area in which the operator desires the plume to be contained. The calculated storage volume estimated at increasing radii from the proposed injection well are provided in **Table 2.47**. These capacities are estimated based on a methodology after Bachu (2006) (**Equation 2.5**). Note, this method does not account for rock compressibility nor migration due to buoyancy; it is simply a volumetric analysis.

Equation 2.5—CO_2 storage volume calculation (after Bachu 2006).

$$V_{CO2} = (A \times H \times \emptyset \times (1 - Sw_{irr}) \times \rho_{CO2} \times EF) \times 10^{-6}$$

Where:

V_{CO2} = CO_2 Storage Volume (Mt)
A = area (m^2)
H = net thickness (m)
$\emptyset$ = porosity (v/v)
Sw_{irr} = irreducible water saturation
ρ_{CO2} = density of CO_2 (reservoir conditions)
EF = Efficiency Factor – defined here as the ratio of the volume of CO_2 injected to the net pore volume (pore volume excluding irreducible water) at the final storage pressure.

Table 2.47—Calculated potential CO_2 storage volumes within [redacted] inside increasing radii from the proposed injection well. At three miles, [redacted] has the capacity to store more CO_2 than proposed by this Project.

Radius (miles)	Area (m^2)	Gross Thickness (m)	Net Thickness (m)	Porosity (v/v)	Swirr (%)	Net Volume (m^3)	CO_2 Density (tonnes/ m^3)*	Theoretical Stor. Volume (Mt)	Est. Efficiency Factor (EF)	Storage Volume (Mt)	Multiple of Anticipated Inj. Volume**
[redacted]											

*Assumes storage pressure of [redacted] and temperature of [redacted].
**Anticipated CO_2 Inj. Volume = [redacted]
Note: does not account for change in volume due to rock compressibility; Swirr = Irreducible water saturation, Mt = Megatonnes

Based on the calculation results, which use conservative inputs for Sw_{irr} [redacted]) and Efficiency Factor ([redacted]), within a three-mile radius of the proposed injection well the [redacted] has the capacity to store approximately one and a half times the anticipated volume of CO_2 to be injected by this project ([redacted]. The available volume increases exponentially with distance from the injection well. Note, simulation results indicate that the Efficiency Factor used here may be a significant underestimation.

2.10.3 Confining Zone Suitability

[redacted] is an ideal confining layer for injected CO_2. [redacted] was deposited in [redacted] environments and filled accommodation overlying preserved [redacted] (**Figure 2.83**). [redacted] consists of [redacted] in the AoR: [redacted] (primary confining layer) and [redacted]t (secondary confining layer). The [redacted] caps the [redacted] (Figure 2.82) and has excellent physical sealing properties, as evidenced by its role in retaining hydrocarbons ([redacted]) and injectate in other areas of the basin (Figure 2.80). Within the AoR, the average depth to the top of the [redacted] is [redacted] ft TVDSS (Figure 2.74). The [redacted] is typically [redacted] ft thick in the basin ([redacted]). The upper facies ranges from [redacted] ft thick, depending on the relict [redacted] of the underlying [redacted], whereby [redacted] are typically thicker than those on the [redacted]. The combined thickness of the [redacted] is approximately [redacted] ft (**Figure 2.84**). Current estimates of porosity and permeability for the confining zone in the AoR are based on neutron-density cross-plot porosity and porosity-based permeability calculations (**Table 2.48**, Juhasz 1979). As additional data is available, these estimates will be supplemented with NMR- and core-based permeability.

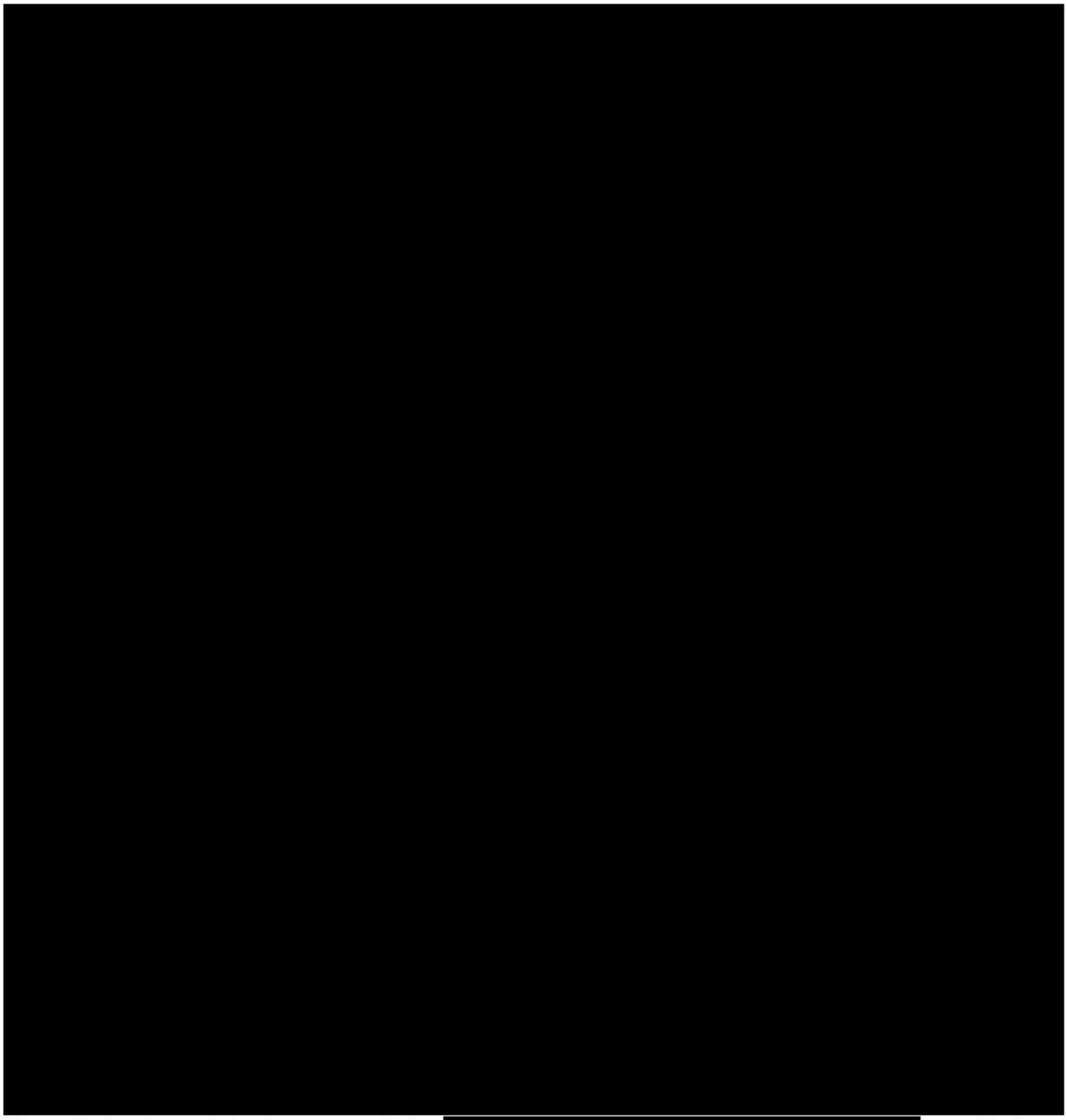

Figure 2.83—Depositional extents of the [redacted]. Solid-phase geochemical data is collected at sample sites shown on map [redacted]).

Figure 2.84— [redacted] thickness map (TST) near the AoR.

Table 2.48—Average ELAN permeability for the [redacted] excluding 15 ft of isolated thin zones with permeability greater than 1 mD.

Todilto Unit:	Gross Thickness (ft)	Net Confining Thickness (ft)	Total Porosity (v/v)	Permeability (mD)
[redacted]				
[redacted]				

No capillary pressure or rock strength data exists for [redacted] within the AoR. Measurements of confining zone capacity via capillary pressure measurements are planned for the [redacted] core from the Strat 1 and in future wells to be drilled within the Project AoR. Rock strength measurements are also planned for the core recovered in Strat 1 to define the yield strength, peak strength, and residual strength at in-situ conditions.

[redacted] is geochemically suitable for confining CO_2 over extended periods. The average composition of [redacted]

[redacted] underlying reservoir is high. Core collected from Strat 1, located approximately [redacted] of the proposed injection well, is being analyzed for mineralogy and elemental composition to confirm the geochemical suitability of [redacted] confining zone.

Additionally, core will be collected and analyzed across the [redacted] from Injector No. 1 before injection commences. Four Corners Carbon plans to input collected AoR-specific solid- and fluid-phase geochemical data into reactive transport models to characterize potential chemical reactions with the confining zone once site-specific data is analyzed.

2.10.4 Mechanical Suitability

The lack of well penetrations in the [redacted] makes this location suitable for injecting CO_2 (Figure 2.80). By the time injection commences, Injector No. 1 and Monitor No. 1 will be the only [redacted] penetrations within the AoR. Four Corners Carbon plans to use SLB's EverCRETE CO_2-resistant cement system[37] (or equivalent) when sealing these wells to mitigate the risk of leakage. The EverCRETE or equivalent cement systems have a lower probability of degrading than traditional Portland cement systems and can self-heal if there is cement damage.

[37] https://www.slb.com/-/media/files/ce/product-sheet/evercrete-ps.ashx

2.11 References

Ajayi, T., Gomes, J. S., & Bera, A. 2019. A review of CO_2 storage in geological formations emphasizing modeling, monitoring and capacity estimation approaches. Petroleum Science, 16(5), 1028–1063. https://doi.org/10.1007/s12182-019-0340-8

[redacted]

Audigane, P., Irina G., Czernichowski-Lauriol, I. and Xu, T. 2007. Two-dimensional reactive transport modeling of CO_2 injection in a saline Aquifer at the Sleipner site, North Sea. American Journal of Science, 307(2007), 974-1008. DOI: 10.2475/07.2007.02

Bachu, S., and Adams, J. J. 2003. Sequestration of CO_2 in geological media in response to climate change: capacity of deep saline aquifers to sequester CO_2 in solution. Energy Conversion and Management, 44(20), 3151–3175. https://doi.org/10.1016/s0196-8904(03)00101-8

Bachu, Stefan, and P. Eng. "The Capacity for Carbon Dioxide Storage in Oil and Gas Pools in Northeastern Alberta." Alberta Energy Research Institute (2006). Baker Atlas Inc. 2002. Introduction To Wireline Log Analysis, Baker Atlas, 2002. Baker Hughes Inc.

Baltz, E.H., 1967. Stratigraphy and Regional Tectonic Implications of Part of Upper Cretaceous and Tertiary Rocks, East-Central San Juan Basin, New Mexico: U.S. Geological Survey (USGS) Professional Paper 552, 101 p.

Bassiouni, Z., 1994. Theory, Measurement and Interpretation of Well Logs. Textbook Series, Society of Petroleum Engineers (SPE), Vol. 4.

Beitler, B., Chan, M. and Parry, W. 2003. Bleaching of Jurassic Navajo Sandstone on Colorado Plateau Laramide highs: Evidence of exhumed hydrocarbon supergiants? Geology, 31(12), 1041-1044. https://doi.org/10.1130/G19794.1

Black, J., Carroll, S. and Haese, R. 2015. Rates of mineral dissolution under CO_2 storage conditions. Chemical Geology, 399, 134-144. https://doi.org/10.1016/j.chemgeo.2014.09.020

Boot-Handford, M., Abanades J., Anthony, E., Blunt, M., Brandani, S., MacDowell, N., Fernández, J., Ferrari, M-C., Gross, R., Hallett, J., Haszeldine, R., Heptonstall, P., Lyngfelt, A., Makuch, Z., Mangano, E., Porter, R., Pourkashanian, M., Rochelle, G., Shah, N., Yao, G. and Fennell, P. 2014. Carbon capture and storage update. Energy & Environmental Science, 7(1), 130–189. https://doi.org/10.1039/C3EE42350F

Busch, A., Alles, S., Gensterblum, Y., Prinz, D., Dewhurst, D., Raven, M, Stanjek, H. and Krooss, B. 2008. Carbon dioxide storage potential of shales. International Journal of Greenhouse Gas Control, 2(3), 297–308. https://doi.org/10.1016/j.ijggc.2008.03.003

Brown, D.R., and Stone, W.J., 1979. Hydrogeology of the Aztec Quadrangle, San Juan County, New Mexico: New Mexico Bureau of Mines and Mineral Resources, Hydrogeologic Sheet 1.

Cather, S.M. 2004. The Laramide Orogeny in Northern New Mexico and Southern Colorado, in Mack, G.G., and Giles, K.A., eds., The Geology of New Mexico, A Geologic History: New Mexico Geological Society Special Pub. 11, pp. 203-248.

Chamberlin, R.M. and Anderson, O.J. 1989. The Laramide Zuni Uplift, southeastern Colorado Plateau: A Microcosm of Eurasian-style Indentation-Extrusion Tectonics? In Anderson, O.J., Lucas, S.G., Love, D.W. and Cather, S.M., eds., Southeastern Colorado Plateau, New Mexico Geological Society 40th Annual Field Conference Guidebook, pp. 81-90.

Condon, S.M., and Huffman, A.C., Jr. 1988. Revisions in Nomenclature of the Middle Jurassic Wanakah Formation, Northwestern New Mexico and Northeastern Arizona, Part 1 of Revisions to Stratigraphic Nomenclature of Jurassic and Cretaceous Rocks of the Colorado Plateau: USGS Bulletin 1633-A, pp. 1-12.

Condon, S.M., and Peterson, F. 1986. Stratigraphy of Middle and Upper Jurassic Rocks of the San Juan Basin – Historical Perspective, Current Ideas, and Remaining Problems, in Turner-Peterson, C.E., Santos, E.S., and Fishman, N.S., eds., A Basin Analysis Case Study The Morrison Formation, Grants Uranium Region, New Mexico: AAPG Studies in Geology No. 22, pp. 7-26.

Cooley, M.E., and Weist, W.G. 1979. Regional Hydrogeology of the San Juan Hydrologic Basin of New Mexico, Colorado, Arizona, and Utah, US Department of the Interior, San Juan Basin Regional Uranium Study, Working Paper 11-C, USGS Open-File Report 79-1498, 66 p.

Craigg, S. D. 2001. Geologic framework of the San Juan structural basin of New Mexico, Colorado, Arizona, and Utah, with emphasis on Triassic through Tertiary rocks. In Geologic framework of the San Juan structural basin of New Mexico, Colorado, Arizona, and Utah, with emphasis on Triassic through Tertiary rocks, USGS Professional Paper, 1420, 70 p. https://doi.org/10.3133/pp1420

Craigg, S.D., Dam, W.L., Kernodel, J.M., Thorn, C.R., and Levings, G.W. 1990. Hydrogeology of the Point Lookout Sandstone in the San Juan Structural Basin, New Mexico, Colorado, Arizona, and Utah, USGS Hydrologic Investigations Atlas HA 720-G, 2 sheets.

Dai, Z., Xu, L., Xiao, T., McPherson, B., Zhang, X., Zheng, L., Dong, S., Yang, Z., Soltanian, M. R., Yang, C., Ampomah, W., Jia, W., Yin, S., Xu, T., Bacon, D. and Viswanathan, H. 2020. Reactive chemical transport simulations of geologic carbon sequestration: Methods and applications. Earth-Science Reviews, 208(103265). https://doi.org/10.1016/j.earscirev.2020.103265

Dam, W.L. 1995. Geochemistry of Ground Water in the Gallup, Dakota, and Morrison Aquifers, San Juan Basin, New Mexico, USGS WRI Report 94-4253, 76 p.

Dam, W.L., Kernodel, J.M., Levings, G.W., and Craigg, S.D. 1990. Hydrogeology of the Pictured Cliffs Sandstone in the San Juan Structural Basin, New Mexico, Colorado, Arizona, and Utah, USGS Hydrologic Investigations Atlas HA 720-D, 2 sheets.

Dickinson, W.R., and Snyder, W.S. 1978. Plate Tectonics of the Laramide Orogeny, in Matthews, Volume 3 edition, Laramide Folding Associated with Basement Block Faulting in the Western United States: Geological Society of America (GSA) Memoir No. 151, p. 355-365.

Doveton, John H. 2011. Principles of Mathematical Petrophysics (International Association for Mathematical Geosciences: Studies in Mathematical Geosciences) Oxford University Press.

Fassett, J.E. 1989. Coal-bed Methane – A contumacious, free-spirited bride; The Geologic Handmaiden of Coal Beds, in Lorenz, J.C. and Lucas, S.G., eds, Energy Frontiers in the Rockies, Albuquerque Geological Society, p. 131-146

Fassett, J.E., 1991. Oil and gas resources of the San Juan basin, New Mexico and Colorado. Economic geology, US: The geology of North America: Geological Society of America, pp.357-372. https://doi.org/10.1016/j.chemgeo.2007.06.009

Gill, J.J., eds., Guidebook to the Geology of the Southwestern San Juan Basin: Four Corners Geological Society, 2nd Field Conference, pp. 44-52.

Green, M.W., and Pierson, C.T. 1977. A Summary of the Stratigraphy and Depositional Environments of Jurassic and Related Rocks in the San Juan Basin, Arizona, Colorado, and New Mexico, in Fassett, J.E., ed., Guidebook of the San Juan Basin III, New Mexico Geological Society, 28th Field Conference, pp. 147-152.

Haerer, D. and McPherson, B. 2009. *Evaluating the Impacts and Capabilities of Long Term Subsurface Storage in the Context of Carbon Sequestration in the San Juan Basin, NM and CO*, Elsevier Energy Procedia I, pp. 2991-2998.

Harrison, A., Tutolo, B. and DePaolo, D. 2019. The Role of Reactive Transport Modeling in Geologic Carbon Storage. Elements, 15(2), 93–98. https://doi.org/10.2138/gselements.15.2.93

Hart, B.S. 2001. Stratigraphy and Hydrocarbon Resources of the San Juan Basin: Lessons for Other Basins, Lessons from Other Basins: The Mountain Geologist, Vol. 58, No. 2, pp. 43-103.

Heidbach, O., M. Rajabi, K. Reiter, M.O. Ziegler, and the WSM Team (2016): World Stress Map Database Release 2016. GFZ Data Services,doi:10.5880/WSM. 2016.001.

Herron, M. M. 1987. Estimating the Intrinsic Permeability of Clastic Sediments from Geochmical Data. *SPWLA*, 23.

Huffman, C. and Taylor, D. 1999. Relationship of Hydrocarbon Resources to Basement Faulting in the San Juan Basin, in Cather, M. ed., Fractured Reservoirs: Characterization and Production, Petroleum Technology Transfer Council: Farmington, NM, pages not consecutively numbered.

Hydrogeology of the Cliff House Sandstone in the San Juan Structural Basin, New Mexico, Colorado, Arizona, and Utah. 1990. USGS Hydrologic Investigations Atlas HA 720-E, 2 sheets.

Hydrogeology of the Menefee Formation in the San Juan Structural Basin, New Mexico, Colorado, Arizona, and Utah. 1990. USGS Hydrologic Investigations Atlas HA 720-F, 2 sheets.

Hydrogeology of the Morrison Formation in the San Juan Structural Basin, New Mexico, Colorado, Arizona, and Utah. 1990. USGS Hydrologic Investigations Atlas HA 720-J, 2 sheets.

Jengten, R.W. 1977. Pennsylvanian Rocks in the San Juan Basin, New Mexico, and Colorado, in Fassett, J.E., ed., San Juan Basin III, New Mexico Geological Society, 28th Field Conference, pp. 129-132.

Johnson, J.W., Nitao, J.J., Morris, J.P. 2004. Modeling the long-term isolation performance of natural and engineered geologic CO_2 storage sites. Greenhouse Gas Control Technologies 9, 1315-1321.

Juhasz, I. 1979. The Central Role of Qv and Formation-Water Salinity in The Evaluation of Shaly Formations, SPWLA 20th annual logging symposium June 3-6, 1979.

Kampman, N., Bickle, M., Wigley, M., and Dubacq, B. 2014. Fluid flow and CO_2–fluid–mineral interactions during CO_2-storage in sedimentary basins. Chemical Geology, 369, 22–50. https://doi.org/10.1016/j.chemgeo.2013.11.012

Kampman, N., Busch, A., Bertier, P., Snippe, J., Hangx, S., Pipich, V., Di, Z., Rother, G., Harrington, J. F., Evans, J. P., Maskell, A., Chapman, H. J., & Bickle, M. J. 2016. Observational evidence confirms modelling of the long-term integrity of CO_2-reservoir caprocks. Nature Communications, 7(1), Article 1. https://doi.org/10.1038/ncomms12268

Kelley, V.C. 1951. Tectonics of the San Juan Basin, in Guidebook of the South and West Sides of the San Juan Basin, New Mexico and Arizona, New Mexico Geological Society, 1st Field Conference, pp.53-55.

Kelley, V.C. 1957. Tectonics of the San Juan Basin and Surrounding Areas, in Little, C.J., and Gill, J.J., eds., Guidebook to the Geology of the Southwestern San Juan Basin: Four Corners Geological Society, 2nd Field Conference, pp. 44-52.

Kelley, V.C. 1967. Tectonics of the Zuni-Defiance Region, New Mexico and Arizona, in Trauger, F.D., ed., Defiance-Zuni-Mt. Taylor Region Arizona and New Mexico, New Mexico Geological Society, 18th Field Conference, pp. 28-31.

Kelley, S., Engler, T., Cather, M., Pokorny, C, Yang, C.H., Mamer, Hoffman, G., Wilch, J., Johnson, P., and Zeigler, K. 2014. Hydrologic Assessment of Oil and Gas Development of the Mancos Shale in the San Juan Basin, New Mexico: N.M. Bureau Geology & Mineral Resources, of Report 566, 64 p.

Kelly, T.E. 1977. Geohydrology of the Westwater Canyon Member, Morrison Formation, of the Southern San Juan Basin, New Mexico, in Guidebook of the San Juan Basin III, northwestern New Mexico: New Mexico Geological Society, 28th Field Conference, pp. 285-290.

Kernodle, J.M. 1996. Simulation Analysis of the San Juan Basin Ground-Water Flow System, New Mexico, Colorado, Arizona, and Utah: USGS WRI Report 95-4187, 117 p.

Kirk, A.R. and Condon, S.M. 1986. Structural Control of Sedimentation Patterns and the Distribution of Uranium Deposits in the Westwater Canyon Member of the Morrison

Formation, Northwestern New Mexico – A Subsurface Study in Turner-Peterson, C.E., Santos, E.S., and Fishman, N.S., eds., A Basin Analysis Case Study: Morrison Formation, Grants Uranium Region, New Mexico, Vol. A179, Tulsa, Energy Minerals Division of the AAPG, p. 105-143.

[redacted]

Lake, L. 2007. Petroleum Engineering Handbook. Richardson, TX: Society of Petroleum Engineers.

Levings, G.W., Craigg, S.D., Dam, W.L., Kernodle, J.M., and Thorn, C.R. 1990. Hydrogeology of the San Jose, Nacimiento, and Animas Formations in the San Juan Structural Basin, New Mexico, Colorado, Arizona, and Utah, USGS Hydrologic Investigations Atlas HA 720-A, 2 sheets.

Levings, G.W., Kernodle, J.M., and Thorn, C.R. 1996. Summary of the San Juan Structural Basin Regional Aquifer-System Analysis, New Mexico, Colorado, Arizona, and Utah, USGS WRI Report 95-4188, 55 p.

Lohman, S.W. 1972. Ground-water Hydraulics: USGS Prof. Paper 708, 70 p.

Lorenz, C.L. and Cooper, S.C. 2001. Tectonic Setting and Characteristics of Natural Fractures in Mesa Verde and Dakota Reservoirs of the San Juan Basin, New Mexico and Colorado, Sandia National Laboratories Report SAND2001-0054, January 2001, 77 p.

Lorenz, J. and Cooper, S. 2003. Tectonic setting and characteristics of natural fractures in Mesaverde and Dakota reservoirs of the San Juan Basin: New Mexico Geology, 25, 3- 14.

Lucas, S. G., Kietzke, K. K., and Hunt, A. P. 1985. The Jurassic System in east-central New Mexico: New Mexico Geological Society, Guidebook 36, pp. 213-242. https://nmgs.nmt.edu/publications/guidebooks/downloads/36/36_p0213_p0242.pdf

Lyford, R.P., and Stone, W.J. 1978. Ground-water Resources of Northwestern New Mexico (abs): Geological Society of America, Abstracts with Programs, V. 10, No. 5, p. 220.

Lyford, F.P. 1979. *Ground Water in the San Juan Basin, New Mexico and Colorado*, USGS Water Resources Investigation 79-73, 22 p.

McCormack, K., Bratton, T., Chen, T. and McPherson, B. 2022. Induced seismicity potential based on probabilistic geomechanics for the San Juan Basin CarbonSAFE project. GEOPHYSICS, 87(6), EN69–EN79. https://doi.org/10.1190/geo2021-0704.1

[redacted]

Merrill, M.D., Drake, R.M., II, Buursink, M.L., Craddock, W.H., East, J.A., Slucher, E.R., Warwick, P.D., Brennan, S.T., Blondes, M.S., Freeman, P.A., Cahan, S.M., DeVera, C.A., and Lohr, C.D. 2016. Geologic framework for the national assessment of carbon dioxide

storage resources—Southern Rocky Mountain Basins, chap. M of Warwick, P.D., and Corum, M.D., eds., Geologic framework for the national assessment of carbon dioxide storage resources: U.S. Geological Survey Open-File Report 2012–1024–M, 59 p., at http://dx.doi.org/10.3133/ofr20121024M.

Molenaar, C.M. 1977. Stratigraphy and Depositional History of Upper Cretaceous Rocks of the San Juan Basin Area, New Mexico and Colorado, with a note on Economic Resources, in Fassett, J.E., ed., Guidebook of the San Juan Basin III, New Mexico Geological Society, 28th Field Conference, pp. 159-166.

Muller, N., Qi, R., Mackie, E., Pruess, K., and Blunt, M. J. 2009. CO_2 injection impairment due to halite precipitation. Energy Procedia, 1(1), 3507–3514. https://doi.org/10.1016/j.egypro.2009.02.143

Owen, D.E. 1973. Depositional History of the Dakota Sandstone, San Juan Basin area, New Mexico, in Fassett, J.E., ed., Cretaceous and Tertiary Rocks of the Southern Colorado Plateau: Four Corner Geological Society Memoir, pp. 37-51.

Palandri, J., & Kharaka, Y. 2004. A Compilation of Rate Parameters of Water-Mineral Interaction Kinetics for Application to Geochemical Modeling. 1068, 71.

Patil, R. S., Banerjee, D., Zhang, C., Thallapally, P. K., and Atwood, J. L. 2016. Selective CO_2 Adsorption in a Supramolecular Organic Framework. Angewandte Chemie International Edition, 55(14), 4523–4526. https://doi.org/10.1002/anie.201600658

Pearce, J., Kirby, G., Lacinska, A., Bateson, L., Wagner, D., Rochelle, C., and M. Cassidy. 2011. Reservoir-scale CO_2-fluid rock interactions: Preliminary results from field investigations in the Paradox Basin, Southeast Utah. Energy Procedia, 4, 5058–5065. https://doi.org/10.1016/j.egypro.2011.02.479

Pecha, M. E., Gehrels, G. E., Karlstrom, K. E., Dickinson, W. R., Donahue, M. S., Gonzales, D. A., and Blum, M. D. 2018. Provenance of Cretaceous through Eocene Strata of the Four Corners Region: Insights from Detrital Zircons in the San Juan Basin, New Mexico and Colorado: Geosphere, v. 14, p. 1-27.

Pruess, K., and Müller, N. 2009. Formation dry-out from CO_2 injection into saline aquifers: 1. Effects of solids precipitation and their mitigation. Water Resources Research, 45(3). https://doi.org/10.1029/2008WR007101

Ridgley, J.L., Green Morris W., Pierson Charles T., Finch Warren I., and Lupe Robert D. 1978. Summary of the Geology and Resources of Uranium in the San Juan Basin and Adjacent Region, New Mexico, Arizona, Utah & Colorado: USGS OFR 78-964, 107 p.

Saadatpoor, E., Bryant, S. L., and Sepehrnoori, K. 2010. New Trapping Mechanism in Carbon Sequestration. Transport in Porous Media, 82(1), 3–17. https://doi.org/10.1007/s11242-009-9446-6

Schmitt, L. J 1982. Petrographic study of sandstones from measured sections of the Morrison Formation and related units, southwestern San Juan Basin, New Mexico (Open-File Report No. 82–991; Open-File Report, p. 63). U.S. Geological Survey. https://pubs.usgs.gov/of/1982/0991/report.pdf

Schmidt, H.-P., Anca-Couce, A., Hagemann, N., Werner, C., Gerten, D., Lucht, W., & Kammann, C. 2019. Pyrogenic carbon capture and storage. GCB Bioenergy, 11(4), 573–591. https://doi.org/10.1111/gcbb.12553

Scholle, P. A. 2003. *Geologic Map of New Mexico* (9/7/2022 ed.) [Open-File Geologic Map #304]. New Mexico Bureau of Geology & Mineral Resources. https://geoinfo.nmt.edu/publications/maps/geologic/ofgm/details.cfml?volume=304

Selvaduria and Suvorov .2022. Poroelastic properties of rocks with a comparison of theoretical estimates and typical experimental results. Sci Rep. 2022 Jun 29;12(1):10975. doi: 10.1038/s41598-022-14912-5.

Slack, P.B. and Campbell, J.A. 1976. Structural Geology of the Rio Puerco Fault Zone and its Relationship to Central New Mexico Tectonics, in Woodward, L.A. and Northrop, S. A., eds., Tectonics and Mineral Resources in Southwestern North America, New Mexico Geological Society Special Publication No. 6, pp. 46-52.

Slack, P.B. 1973. Structural Geology of the Northeast Part of the Rio Puerco Fault Zone, Sandoval County, New Mexico, University of New Mexico unpublished M.S. thesis, 74 p.

Steven, T.A. 1975. Middle Tertiary Volcanic Field in the Southern Rocky Mountains, Cenozoic History of the Southern Rock Mountains, GSA Memoir 144, pp. 75-93.

Stone, W.J., Lyford, F.P., Frenzel, P.F., Mizell, N.H., and Padgett, E.T. 1983. *Hydrology and* Water Resources of San Juan Basin, New Mexico, New Mexico Bureau of Mines and Mineral Resources, Hydrologic Report 6, 70 p.

[redacted]

Taylor, D. J., & Huffman Jr., A. C. 1998. Map showing inferred and mapped basement faults, San Juan Basin and vicinity, New Mexico and Colorado (Report No. 2641; IMAP). USGS Publications Warehouse. https://doi.org/10.3133/i2641

Thaden, R.E. and Zech, R.S. 1984. Preliminary Structure Contour Map on the Base of the Cretaceous Dakota Sandstone in the San Juan Basin and Vicinity, New Mexico, Arizona, Colorado and Utah: USGS Miscellaneous Field Studies Map MF-1673.

Thorn, C.R., Levings, G.W., Craigg, S.D., Dam, W.L., and Kernodle, J.M. 1990. Hydrogeology of the Ojo Alamo Sandstone in the San Juan Structural Basin, New Mexico, Colorado, Arizona, and Utah, USGS Hydrologic Investigations Atlas HA 720-B, 2 sheets.

Tian, X., Chang, M., Shi, F., & Tanikawa, H. 2014. How does industrial structure change impact carbon dioxide emissions? A comparative analysis focusing on nine provincial regions in China. Environmental Science & Policy, 37, 243–254. https://doi.org/10.1016/j.envsci.2013.10.001

[redacted]

Wang, J., Cao, Y., Liu, K., Liu, J., Xue, X., & Xu, Q. 2016. Pore fluid evolution, distribution and water-rock interactions of carbonate cements in red-bed sandstone reservoirs in the Dongying Depression, China. Marine and Petroleum Geology, 72, 279–294. https://doi.org/10.1016/j.marpetgeo.2016.02.018

Wigley, M., N. Kampman, B. Dubacq, and M. Bickle. 2012. Fluid-Mineral Reactions and Trace Metal Mobilization in an Exhumed Natural CO_2 Reservoir, Green River, Utah, Geology, 40, 555-558, https://doi.org/10.1130/G32946.1.

Woodward, L.E. and Callender, J.F. 1977. Tectonic Framework of the San Juan Basin, in Fassett, J.E. ed., Guidebook of the San Juan Basin III, New Mexico Geological Society, 28th Field Conference, pp. 209-212.

[redacted]

Xu, T., Apps, J. A., & Pruess, K. 2001. Analysis of mineral trapping for CO_2 disposal in deep aquifers. published. https://doi.org/10.2172/789133

Zoback, M. 2007. *Reservoir Geomechanics*. Cambridge: Cambridge University Press. https://doi.org/10.1017/CBO9780511586477

3.0 AoR and Corrective Action [40 CFR 146.82(a)(13) and 146.84(b)]

All information satisfying 40 CFR 146.82(a)(13) and 146.84(b-c) is described in **3.0_aor_ca_plan_SJB_2023.06.09.pdf**.

4.0 FINANCIAL ASSURANCE [40 CFR 146.82(A)(14) AND 146.85]

Four Corners Carbon has submitted to the Financial Responsibility Demonstration module all the information and files required by 40 CFR 146.82(a)(14) to demonstrate that it meets the financial responsibility requirements of 40 CFR 146.85.

The information and files submitted show the estimated costs provided by a third-party entity care and site closure, and do any emergency or remedial response that may be needed. Four Corners Carbon will obtain and submit EPA compliant financial instruments to meet the financial responsibility requirements of 40 CFR 146.85.

Document **4.0_fa_demonstration_SJB_2023.06.09.pdf** has been submitted which includes all requirements required by 40 CFR 146.82(a)(14) and 146.85.

5.0 INJECTION WELL CONSTRUCTION [40 CFR 146.86]

This section includes the text, tables, and figures to fulfill the injection well construction data requirements listed at 40 CFR §146.82(a)(9), (11), and (12). There are three wells planned for the Project, Injector 1, Monitor 1 and Strat 1. Injector 1 and Monitor 1 are new wells that will be constructed. The Strat 1 well is an existing well that was constructed for CO_2 service and will be utilized as a characterization well for this Project. The Injection Well Construction Plan includes all the information necessary to meet the requirements at 40 CFR §146.86. **Figures 5.1**, **5.2**, and **5.3** are wellbore diagrams of the proposed Injector 1, Monitor 1, and the existing Strat 1. Detail specifications for the casing, cement, tubing, and packer for Injector 1 are discussed below. More detailed information is provided in the "Construction Details" document (**5.0_Construction_Details_SJB_2023.06.09.pdf**) for the newly constructed wells for the Project.

5.1 Proposed Stimulation Program [40 CFR 146.82(a)(9)]

Injector 1 is anticipated to need a stimulation program, after initial well perforation, over selected intervals. The zones that are perforated and acidized will be chosen based upon advanced well log, core, and formation testing evaluations. Additional data obtained from future wells (e.g., Injector 1, Monitor 1) that are drilled and operated by Four Corners Carbon are anticipated to indicate the need for stimulation to remediate any drilling damage or improve injectivity caused by low formation porosity and/or permeability. Over the course of the project timeline, additional well data will become available as Monitor 1 and Injector 1 are drilled, and data is gathered. Core testing will be performed for fluid compatibility and reactivity. If a stimulation program is needed this data will be utilized in the stimulation design, that will be submitted to the USEPA Region 6 for approval. Any downhole, injected chemicals will comply with state(s) and federal regulations.

5.2 Construction Procedures [40 CFR 146.82(a)(12)]

Permanently sequestering and preventing movement of the CO_2 injectate into the USDW is a critical design criterion for Class VI wells. The design and operations of the injection and monitoring wells considers the injection volume, rate, chemical composition, and physical properties of the injectate fluid. Also considered in well design are the corrosive nature of the injectate fluid, and the interaction of the fluid with wellbore components. Operation of Injector No. 1 is designed to manage pore space utilization in the reservoir and to contain the CO_2 in the authorized injection interval.

Specialty metallurgy is often required to handle the potential for corrosive fluids, commonly referred to as Corrosion Resistant Alloys (CRA) in the industry. CO_2 alone is not corrosive, but when combined with water, it can create carbonic acid with a pH as low as 3. In addition, other compounds such as hydrogen sulfide (H_2S) can create a corrosive environment. The metallurgy selection for the Injector No. 1 considers the injectate makeup and is designed to withstand the potentially harsh environment presented by injecting CO_2. The casing and cement are engineered to protect the USDW and prevent the injectate fluids from migrating out of the injection interval.

The injection and monitoring well designs will meet or exceed the following standards:

- American Petroleum Institute Specification 5CT
- American Petroleum Institute RP 5C1
- American Petroleum Institute RP 10B-2
- American Petroleum Institute Specification 10A
- American Petroleum Institute RP 10D-2
- American Petroleum Institute Specification 11D1
- American Petroleum Institute RP 14B
- American Petroleum Institute RP 14C

The design and construction of Injector No. 1 is dedicated to CO_2 injection. All well materials, including but not limited to the casing, cement, tubing, and packer are compatible with all fluids these materials are expected to come into contact with and meet or exceed standards developed for such materials by the American Petroleum Institute, American Society for Testing and Materials (ASTM) International, or comparable standard. The Injector No. 1 wellbore diagram is provided in **Figure 5.1**.

5.2.1 Casing and Cementing

The proposed wellbore design consists of [redacted]. surface casing below the USDW and would be cemented to surface per EPA Class VI standards. This injection well is designed to inject approximately [redacted] metric tons per year at a wellhead pressure of [redacted] psi and a maximum annular pressure of [redacted] psi. The production casing will be a [redacted], "long string" beginning at the surface to an approximate depth of [redacted] ft across the planned injection zone in [redacted] The injection zone will span approximately [redacted] ft. To ensure sufficient corrosion resistance for CO_2 injection, CRA material will be used across the injection zone and upper confining interval. **Table 5.1** details the casing design. CO_2 resistant cement like EverCrete or equivalent will be placed in the lower portion of the well from TD across both the injection and confining zones. The use of both CRA casing and EverCrete or equivalent type cement across the [redacted] and confining zone will ensure injectate will not migrate out of the intended storage zone.

The injectate stream is anticipated to be dry and non-corrosive, the planned design allows for the possibility of a surface upset or invasion of connate water[38] from the reservoir. A complete metallurgical study of the injectate and well conditions is planned to be performed, to validate the material selection used in this application. Casing design load cases were run for each of the casing strings and tubing. The design/load cases are provided in the document—Construction Details, for each string. Haliburton's Wellcat software, version 17.0.01 was used for design calculations.

5.2.2 Tubing and Packer

Like the casing string, it is important to consider the injectate and the potential for a corrosive environment when selecting the tubing. The UIC Class VI regulations state that proper tubing and packer should be installed near the bottom of the tubing string for the CO_2 injection. **Table 5.2**

[38] Connate water is water that is trapped in the pores of a rock during formation of the rock. connate water. | Energy Glossary (slb.com) accessed March 2023.

represents the tubing specifications which will be utilized for the injection well. Taking into consideration the possibility of a water and CO_2 mixture leading to the presence of carbonic acid, the injection tubing will be comprised of [redacted] material[39].

The tubing size of [redacted] outside diameter (OD) was selected by considering the total proposed injection volume of CO_2 during the project life. Premium tubing connections using metal to metal sealing surfaces will assure the integrity of the tubing string and avoid weakness at connections.

The packer provides a means for anchoring the tubing string, structural stability for the tubing and isolation of the overlying annulus space from the injection interval so that the annular fluid can be monitored for tubing and packer leaks. The packer will be installed inside the [redacted] long-string casing at a point near the top of the injection interval. The completion and monitoring assembly will employ a [redacted] rated injection packer with a floating seal assembly, manufactured from CRA material. **Table 5.3** details the packer design. The packer will be rated to withstand the differential pressure that it will experience during installation, workovers, and the injection phase plus a factor margin of safety.

During the life of the injection phase of the Project it may be occasionally necessary to remove the tubing in the injection well. A permanent injection packer with a seal bore assembly and nipple profiles below the seal bore will allow mechanical isolation between the tubing and [redacted] making it possible to pull the tubing without injecting kill weight fluid into the [redacted]. The packer is available in sizes compatible with the [redacted].-diameter tubing and the [redacted] diameter [redacted] long-string casing. In addition, the packer will be manufactured using carbon dioxide-compatible elastomer materials (e.g., nitrile rubber) and corrosion-resistant steel materials.

Table 5.1—Casing specifications.

Name	Depth Interval (ft)	Outside Diameter (in.)	Inside Diameter (in.)	Weight (lbm/ft)	Grade (API)	Design Coupling (Short or Long Threaded)	Thermal Conductivity (W/M/°C)	Burst Strength (psi)	Collapse Strength (psi)
Conductor	[redacted]	[redacted]	[redacted]	[redacted]	[redacted]				
Surface	[redacted]	[redacted]	[redacted]	[redacted]	[redacted]	[redacted]	[redacted]	[redacted]	[redacted]
Long String	[redacted]	[redacted]	[redacted]	[redacted]	[redacted]	[redacted]	[redacted]	[redacted]	[redacted]
Long-string	[redacted]	[redacted]	[redacted]	[redacted]	[redacted]	[redacted]	[redacted]	[redacted]	[redacted]

[39] [redacted]

Table 5.2—Tubing specifications.

Name	Depth Interval (ft)	Outside Diameter (in.)	Inside Diameter (in.)	Weight (lbm/ft)	Grade (API)	Design Coupling (Short or Long Thread)	Burst strength (psi)	Collapse strength (psi)
Injection tubing	[redacted]	[redacted]	[redacted]	[redacted]	[redacted]	[redacted]	[redacted]	[redacted]

Table 5.3—Packer specifications.

Packer Type and Material	Packer Setting Depth (ft)	Length (ft)	Nominal Casing Weight (lbm/ft)	Packer Main Body Outer Diameter (in.)	Packer Inner Diameter (in.)
Premium packer with V0 rating	[redacted]	[redacted]	[redacted]	[redacted]	[redacted]

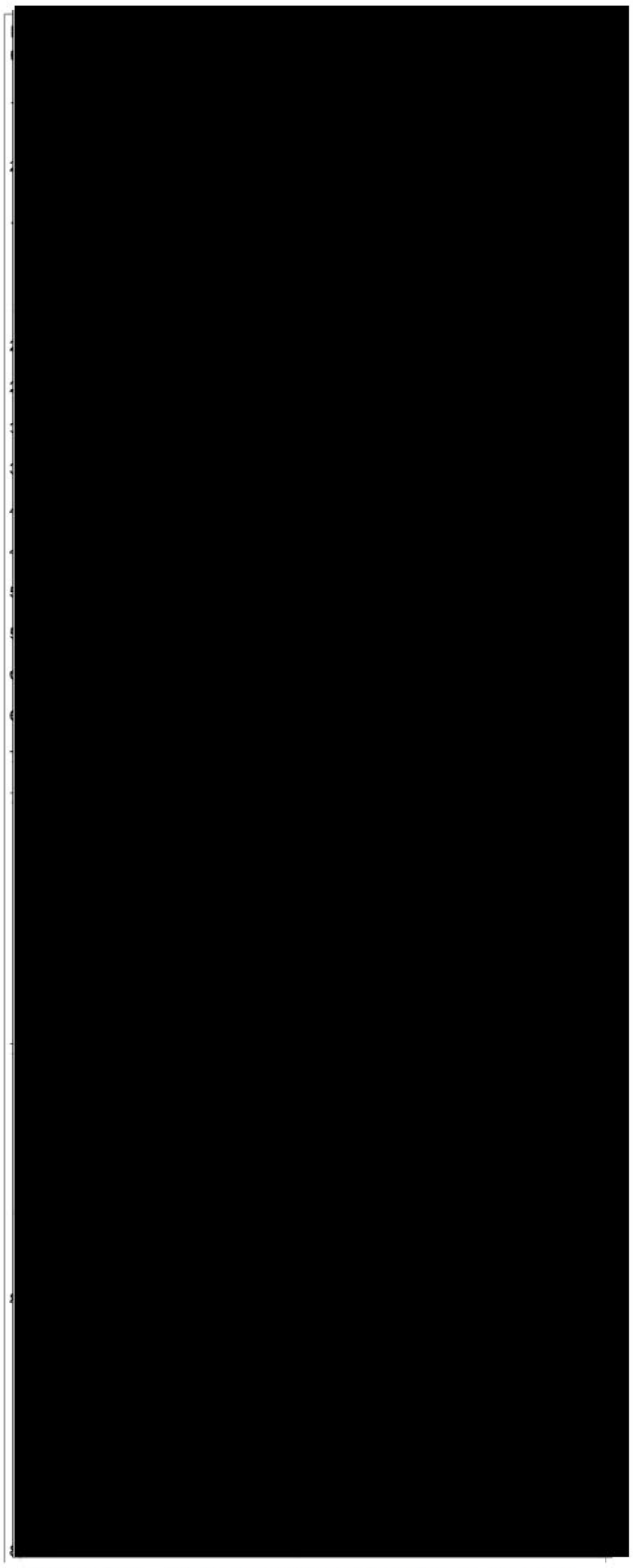

Figure 5.1—Proposed Injector 1 wellbore diagram.

5.2.3 Monitor 1 Well Construction

The construction of Monitor No. 1 well will follow a similar design to the injection well to ensure that there is no conduit of fluids from [redacted] to any USDWs. The primary difference between the design of Injector No. 1 and Monitor No.1 is the long string production casing which is [redacted]. Monitor No. 1 well will be perforated in [redacted] to allow for pressure monitoring and fluid sampling. External (to the [redacted] casing) pressure gauges will be installed to monitor pressures above and below [redacted] The well diagram for Monitor No. 1 is shown in **Figure 5.2** and additional construction detail is provided in the document—Construction Details.

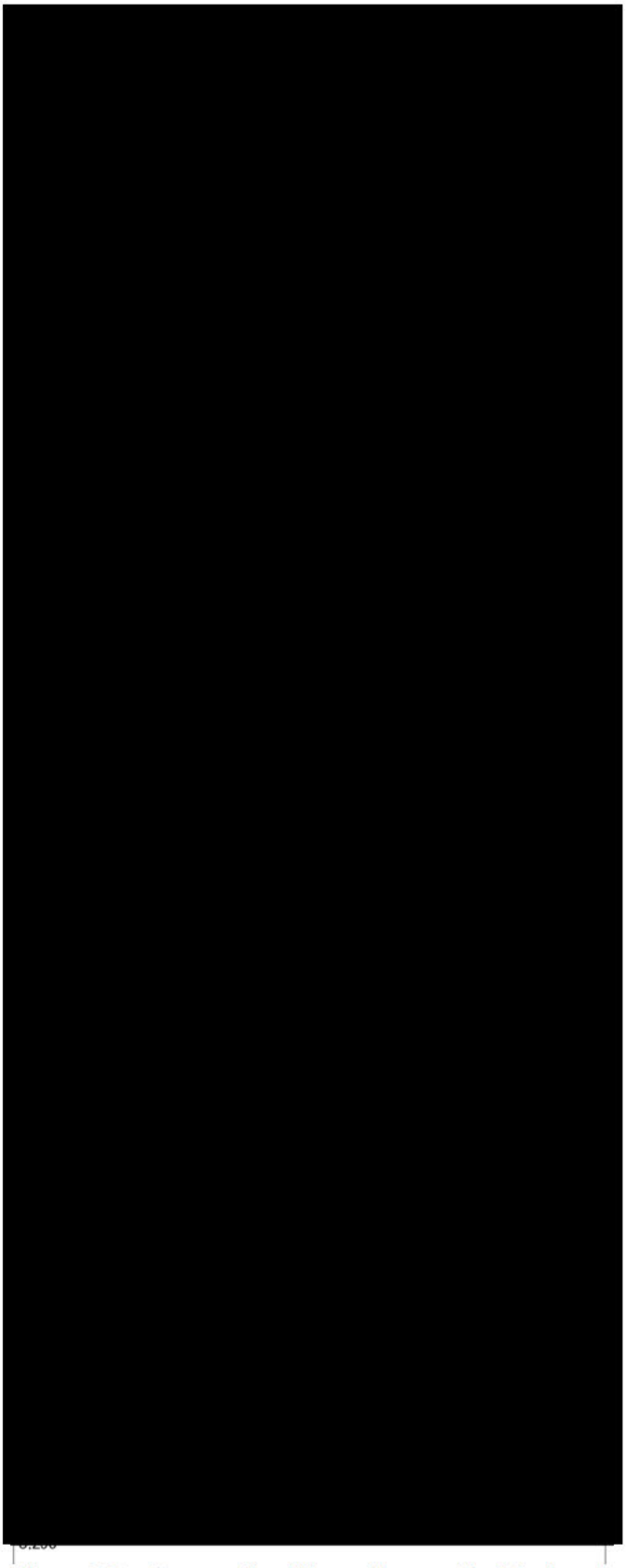

Figure 5.2—Proposed wellbore diagram for Monitor 1.

5.2.4 Continuous Monitoring Devices

During and after injection, Four Corners Carbon will implement a continuous monitoring plan consisting of the following elements:

Continuous Recording of Injection Mass Flow Rate

The continuous mass flow rate of CO_2 injected into the storage complex will be measured by a Coriolis flow meter transmitter for the injection well. The CO_2 flow transmitters will be networked to the main CO_2 storage site control center via a supervisory control and data acquisition (SCADA)-like system.

Continuous Recording of Injection Pressure

The continuous injection pressure of the CO_2 will be measured at the injection well by a pressure transmitter. The pressure transmitter will be networked to the main CO_2 storage site control center via a SCADA-like system. If the injection pressure exceeds 90% of [redacted] fracture pressure it will send an alarm to the control center for corrective action.

Continuous Recording of Injection Temperature

The continuous temperature of the CO_2 will be measured at the injection well by a temperature transmitter. The temperature transmitters will be networked to the main CO_2 storage site control center via a SCADA-like system.

Continuous Recording of Annulus Pressure

The continuous annulus pressure between the long string [redacted]. casing and the [redacted]. casing will be networked to the control room via a SCADA-like system and will provide the operators with an alarm and high pressure shut-down.

Bottomhole Pressure and Temperature

Electronic pressure and temperature gauges will be installed in the borehole of each injection well to continuously monitor CO_2 injection pressure and temperature (P/T) inside the tubing at the injection reservoir. The borehole P/T data will be networked to the main CO_2 storage site control center via a SCADA-like system.

6.0 PRE-OPERATIONAL LOGGING AND TESTING [40 CFR 146.82(A)(8) AND 146.87]

Document **6.0_pre-operational_testing_SJB_2023.06.09.pdf** has been submitted including all requirements required by 40 CFR 146.82(a)(8) and 146.87.

7.0 INJECTION WELL OPERATION

7.1 Operational Procedures [40 CFR 146.82(a)(10)]

The following information (**Table 7.1**) provides the operating parameters and engineering criteria during injection operations required under 40 CFR 146.82(a)(7) and (10). Using these criteria, the injection well will be operated to prevent the migration of CO_2 from the approved zone and into a USDW.

Table 7.1—Proposed injection well operating parameters.

Item	Values	Description/Comments
	Injected Volume	
Total Injected Volume	[redacted]	Based on expected injection
	Injection Rates	
Proposed Average Injection Rate	[redacted]	Based on expected injection
Calculated Maximum Daily Injection Rate	Under Review	Under Review
	Pressure	
Formation Fracture Pressure at Top Perforation	[redacted]	Estimated formation fracture gradient of [redacted] psi/ft
Average Operating Surface Injection Pressure	[redacted]	Proposed average surface injection pressure
Surface Maximum Injection Pressure	[redacted]	Based on SLB modeling maximum pressure [redacted].
Average Operating BHP	[redacted]	Based on expected injection (< 90% of fracture gradient)
Maximum BHP	[redacted]	Based on expected injection (< 90% of fracture gradient)
Tubing-Casing Annular Pressure	[redacted]	100 psi above maximum surface injection pressure

7.1.1 Injection Rate

The injection rate for CO_2 into [redacted] is modelled and estimated to be stable at [redacted].

7.1.2 Maximum Injection Pressure

The fracture gradient of [redacted] is estimated to be [redacted] psi/ft. The maximum allowable sand face pressure gradient is calculated by multiplying the fracture gradient by 90%. This yields a maximum sand face pressure gradient of [redacted] psi/ft.

7.1.3 CO_2 Volume

The total volume of CO_2 injected and stored in the Entrada Sandstone is estimated to be [redacted] Mt.

7.1.4 Annulus Pressure

The annulus will be filled with base oil with a nitrogen cap. There can be significant temperature fluctuations downhole during startup and shutdown of injection. The requirement to keep the annulus pressure 100 psi or greater over the tubing pressure will be impacted by the annulus temperature and hence the pressure. The nitrogen cap will provide a compressible cushion to absorb pressure fluctuations in the annulus. The annulus pressure will be set to be at least 100 psi above the tubing wellhead pressure. The expected maximum allowable annulus pressure is [redacted] psi. SLB's modeling indicated a maximum injection pressure of [redacted] psi will result in an annulus pressure of [redacted] psi. Therefore, the annulus pressure is expected to range from [redacted] psi to a maximum of [redacted] psi.

7.1.5 Well Stimulation Procedures

Injector No. 1 is anticipated to need a stimulation program after initial well perforation, over selected intervals. The zones will be chosen based upon advanced well log, core, and formation testing evaluations. Over the course of the project timeline, additional well data will become available as the characterization well (Monitor 1) and injection well (Injector 1) are drilled, and data is gathered. Core testing will be performed for fluid compatibility and reactivity. The additional data will be used to design stimulation procedures that will be submitted to EPA Region 6 for approval. Any downhole, injected chemicals will comply with state(s) and federal regulations.

7.2 Proposed Carbon Dioxide Stream [40 CFR 146.82(a)(7)(iii) and (iv)]

The following is a typical composition of an injectate stream which will be validated by future samples and laboratory testing. (**Table 7.2**).

Table 7.2— Typical composition of an injectate stream.

Constituent	Limit
CO_2	[redacted]
CO	[redacted]
H_2	[redacted]
H_2S	[redacted]
Total Sulfur	[redacted]
Total NO_X	[redacted]
O_2	[redacted]
H_2O	[redacted]
Hydrocarbons	[redacted]
Glycol	[redacted]
Maximum dew point at 400 psig	[redacted]
Non-condensable gases	[redacted]

Four Corners Carbon plans to inject [redacted] of CO_2 for [redacted] years into Injector No. 1. The total volume to be injected is [redacted] over the Project's life. The maximum bottom hole injection pressure of [redacted] psi is less than 90% of the formation fracture pressure ([redacted]) and, therefore, does not significantly alter USDWs.

8.0 TESTING AND MONITORING [40 CFR 146.82(A)(15) AND 146.90]

The information and files have been submitted to the EPA as required by 40 CFR 146.82(a)(15), that the proposed Testing and Monitoring Plan meets the requirements of 146.90.

The plan is described in: **8.0_tm_plan_SJB_2023.06.09.pdf**.

9.0 INJECTION WELL PLUGGING [40 CFR 146.82(A)(16) AND 146.92(B)]

The information and files submitted demonstrate, as required by 40 CFR 146.82(a)(16), that the proposed Injection Well Plugging Plan meets the requirements of 40 CFR 146.92(b).

This section describes the injection well plugging plan the operator will implement in compliance with 40 CFR 146.92 after CO_2 injection has ceased and injection well monitoring activities have been completed. The plan is described in: **9.0_plugging_plan_SJB_2023.06.09.pdf**.

10.0 POST-INJECTION SITE CARE AND SITE CLOSURE [40 CFR 146.82(A)(17) AND 146.93(A)]

The information and files submitted demonstrate, as required by 40 CFR 146.82(a)(17), that the proposed Post-Injection Site Care (PISC) and Site Closure Plan, meets the requirements of 146.93(a).

The Post-Injection Site Care and Site Closure plan is provided in: **10_pisc_sc_plan_SJB_2023.06.09.pdf**

11.0 EMERGENCY AND REMEDIAL RESPONSE [40 CFR 146.82(A)(19) AND 146.94(A)]

The information and files submitted as required by 40 CFR 146.82(a)(19) show that the proposed Emergency and Remedial Response Plan (ERRP) meets the requirements of 146.94(a).

The ERRP is provided in **11.0_err_plan_SJB_2023.06.09.pdf**.

12.0 INJECTION DEPTH WAIVER AND AQUIFER EXEMPTION EXPANSION

Not Applicable—No injection depth waiver nor aquifer exemption expansion is requested or required.

13.0 OPTIONAL ADDITIONAL PROJECT INFORMATION [40 CFR 144.4]

13.1 Environmental Justice

The United States Environmental Protection Agency has established Class VI requirements to safeguard underground sources of drinking water and mitigate potential health hazards, particularly for populations located within or near the delineated area of review (AoR). The Regional EPA Underground Injection Control Directors play a vital role in protecting public health and must assess the risks associated with a proposed Class VI injection well within their jurisdiction. This includes identifying and addressing any potential environmental impacts on minority and low-income populations, as part of environmental justice (EJ) screening.

According to the EPA, environmental justice (EJ) is defined as the fair treatment and meaningful involvement of all people regardless of race, color, national origin, or income with respect to the development, implementation, and enforcement of environmental laws, regulations, and policies (USEPA 1998).

In evaluating potential EJ concerns resulting from the proposed Project, Four Corners Carbon followed the EPA's guidance provided in "*Geologic Sequestration of Carbon Dioxide - UIC Quick Reference Guide, Additional Tools for UIC Program Directors Incorporating Environmental Justice Considerations into the Class VI Injection Well Permitting Process*" (USEPA 2011). According to this document, environmental justice is employed by UIC Program Directors and project owners or operators to "determine if any minority or low-income communities might be impacted by the proposed well" (USEPA 2011). As outlined in Step 2 of the guidance, under "EJ Steps for UIC Program Directors and Owners or Operators," Four Corners Carbon "review[ed] site characterization data to determine if EJ communities reside within the AoR and may be impacted" (USEPA 2011).

To evaluate any potential EJ communities residing within the Project AoR, Four Corners Carbon reviewed geospatial data to determine the demographics within the AoR. The geospatial review indicated that no structures for human occupancy are present in the AoR; thus, the population within the AoR is zero residents. This conclusion was formed by analyzing the New Mexico Department of Finance and Administration Address Point database accessed via RGIS[40] that is used to for New Mexico's 911 program. This search found two address points present within the AoR (**Figure 13.1**). Next, a satellite imagery review of these locations indicated that no structures for human occupancy are present at these locations. Further review across the AoR confirmed a lack of additional structures (**Figure 13.2**). Since the AoR is not populated there are no demographics to be assessed and no EJ communities reside within the AoR.

The EPA's EJScreen tool inaccurately indicates that a population of [redacted] people resides within the AoR. The tool is likely referencing population statistics that are mapped coarser than the size of the AoR. A disclaimer provided by EJScreen acknowledges this limitation: "Users should keep in mind that screening tools are subject to substantial uncertainty in their demographic and environmental data, particularly when looking at small geographic areas." Four Corners Carbon

[40] https://rgis.unm.edu/rgis6/dataset.html?uuid=cef558f9-9312-45b4-8e84-93450b38278e

relied on a review of geospatial data and satellite imagery to determine that there are no EJ communities residing within the AoR.

Four Corners Carbon remains committed to the principles of environmental justice and will continue to consider potential impacts on all communities, particularly those that are historically marginalized and vulnerable, in this and future projects. This will include updating this population analysis regularly throughout the injection and monitoring periods and taking action to address potential EJ concerns should they arise.

Even though no EJ communities reside within the AoR, Four Corners Carbon has prepared a community engagement plan to support meaningful engagement with surrounding communities outside of the AoR for all phases of injection well operation, construction operations, and eventually decommissioning. This engagement plan will ensure culturally appropriate engagement with traditionally underserved or disadvantaged communities and Four Corners Carbon will create and distribute all communication materials in an effective and culturally appropriate manner for all involved.

The engagement plan will include a feedback loop to enable nearby communities to meaningfully participate and engage in discussions regarding project activities. The grievance mechanism will be transparent and well-documented to ensure that community members have equitable access to raise concerns and receive answers to questions, concerns, and comments about the injection well and its associated project activities. Opportunities for anonymous engagement and dialogue will be integrated into the engagement plan to ensure there is no retaliation against any community members.

Plan revision number: 0

Figure 13.1—Map of all addresses in the vicinity of the AoR identified in the New Mexico Department of Finance and Administration Address Point database.

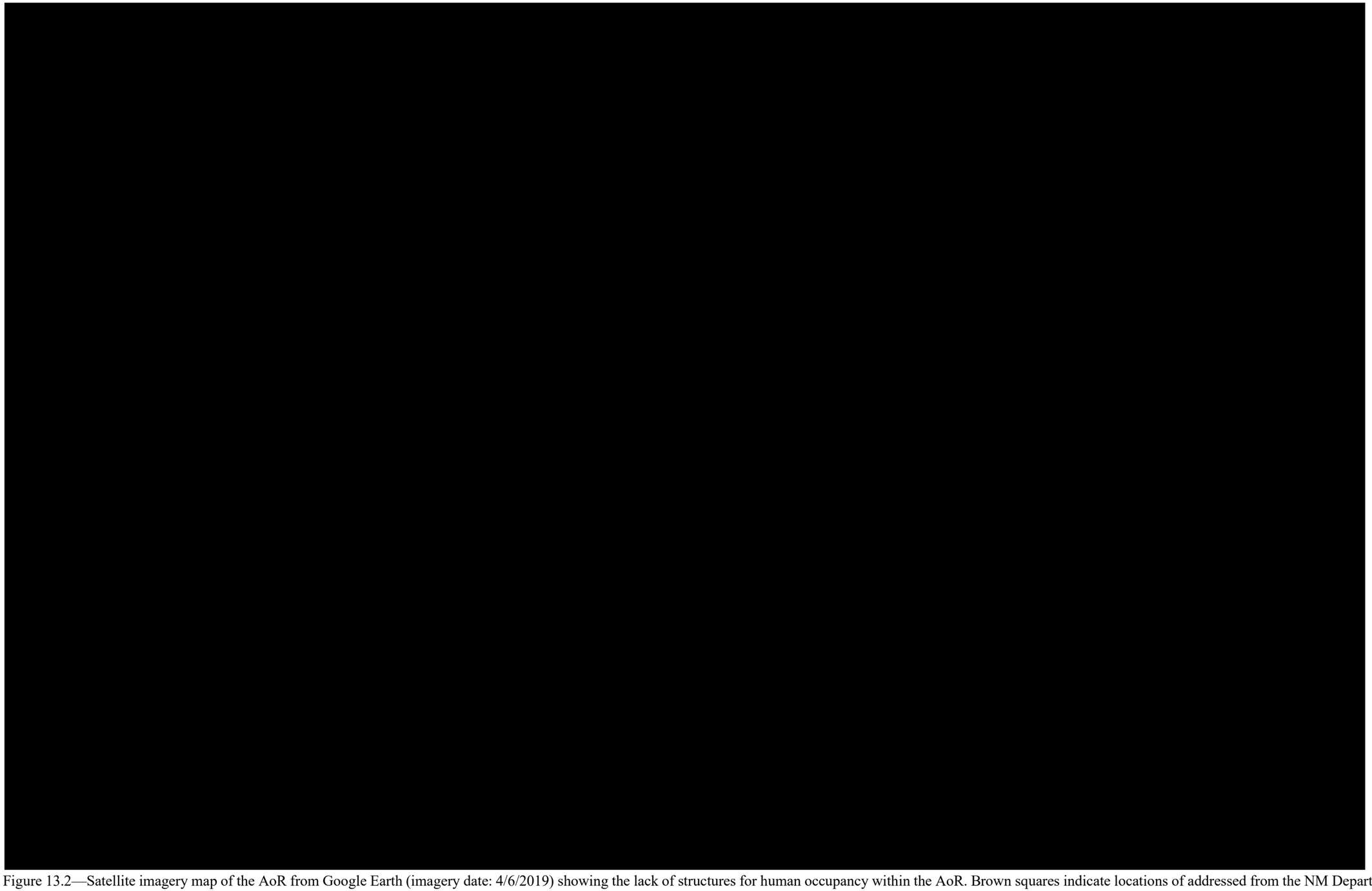

Figure 13.2—Satellite imagery map of the AoR from Google Earth (imagery date: 4/6/2019) showing the lack of structures for human occupancy within the AoR. Brown squares indicate locations of addressed from the NM Department of Finance and Administration Address Point database. No enclosed structures are present at these locations.

13.2 The National Historic Preservation Act of 1966 [16 U.S. Code 470]

Four Corners Carbon evaluated the existence of historic places recorded in the National Register of Historic Places within the AoR of Injector No. 1 (**Figure 13.3**). There are no historic places in the Register within the AoR or plume boundary.

13.3 The Endangered Species Act [16 U.S. Code 1531]

Four Corners Carbon reviewed the U.S. Fish & Wildlife Service's Information for Planning and Consultation tool[41] (IPAC) to evaluate the potential presence of endangered, threatened, and candidate species ranges and critical habitat within the AoR. No critical habitats are present within the AoR. The AoR is within the known or expected ranges of the species listed in **Table 13.1** below.

For Corners Carbon will comply with all federal and state laws for surface operations, such as drilling permits and seismic surveys, for the planned injection and monitoring well.

[41] https://ipac.ecosphere fws.gov – accessed 5/4/2023

Table 13.1—List of known or expected endangered, threatened, and candidate species ranges within the AoR. From the USFWS IPAC tool.

Mammals

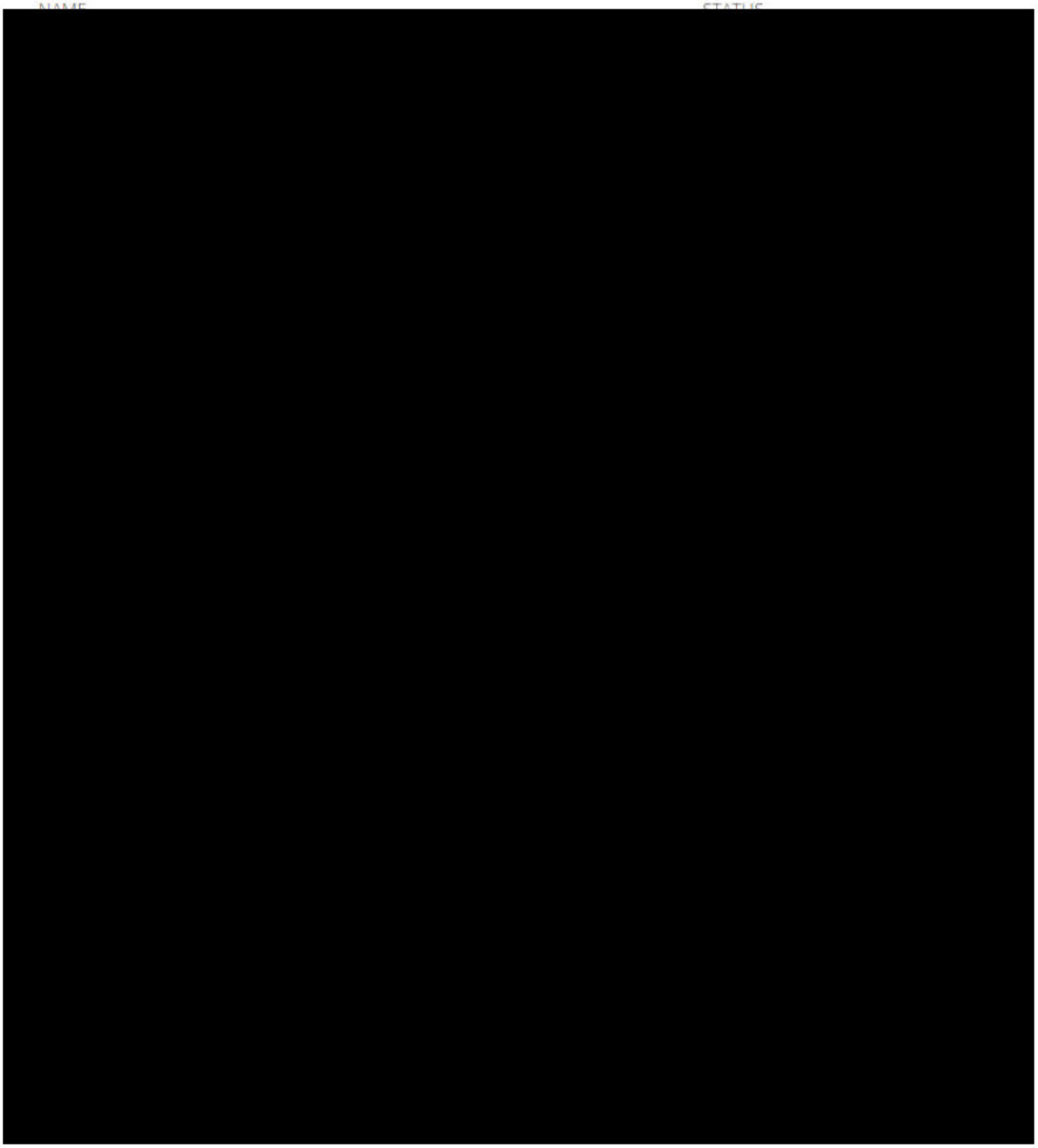

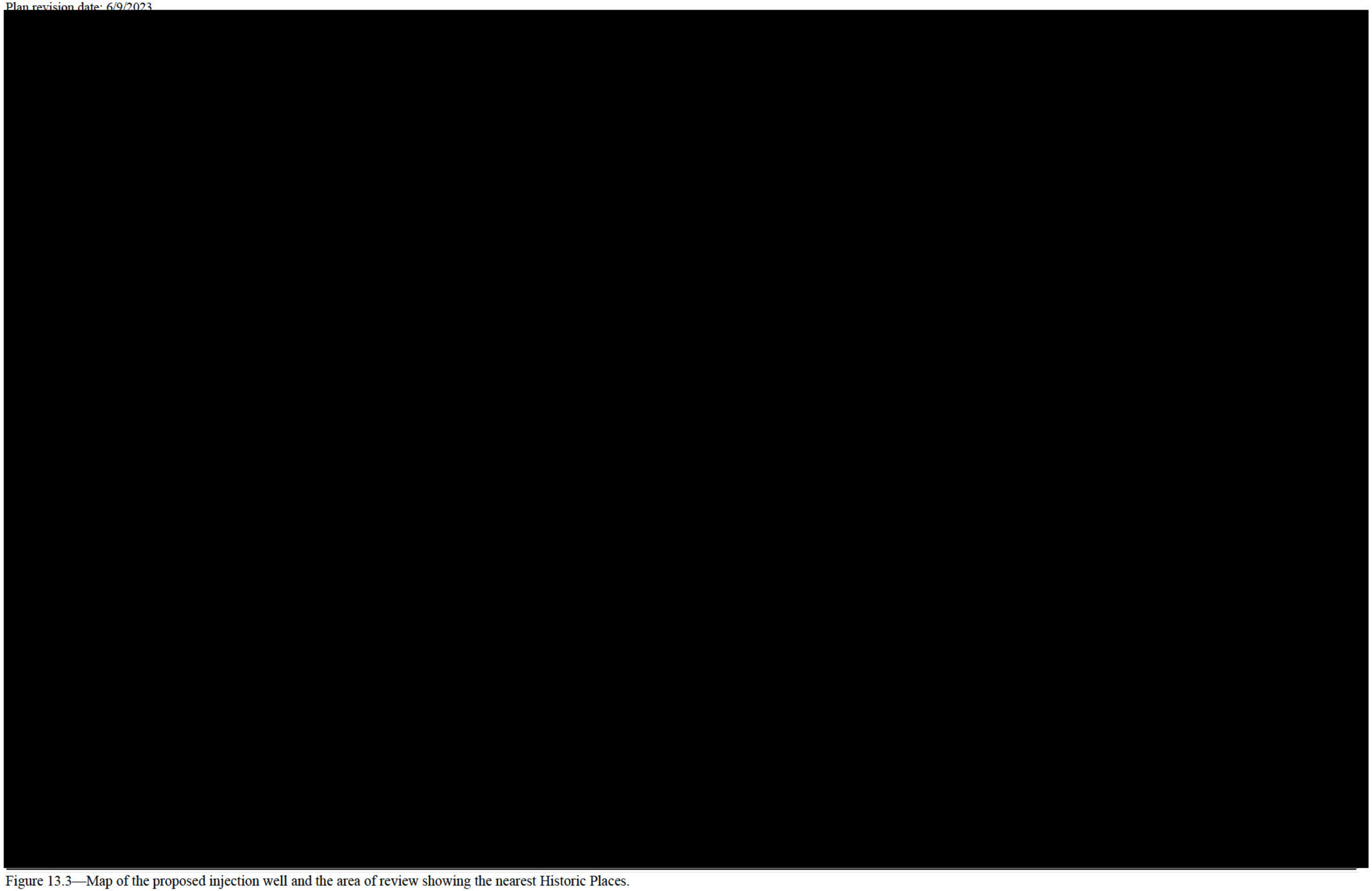

Figure 13.3—Map of the proposed injection well and the area of review showing the nearest Historic Places.

14.0 OTHER INFORMATION

Additional information and data that may be helpful to the review process have been provided in separate attachments. These include:

File Name	Description
FourCornersCarbonSJ_geodatabase.gdb	An ESRI file geodatabase containing project specific data (proposed well locations, AoR boundary, etc.) and other pertinent spatial data referenced in the application narrative
References	A folder containing references cited
2.1.2_RegionalTopographicMap.pdf	Regional topographic map of the Northern San Juan Basin showing the location of the proposed injection well (blue) and AoR. Regional topographic map of the Northern San Juan Basin showing the location of the proposed injection well (blue) and AoR. The approximate extent of the San Juan Basin is shown with a dashed dark red line and the approximate Central Basin extent is shown with a thin dotted red line
2.1.3_TypeWellLog.pdf	Type well log for the project area showing all key stratigraphic markers and zones from surface down to the lower confining zone
2.2.1a_FourCornersCarbon_Inj1_AoR_Map_ArchD_1-18k_land-topo.pdf	A map of the AoR with all required information per 14 CFR §146.82 at a scale of 1 in. to 1,500 ft (1:18,000).
2.2.1b_FourCornersCarbon_Inj1_AoR_Map_ArchD_1-12k_SatImage.pdf	An AoR basemap version at 1:12,000 scale with a recent satellite imagery basemap
2.2.1c_AoRMap-let.pdf	A smaller scale letter sized version of the AoR basemap
2.2.2_[redacted]_1-24k_ArchE.pdf	Large scale structure contour map on the top of the proposed injection zone, [redacted]
2.2.2_[redacted]_1-24k_ArchE.pdf	Large scale structure contour map on the top of the upper confining zone, [redacted]
2.2.3_CrossSections.pdf	Structural cross section A and B running NW-SE and SW-NE, respectively, through the proposed injection well location
2.3.1_BasementFaultsMap.pdf	Map of approximate locations of basement faults (after Taylor and Huffman 1998)
2.4.1a[redacted]_SCM_1-250k_let.pdf	[redacted] structure contour map at 1:250k scale
2.4.1b[redacted]Isopach_1-250k_letter.pdf	[redacted] gross isopach map at 1:250k scale
2.4.2a_[redacted]_SCM_1-250k_letter.pdf	[redacted] structure contour map at 1:250k scale
2.4.2b_[redacted]_Isopach_1-250k_letter.pdf	[redacted] gross isopach map at 1:250k scale
2.5.3_WSMLetter-final.pdf	Basin scale stress orientations map from the World Stress Map database
2.6.2_SeismicHistoryMap.pdf	Seismic events map of the SJ basin from the USGS
2.7.3_AoRWaterWellsBasemap.pdf	Map of water wells within the AoR
3.4.1a_AoR Oil and Gas Well List (NM OCD)-dist.xlsx	Spreadsheet with a list of all oil and gas wellbores within the AoR and pertinent information (depths etc.) from the New Mexico Oil Conservation Division.
3.4.1b_AoR Water Well List (NM OSE PODs)-dist.xlsx	Spreadsheet with all water wells within the AoR from the New Mexico Office of the State Engineer's Points of Diversion database.
3.4.1c_Oil and Gas Well Files NM-OCD.zip	Well files and logs for all oil and gas wells within the AoR
3.4.1d_Water Well Files_NM-OSE.zip	Well files for all water wells within the AoR
13.1a_EJ_AddressesMap.pdf	Map showing address points within and adjacent to the AoR

File Name	Description
13.1b_EJ_SatImage.pdf	Google Earth satellite imagery map of the AoR
13.2_HistoricPlacesMap.pdf	Map of the proposed injection well and the area of review showing the nearest Historic Places.